Targeting ribosome biogenesis and metabolism in acute myeloid leukaemia

Laura Llewellyn Ferguson

A thesis submitted for the degree of Doctor of Philosophy of The Australian National University

May 2020

The John Curtin School of Medical Research
The Australian National University

Declaration

This is to certify that:

1. The work described in this thesis was designed, performed and analysed by myself under the supervision of Dr. Katherine Hannan and Dr. Anneke Blackburn.

2. This thesis contains no material which has been accepted for the award of any other degree or diploma in any university.

3. This thesis comprises only my original work, except where due acknowledgement has been made in the text to other materials referenced.

4. This thesis is less than 100,000 words in length, exclusive of tables, legends, and the bibliography.

Laura Llewellyn Ferguson

May 2020

Acknowledgements

Abstract

Targeting ribosome biogenesis, a cellular process frequently upregulated in cancer, with the novel Pol I transcription inhibitor CX-5461 is highly efficacious in pre-clinical models of solid and haematological cancers, which lead to the commencement of clinical trials. However, as is common with single-agent therapies in the mouse models (similar to challenges with treating human patients), the mice eventually succumb to disease, highlighting the need for a combination therapy approach. Based on the strong link between altered ribosome biogenesis and metabolism in cancer it was hypothesised that targeting these two processes in combination would prove efficacious in cancer, and acute myeloid leukaemia (AML) was chosen to test this as it is an aggressive malignancy with poor therapeutic options. In order to address this hypothesis *In vitro* drug synergy testing in AML cell lines was performed to identify promising combinations (Chapter 3), these were then tested for efficacy in *in vivo* transplant models of AML (Chapter 4). Finally, *in vitro* mechanistic analysis of the most promising drug combination was performed in order to understand the mechanisms of synergy (Chapter 5).

In vitro testing of CX-5461 in combination with 10 clinically-approved metabolism-modifying drugs confirmed that orlistat, dichloroacetate (DCA), ritonavir, omeprazole and chloroquine act synergistically with CX-5461 to reduce cell viability in multiple AML cell lines. Three such combination therapies were evaluated in a syngeneic mouse AML model. Neither orlistat nor DCA improved survival in combination with CX-5461 compared to CX-5461 alone, however, synergy was observed with the autophagy inhibitor chloroquine. Interestingly, the combination of CX-5461 and chloroquine had limited efficacy in human cell line xenograft mouse models, despite strong *in vitro* results. As the dosing of CX-5461 and chloroquine could not be increased due to toxicity, mechanistic analysis was performed in order to identify an alternative to chloroquine with reduced toxicity, and potentially improved efficacy.

CX-5461 and chloroquine were found to synergise through cell cycle arrest and cell death in all four cell lines tested. Metabolic flux analysis revealed that the combination of drugs significantly affected mitochondrial activity, indicating that the combination of

CX-5461 and chloroquine is placing the cells in mitochondrial stress. Therefore, direct targeting of the mitochondria was identified as a promising approach in combination with ribosome biogenesis inhibition with CX-5461, and various clinically-approved drugs that target mitochondria were identified for future combination testing.

Table of contents

Chapter 4   Testing promising combination therapies *in vivo* in transplant models of AML 90

List of figures

List of tables

List of abbreviations

Abbreviation	Full name
3'UTR	3 prime untranslated region
5SRNP	Ribosomal protein L5/L11/5S ribonucleolar protein
AHR	Aryl hydrocarbon receptor
ALDH1	Aldehyde dehydrogenase 1
ALL	Acute lymphoblastic leukaemia
AML	Acute myeloid leukaemia
AMPK	5' adenosine monophosphate-activated protein kinase
ANOVA	Analysis of variance
APL	Acute promyelocytic leukaemia
ATG	Autophagy-related gene
ATM	Ataxia-telangiectasia mutated
ATO	Arsenic trioxide
ATP	Adenosine triphosphate
ATR	ATM and Rad 3-related
ATRA	All-trans retinoic acid
B-CLL	B-chronic lymphocytic leukaemia
BECN1	Beclin 1
BLI	Total body bioluminescence
BrdU	5-bromo-2'-deoxyuridine
BSA	Bovine serum albumin
BSABB	Bovine serum albumin blocking buffer
CAR	Chimeric antigen receptor
CDC25A	Cell division cycle 25 A
CDK2	Cyclin-dependent kinase 2
CEBPA	CCAAT/enhancer-binding protein alpha
CI	Combination Index
CLL	Chronic lymphocytic leukaemia
C_{max}	Peak serum concentration
CML	Chronic myeloid leukaemia
CNS	Central nervous system
Core	Core region
Cox	Cytochrome C oxidase
CrTac:Ncr-Foxn1nu	Athymic nude mice
DAPI	4',6-diamidino-2-phenylindole
DCA	Dichloroacetate
ddH_2O	Double-distilled water

Abbreviation	Full name
DMSO	Dimethyl sulfoxide
DNMT3α	DNA methyltransferase 3 α
DSMZ	German Collection of Microorganisms and Cell Cultures
ECAR	Extracellular acidification rate
EDTA	Ethylenediaminetetraacetic acid
ETC	Electron transport chain
ETS	External transcribed spacer
FAB	French-American-British
FASN	Fatty acid synthase
FBS	Fetal bovine serum
FC	Flow cytometry
FCCP	Carbonylcyanide p-trifluoromethoxy-phenylhydrazone
FCSB	Flow cytometry staining buffer
FLT3	FMS-like tyrosine kinase 3
FSC	Forward scatter
G6P	Glucose 6-phosphate
GFP	Green fluorescent protein
GI_{50}	Concentration of drug resulting in 50% growth inhibition
GLS	Glutaminase
GLUT	Glucose transporter
Gy	Gray (unit)
h	Hour/s
HCl	Hydrochloric acid
HEPES	4-(2-hydroxyethyl)-1 piperazineethanesulfonic acid
HI-FBS	Heat-inactivated fetal bovine serum
HIV	Human immunodeficiency virus
HMG-CoA	3-hydroxy-3-methyl-glutaryl-coenzyme A
HRP	Horseradish peroxidase
HSCs	Haematopoietic stem cells
HSCT	Haematopoietic stem cell transplantation
IDH	Isocitrate dehydrogenase
IGF-IR	Insulin growth factor-I receptor
ITD	Internal tandem duplication
ITS	Intergenic spacers
IV	Intravenously
LAMP1	Lysosomal-associated membrane protein 1
LD_{50}	50% lethal dose
luc	Luciferase

Abbreviation	Full name
mCMV	Murine cytomegalovirus
MCV	Mean corpuscular volume
MDS	Myelodysplastic syndrome
min	Minute(s)
miRNA	Micro RNA
MLL	Mixed-lineage leukaemia
mRNA	Messenger RNA
MSCs	Mesenchymal stem cells
MTD	Maximum tolerated dose
mTOR	Mammalian target of rapamycin
mTORC1	mTOR complex 1
MTT	Thiazolyl blue tetrazolium bromide
NaCl	Sodium chloride
NaH_2PO_4	Sodium dihydrogen phosphate
NAPDH	Reduced nicotinamide adenine dinucleotide phosphate
NF-κB	Nuclear factor kappa-light-chain-enhancer of activated B cells
NH_4Cl	Ammonium chloride
NK cell	Natural killer cell
NORs	Nucleolar organiser regions
NPM1	Nucleophosmin
NSG	NOD-scid-gamma
OCR	Oxygen consumption rate
OCT	Organic cation transporter
ORF	Open reading frame
OXPHOS	Oxidative phosphorylation
PBS	Phosphate-buffered saline
PCR	Polymerase chain reaction
PDH	Pyruvate dehydrogenase
PDK	Pyruvate dehydrogenase kinase
PE	Phosphatidylethanolamine
PEG-400	Polyethylene glycol-400
PEI	Polyethylenimine
PENAO	Phenylarsonous acid
PIC	Pre-initiation complex
PML	Promyelocytic leukaemia
Pol I	RNA polymerase I
Pol II	RNA polymerase II
Pol III	RNA polymerase III
PPAR	Peroxisome proliferator-activated receptors

Abbreviation	Full name
PSA	Prostate-specific antigen
PVDF	Polyvinylidene difluoride
RARα	Retinoic acid receptor α
RFP	Red fluorescent protein
RNAseq	RNA sequencing
ROI	Regions of interest
ROS	Reactive oxygen species
RP	Ribosomal proteins
rRNA	Ribosomal RNA
SDS	Sodium dodecyl sulphate
SDS-PAGE	Sodium dodecyl sulphate polyacrylamide gel electrophoresis
SL-1	Selectivity factor 1
SLC1A5	Solute carrier family 1 member 5
SMBB	Skim milk blocking buffer
snoRNA	Small nucleolar RNA
snRNA	Small nuclear RNA
SSC	Side scatter
t-AML	Treatment-related acute myeloid leukaemia
$t_{1/2}$	Biological half-life
TAFs	TATA-box-binding protein -associated factors
TBP	TATA-box-binding protein
TBS	Tris-buffered saline
TBST	Tris-buffered saline with tween-20
TCA	Tricarboxylic acid cycle
TEM	Transmission electron microscopy
TET	Tetracycline
TET2	Tet methylcytosine dioxygenase 2
TIF-IA	Transcription Initiation Factor IA
TopIIα	Topoisomerase II α
tRNA	Transfer RNA
UBF	Upstream binding factor
UCE	Upstream control element
VCAM-1	Vascular cell adhesion molecule 1
VLA-4	Very late antigen-4
WB	Western blot
WHO	World Health Organisation
XIAP	X-linked inhibitor of apoptosis protein

Chapter 1 Introduction

1.1 Acute myeloid leukaemia: an aggressive malignancy with poor therapeutic options

1.1.1 Epidemiology and aetiology

Acute myeloid leukaemia (AML) is a heterogeneous cancer resulting from the clonal expansion of myeloid progenitor cells, leading to an accumulation of myeloid blasts in the peripheral blood or bone marrow [8]. It is the most common acute leukaemia in adults [9], and approximately 1000 Australians are diagnosed with AML each year (or 4 new cases per 100,000 people) [10]. The 5-year survival rate is poor, at approximately 30%, compared to over 90% for more common cancers such as breast and prostate cancer [10]. The risk of developing AML increases with age and the highest risk age group is those over 65 [11]. Other risk factors include pre-existing haematological disease, genetic conditions (e.g. Down syndrome, Li-Fraumeni syndrome), radiation exposure, chemical exposure (e.g. pesticides, cigarette smoke) or previous chemotherapy [12]. Investigation of correlations between specific risk factors and AML genetics has revealed that cigarette smoke and occupational chemical exposure (e.g. pesticides) are associated with AML with increased incidence of complex chromosomal abnormalities and oncogene activation [13-15]. However, specific risk factors account for only a relatively small fraction of total AML cases, the majority of which are considered de-novo AML (~90%)[16]. Of the non-de-novo cases, most arise after cytotoxic and/or radiation therapy (treatment-related/t-AML) or myelodysplastic syndrome (MDS) [16], a heterogeneous group of disorders characterised by ineffective haematopoiesis that progresses to AML in approximately 15% of cases [17], through complex mechanisms that remain to be fully elucidated.

1.1.2 Genetics of AML

While AML has a comparatively low mutational burden compared to cancers such as melanoma and lung carcinoma [18], there are numerous recurrent mutations which are found at low frequency (Table 1-1) [2]. These mutations can be broadly characterised

into groups associated with DNA methylation, tumour suppressors, activated signalling, myeloid transcription factors, chromatin modifiers, cohesion, spliceosome and transcription factor fusions. Certain mutations have been associated with either a favourable, intermediate or poor outcome for patients [19] (Table 1-1). Of the most common mutations, the presence of mutations in phosphoprotein nucleophosmin (NPM1) has been associated with a favourable outcome for patients [20,21], while those in the signal transduction protein FMS-like tyrosine kinase 3 (FLT3), including FLT3 internal tandem duplication (ITD), are associated with a poor outcome [3,4]. Cytogenetic analysis also provides a powerful prognostic tool for predicting outcomes in patients with this disease, with approximately 50-60% of AML patients having cytogenetic abnormalities at diagnosis [2,22], up to 75% in t-AML [16]. For example, translocations of the mixed-lineage leukaemia (MLL) gene/11q23, which encodes a histone methyltransferase involved in haematopoiesis, results in specific fusion proteins which are associated with a poor patient outcome [6,23]. The MLL fusion gene partners, of which there are over 70 [24], further dictate the prognosis for these cancers. Of the more common rearrangements, MLL-AF6/t(6;11) is associated with a very poor prognosis, while MLL-AF9/ t(9;11) is more favourable [25]. The translocation t(15;17) is characteristic of a subtype of leukaemia known as acute promyelocytic leukaemia (APL), fusing the promyelocytic leukaemia (PML) gene and retinoic acid receptor α (RARα), which blocks differentiation and promotes survival of promyelocytic cells [26].

Category	Mutation	Frequency (%)	Favourable (F), Intermediate (I) or Unfavourable (U) prognosis	Present in models in this thesis?	
				In vitro	*In vivo*
NPM1	NPM1	27	F		
Activated signalling	FLT3	28	U	+	+
	KRAS or NRAS	12	I	+	+
	KIT	4	I		
	PTPN11	4	I		
DNA methylation	DNMT3A	26	I		
	IDH1 or IDH2	20	I		
	TET2	8	I	+	
Tumour suppressors	TP53	8	U	+	+
	WT1	6	I		
Myeloid transcription factors	RUNX1	10	I		
	CEBPA	6	F		
Transcription factor fusions	t(15;17)/PML-RARα	9	F		
	inv(16)/MYH11-CBFB	6	F		
	t(8;21)/RUNX1/RUNX1T1 (AML1-ETO)	4	F	+	
Chromatin modifiers	11q23/MLL fusions	4	U	+	+
Other	Loss of 7 or del (7q)	10	U		
	Loss of 5 or del(5q)	8	U		

Table 1-1: Recurrent mutations in AML with functional categorisation and prognostic significance

Mutation frequency and functional characterisation adapted from [2]. Prognostic significance adapted from [3-6]. Genetic information of individual cell lines used in this thesis is in Table *3-1*.

With such a heterogeneous genetic profile, and the evidence that single mutations are not sufficient to cause AML [27], it is clear that the development of AML is a multistep process. A 'two-hit' model of AML development has been proposed where 'Class I' mutations, which activate signal transduction to confer a survival or proliferation advantage, cooperate with 'Class II' mutations, which affect transcription factors to block differentiation [27]. Common Class I mutations include FLT3 and receptor tyrosine kinase c-KIT, while common Class II mutations include NPM1 and transcription factor CCAAT/enhancer-binding protein alpha (CEBPA). Mutations in epigenetic regulators have more recently emerged as a third class of mutations, including tet methylcytosine dioxygenase 2 (TET2) and DNA methyltransferase 3 α (DNMT3α) [2]. Together these different classes of mutation cooperate to facilitate the survival and abnormal clonal proliferation of myeloid progenitor cells, resulting in AML.

1.1.3 Classification of AML subtypes

Classifying subtypes of AML has proved difficult due to its inherent heterogeneity. The older French-American-British (FAB) classification uses cell morphology and cytochemical characteristics to divide AML into 10 subtypes [28] but this did not provide a high reproducibility and prognostic value [29,30]. The more recent World Health Organisation (WHO) classification incorporates the FAB classification, as well as cytogenetic abnormalities, specific gene mutations and distinct subtypes including t-AML, myeloid sarcoma (a solid myeloblast tumour) and myeloid proliferations related to Down syndrome [8] (Table 1-2). The sheer number of subtypes of AML highlights the heterogeneity of this disease and the challenges this creates for treatment.

WHO subtype
AML with recurrent genetic abnormalities
AML with t(8;21)(q22;q22); RUNX1-RUNX1T1
AML with inv(16)(p13.1q22) or t(16;16)(p13.1;q22); CBFB-MYH11
Acute promyelocytic leukaemia with t(15;17)(q22;q12); PML-RARα
AML with t(9;11)(p22;q23); MLLT3-MLL
AML with t(6;9)(p23;q34); DEK-NUP214
AML with inv(3)(q21q26.2) or t(3;3)(q21;q26.2); RPN1-EVI1
AML (megakaryoblastic) with t(1;22)(p13;q13); RBM15-MKL1
AML with mutated NPM1
AML with mutated CEBPA
AML with myelodysplasia-related changes
Therapy-related myeloid neoplasms
Acute myeloid leukaemia, not otherwise specified (NOS)
AML with minimal differentiation (FAB M0)
AML without maturation (FAB M1)
AML with maturation (FAB M2)
Acute myelomonocytic leukaemia (FAB M4)
Acute monoblastic and monocytic leukaemia (FAB M5)
Acute erythroid leukaemia (FAB M6)
Acute megakaryoblastic leukaemia (FAB M7)
Acute basophilic leukaemia
Acute panmyelosis with myelofibrosis
Myeloid sarcoma
Myeloid proliferations related to Down syndrome
Blastic plasmacytoid dendritic cell neoplasm

Table 1-2: The WHO Classification of AML

Outlined in the WHO Classification of tumours of haematopoietic and lymphoid tissues (4th Edition, 2008) [8].

1.1.4 Models for studying AML

1.1.4.1 Cell lines

AML cells of both human and mouse origin are readily culture-adaptable, with more than 200 such cell lines currently described [31]. These cell lines vary in the mutations present, the disease subtype they are derived from and their previous exposure to chemotherapy, allowing these various parameters to be studied *in vitro*. The cell lines used in this thesis are outlined in Table *2-1* and Table 3-1.

1.1.4.2 Mouse models

Many of these cell lines readily engraft in mice. Established *in vivo* models include mouse AML cell lines injected into genetically matched immune-competent hosts (syngeneic) [32], and human AML cells injected in to immune-compromised mice (xenograft) [33], with many disease features, such as bone marrow involvement, recapitulating human disease when the cells are injected intravenously (further discussed in Sections 4.1.2 and 4.3.3). Some fresh/non-culture-adapted AML patient samples can also be successfully engrafted in immune-compromised mice generating a patient-derived xenograft (PDX) model. While these can be difficult to establish, advances in immunodeficient mouse strains has improved the success of these models [34]. Both syngeneic and cell line xenograft mouse models are used in this thesis and are described in Section 4.1.2.

1.1.5 Current treatment and treatment challenges

The standard treatment for the majority of AML subtypes has changed little in the last few decades, relying heavily on standard chemotherapeutics and hematopoietic stem cell transplantation (HSCT). Treatment of AML usually begins with aggressive induction chemotherapy, the goal of which is to achieve remission, often in a standard 7+3 combination; 7 days of cytarabine therapy combined with 3 days of anthracycline therapy [35,36]. Cytarabine (cytosine arabinoside) is an antimetabolite that incorporates into newly synthesised DNA and inhibits further DNA synthesis, and is thus particularly effective against rapidly diving cells including leukaemia [37], but also affects non-cancerous dividing cells, such as intestinal cells [38] and embryonic cells [39]. Anthracyclines, such as daunorubicin, are mainly thought to mediate anti-cancer

effects through intercalating with DNA [40]. Bone marrow biopsies are performed 14-21 days post-therapy initiation to measure the efficacy of the induction therapy, after which induction treatment is repeated, if required, or post-remission chemotherapy, HSCT or registration in a clinical trial are undertaken depending on patient age, cytogenetics, co-morbidities and other factors [41,42]. These standard therapeutic regimes with cytotoxic therapeutic agents achieve approximately a 20% 5-year survival rate overall [43], which reduces to 5-10% in older patients, who account for the majority of diagnoses and have a high therapy-associated mortality and increased risk of unfavourable cytogenetics [44,45]. As these therapies are non-specific for cancer cells there are significant side-effects associated with their use. Myelotoxicity/bone marrow suppression is a common and sometimes life-threatening side effect of standard AML chemotherapy, resulting in conditions such as neutropenia, thrombocytopenia, bacteraemia, pneumonia and sepsis [46,47]. Heart failure is also a common complication of anthracycline treatment, occurring in approximately 20% of patients due to anthracycline-induced cardiotoxicity, sometimes decades after the treatment [48]. HSCT is often the most effective method of achieving remission and preventing AML recurrence [49], but has a high risk of treatment-associated morbidity and mortality, particularly in older patients due to increased levels of pre-existing comorbidities, requiring serious risk-benefit analysis and adjustment of the intensity of the therapy [50-52].

In contrast to other AML subtypes, there have been dramatic improvements in the treatment of APL in the last few decades, particularly through targeting of the PML-RARα fusion protein that is characteristic of this subtype. The introduction of differentiation therapy all-trans retinoic acid (ATRA), which binds the fusion PML-RARα protein leading to its degradation, in combination with standard chemotherapies such as cytarabine significantly improved outcomes for APL patients, with complete remission of greater than 90% and cure rate exceeding 80% in some cases [53-56]. Long-term remission was further improved with the introduction of arsenic trioxide (ATO), which also binds the fusion protein, and may be used in combination with ATRA [57,58]. While ATRA and ATO therapy have mild, reversible side effects [59], the side effects of conventional chemotherapies used in combination with them, as outlined previously, are often severe and can be life-threatening.

Despite current efforts to develop more targeted therapies for AML, such as therapies targeting FLT3-ITD mutated AML [60], the treatment landscape of AML is predominated by cytarabine in combination with anthracyclines. The lack of effective therapies and often severe treatment-related side effects for this aggressive malignancy makes it an ideal focus for new therapy development, however attempting to treat such a heterogeneous disease presents a significant challenge. A promising approach is to target the oncogenic processes in cancer cells that are common between many different cancer types and subtypes, with the aim of improving efficacy and reducing the development of drug resistance.

1.2 Targeting ribosome biogenesis in cancer

1.2.1 The nucleolus and ribosome biogenesis

Ribosome biogenesis, or the synthesis of ribosomes, is a highly conserved, complex process that occurs within a sub-nuclear, non-membrane bound structure known as the nucleolus [61]. Ribosomes are encoded by hundreds of copies of the ribosomal DNA (rDNA) gene in head-to-tail tandem repeats in nucleolar organiser regions (NORs), which cluster on the short arms of five human acrocentric chromosomes (13, 14, 15, 21, 22) [62]. In eukaryotes, the repeating units consists of the rDNA gene encoding the 18S, 5.8S and 28S ribosomal RNA (rRNA), separated by internal intergenic spacers (ITS) and flanked by a 5' and 3' external transcribed spacer (ETS) [63,64] and these rDNA genes are transcribed exclusively by RNA polymerase I (Pol I) . At the core region (Core) and upstream control element (UCE) of the rDNA promoter, transcription requires the formation of a pre-initiation complex (PIC), the main components of which include Pol I, human selectivity factor 1 (SL-1) complex, upstream binding factor (UBF), Pol-I-associated factor RRN3 and topoisomerase II α (TopIIα) [65] (Figure 1-1). SL-1, which is a complex of the TATA-box-binding protein (TBP) and multiple TBP-associated factors (TAFs) [66], plays a crucial role in recruiting Pol I through its interaction with RRN3 [67] and TopIIα [68]. Regulation of rDNA transcription by Pol I is dynamic, with cell cycle cues and growth factors able to modulate the rate of rRNA transcription [69]. Transcription of the rDNA gene generates a single polycistronic 47S transcript, which is processed into the mature 18S, 5.8S and 28S rRNAs [70]. Functional ribosomes also require 5S RNA,

transcribed by RNA polymerase III (Pol III) in the nucleus [71], and various ribosomal proteins (RPs), transcribed by RNA polymerase II (Pol II) also in the nucleus and translated in the cytoplasm [72], which are imported into the nucleolus. Together these elements are assembled into pre-40S and pre-60S ribosomal subunits, which are then exported to the cytoplasm to form mature 80S ribosomes, which can then translate mRNA into protein [73].

1.2.2 Elevated ribosome biogenesis in cancer

Elevated growth and proliferation of cells is accompanied by an increased abundance of ribosomes to support the high protein translation requirement of the cells during this time [74,75]. Elevated transcription of the rDNA by Pol I and subsequent increases in ribosome biogenesis are features common to many human cancers, as enhanced translational capacity is required to facilitate the proliferation of cancerous cells [76]. Indeed, changes in the morphology and number of nucleoli has long been recognised as a feature of cancerous cells and is used as a diagnostic tool by pathologists as a marker of aggressive disease [77]. Elevated ribosome biogenesis has also been observed in the premalignant state. For example, in a mouse lymphoma model, pre-malignancy is accompanied by increases in Pol I transcription, including increased total RNA per cell, 18S and 28S RNA, pre-RNA and expression of Pol I transcription factors [78], highlighting the role of increased ribosome biogenesis in malignant transformation and progression.

1.2.3 Targeting ribosome biogenesis with the novel Pol I inhibitor CX-5461

The relationship between rDNA transcription rate and cellular proliferation makes rDNA transcription an attractive target for broad-spectrum cancer therapies. Indeed, some standard cancer chemotherapies have been shown to significantly perturb various stages of ribosome biogenesis including rRNA transcription (e.g. doxorubicin, oxaliplatin), early rRNA processing (e.g. camptothecin, flavopiridol) and late rRNA processing (e.g. 5-fluorouracil), which might contribute to their anti-cancer properties [79]. However, a more targeted approach to ribosome biogenesis inhibition is likely to prove even more efficacious against cancer cells.
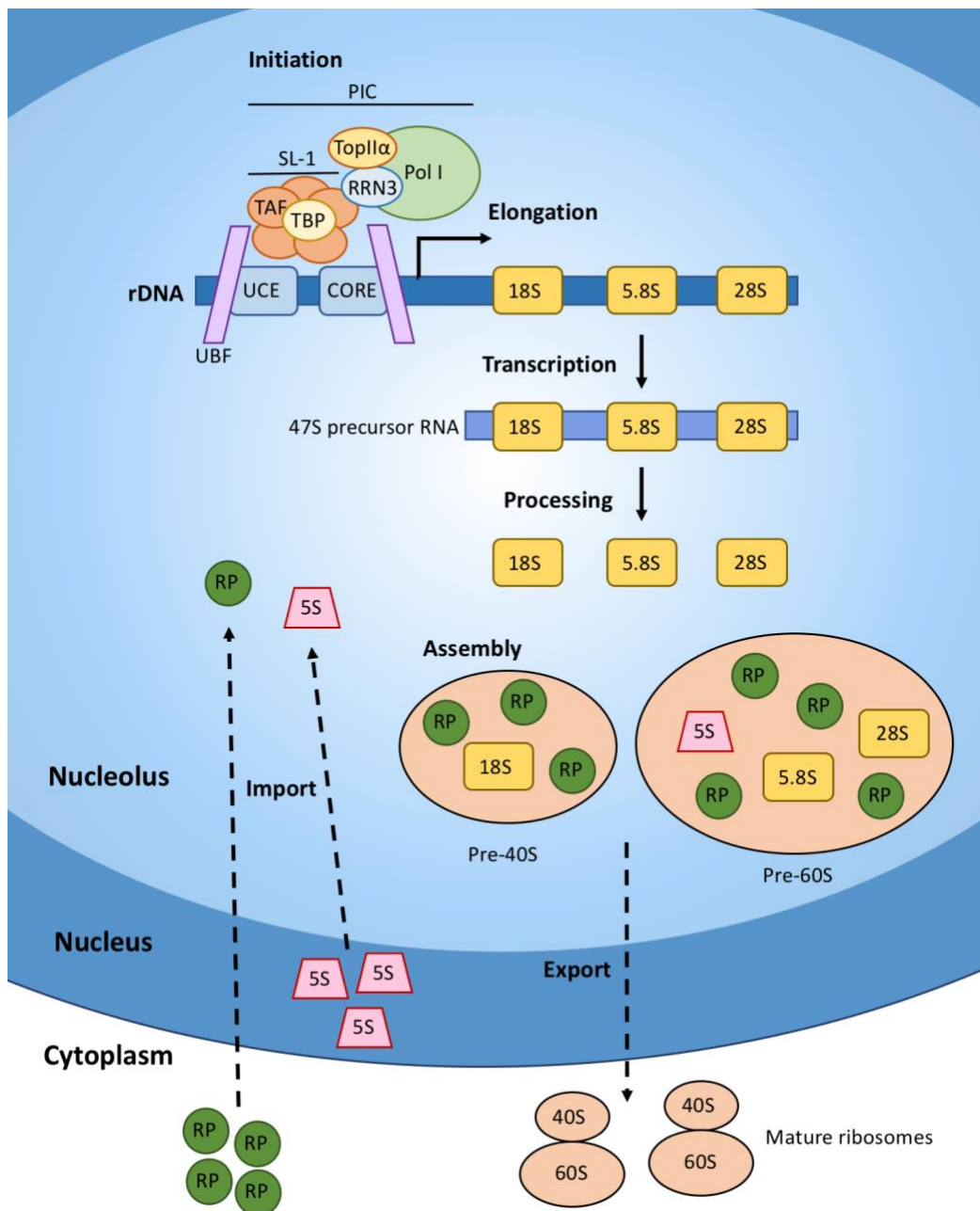
Figure 1-1: Schematic representation of ribosome biogenesis

Transcription of the ribosomal DNA (rDNA) gene occurs within the nucleolus. Transcription initiation requires the formation of a pre-initiation complex (PIC) at the core and upstream control elements (UCE) of the rDNA promoter. The PIC consists of upstream binding factor (UBF), the SL-1 complex (comprised of TATA-box-binding protein (TBP) and five TATA-box-associated factors (TAFs)), RNA polymerase I (Pol I) and RRN3. The 47S rDNA repeats are then transcribed by Pol I, producing a 47S precursor RNA, which is processed into 18S, 5.8S and 28S RNA. Ribosomal proteins (RP) and 5S RNA are imported into the nucleolus, where pre-40S and pre-60S subunits are then assembled from the rRNA and RPs, and exported to the cytoplasm to produce mature ribosomes.

In eukaryotes, gene transcription is performed by three different RNA polymerases: Pol I (which transcribes the rDNA gene), Pol II (which transcribes messenger RNA (mRNA), micro RNA (miRNA), small nuclear RNA (snRNA), and small nucleolar RNA (snoRNA) genes) and Pol III (which transcribes transfer RNA (tRNA) and 5S rRNA genes).[80] As the only polymerase exclusively involved in the transcription of the rDNA, Pol I is an ideal target for inhibition of rDNA transcription without affecting global transcription.

Identified in a screen for inhibitors of rRNA synthesis, the novel drug CX-5461 selectively targets rDNA transcription by disrupting the interaction of SL-1 with the rDNA, preventing the recruitment of Pol I [81] (Figure 1-2). Importantly, CX-5461 is highly selective for Pol I, showing a 200-fold specificity for Pol I over Pol II, thus has limited effects on global transcription [81]. CX-5461 inhibits rDNA transcription initiation in both non-malignant and malignant cells to a similar extent, however, non-malignant cells are approximately 30 times less sensitive to CX-5461 in terms of viability, highlighting the addiction of malignant cells to rDNA transcription and the therapeutic window this creates [81]. CX-5461 has shown significant efficacy in various solid and haematological malignancies *in vivo*, for example, mediates p53-dependent apoptosis and prolonged survival in animal models of B-cell lymphoma and acute myeloid leukaemia [78].

A Phase I dose-escalation study of CX-5461 in patients with haematological cancers, conducted at the Peter MacCallum Cancer Centre in Melbourne, revealed that administration of CX-5461 intravenously once every 3 weeks resulted in rapid, on-target inhibition of rDNA transcription in peripheral blood mononuclear cells (PBMCs) and cancer cells, and a prolonged partial response was achieved in one patient with anaplastic large cell lymphoma [82]. In this study, the maximum tolerated dose was found to be 170 mg/m^2, with a dose-limiting toxicity of palmar-plantar erythrodysesthesia, and manageable incidences of photosensitivity in 50% of patients, irrespective of dose. CX-5461 has also shown significant efficacy in solid tumour preclinical models including osteosarcoma [83], ovarian cancer [84] and breast cancer [81] leading to the commencement of a Phase I/II clinical trial of CX-5461 in solid tumours in Canada (ClinicalTrials.gov Identifier: NCT02719977), with results so far indicating CX-5461 is tolerable and has activity in patients [85].
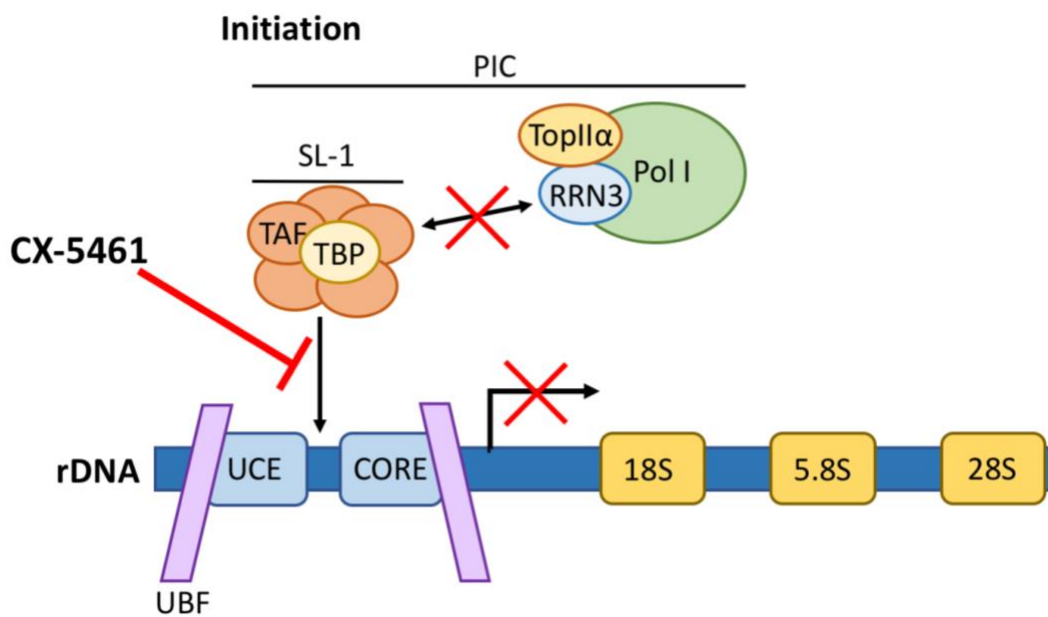
Figure 1-2: Mechanism of action of the novel Pol I inhibitor CX-5461

Novel cancer therapeutic CX-5461 inhibits ribosome biogenesis at the stage of rDNA transcription initiation by interfering with SL-1/rDNA binding, preventing the recruitment of Pol I to the pre-initiation complex (PIC).

Despite the remarkable potential of CX-5461 in animal models of malignancy, eventually the mice succumb to the disease. For example, in the aggressive syngeneic MLL/ENL (t[11;19][q23;p13.3]) p53 null mouse model, treatment with CX-5461 significantly improved survival compared to the vehicle-treated mice, increasing the median survival from 11 days to 24 days post-transplant, however, the CX-5461-treated mice still eventually succumb to disease [1] (Figure 1-3). This indicates that CX-5461 as a single agent is not sufficient to completely halt cancer progression in this model. Thus, CX-5461 is likely to be more effective and have broader applications in cancer therapy if it is used in combination with other anti-cancer molecules, presumably that impact on different or complementary mechanisms of action to reduce cancer cell growth or induce cell death.
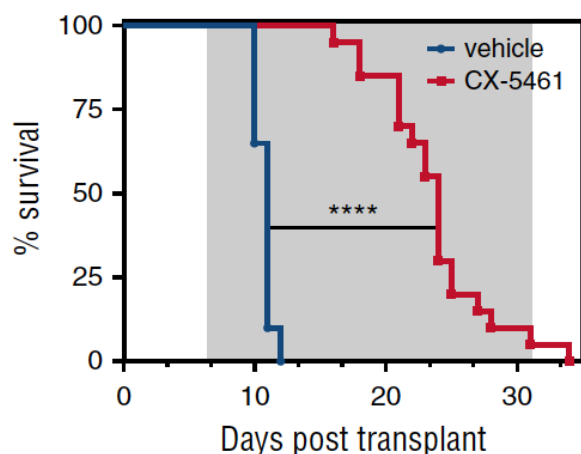
Figure 1-3: CX-5461 significantly improves the survival of AML-bearing mice, however they eventually succumb to disease

Figure 3B from Hein et al [1]. Mice were injected with mouse-derived MLL/ENL p53 null AML cells intravenously in the tail vein. Engraftment was confirmed through bioluminescent imaging (described in Section 2.6). At 7 days post-transplant treatment was commenced with either CX-5461 (35mg/kg every 3 days) or vehicle (NaH_2PO_4). Treatment continued until the mice reached an ethical endpoint and the survival time was calculated. Grey shading indicates the treatment period. ****P < 0001. N=20 mice/group.

1.3 Targeting cancer cell metabolism

1.3.1 Metabolic rewiring in cancer

Deregulated cellular energetics has formally been recognised as a hallmark of cancer since 2011, and thus is considered an important target for cancer therapies [86]. Rapidly proliferating cells, including cancer cells, require maintenance of a higher metabolic rate in order to produce energy in the form of adenosine triphosphate (ATP), macromolecules to facilitate their growth and to maintain redox balance [87]. There are many metabolic pathways that are dysregulated in cancer cells that could be potential targets for combination therapy (Figure 1-4).

Figure 1-4: Metabolic pathways altered in cancer

Various metabolic pathways are altered in cancer to facilitate the abnormal growth and proliferation of the cells, including glucose transport, glycolysis, nucleotide synthesis, fatty acid synthesis, cholesterol synthesis, autophagy, glutaminolysis and the electron transport chain (ETC). Alterations in these pathways provide the cancer cells with increased capacity for bioenergetics, biosynthesis and redox balance, conferring a survival and proliferation advantage over non-cancerous cells. FASN = fatty acid synthase, G6P= glucose 6-phosphate, GLS = glutaminase, GLUT = glucose transporter, HMG-CoA = 3-hydroxy-3-methyl-glutaryl-coenzyme A, NAPDH = reduced nicotinamide adenine dinucleotide phosphate, PDH = pyruvate dehydrogenase, PDK = pyruvate dehydrogenase kinase, PPAR = peroxisome proliferator-activated receptors, SLC1A5 = solute carrier family 1 member 5, TCA = tricarboxylic acid cycle.

Aerobic glycolysis (Warburg effect), the preference of some cells to metabolise pyruvate to lactic acid, even in the presence of oxygen, was a phenomenon first described by Otto Warburg almost 100 years ago [88,89], and has since been recognised as a feature of cancer [90]. Glycolysis is a relatively inefficient means of generating ATP per unit of glucose when compared to mitochondrial respiration, however, metabolism through this pathway is thought to benefit cancer cells by providing them with more rapid ATP generation and increased macromolecule synthesis capacity [91]. Targeting this pathway shifts the metabolism of pyruvate to mitochondrial oxidative phosphorylation which can reduce the growth of tumour cells that are dependent on glycolysis, while leaving normal cells unaffected [92]. Mitochondrial metabolism is also an important process in tumour development. Functional mitochondria are present in many cancers, with the upregulation of one or more mitochondrial pathways providing the additional energy and macromolecules necessary for cancer cell growth and proliferation [93]. Non-glucose metabolism also has an important role in tumours, including fatty acid [94,95] and glutamine metabolism [96,97] which are altered in haematological malignancies. Increased synthesis of cellular building blocks including nucleotides [98] and cholesterol [99,100], further fuels cell growth, including that of cancer cells. Autophagy, a process of intracellular recycling, provides the cells, including cancer cells, with nutrients in times of stress [101] and reduces oxidative stress by degrading dysfunctional organelles [102]. Targeting these metabolic pathways could improve the efficacy of CX-5461, as well as reduce acquired resistance to this drug.

1.3.1.1 Metabolic rewiring in AML

Metabolic rewiring has also been found to play a role in AML development and progression. Isocitrate dehydrogenase (IDH) mutations, commonly found in AML (Table 1-1), lead to the abnormal production of oncometabolite 2-hydroxyglutarate (HG), resulting in inhibition of cytochrome c oxidase (COX) activity in the mitochondrial electron transport chain (ETC) [103] and making cells more dependent on glutamine for survival [104]. Indeed, glutamine dependency is a feature of AML cells with various genetic mutations, as knocking out solute carrier family 1 member 5 (Slc1a5), which transports neutral amino acids such as glutamine, has been found to decrease leukaemia initiation and progression in mouse models of AML, while having comparatively mild effects on bone marrow and blood cell development [105].

Mitochondria, which contribute to many core metabolic processes, are also altered in AML, with AML blasts having a higher mitochondrial (mt)DNA copy number and oxygen consumption rate, indicating an increased number of mitochondria and thus functional capacity, in comparison to normal hematopoietic cells [106]. Dependency on glycolysis is another feature common to AML, as targeting glycolysis with inhibitor dichloroacetic acid 'primed' human AML cell lines with various genetic mutations for the cytotoxic effects of ATO treatment [107]. In particular, AML cells with FLT3-ITD mutation, a common mutation (Table 1-1), have a significant increase in aerobic glycolysis compared to normal blood cells, a dependency which can be targeted therapeutically *in vivo* [108]. Cholesterol pathways are also dysregulated in AML, with increased processing of low-density lipoprotein [109] and HMG-CoA reductase activity [110] in AML patient cells compared to normal blood cells, in order meet the increased cholesterol demands of rapidly dividing tumour cells for membrane synthesis. Autophagy, a process of intracellular recycling, has been found to be both upregulated and downregulated in AML cells. A reduced rate of autophagy results in an increase in the number of damaged organelles [111], increasing reactive oxygen species (ROS) levels [112], genome instability [102] and inflammation [113], creating a tumour permissive environment for AML cells [114]. Conversely, increased levels of autophagy can have a cytoprotective role in response to cellular stress, including chemotherapy, and have been shown to play a role in the maintenance of leukemic stem cells [115]. Both fatty acid synthesis and oxidation have been shown to play a key role in AML cell maintenance, including through bone marrow adipocytes providing AML cells with fatty acids which promote AML cell survival [116].

1.3.2 Metabolic changes accompanying drug insensitivity

Given the role metabolic pathways play in supporting cancer cell growth, stress responses and survival it is unsurprising that many have also been linked to both intrinsic and acquired insensitivity to chemotherapy.

Chemotherapy-resistant prostate cancer cells have an increased expression of HMG-CoA reductase (HMGCR), a critical enzyme in cholesterol synthesis, and knocking down or inhibiting the function of this enzyme with simvastatin re-sensitised the cells to

chemotherapy [99]. In glioma cells resistant to standard chemotherapy temozolomide, upregulation of autophagy was found to be associated with poor prognosis in patients and chemoresistance, and genetic or chemical inhibition of autophagy re-sensitised the cells to temozolomide [117].

Metabolic changes have also been implicated in chemotherapy-resistance in AML. In cytarabine-resistant cells from patient-derived xenograft mouse models, a high oxidative phosphorylation (OXPHOS) phenotype was observed including increased expression of genes involved in lipid metabolism, elevated ROS, and increased mitochondrial mass and activity [118]. Targeting mitochondrial function re-sensitised the cells to the effects of cytarabine, indicating mitochondrial activity is playing an important role in AML cell resistance to cytarabine. Statins, which target cholesterol synthesis, are toxic to both AML cell lines and patient samples through preventing protective cholesterol responses to chemotherapeutics cytarabine and daunorubicin [100].

Together these findings highlight the important role metabolism plays in the response of cancer cells to chemotherapy and in acquired resistance, making targeting cancer metabolism an ideal angle for combination therapy, such as with ribosome biogenesis inhibition.

1.4 Combination therapy rationale

Targeting metabolism in combination with CX-5461 is a logical approach as ribosome biogenesis is intimately linked to energy production and thus metabolism. Indeed, the process of ribosome biogenesis can account for up to 80% of energy consumption in a rapidly dividing cell [74]. In return, increased numbers of ribosomes provide more proteins in the cell which are involved in signalling and are building blocks in metabolism. As outlined in Section 1.3.2, adaptive metabolic responses play an important role in drug resistance, and targeting these pathways re-sensitises cancer cells to chemotherapy. Interestingly, RNA sequencing (RNAseq) analysis of mouse leukemic cells performed by our laboratory demonstrated that short-term CX-5461 treatment induced multiple changes in metabolic gene expression including

upregulation of transcription of enzymes involved in fatty acid and cholesterol synthesis (Figure 1-5, Hein & Blackburn, unpublished), which confirms that ribosome biogenesis and metabolism are intimately linked and provides a clue as to how these cells might be overcoming their sensitivity to CX-5461. Thus, targeting these two aspects of cancer cells is a promising approach to improve efficacy.
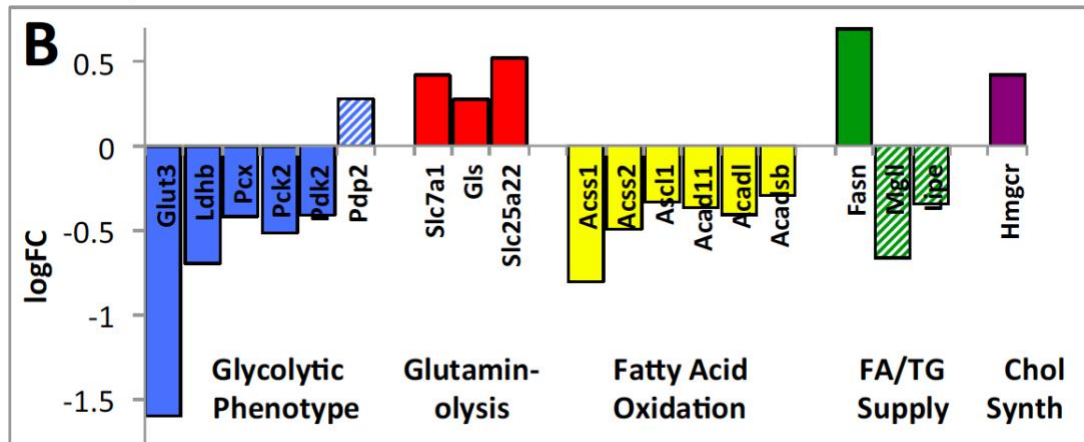
Figure 1-5: Changes in mRNA levels of metabolic genes in MLL/ENL NRAS AML cells after 10 hours of CX- 5461 treatment *in vivo*

Fold change compared to untreated cells. False discovery rate (FDR) < 0.1. Hatched columns contribute to the pathway in the opposite direction to others in the same pathway. Hein & Blackburn, unpublished. Chol synth = cholesterol synthesis, FA = fatty acid, FC = fold change, TG = triglyceride.

1.5 Hypothesis

Combining the novel Pol I inhibitor CX-5461 with metabolism-modifying drugs will improve efficacy in acute myeloid leukaemia.

To examine this hypothesis the following aims were addressed.

1.6 Aims

1. **Identify established metabolism-modifying therapies that work synergistically with CX-5461 to target AML *in vitro* (Chapter 3)**

A panel of human and mouse AML cells lines will be used to identify established metabolism-modifying drugs that enhance the effects of CX-5461 to reduce AML cell number *in vitro.*

2. **Test promising combination therapies in *in vivo* syngeneic and xenograft models of AML (Chapter 4).**

Metabolism-modifying drugs that are found to act synergistically with CX-5461 to reduce AML cell number *in vitro* (Chapter 3) will be tested for their efficacy in improving survival *in vivo* in transplant models of AML.

3. **Investigate the mechanism/s of synergy for promising drug combinations (Chapter 5).**

Promising drug combinations will be identified based on the studies in Chapters 3 and 4. Given the published effects of the drugs as individual agents, mechanistic analysis will be performed to determine how the drugs act synergistically together.

Chapter 2   Methods

2.1 Cell lines and tissue culture

Human cell lines MV4-11 (ACC 102), THP-1 (ACC 16), MOLM-13 (ACC 554), KG-1 (ACC 14), NB-4 (ACC 207) and SKM-1 (ACC 547) were purchased from the German Collection of Microorganisms and Cell Cultures (DSMZ; Braunschweig, Germany). Mouse MLL/AF9 NRAS cells were generated by others using fetal liver transduction to introduce the MLL/AF9 fusion protein with green fluorescent protein (GFP) tag and Nras^{G12D} mutation with luciferase tag [32]. Cells were maintained in RPMI-1640 media (Gibco, via ThermoFisher Scientific, Cat no. 11875093) supplemented with 20% heat-inactivated fetal bovine serum (HI-FBS, Sigma-Aldrich, Cat no. F9423-500mL) and GlutaMAX (Gibco, Cat no. 35050061) at 37°C in 5% (human cells) or 10% CO_2 (mouse cells). Cell lines were certified to be free of mycoplasma contamination through polymerase chain reaction (PCR) testing. Cells were sub-cultured every 3-4 days, at a 1 in 2 (human) or 1 in 3-4 (mouse) split, by adding the existing cell mixture to fresh media. When media removal was required, cells were centrifuged at 450 x g for 5 minutes, unless specified otherwise.

Cell line name	Origin	Culture conditions	Doubling time (approximate hours [h])
MV4-11	DSMZ: ACC 102	RPMI 1640 + 20% HI-FBS + Glutamax, 37°C with 5% CO_2	50
THP-1	DSMZ: ACC 16	RPMI 1640 + 20% HI-FBS + Glutamax, 37°C with 5% CO_2	72
MOLM-13	DSMZ: ACC 544	RPMI 1640 + 20% HI-FBS + Glutamax, 37°C with 5% CO_2	50
KG-1	DSMZ: ACC 14	RPMI 1640 + 20% HI-FBS + Glutamax, 37°C with 5% CO_2	38
SKM-1	DSMZ: ACC 547	RPMI 1640 + 20% HI-FBS + Glutamax, 37°C with 5% CO_2	48
MLL/AF9 NRAS	[32]	RPMI 1640 + 20% HI-FBS + Glutamax, 37°C with 10% CO_2	24

Table 2-1: Cell line origin and growth conditions

*Doubling times based on DSMZ information and personal observation. See Table 3-1 for genetic information.

2.2 Buffers

Buffer	Composition
Western solubilisation buffer	0.5mM EDTA, 20mM HEPES, 2% (w/v) SDS pH 7.9
Western sample loading buffer (6X)	2% (w/v) SDS, 0.4M tris-HCl pH 6.8, 48% (v/v) glycerol, 58mM 2-mercaptoethanol, 0.25% (w/v) bromophenol blue
SDS-PAGE buffer	25mM tris, 190mM glycine, 0.1% (w/v) SDS
Semidry transfer buffer (Bjerrum Schafer-Nielson Buffer with SDS)	48mM tris, 39mM glycine, 0.00375% (w/v) SDS, 20% (v/v) methanol
Tris-buffered saline (TBS)	50mM tris, 150mM NaCl
Tris-buffered saline with tween (TBST)	0.1% (v/v) tween-20 in TBS
Skim milk blocking buffer (SMBB)	5% (w/v) skim milk in TBST
Bovine serum albumin (BSA) blocking buffer (BSABB)	1% (w/v) BSA in TBST
Flow cytometry staining buffer (FCSB)	2% FBS and 0.5% Tween-20 in PBS
Red cell lysis buffer	144mM NH_4Cl, 17mM tris-HCl pH 7.65

Table 2-2: Buffer composition

EDTA = ethylenediaminetetraacetic acid, FBS = fetal bovine serum, HEPES = 4-(2-hydroxyethyl)-1 piperazineethanesulfonic acid, SDS = Sodium dodecyl sulphate, HCl = hydrochloric acid, SDS-PAGE = sodium dodecyl sulphate polyacrylamide gel electrophoresis, NaCl = sodium chloride, PBS = phosphate-buffered saline, NH_4Cl = ammonium chloride.

2.3 Antibodies and dyes

Antibody	Species	Supplier	Assay	Concentration used	Buffer
LC3B	Rabbit	Cell signalling #2775S	WB	1:3000	BSABB
P62/Sequestome	Mouse	Abnova #H00008878-M01	WB	1:4000	SMBB
Beclin 1	Rabbit	Cell signalling #3495S	WB	1:1000	SMBB
ATG7	Rabbit	Cell signalling #8558S	WB	1:750-1:1000	SMBB
BrdU (B44 clone)	Mouse	BD Pharmingen #347580	FC	1:50	FCSB
Anti rabbit-HRP	Goat	Bio-Rad #170-6515	WB	1:3000	SMBB or BSABB
Anti mouse-HRP	Goat	Bio-Rad #170-6516	WB	1:3000	SMBB or BSABB
Beta Actin-HRP (C4)	Mouse	Santa Cruz # sc-47778 HRP	WB	1:10 000	SMBB or BSABB
Anti mouse Alexafluor 488	Goat	Invitrogen #A11001	FC	1:500	FCSB
DAPI	N/A	Sigma #10236276001	FC	1µg/mL	FCSB

Table 2-3: Antibodies and dyes

HRP = horseradish peroxidase, WB = western blot, FC = flow cytometry, DAPI = 4',6-diamidino-2-phenylindole, SMBB = skim milk blocking buffer, BSABB = bovine serum albumin (BSA) blocking buffer. See Table *2-2* for buffer composition.

2.4 Chemicals and drugs

MTT (Thiazolyl blue tetrazolium bromide, Sigma, Cat no. M2128) was dissolved in PBS to make a 5mg/mL solution, filter sterilised, aliquoted and stored at -20°C.

Neutral red (Sigma, Cat no. N4638) was dissolved in ddH$_2$O at 3.3mg/mL, filter sterilised and stored at 4°C for up to 2 months.

Luciferin (Xenolight D-luciferin K+ Salt, Perkin Elmer, Cat no. 122799) was dissolved in PBS to make a 5mg/mL solution, filter sterilised, aliquoted and stored at -20°C in the dark.

BrdU (5-bromo-2'-deoxyuridine; Sigma, Cat no. 10280879001) was dissolved in double-distilled water (ddH$_2$O) to make a 10mM solution, filter sterilised, aliquoted and stored at --20°C.

CX-5461: For *in vitro* work, CX-5461 (Cylene) was dissolved in 50mM NaH_2PO_4 pH4.5 to make a 10mM stock solution, aliquoted and stored at -20°C in the dark. For *in vivo* work, CX-5461 solution was prepared fresh from powder before dosing using the same vehicle as *in vitro*.

Orlistat: For *in vitro* work, orlistat (Sigma-Aldrich, Cat no. O4139) was dissolved in dimethyl sulfoxide (DMSO) to make a 15mM stock solution, aliquoted and stored at -20°C. For *in vivo* work, orlistat was extracted from Xenical capsules (Roche), adapted from the methods of Kridel et al [119]. The contents of a Xenical capsule were placed in 250μL absolute ethanol for 20 minutes (min), vortexed every 10 min, then 500μL PEG-400 (BioUltra, Sigma, Cat no. 91893) was added, vortexed and left for 10 min, then vortexed again. The tube was spun at 14 000 x g for 5 min to pellet the filler material, then the resulting supernatant was removed, and stored at -20°C.

Chloroquine: For *in vitro* work, chloroquine diphosphate salt (Sigma, Cat no. C6628) was dissolved in PBS to make a 50mM stock solution, filtered sterilised and stored at 4°C in the dark for up to 3 months. For *in vivo* work, chloroquine solution was prepared using 50mM NaH_2PO_4 pH4.5.

Dichloroacetate (DCA): For *in vitro* work, DCA liquid (Sigma, Cat no. D54702) was diluted in PBS to make a 100mM solution, the pH adjusted to 6.9-7.5, then filter sterilised and stored at 4°C. For *in vivo* work, DCA solution was prepared in 50mM NaH_2PO_4 pH4.5.

Ritonavir: For *in vitro* work, ritonavir powder (Sigma, Cat no. SML0491) was dissolved in DMSO to make a 15mM stock solution, aliquoted and stored at -20°C. For *in vivo* work, ritonavir powder (Selleckchem, Cat no. S1185) was dissolved in 7.5% ethanol in PBS and used immediately.

Omeprazole: For *in vitro* work, omeprazole powder (Sigma, Cat no. O104) was dissolved in DMSO to make a 150mM stock solution, aliquoted and stored at -20°C in the dark. For *in vivo* work, omeprazole powder (Selleckchem, Cat no. S1389) was dissolved in 7.5% ethanol in PBS and used immediately.

Metformin: Metformin/1,1-dimethylbiguanide hydrochloride powder (Sigma, Cat no. D150959) was dissolved in PBS to make a 50mM stock solution, then filter sterilised and stored at 4°C.

Simvastatin: Simvastatin powder (Sigma, Cat no. S6196) was dissolved in DMSO to make a 10mM solution, aliquoted and stored at -20°C.

Fenofibrate: Fenofibrate powder (Sigma, Cat no. F6020) was dissolved in DMSO to make a 100mM stock solution, aliquoted and stored at -20°C.

Bezafibrate: Bezafibrate powder (Sigma, Cat no. B7273) was dissolved in DMSO to make a 100mM stock solution, aliquoted and stored at -20°C.

Rosiglitazone: Rosiglitazone powder (Sigma, Cat no. R2408) was dissolved in DMSO to make a 50mM solution, aliquoted and stored at -20°C.

Bafilomycin A1: Bafilomycin A1 powder (Selleckchem, Cat no. S1413) was dissolved in DMSO to make a 150µM solution, aliquoted and stored at -20°C.

2.5 Viability assays and synergy analysis

In Chapter 3, three different methods of measuring total viable cell number were utilised in order to determine if any of the drugs were impacting on the mechanism of action of the viability assay; the neutral red assay, the MTT assay and Coulter counts.

2.5.1 Neutral red

The neutral red assay estimates viable cell number based on the uptake and binding of the neutral red dye in the lysosomes of the cells [120]. Uptake and retention of the dye will only occur if a pH gradient is present in the lysosomes, as the dye then becomes charged when it enters the lysosome and accumulates. Maintenance of active pH gradients through ATP production is a characteristic of a viable cell, therefore, the amount of retained dye is proportional to the number of viable cells. However, if a drug interferes with the accumulation of neutral red without affecting the viability of the cell this assay will not be an accurate measure of cell viability.

2.5.2 MTT

The MTT assay is based on the conversion of the water-soluble MTT tetrazolium salt (3-(4,5-dimethylthiazol-2-yl)-2,5-diphenyl tetrazolium bromide) to coloured formazin crystals via succinate dehydrogenase in the mitochondria [121]. This process requires functional mitochondrial enzymes, which is a characteristic of viable cells. Therefore,

the amount of converted MTT is proportional to the number of viable cells. However, if a drug interferes with normal mitochondrial enzyme function without affecting the overall viability of the cell the MTT assay will not be an accurate measure of cell viability.

2.5.3 Coulter count

A physical particle counting method is a 'gold-standard' measure of cell viability. The Z2 Coulter Counter (Beckman Coulter) counts and determines the size of cells by utilising changes in electrical resistance when a cell suspended in a conductive liquid passes through an aperture. Viable and dead cells can then be distinguished by their size.

2.5.4 Measuring total viable cell number

Cells were seeded in 96-well round-bottom plates at a pre-determined density so that the cells were still in the exponential growth phase at the end of the assay. At the time of plating, drug dilutions (with equal final concentration of vehicle) were added to the plate in quadruplicate wells and the cells cultured for 96 h.

- Coulter count: Following treatment, a 1:100 dilution was made of the cells in Isoflow Sheath Fluid (Beckman Coulter, Cat no. A48466) and counting performed using the Z2 Coulter counter (Beckman Coulter). Gating was performed on events with volume 200fL+.
- MTT: Following treatment 20µL of 2.5mg/mL MTT solution was added to each well and the plates incubated at 37°C for 1-2 h. The media was removed and replaced with DMSO. The resulting solutions were transferred to a flat-bottom 96 well plate and the absorbance read at 570nm using an Epoch Microplate Spectrophotometer (BioTek).
- Neutral red: Following treatment the media was removed and replaced with 200µL /well pre-warmed media containing neutral red (200µL of 3.3mg/mL neutral red stock solution/20mL media) and the plates incubated at 37°C for 3 h. The plates were washed 3 times with PBS then the contents solubilised in 3:1 methanol:acetic acid de-stain solution. The resulting solutions were transferred to a flat-bottom 96 well plate and the absorbance read at 540nm using an Epoch Microplate Spectrophotometer (BioTek).

N=1 for testing suitability of MTT or neutral red as viability assays with the different metabolism-modifying drugs.

2.5.5 GI$_{50}$ and synergy analysis

The cell lines were treated with the drugs as single agents at a range of concentrations in order to determine the dose-response curves for viability. Viability (as a % of the vehicle-treated cells) was calculated as an average of n=3 experiments. The concentration resulting in 50% growth inhibition (GI$_{50}$) values were calculated using sigmoidal dose-response curve analysis in Prism (GraphPad Software, San Diego, USA). A non-linear curve (sigmoidal) was fitted to the data points. Where a sigmoidal dose curve could not be fitted, an estimate only of the GI$_{50}$ was shown.

Synergy analysis of n=3 experiments was performed using the Chou-Talalay Combination Index method [122]. This method is based on the median-effect equation, which incorporates various well-established equations in biochemistry and biophysics, including the Michaelis-Menten model of enzyme kinetics and the Scatchard equation which describes the affinity of a ligand with a binding site. Dose response curves are fitted, or predicted, to the data points of the effects of the single drugs and used to determine if a drug combination effect is synergistic. Non-constant ratio synergy analysis was performed using CompuSyn software (ComboSyn Inc.) using the viability results to determine the 'effect' (as 1 – [%viability/100]) and synergy defined as a combination index of 0.75 or lower, based on recommended guidelines for categorising synergism [123]. Where the viability was 100% the effect was entered as 0.001 as an effect of 0 cannot be entered.

2.6 Tumour models and *in vivo* drug studies

In Chapter 4, metabolism-modifying drugs that were found to act synergistically with CX-5461 *in vitro* (Chapter 3) were tested for their tolerability in non-tumour-bearing mice, followed by efficacy testing (improving survival *in vivo* in transplant models of AML). Animal experimentation was approved by the Animal Experimentation Ethics Committee at ANU (under protocol A2015/12).

2.6.1 Tolerability studies

Tolerability of the drugs as single agents and in combination were tested in non-tumour-bearing mice. 8-12 week old female C57Bl/6 Jax mice (provided by Australian Phenomics Facility, Canberra, Australia), were administered drugs as below in groups of approximately 3/dosing schedule. Dosing of the single agents was performed over a 2-3 week period with daily weighing, followed by a week of monitoring only. In some cases, if the mice were tolerating the drug well (no weight loss) after 1-2 weeks of dosing, an additional cohort of mice was started at a higher drug dose. In cases where the tolerability of the vehicle was unknown, a vehicle only treated group was also tested. Once the MTD or tolerable range of the metabolism drug was established, combination tolerability testing with CX-5461 was commenced. The dosing schedules were as follows:

- Orlistat: 240mg/kg/day orlistat or vehicle (33% ethanol, 67% polyethylene glycol-400 [PEG-400]) by intraperitoneal injection at 15μL/10g mouse body weight using 50μL Hamilton syringes (Hamilton Company, Nevada, United States, Cat no. 20701).

- Chloroquine: 50-400mg/kg/day chloroquine dissolved in PBS, dosed by oral gavage (using 20ga plastic feeding tubes, Instech, Cat no. FTP-20-38) at 100μL/10g body weight.

- CX-5461 and chloroquine: 50-100mg/kg/day chloroquine with 30-35mg/kg CX-5461 dissolved in 50mM NaH$_2$PO$_4$, dosed by oral gavage at 100μL/10g body weight.

- CX-5461 and DCA: 200mg/kg/day DCA with 35mg/kg CX-5461 dissolved in 50mM NaH$_2$PO$_4$, dosed by oral gavage at 100μL/10g body weight.

- Omeprazole: 100-400 mg/kg/day omeprazole dissolved in 7.5% ethanol in PBS, dosed by oral gavage at 100μL/10g body weight.

- Ritonavir: 50-400 mg/kg/day ritonavir dissolved in 7.5% ethanol in PBS, dosed by oral gavage at 100μL/10g body weight.

Weight was monitored daily as a sign of drug toxicity, and the percentage weight change from the initial weight calculated. Mice were euthanised if they lost more than 20% body weight from their initial weight. The maximum tolerated dose was defined

as a maximum weight loss of 10% of initial, from which the mice recovered over the next couple of days.

2.6.2 Efficacy studies

2.6.2.1 Syngeneic model

5×10^5 MLL/AF9 NRAS cells were injected intravenously (tail vein) in 8-10 week old female C57Bl/6 Jax mice (provided by Australian Phenomics Facility, Canberra, Australia). Engraftment was confirmed 7 days post-transplant through the following procedure: intraperitoneal injection of 200μL/mouse 5mg/mL XenoLight D-Luciferin K Salt Substrate (Perkin Elmer) in PBS, 5 min wait, induction of anaesthesia using Isofluorane gas (Cat # ISOF 03, Provet), followed by bioluminescent imaging using an IVIS Spectrum machine (Perkin Elmer) on automatic acquire settings. Living Image software (Perkin Elmer) was used for visualisation and quantification of the bioluminescence. Mice were randomised into groups of 5-8 based on tumour burden and dosing commenced.

2.6.2.2 Human cell line xenograft models

8-12 week old female NOD-scid-gamma (NSG) mice (provided by the Australian Phenomics Facility) were injected intravenously (tail vein) with 2×10^6 human AML cell lines (MV4-11 GFP luc or MOLM-13 GFP luc cells), or irradiated with 1 Gray (Gy) single dose, whole-body irradiation, then injected with cells the next day (THP-1 GFP luc cells). See Section 2.6.3 for generation of the GFP luc human cell lines. Mice were placed on Baytril (Enrofloxacin 25mg/mL oral solution, ProVet, Cat no. BAYT O) in drinking water immediately following irradiation, or for the non-irradiated mice at least 3 days before the first bioluminescent image, and antibiotic treatment continued for the duration of the experiment. Engraftment was confirmed 3-7 days post-transplant through bioluminescent imaging as above, mice randomised into groups of 8 based on tumour burden and dosing commenced. Groups of 3-6 mice were used for characterising the disease model.

2.6.2.3 Dosing schedules

Mice were dosed as follows in groups of 5-8/treatment, at 100μL/10g body weight unless indicated otherwise:

- CX-5461 and orlistat: treatment groups received dosing by oral gavage of CX-5461 vehicle (50mM NaH$_2$PO$_4$ buffer) or CX-5461 at 35mg/kg Monday, Wednesday and Friday, intraperitoneal injection of orlistat vehicle (33% ethanol, 67% PEG-400) at 15μL/10g mouse body weight using 50μL Hamilton syringes (Cat no. 20701) or orlistat solution daily Monday-Friday, or the combination of the two drugs.
- CX-5461 and chloroquine: treatment groups received dosing by oral gavage of either vehicle (50mM NaH$_2$PO$_4$ buffer), CX-5461 at 30mg/kg Monday, Wednesday and Friday, chloroquine at 50-80mg/kg daily Monday-Friday or the combination of the two drugs.
- CX-5461 and DCA: treatment groups received dosing by oral gavage of either vehicle (50mM NaH$_2$PO$_4$ buffer), CX-5461 at 30mg/kg Monday, Wednesday and Friday, DCA at 200mg/kg daily Monday-Friday or the combination of the two drugs.

Ensure (Abbott Nutrition, Cat no. S619.185) was mixed with powder from the food pellet bags and water to form a paste, which was provided daily for the duration of dosing to help the mice maintain weight. Dosing was continued until an ethical endpoint was reached (e.g. hunching, difficulty breathing, reluctance to move, >20% weight loss), at which point the mice were euthanised. The treatment groups were not blinded to the researcher who was determining the ethical endpoint.

2.6.2.4   Weight changes

Weight was monitored 5-7 days/week as an indicator of general health, and the percentage weight change from the initial weight calculated. Mice were euthanised if they lost more than 20% body weight from their initial weight.

2.6.2.5   Survival analysis

Differences in survival times were determined using Kaplan-Meier survival curves in Prism (GraphPad Software), followed by a Log-rank test. The Bonferroni corrected threshold was applied for comparison of multiple survival curves, such that a P value of <0.0083 was considered significant for these analyses.

2.6.2.6 Bioluminescent imaging analysis

Quantification of total bioluminescence was performed using the Living Image software (Perkin Elmer). Rectangular regions of interest (ROI) of the same size was placed over each mouse in the image and the total flux (photons/second) calculated. For image visualisation the colour scale on the images was adjusted until the areas of disease burden could be easily visualised. Images from the same day are all on the same scale, however, images from different days of the same experiment are on different scales due to the differences in disease burden.

2.6.2.7 Spleen weight

When the mice reached an ethical endpoint, the mice were euthanised and the spleen was removed and weighed.

2.6.2.8 Full blood counts

When the mice reached an ethical endpoint, blood was collected through terminal cardiac puncture under anaesthesia with isofluorane and transferred to a tube containing 0.5M EDTA. Samples were diluted 1:4 in 2% fetal bovine serum in PBS and full blood count (FBC) analysis run on the ADVIA hematology system (Siemans) for FBC + differential.

2.6.3 Generation of GFP-luc tagged human AML cell lines

Green fluorescent protein (GFP)-luciferase (luc) tagged human AML cell lines were generated to inject into mice for the drug efficacy studies, as outlined in Section 2.6.2.2. Retroviral gene delivery was performed using MSCV-GFP-luc2 constructs (a gift from Ricky Johnstone at the Peter MacCallum Cancer Centre in Melbourne). This construct was transfected into 293T cells using polyethylenimine (PEI) transfection, and the resulting retroviral particles collected and concentrated using the Retro-X concentrator (Clontech, Cat no. 631455) according to the manufacturer's instructions. The concentrated retrovirus was then used to transduce the MV4-11, THP-1 and MOLM-13 human AML cell lines through retroviral spin infection with retronectin-coated plates (Takara Cat no T202), according to the manufacturer's instruction. Transduced cells were identified by GFP positivity and cell sorted using flow cytometry. The resulting cell lines were named '(cell line) GFP luc'. Luciferase activity was

confirmed *in vitro*, and *in vitro* sensitivity to CX-5461 was compared between the parental and tagged cell lines. The tagged cells were all found to express luciferase and to have the same sensitivity to CX-5461 as the parental lines (results not shown).

2.7 Cell cycle and cell death analysis by flow cytometry

In Chapter 5, flow cytometry was used to perform cell cycle and cell death analysis. Cells were seeded in 96-well round-bottom plates at a pre-determined density so that the cells were still in the exponential growth phase at the end of the assay. Drugs were added at the indicated timepoints. 30 min before harvesting BrdU was added to a final concentration of 10μM. Cells were washed once with PBS then fixed in 150μL/well 80% ethanol for at least 3 h at 4°C. The ethanol was removed and DNA was denatured for 30 min by adding 100μL/well 2N HCl with 0.5% (v/v) Triton X-100, then neutralised with 100μL/well 0.1M $Na_2B_4O_7.10H_2O$ (pH 8.5). Cells were stained with 20μL of 1:50 anti-BrdU antibody in PBS containing 2% FBS and 0.5% Tween-20 at room temperature for 30 min, washed once with PBS containing 2% FBS, then stained with 20μL 1:500 Alexa Fluor 488 secondary antibody in PBS containing 2% FBS and 0.5% Tween-20 at room temperature in the dark for 30 min and washed once with PBS containing 2% FBS. Samples were resuspended in PBS containing 2% FBS and 1μg/mL DAPI (Table *2-3*), incubated for 15 min in the dark at room temperature and analysed using an LSR-II flow cytometer (BD) or iQue Screener PLUS (Intellicyt). The gating strategy is shown in Figure *2-1*. Results are presented as the percent of cells in each cell cycle phase. N=3 experiments were performed and the mean results shown.
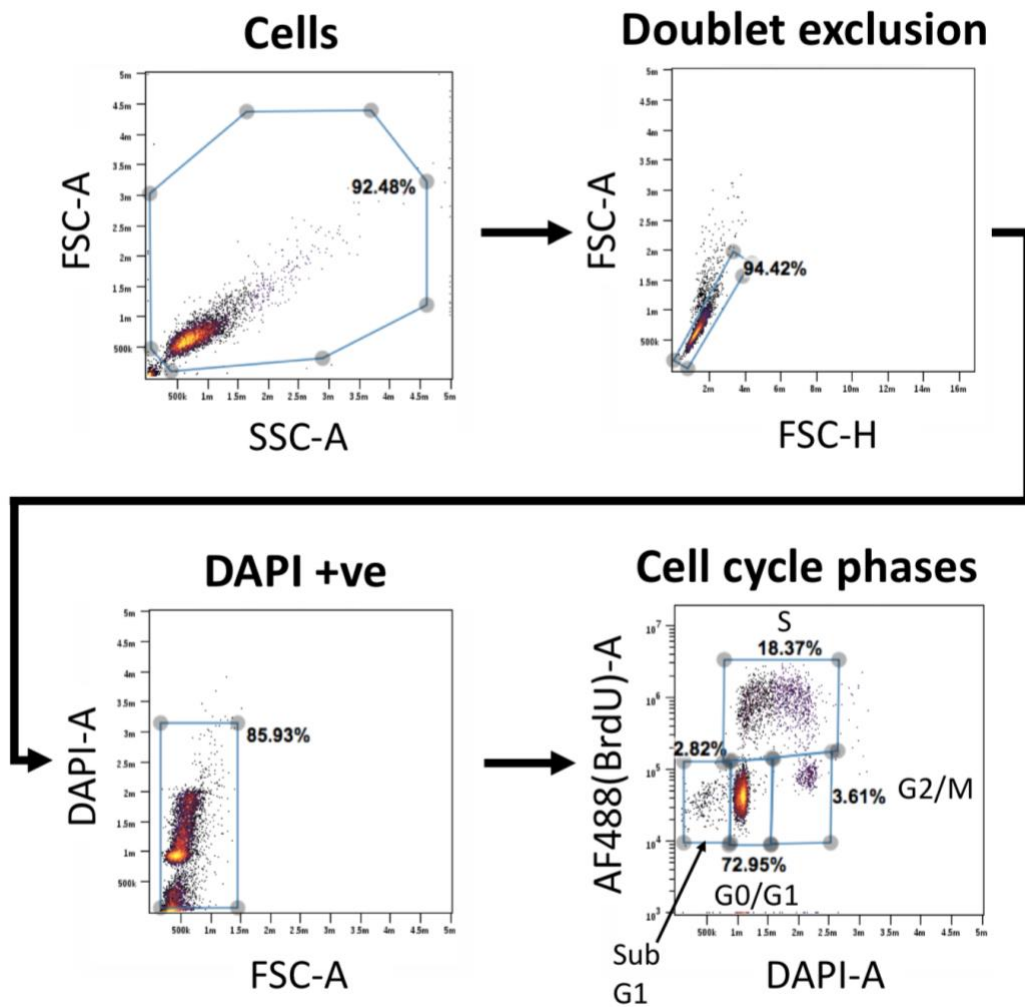
Figure 2-1: Gating strategy used for cell cycle analysis

First, cells were gated based on their forward scatter (FSC, size) and side scatter (SSC; granularity) area (A) parameters. Next, doublets were excluded based on FSC-A versus FSC-height (H). Cells that were stained DAPI positive (+ve), indicating DNA content, were then selected, then the different cell cycle phases were gated based on Alexa Fluor (AF) 488 positivity, as a marker of BrdU incorporation/DNA synthesis, and DAPI, as a marker of DNA content. Cells with sub G1 DNA content (DAPI fluorescence) were considered "dead" cells (including dying/apoptotic cells [124]).

2.8 Western blot

In Chapter 5, western blotting was used to analyse the expression levels of autophagy-related proteins.

1×10^6 cells were treated with the indicated conditions overnight. Cells were then harvested and lysed in western solubilisation buffer (Table *2-2*). Protein lysates were

quantified using the DC protein assay (Bio-Rad, Cat no. 5000111) according to the manufacturer's instructions, then equal protein amounts of protein were separated by SDS-PAGE, transferred to Immobilon-P polyvinylidene difluoride (PVDF) membrane (Millipore) through 30 min semi-dry transfer using the Biorad system, blocked with 5% skim milk or 1% BSA in Tris-buffered saline/0.1% Tween-20 (Table *2-2*) for 1 h at room temperature, then incubated with primary antibody overnight at 4°C, followed by HRP conjugated secondary antibody (Table *2-3*). Membranes were imaged with Clarity Western ECL Substrate (Bio-Rad, Cat no. 1705061) on a ChemiDoc Touch Imaging System (Bio-Rad). Image analysis and quantification was performed using Image Lab (Bio-Rad). Loading was normalised using beta-actin levels on the same blot. N=3 experiments were performed and the mean quantification shown.

2.9 Transmission electron microscopy

In Chapter 5, electron microscopy was performed with assistance from the Centre for Advanced Microscopy at the Australian National University, for the purpose of examining autophagy structures.

1×10^6 cells were treated for 24 h with the indicated conditions. Cells were then harvested (450 x g spin speed) and fixed overnight in 2.5% glutaraldehyde and 4% paraformaldehyde in PBS at 4°C, then secondary fixation was performed with 1% osmium tetroxide for 1 h at room temperature. Cells were embedded in agarose than stained overnight with 2% aqueous uranyl acetate at 4°C. Graduated dehydration was performed in increasing concentrations of ethanol for at least 30 min each (30%, 50%, 70%, 90%, 100%, 100%, 100%), then the sample was infiltrated with increasing concentrations of LR white resin for at least 1 h each (25%, 50%, 75%, 100%, 100%, 100%). Samples were polymerised overnight at 60°C. Ultrathin sections (approximately 60-70nm) were prepared and stained with 2% uranyl acetate for 15 min and lead citrate for 10 min and imaged on the Hitachi HA7100 Transmission Electron Microscope. At least 10 cells/treatment were imaged. Samples were de-identified before imaging, and re-identified once counting of the autophagy structures was complete.

2.10 Creation of inducible shRNA human AML cell lines

Glycerol stocks of the SMART vector human inducible lentiviral shRNA (murine cytomegalovirus (mCMV) promoter, with turbo red fluorescent protein (RFP) reporter) were purchased from Dharmacon. The following targeting sequences were selected:

- Beclin 1 (BECN1) #1: Cat no. V3SH11252-227864843: GAGAGCTTTTGTCCACTGC (targets 3 prime untranslated region (3'UTR) and open reading frame (ORF)).
- BECN1 #2: Cat no. V3SH11252-230157716: TATTGATTGTGCCAAACTG (targets ORF).
- ATG7 #1: Cat no. V3SH11252-226351133: CAACACATCAGTTTGAGAT (targets Non-Coding and ORF).
- ATG7 #2: Cat no. V3SH11252-229968263: CAAGGAAACCAGCACCATG (targets 5'UTR, Non-Coding and ORF).

The SMARTvector inducible non-targeting shRNA vector (Cat no. VSC11655) was used as a control.

Bacteria were expanded in Luria broth overnight, then plasmid DNA extracted using the NucleoBond Xtra Maxiprep kit (Macherey Nagel Cat no. 740414.50), according to the manufacturer's instructions. DNA concentration was quantified via Nanodrop. The Trans-lentiviral shRNA packaging kit (Dharmacon, Cat no. DHA-TLP5912) was used to transfect the plasma DNA into 293T cells, according to the manufacturer's instructions. After 72 h, the resulting virus was collected, concentrated using the Retro-X concentrator (Clontech, Cat no. 631455) according to the manufacturer's instructions and frozen at -80°C. Lentiviral spin infection was then performed on MV4-11, THP-1 and MOLM-13 cells in the same manner as the retroviral spin infection in Section 2.6.3. Puromycin selection at 1µg/mL was performed for 1 week to select the transduced cells. shRNA cell lines were maintained in RPMI with GlutaMAX (Gibco, Cat no. 35050061) and 20% tetracycline (TET) system approved/tetracycline-free HI-FBS (Clontech #631367), which was also used for shRNA induction experiments.

Cells were treated with 1µg/mL doxycycline and knockdown of the target proteins was confirmed at 72 h and 96 h post-induction (N=1, results not shown), as such 72 h was selected as the timepoint for combining shRNA knockdown and CX-5461 treatment.

2.10.1   Combining shRNA knockdown with CX-5461 treatment

Induction of the shRNA was performed by treating the shRNA cell lines with 1µg/mL doxycycline for 72 h, the cells were then counted, media removed and plated at 10,000 cells/well in a 96 well plate with fresh doxycycline and CX-5461 at a range of concentrations. After 96 h of CX-5461 treatment cell viability was assessed using the MTT assay (as in Section 2.5.4). Protein extraction of cells +/- doxycycline treatment was performed at 3 and 7 days post doxycycline induction and western blot analysis for BECN1, ATG7 and LC3B expression was performed as in Section 2.8.

2.11 Extracellular flux analysis

The oxygen consumption rate (OCR) and extracellular acidification rate (ECAR) of AML cell lines were measured using a Seahorse XFe96 extracellular flux analyser (Seahorse Bioscience). A mitochondrial stress test was performed, which uses various inhibitors to measure the respiratory capabilities of the mitochondria, including the maximum respiration. Cells were pre-treated with indicated compounds for 24 h, or injection of drugs performed at the time of the assay (acute treatment), washed and resuspended in unbuffered DMEM (Seahorse, Cat no. 102353-100) containing 10mM D-glucose, 4mM L-glutamine and 1mM pyruvate, pH 7.4 +/- 0.05. The Seahorse culture plate was coated with 25µL/well of 22.4 µg/mL Cell-Tak (Corning Cell-Tak Cell and Tissue Adhesive, 1 mg Cat. # 354240), in 0.1M $NaHCO_3$ (pH=8) for 20 min. The plate was then washed twice with sterile water. Cells were plated at 100,000 cells/well in the coated Seahorse culture plate and spun at 200 x g with zero braking for 1 min to ensure cell attachment, then incubated at 37°C for 40 min in a non-CO_2 incubator. Using the Seahorse XFe96 extracellular flux analyser, OCR and ECAR were then measured at 37°C following a mitochondrial stress test using sequential injections of ± drugs (for acute treatment), ATP synthase inhibitor oligomycin (1µM), proton ionophore carbonylcyanide p-trifluoromethoxy-phenylhydrazone (FCCP, 0.4µM for THP-1, 0.75µM for MOLM-13), and a mixture of the mitochondrial complex III inhibitor

antimycin A and the complex I inhibitor rotenone (1μM of each). Three readings were conducted for the basal levels and after each of the injections. N=3 experiments were performed and the mean results shown. One-way ANOVA was performed with a Tukey's multiple comparison test, the adjusted p-value is shown. Parameters were defined as follows: energy map/profile = basal levels of OCR versus ECAR, basal respiration rates = OCR in the absence of inhibitors, maximal respiration rate = OCR following mitochondrial uncoupling with FCCP, spare respiratory capacity = difference in the OCR between the maximum respiration rate and basal rate, acute response = difference in the OCR following drug injection and basal respiration.

Chapter 3　Identifying metabolism-modifying drugs that synergise with CX-5461 *in vitro*

3.1 Introduction

The novel Pol I inhibitor CX-5461 has been shown to be effective in mouse models of AML, however, resistance to the drug eventually develops [1] (Section 1.2.3). Rational combination therapies with CX-5461 are required to enhance its efficacy and reduce the development of drug resistance. Metabolic reprogramming, a hallmark of cancer [86], is a well-described process by which cancer cells become resistant to chemotherapy. In addition, changes in metabolic gene expression in cancer cells following CX-5461 treatment (Hein et al, unpublished) suggests that targeting metabolic pathways may be a promising approach in combination therapies with CX-5461.

In order to address this hypothesis 6 AML cell lines were selected to evaluate established metabolism-modifying drugs in combination with CX-5461 *in vitro*, addressing Aim 1: 'Identify established metabolism-modifying therapies that work synergistically with CX-5461 to target acute myeloid leukaemia *in vitro*'.

3.1.1 Selection of AML cell lines

AML cell lines covering the various genetic abnormalities commonly observed in AML patients (Table 1-1) were chosen to evaluate these drug combinations (Table 3-1). Four cell lines that express an MLL fusion protein, a particularly aggressive subtype of AML with a poor prognosis for patients [6,23], were selected for the initial testing of all drug combinations. Three of these four cell lines are of human origin; MV4-11, MOLM-13 and THP-1. The fourth is a mouse-derived MLL/AF9 NRAS cell line, generated by fetal liver transduction with a construct expressing the MLL/AF9 fusion protein tagged with green fluorescent protein (GFP) and mouse $Nras^{G12D}$ mutation tagged with luciferase [32]. These four cell lines were used to evaluate a panel of metabolism-modifying drugs in combination with CX-5461. The most promising combinations were then tested in a

further two cell lines selected based on the absence of MLL translocations and the presence of p53 mutations to cover more of the genetic diversity of AML (Table 1-1). These cell lines were the KG-1 and SKM-1 cell lines.

Cell line	Origin of cells	Patient information	P53 status	Other mutations	Fusion protein
MV4-11	Human	10-year-old with acute monocytic leukaemia (AML FAB M5), at diagnosis	WT	FLT3-ITD, KRAS	MLL/AF4
MOLM-13	Human	20-year-old with AML FAB M5a, at relapse after initial myelodysplastic syndromes, relapse	WT	FLT3-ITD	MLL/AF9
THP-1	Human	1-year-old with acute monocytic leukaemia (AML), relapse	Null	NRAS	MLL/AF9
MLL/AF9	Mouse	-	WT	NRAS	MLL/AF9
KG-1	Human	59-year-old with erythroleukaemia that developed into acute myeloid leukaemia (AML), relapse	Null	NRAS, TET2	AML1-ETO
SKM-1	Human	76-year-old with acute monoblastic leukaemia (AML M5) following myelodysplastic syndromes	Mt	KRAS	-

Table 3-1: Genetic characteristics of AML cell lines used for *in vitro* evaluation.

Patient and genetic information according to the DSMZ German Collection of Microorganisms and Cell Cultures. Common AML mutations with functional characterisation are shown in Table *1-1*. Cell line growing conditions are shown in Table *2-1*.

3.1.2 Selection of metabolism-modifying drugs to test in combination with CX-5461

Metabolism-modifying drugs were selected based on the literature reported to target the main metabolic pathways altered in AML (Section 1.3.1.1) and those implicated in chemotherapy insensitivity (Section 1.3.2). While there is still the need for development of new compounds targeting metabolism in cancer, there are also many established metabolism-modifying drugs that could be repurposed as cancer therapies.

Since it can take in excess of $2.6 billion and over a decade to take a new pharmaceutical drug from development to the clinic [125] the utility of established metabolism-modifying drugs is clear as typically they are readily available, low cost and have relatively low toxicity compared to standard chemotherapeutics. Also, their safe dose in humans has already been established making them ready for clinical trials, which would facilitate the translation of any novel combination cancer therapies with these drugs to the clinic. Based on this, the therapies selected include dichloroacetate, metformin, chloroquine, orlistat, omeprazole, ritonavir, simvastatin, fenofibrate, bezafibrate and rosiglitazone (Table 3-2), which were selected for testing. These drugs were selected based on their known inhibition of key metabolic pathways altered in cancer (Figure 3-1), which could potentially be upregulated by AML cells to subvert the effects of CX-5461.

Drug	Traditional Use	Proposed mechanism of action in cancer
Dichloroacetate	Treatment for lactic acidosis	Activation of PDH through inhibition of PDK, reversal of glycolytic phenotype
Metformin*	Anti-diabetic	Activates AMPK, inhibits the electron transport chain complex I
Chloroquine *	Anti-malarial	Inhibits autophagy through interfering with lysosomal function
Orlistat	Weight loss	Inhibits fatty acid synthase
Omeprazole*	Proton pump inhibitor/heartburn	Inhibits fatty acid synthase
Ritonavir*	Anti-retroviral	Inhibits glucose transporter GLUT 4
Simvastatin*	Treatment for hypercholesterolemia	Inhibits HMG-CoA reductase and cholesterol synthesis
Fenofibrate	Treatment for hypercholesterolemia	PPARα agonist, lowers cholesterol
Bezafibrate	Treatment for hypercholesterolemia	PPARα agonist, lowers cholesterol
Rosiglitazone	Anti-diabetic	PPARγ agonist, lowers cholesterol

Table 3-2: Candidate metabolism-modifying drugs for evaluation with CX-5461 and their proposed mechanism of action in cancer.

*On the World Health Organisation's Model List of Essential Medicines [7], a list of safe and cost-effective medicines for common medical conditions and diseases globally.
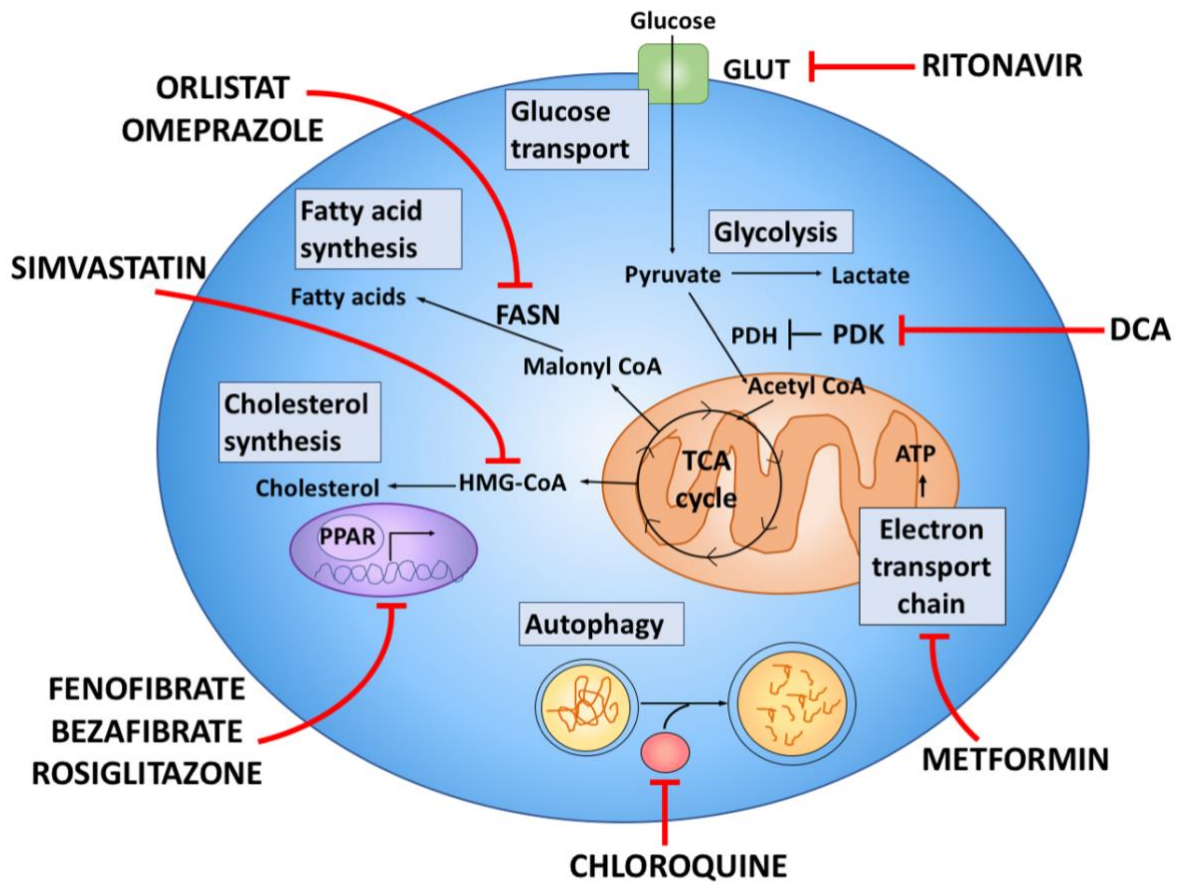
Figure 3-1: Metabolic pathways targeted by the drugs selected for evaluation with CX-5461

Various metabolic pathways are altered in cancer cells, facilitating their growth and proliferation, and even chemotherapy resistance. There are many established metabolism-modifying therapies which target these pathways. Ritonavir, a HIV medication, reduces glucose uptake by inhibiting the GLUT 4 glucose transporter. Dichloroacetate (DCA) shuttles pyruvate from glycolysis to mitochondrial respiration by inhibiting pyruvate dehydrogenase kinase (PDK), an inhibitor of pyruvate dehydrogenase (PDH). Metformin, a diabetes medication, inhibits complex I of the mitochondrial electron transport chain (ETC). Anti-malarial chloroquine inhibits autophagy by interfering with lysosomal function preventing the fusion of lysosomes with autophagosomes. Weight loss medication orlistat and proton pump inhibitor omeprazole both disrupt fatty acid synthesis by inhibiting the fatty acid synthase (FASN) enzyme. Cholesterol medications fenofibrate and bezafibrate, and anti-diabetic rosiglitazone interfere with cholesterol synthesis by acting as peroxisome proliferator-activated receptor (PPAR) agonists, therefore interfering with gene regulation of cholesterol synthesis. Cholesterol medication simvastatin inhibits cholesterol synthesis by inhibiting 3-hydroxy-3-methyl-glutaryl-coenzyme A (HMG-CoA) reductase.

3.1.2.1 Targeting the glycolytic phenotype

Dichloroacetate (DCA) is a drug that has historically been used as a treatment for lactic acidosis as it reduces lactate production. It does this by directing the metabolism of pyruvate to mitochondrial oxidation and away from glycolysis through inhibition of pyruvate dehydrogenase kinases (PDKs), therefore activating pyruvate dehydrogenase (PDH) [126]. DCA has more recently been investigated as an anti-cancer agent due to its ability to reverse the Warburg effect/glycolytic phenotype, a characteristic of cancer cells, through this same process [127]. DCA has been tested in many solid cancers, including breast cancer where it has been shown to be cytostatic as a single agent [92], and enhanced apoptosis in combination with mitochondrial-targeting agents arsenic trioxide [128] and phenylarsonous acid (PENAO) [129]. DCA has also shown efficacy in blood cancers; promising pre-clinical testing of DCA in multiple myeloma has led to the commencement of a Phase II clinical trial of DCA in plateau phase multiple myeloma in Australia (DiCAM trial; ANZCTR #ACTRN12615000226505). In pre-clinical models of B-chronic lymphocytic leukaemia (B-CLL) DCA was shown to have anti-leukemic effects in patient samples and cell lines and to synergise with p53 activator Nutlin-3 [130], as well as to reduce viability of AML cells in combination with arsenic trioxide [107]. Given the literature which shows that targeting glycolysis with DCA can 'prime' AML cells for death by other agents [107], combination therapy with DCA could be a promising approach.

3.1.2.2 Targeting mitochondrial function

Metformin is an anti-diabetic medication which lowers blood glucose concentrations in part through targeting the key energy sensor 5' adenosine monophosphate-activated protein kinase (AMPK), thereby decreasing hepatic glucose production and increasing glucose uptake [131], although the exact mechanisms were previously not well understood. Further investigation of the actions of metformin led to the discovery that it inhibited complex I of the mitochondrial electron transport chain [132], and thus was able to modulate the function of the mitochondria. The investigation of metformin as a cancer therapeutic began when retrospective analysis of cancer incidence in diabetic patients revealed that metformin-treated patients had a significantly lower risk of developing cancer, compared to those on insulin or other therapies [133]. Given the previous findings that metformin could modulate mitochondrial function, this was

investigated in various cancer cells and *in vivo* cancer models. Metformin induced apoptosis and reduced tumour growth in preclinical models of acute myeloid leukaemia through inhibition of electron transport chain complex I [134]. Metformin treatment also induced apoptosis and cell cycle arrest alone and in combination with dexamethasone in multiple myeloma through inhibiting the expression of insulin growth factor-I receptor (IGF-IR) [135], indicating more than one potential mode of action in cancer. It has also been found to be effective in solid tumours such as ovarian cancer [136] and neuroblastoma [137]. Such promising preclinical results in a wide range of tumour models has led to the initiation of hundreds of clinical trials with cancer patients utilising metformin based on its metabolism-modifying properties, including trials for breast cancer (ClinicalTrials.gov Identifiers: NCT01266486 and NCT01310231), lung cancer (ClinicalTrials.gov Identifier: NCT02115464), prostate cancer (ClinicalTrials.gov Identifier: NCT01243385), multiple myeloma and chronic lymphocytic leukaemia (ClinicalTrials.gov Identifier: NCT02948283) and AML (ClinicalTrials.gov Identifier: NCT01849276). In a clinical trial of patients with advanced prostate cancer, metformin + castration was found to reduce the disease marker prostate-specific antigen (PSA) levels by 7 fold compared to the placebo + castration group (ClinicalTrials.gov Identifier: NCT01620593). This supports that metformin can modulate metabolic responses in cancer patients. Given the role that mitochondria play in AML cells [106], combination therapy with metformin could be a promising approach, particularly as its efficacy as a metabolism-modifying therapy is already well-established in humans.

3.1.2.3 Targeting autophagy

Chloroquine has a long history of use in humans including as an antimalarial drug, with its efficacy thought to be due to its inhibition of heme polymerase through an unknown mechanism, leading to the accumulation of free heme which is toxic to the parasite [138]. Chloroquine and its derivate hydroxychloroquine have also been used to treat some immune disorders like rheumatoid arthritis based on its immune suppressive effects [139], in part through inhibition of inflammatory cytokine signalling [140] and toll-like receptor signalling through raising endosomal and lysosomal pH [141]. Chloroquine has also been recognised to have anti-cancer properties for many decades [142], and was subsequently found to inhibit autophagy through interfering with lysosomal function, thus preventing the fusion of lysosomes with autophagosomes [143].

Inhibition of autophagy through chloroquine has since been studied as a therapeutic target in various cancer models, with chloroquine acting to reduce the growth of hepatocellular carcinoma *in vitro* and *in vivo* [144], reducing the growth and metastasis of breast cancer [145], including through inducing mitochondrial damage and impairing DNA break repair [146], and inhibiting proliferation, inducing apoptosis and cell cycle arrest *in vitro* in acute promyelocytic leukaemia [147]. Clinical trials of chloroquine or hydroxychloroquine have commenced in various malignancies including breast cancer as a single agent (ClinicalTrials.gov Identifier: NCT02333890) or in combination with standard chemotherapy (ClinicalTrials.gov Identifier: NCT01446016) and in relapsed and refractory multiple myeloma where a 30% response rate was achieved after 2 cycles with a combination of bortezomib, cyclophosphamide and chloroquine (ClinicalTrials.gov Identifier: NCT01438177). Given the role autophagy has been demonstrated to play in AML cell survival [115], combination treatment with chloroquine could be a promising approach.

3.1.2.4 Targeting fatty acid synthesis

Orlistat is a weight-loss medication that reduces fat absorption by inhibiting pancreatic and gastric lipases through binding to the active site of the enzymes and preventing enzyme activity [148]. In the search for novel agents targeting fatty acid synthesis, a process upregulated in cancer, an activity-based proteomics screen revealed that orlistat was also a novel inhibitor of the thioesterase domain, key for the function of the enzyme, of fatty acid synthase (FASN) and was efficacious in an *in vivo* mouse model of prostate cancer [119]. Orlistat has since been tested *in vitro* and *in vivo* in various cancer models including leukaemia [149] and multiple myeloma [150]. Despite these promising results, clinical development of orlistat as a cancer therapy has been hindered by its poor oral bioavailability [151], as such there are currently no clinical trials in cancer with this drug. The search for novel inhibitors of FASN with improved bioavailability revealed that certain proton pump inhibitors, including omeprazole, also inhibit the thioesterase domain of FASN [152]. Omeprazole is traditionally a medication to treat reflux and has proton pump inhibitor activity by inhibiting the gastric H^+,K^+-ATPase [153]. Before omeprazole was identified as a FASN inhibitor, it had been shown to inhibit proliferation and modulate autophagy *in vitro* in pancreatic cancer cells, hypothesised to be due to its effects on the lysosomal transport pathway [154]. It has

also been shown to reduce invasion and metastasis in models of triple negative breast cancer *in vitro* and *in vivo,* hypothesised to be due to its action as an aryl hydrocarbon receptor (AHR) ligand [155]. This more recently discovered mechanism of action of omeprazole as a FASN inhibitor has led to the commencement of a Phase II clinical trial to improve the efficacy of neoadjuvant chemotherapy in breast cancer (ClinicalTrials.gov Identifier: NCT02595372) with results yet to be published. Given that fatty acids have been shown to promote AML cell survival [116], combination therapy with orlistat or omeprazole and CX-5461 could be a promising approach.

3.1.2.5 Targeting glucose uptake

Ritonavir is an anti-retroviral human immunodeficiency virus (HIV) medication that prevents the formation of mature, infectious HIV particles by inhibiting the action of the HIV protease enzyme to cleave the gag-pol polyproteins, an essential step in the HIV lifecycle [156]. First approved for clinical use in the 1990's, ritonavir is now more commonly used to boost the effects of other protease inhibitors due to its inhibition of liver cytochrome P450 3A-mediated metabolism, increasing the concentration of other protease inhibitors and improving their efficacy [157]. Metabolic side effects, including insulin resistance and type II diabetes, have long been associated with the use of retroviral protease inhibitors in the treatment of HIV, leading to the discovery that these drugs inhibit glucose uptake [158]. Given the association of increased glucose uptake with cancer cells, this is of great interest as a potential cancer therapy. Ritonavir is an inhibitor of glucose transporter type 4 (GLUT4) and has been shown to be effective in models of multiple myeloma [159] and chronic lymphocytic leukaemia (CLL) [160] in combination with metformin. Current clinical trials with ritonavir in cancer include in combination with external beam radiation in patients with brain metastasis (ClinicalTrials.gov Identifier: NCT00637637) and in patients with relapsed and refractory multiple myeloma and CLL in combination with metformin (ClinicalTrials.gov Identifier: NCT02948283) with results yet to be published. Given the role that glucose plays in both glycolysis and mitochondrial metabolism, which have both been shown to be dysregulated in AML [106,107], combination treatment with ritonavir could be a promising approach.

3.1.2.6 Targeting cholesterol metabolism

The cholesterol-lowering medication simvastatin inhibits the action of the enzyme HMG-CoA reductase to convert HMG-CoA to mevalonate, which is a rate-limiting step in cholesterol synthesis [161]. Given that cholesterol synthesis is upregulated in cancer, simvastatin was tested as a single agent and found to reduce proliferation and colony-forming potential of AML cell lines *in vitro*, and to sensitise the cells to the effects of cytarabine [162]. In multiple myeloma cell lines, simvastatin was found to induce cell cycle arrest and death [163]. In a clinical trial of simvastatin in breast cancer, immunohistochemistry analysis revealed that several weeks of treatment resulted in increased apoptosis and reduced the levels of proliferative markers in the primary tumours [164]. Fibrates and glitazones are other classes of cholesterol-modifying agents that activate specific transcription factors of the superfamily of nuclear hormone receptors, known as peroxisome proliferator-activated receptors (PPARs). Fibrates are agonists of PPARα and glitazones are agonists of PPARγ, and the downstream consequences of the activation of these factors is the lowering of blood triglycerides and cholesterol [165]. Fenofibrate has been shown to induce apoptosis in triple-negative breast cancer [166] and mantle cell lymphoma [167]. In a clinical trial of patients with various relapsed and progressive cancers when given fenofibrate in a 5-drug metronomic regimen with thalidomide, celecoxib, etoposide and cyclophoshamide, 31% of patients achieved progression-free survival after 27 weeks treatment (ClinicalTrials.gov Identifier: NCT00357500). Bezafibrate was found to inhibit proliferation and induce cell cycle arrest in an *in vitro* model of lung adenocarcinoma [168]. In chronic myeloid leukaemia (CML), glitazones were shown to target the leukaemia stem cell pool [169] and rosiglitazone synergised with carboplatin to induce apoptosis and reduce cell growth in a mouse model of lung cancer [170]. Given the dysregulation of cholesterol metabolism in AML cells [110], combination treatment with simvastatin, fenofibrate, bezafibrate or rosiglitazone could be a promising approach.

Together this literature indicates that metabolism-modifying agents can both have efficacy against cancer cells as single agents and/or sensitise cancer cells to the effects of other anti-neoplastic drugs, and thus potentially be effective as cancer therapeutics.

3.1.2.7 Metabolism-modifying drugs that potentially modulate ribosome biogenesis

In addition to their metabolism-modifying mechanism of action, some of the drugs that were selected for testing in combination with CX-5461 also have reported effects on ribosome biogenesis. The key considerations when evaluating these studies include the concentration of drug used, the cell type and the duration of treatment.

Metformin activates AMPK [131], which has been shown to downregulate rRNA synthesis through impairing the interaction between TIF-1A and SL-1 [171]. Treatment of MCF7 breast cancer cells with 2.5mM metformin for 4 hours resulted in a significant reduction in rRNA transcription, following AMPK activation and subsequent activation of histone demethylase KDM2A at the rDNA promoter [172]. Gene expression analysis of human peripheral blood mononuclear cells from patients treated with 100 mg ritonavir once or twice daily for 14 days, has shown significant modulation of 13 genes involved in ribosome biogenesis and assembly [173], although it is not clear whether these are upregulated or downregulated. Omeprazole treatment has been shown to decrease expression of the transcription factor c-myc, a key regulator of ribosome biogenesis [174], in human peripheral blood mononuclear cells cultured for 21 days *in vitro* with 1µM omeprazole[175]. However, it was not confirmed in this study if the rate of rDNA transcription was decreased. Chloroquine is known to intercalate with DNA [176], which could reduce the rate of rDNA transcription.

While none of the metabolism modifying agents selected for testing in these studies is a selective inhibitor of ribosome biogenesis, as evidenced above, some of these agents may dysregulate factors involved in ribosome biogenesis. This must also be taken into consideration when examining promising combination therapies with CX-5461.

3.1.3 Determination of drug concentrations to be used for testing

In order to evaluate the drugs at biologically relevant concentrations, a maximum concentration for testing was selected for each drug based on the literature, taking into consideration, if reported, achievable plasma concentrations in patients and/or mice, concentrations reported in *in vitro* studies and concentrations known to achieve on-target effects for the mechanisms being investigated in cancer.

CX-5461. A maximum concentration of 1μM was used for CX-5461 in order for the drug to remain an on-target inhibitor of Pol I and not Pol II or Pol III [81].

DCA. With repeated dosing of DCA, plasma concentrations of around 1-2mM are achievable [177], as such 5mM was chosen as the maximum concentration for testing.

Metformin. When used as an antidiabetic medication, metformin serum levels average around 700μM [178], however, 10mM was selected as a maximum concentration as metformin has been shown to inhibit mitochondrial complex I activity in the millimolar range in leukaemia cells [134].

Chloroquine. In studies of malaria-infected patients, chloroquine plasma concentrations peak at around 1-2μM during a 3 day course of chloroquine treatment [179] and similar levels were observed in malaria-infected mice [180], however for the purpose of studying autophagy inhibition a maximum concentration of 40μM was selected as chloroquine is well established to inhibit autophagy at this concentration [111,181].

Orlistat. There is minimal absorption of orlistat when taken through the traditional oral route in humans [151] and testing of injectable orlistat has not been performed in humans thus far. However, in mice that have been injected with orlistat solution by intraperitoneal injection, plasma concentrations have been measured to reach 10μM and been predicted to reach approximately 16μM with a higher dosing schedule [119]. As such, a maximum concentration of 30μM was selected for *in vitro* testing.

Omeprazole. Omeprazole inhibits the thioesterase domain of FASN at a micromolar range, with a concentration that inhibits the activity of the enzyme by 50% (IC_{50}) of approximately 30μM [152]. As such, 200μM was the highest concentration utilised for testing to ensure maximum inhibition of FASN.

Ritonavir. Ritonavir plasma levels in patients peak at approximately 25-30μM [182] and glucose uptake has been shown to be significantly inhibited by 50μM of ritonavir[158]. As such, ritonavir was tested up to a maximum concentration of 50μM.

Simvastatin. In healthy human volunteers, plasma levels of approximately 20μM simvastatin were readily achieved [183], therefore a maximum concentration of 40μM was utilised for testing.

Fenofibrate and bezafibrate. Plasma levels of approximately 30μM fenofibrate and bezafibrate are achievable in healthy volunteers [184], therefore a maximum concentration of 100μM was used for testing.

Rosiglitazone. Rosiglitazone levels reach approximately 2μM in the plasma of patients [185], as such 30μM maximum was used for testing.

3.1.4 Analysis of drug synergy

Determining synergistic drug combinations is of great interest in the medical field as, in general, lower concentrations of the individual drugs are used, resulting in less severe side effects and reduces the occurrence of drug resistance [186]. To be defined as synergistic (also known as super-additive), the combination effects of the drugs must be in excess of what would be predicted given the individual effects of the drugs. If the combination effect matches what is expected given the individual drug potencies the combination is considered additive, while if the effect is less than predicted the combination is considered antagonistic. Various methods of analysis exist for determining drug synergy; one such well-established method is the Chou-Talalay Combination Index method [122]. The Combination Index (CI) method provides a quantitative measure of synergy between two or more drugs; an additive effect has a CI = 1, a synergistic effect has a CI<1 and an antagonistic effect has a CI>1. This method has been incorporated into a freely-available program called CompuSyn. Further details of this method are included in Section 2.5.5.

3.1.5 Assays for measuring cell viability

Total viable cell number was chosen as the read-out for the analysis, rather than a more narrow effect such as cell death, as this read-out can evaluate multiple consequences of drug treatment over time (e.g. cell cycle arrest, apoptosis, senescence, cell death). The mechanism of action mediating altered cell viability would be determined once promising combinations had been identified, to help identify the mechanisms of synergy (see Chapter 5). In order to evaluate the effects of the metabolism drugs with CX-5461, colourimetric viability plate-based assays were utilised (Section 2.5). There are a number of such assays including the neutral red assay and the thiazolyl blue tetrazolium bromide (MTT) assay. The neutral red assay

estimates viable cell number based on the uptake and binding of the neutral red dye in the lysosomes of the cells, which can only occur in viable cells (Section 2.5.1) [120]. The MTT assay is based on the conversion of the water-soluble MTT tetrazolium salt (3-(4,5-dimethylthiazol-2-yl)-2,5-diphenyl tetrazolium bromide) to coloured formazin crystals via succinate dehydrogenase in the mitochondria (Section 2.5.2)[121]. Alternatively, cell counting using the Coulter counter, which measures particle number and size, was used as a control to determine the suitability of the assays with the different drugs (Section 2.5.3).

3.2 Results

3.2.1 Optimising conditions for viability testing

In order to ensure that the cells are in an exponential growth phase at the time that viability is assessed, various plating densities were evaluated with viable cell number determined using the neutral red assay after 96 h culturing in untreated conditions (Figure 3-2). Importantly, a 96 h timepoint was chosen as this provided the cells time to divide at least 1-2 times in untreated conditions (refer to Table *2-1* for doubling times of each cell line). This is important as cells often display a lag phase on replating, and if the cells become confluent they may be contact inhibited and run out of nutrients which reduces the proliferation rate. Human AML cell lines were plated at a range of 0.5-10 x 10^4 cells/well and the mouse AML cell lines at 0.25-5 x 10^4 cells/well.

Figure 3-2 shows that after 96 h culturing in untreated conditions the MV4-11, THP-1 and SKM-1 cells were in the exponential growth phase from 0.5-5 x 10^4 cells/well plated then plateau in number at higher plating densities, indicating they were confluent. The MOLM-13 and MLL/AF9 NRAS cells were in exponential growth phase from 0.5-2 x 10^4 cells/well plated then become confluent at higher plating densities. The KG-1 cells were in exponential growth phase from 0.5-3 x 10^4 cells/well plated then become confluent at higher plating densities. Thus, for the MV4-11, THP-1 and SKM-1 cell lines 4 x 10^4 cells/well, KG-1 2 x 10^4 cells/well, MOLM-13 1.5 x 10^4 cells/well and MLL/AF9 NRAS 1 x 10^4 cells/well were chosen as optimal plating densities for the 96 h drug treatment viability assays.
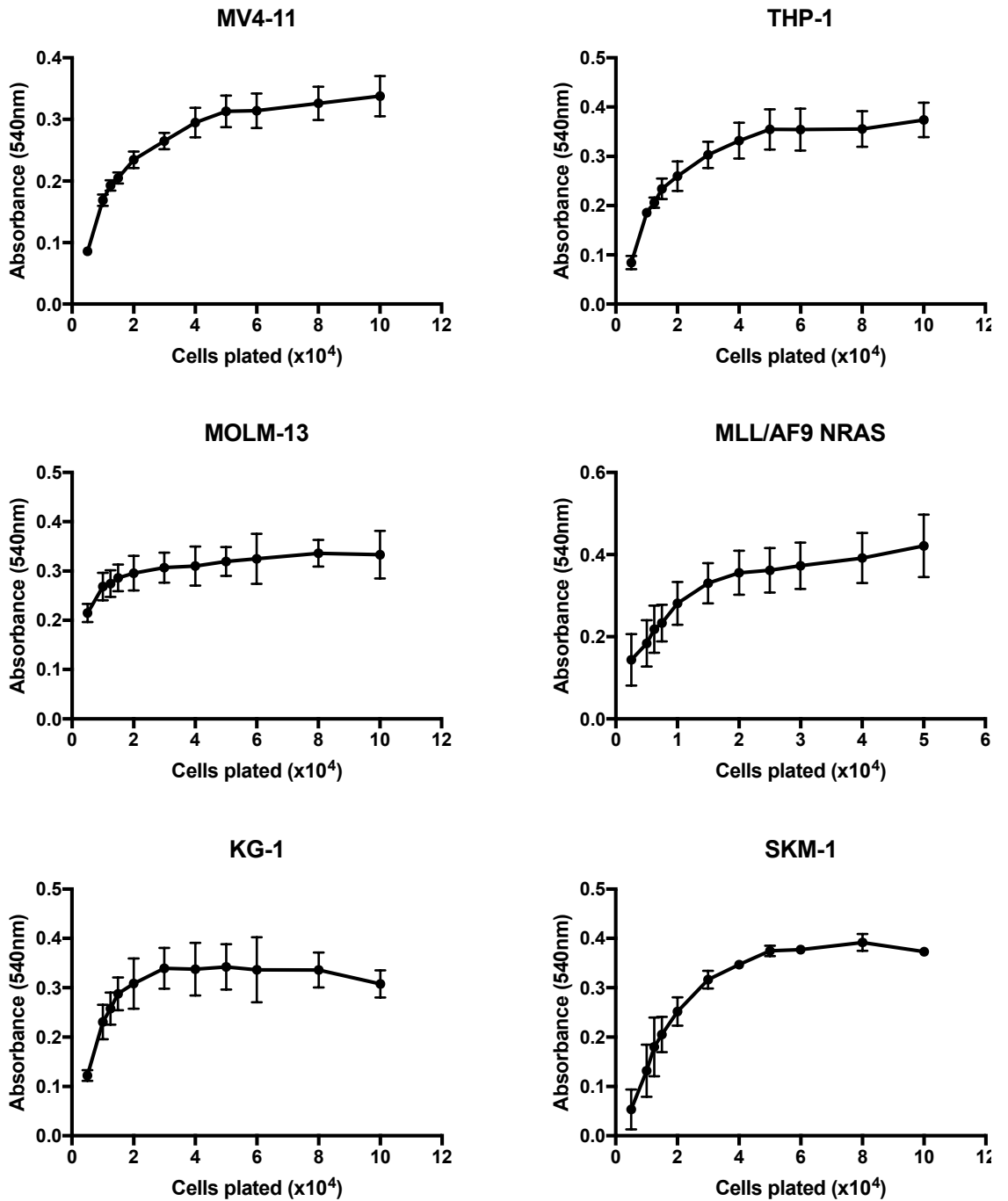
Figure 3-2: Determining cell plating density for viability assays

AML cell lines MV4-11, THP-1, MOLM-13, MLL/AF9 NRAS, KG-1 and SKM-1 were plated at a range of cell numbers per well in a 96 well plate and cultured in untreated conditions for 96 h. Total viable cell number was determined using the neutral red assay (Methods section 2.5.1). Graphs show the mean±SD of n=2-3 experiments.

The accuracy of the viability assay used (neutral red or MTT) was confirmed using a physical counting method (Coulter count), using the MV4-11 cell line. When comparing the effect of these drugs between the neutral red assay and Coulter counting (Figure 3-3), the results were consistent for CX-5461, orlistat, ritonavir, DCA, omeprazole, fenofibrate, bezafibrate and rosiglitazone. Interestingly, treatment with metformin and simvastatin resulted in an underestimate of viability, while chloroquine treatment resulted in an overestimation of viability with the neutral red assay. As the neutral red assay measures the uptake and retention of the neutral red dye in the lysosomes [120] this suggests that the drugs are affecting the number and/or function of the lysosomes in the MV4-11 cells. Simvastatin has been reported to induce autophagy (which, at least in the short term, would result in a decrease in lysosomes) as a cytoprotective effect in leukaemia cells [187] and metformin is a well-known autophagy inducer in cancer cells due to activation of AMPK and downstream reduction in mTOR [188,189], so this underestimation of cell viability with neutral red is consistent with the literature. The overestimation of cell viability with neutral red following chloroquine treatment is also unsurprising given the inhibitory effect chloroquine has on autophagy [143], resulting in the accumulation of lysosomes and thus artificially inflating the neutral red readings.
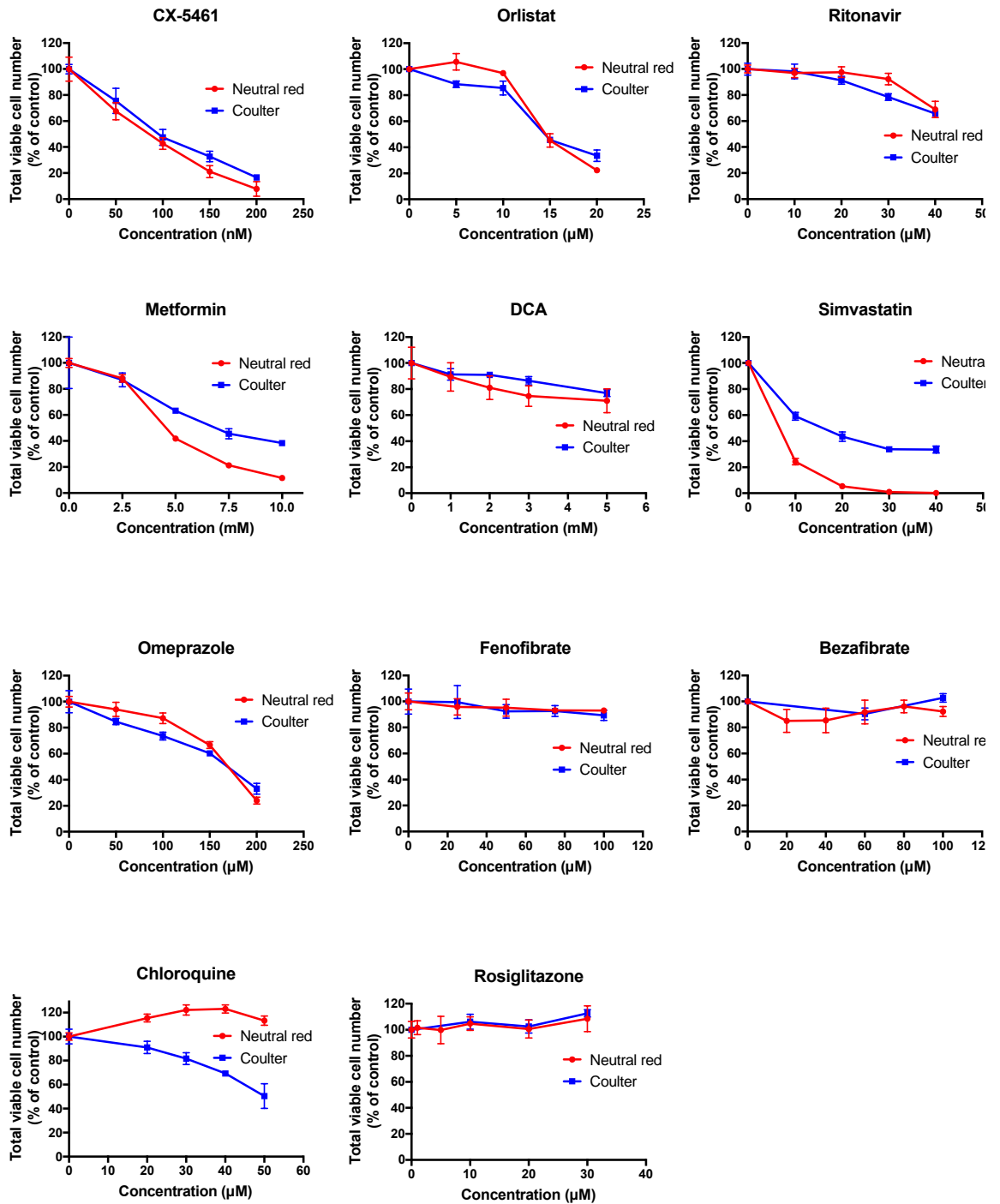
Figure 3-3: Comparison of neutral red and Coulter count results for cell viability.

MV4-11 cells were treated with the indicated drugs for 96 h then cell viability was simultaneously assayed using neutral red staining and Coulter counting in order to determine if any of the drugs were inferring with the mechanism of action of the neutral red assay. Graphs show the mean±SD of 2-4 technical replicates per data point, n=1.

In light of these results, metformin, simvastatin and chloroquine were further tested using the MTT assay and compared to Coulter counting to measure cell viability (Figure 3-4). The results of the MTT and Coulter counts correlate for chloroquine treatment, but again this did not correlate for metformin and simvastatin. As the MTT assay measures the activity of mitochondrial reductases [121], these results suggest that metformin and simvastatin are affecting the function of the mitochondria. Metformin has previously been reported to have various effects on mitochondrial function including complex I inhibition [134], limiting respiration and citric acid cycle activity [190] and inhibiting ATP synthase [191] which could affect the results of the MTT assay. Statins,
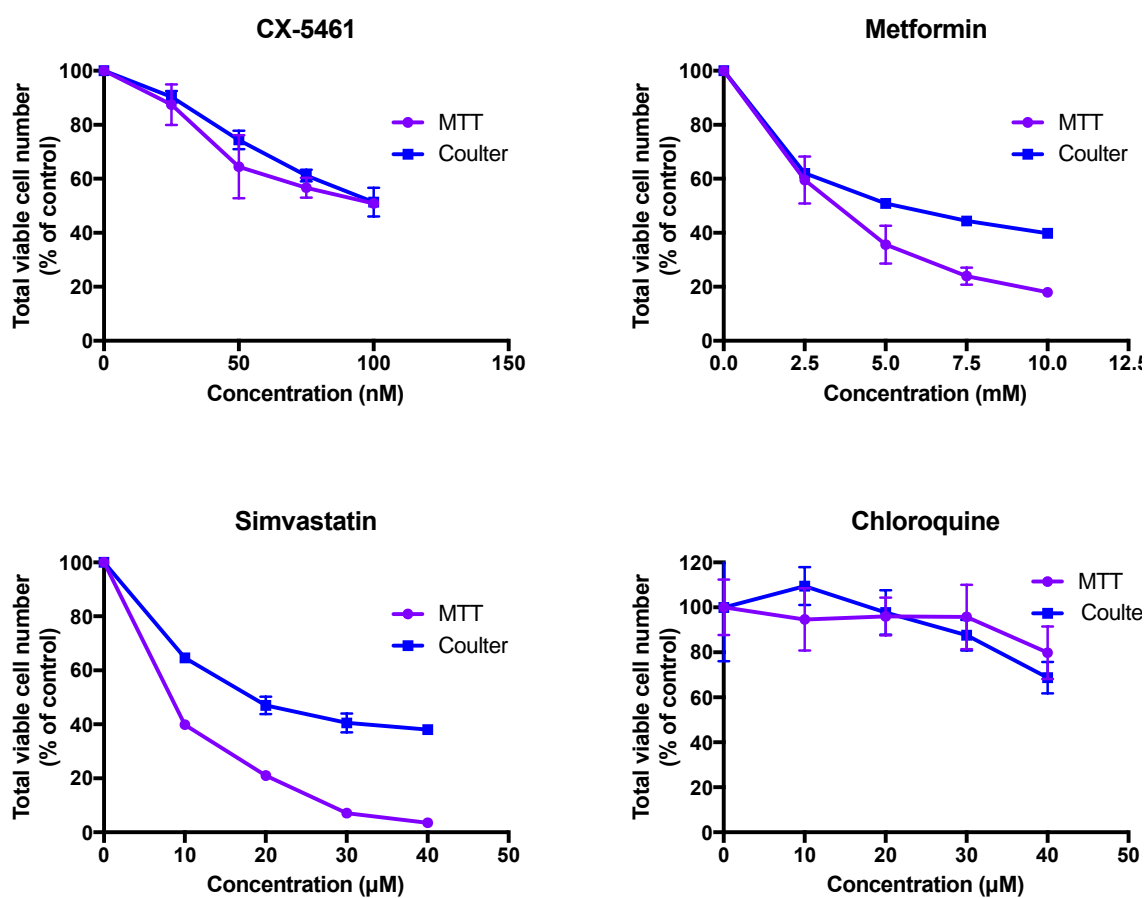
Figure 3-4: Comparison of MTT assay and Coulter count results for cell viability.

MV4-11 cells were treated with the indicated drugs for 96 h then cell viability was simultaneously assayed using MTT staining and Coulter counting in order to determine if any of the drugs were inferring with the mechanism of action of the MTT assay. Graphs show the mean±SD of 2-4 technical replicates per data point, n=1.

including simvastatin, have been reported to induce mitochondrial dysfunction by inhibiting complex III in muscle cells [192] and could potentially also affect the mitochondria in leukaemia cells. Any future viability evaluation with these drugs should not be metabolism-based, instead a method such as cell counting through high-throughput flow cytometry would be preferable as this technique would not be affected by the mechanism of action of the drugs. This technique was not available in house at the commencement of testing, but has since been set up and could be used for future evaluation of cell viability with suspension cells such as AML. Since a suitable assay for measuring cell viability was not identified for metformin and simvastatin at the time the experiments were conducted, these drugs were not evaluated further. As the aim of the study is to evaluate combination therapies with CX-5461 this was also tested with the MTT assay and found to correlate with the Coulter counts, and thus the MTT assay was deemed accurate to determine cell viability following CX-5461 treatment. The results of the viability assay comparison testing are summarised in Table 3-3.

Drug	Suitability with neutral red?	Suitability with MTT?
CX-5461	Yes	Yes
Orlistat	Yes	Not tested
Ritonavir	Yes	Not tested
Metformin *	No	No
DCA	Yes	Not tested
Simvastatin *	No	No
Omeprazole	Yes	Not tested
Fenofibrate	Yes	Not tested
Bezafibrate	Yes	Not tested
Chloroquine	No	Yes
Rosiglitazone	Yes	Not tested

Table 3-3: Summary of suitability testing of viability assays for each drug as a single agent.

*These drugs were not carried forward for further evaluation.

3.2.2 Dose-response curves and GI50s of drugs as single agents

Each drug was tested as a single agent across a range of concentrations (Section 3.1.3) in 4 cell lines (MV4-11, THP-1, MOLM-13 and MLL/AF9 NRAS). Total viable cell number

after 96 h of treatment was determined using the assay appropriate for each drug (Table 3-3). For each drug and cell line the concentration versus the cell viability was graphed (Figure 3-5-Figure 3-8). The dose resulting in a 50% growth inhibition (GI_{50}) was then calculated for each cell line after fitting a non-linear dose curve to the data points (Methods Section 2.5.5). GI_{50} values are summarised in Table 3-4.

3.2.2.1 Ribosome biogenesis

In response to treatment with ribosome biogenesis inhibitor CX-5461 (up to a maximum concentration of 1µM, as justified in Section 3.1.3), dose-response curves from 100% viability to close to 0% viability were achieved in the MLL/AF9 NRAS (Figure 3-8) and MV4-11 (Figure 3-5) cell lines, with the MLL/AF9 NRAS cells being the most sensitive by about 10-fold. In the MOLM-13 cell line (Figure 3-6) viability plateaued at approximately 200nM, thus a true GI_{50} could not be determined. Given the effects CX-5461 is known to have on cell cycle in this cell line [1] it is possible that this plateau is due to CX-5461 inducing cell cycle arrest in the cells, particularly at 200nM or higher. The THP-1 cell line (Figure 3-7) showed no sensitivity to CX-5461 treatment.

3.2.2.2 Glucose uptake and glycolysis

In response to treatment with glucose uptake inhibitor ritonavir (up to a maximum concentration of 50µM, as justified in Section 3.1.3) dose-response curves from 100% viability to close to 0% viability were achieved in the MLL/AF9 NRAS cells, MOLM-13 and MV4-11, in ascending order of GI_{50}. The THP-1 cell line showed some limited sensitivity at the higher concentrations of ritonavir only.

In response to treatment with glycolysis inhibitor DCA, no dose-response curves were achieved in any of the cells lines, however, at the maximum concentration of 5mM (as justified in Section 3.1.3) viability of the MLL/AF9 NRAS cells dropped to approximately 30%. The MV4-11 and THP-1 cell lines showed a small drop in viability at 5mM, while there was no change in the MOLM-13 cell line.

Drugs	Maximum concentration tested*	GI$_{50}$±SD			
		Human			Mouse
		MV4-11 (MLL/AF4, p53 WT)	MOLM-13 (MLL/AF9, p53 WT)	THP-1 (MLL/AF9, p53 null)	MLL/AF9 NRAS (p53 WT)
Ribosome biogenesis					
CX-5461 (nM)	1000	115.6±27	~200	>1000	10.3±2
Glucose uptake and glycolysis					
Ritonavir(µM)	50	41.0±0.2	40.4±11	>50	13.3±3
DCA (mM)	5	>5	>5	>5	~4
Fatty acid synthesis					
Orlistat (µM)	30	19.2±3	23.4±2	>30	~30
Omeprazole (µM)	200	~180	>200	>200	125.6±2
Autophagy					
Chloroquine (µM)	40	>40	>40	>40	25.9±5
Cholesterol synthesis					
Fenofibrate (µM)	100	>100	>100	>100	25.5±4
Bezafibrate (µM)	100	>100	>100	>100	>100
Rosiglitazone (µM)	30	>30	>30	>30	>30

Table 3-4: GI$_{50}$ values of drugs as single agents

Data from Figure *3-5* - Figure *3-8*. Colour code: No colour = Sensitive (>25% drop in cell viability at maximum concentration Light grey = Some sensitivity (10-25% drop in cell viability at maximum concentration) Dark grey = Not sensitive (<10% drop in cell viability at maximum concentration). * Justified in Section 3.1.3.

3.2.2.3 Fatty acid synthesis

In response to treatment with fatty acid synthesis inhibitor orlistat (up to a maximum concentration of 30µM, as justified in Section 3.1.3) dose-response curves from 100% viability to close to 0% viability were achieved in the MV4-11 and MOLM-13 cell lines.

At 30µM orlistat the viability of the MLL/AF9 NRAS cells dropped to approximately 60%, while the THP-1 cells showed no sensitivity.

In response to treatment with fatty acid synthesis inhibitor omeprazole (up to a maximum concentration of 200µM, as justified in Section 3.1.3) a dose-response curve from 100% viability to close to 0% viability was achieved in the MLL/AF9 NRAS cell line. At 200µM treatment, viability of the MV4-11 and MOLM-13 cells had dropped to 30% and 80%, respectively, while the THP-1 cells showed no sensitivity.

3.2.2.4 Autophagy

In response to treatment with autophagy inhibitor chloroquine (up to a maximum concentration of 40µM, as justified in Section 3.1.3) a dose-response curve from 100% viability to close to 0% viability was achieved in the MLL/AF9 NRAS cell line. The MV4-11, MOLM-13 and THP-1 cell lines showed limited or no sensitivity to chloroquine, up to 40µM.

3.2.2.5 Cholesterol synthesis

In response to treatment with cholesterol synthesis inhibitors fenofibrate, bezafibrate and rosiglitazone (up to a maximum concentration of 100µM, 100µM,and 30µM, respectively, as justified in Section 3.1.3) dose-response curves from 100% viability to close to 0% viability were achieved in the MLL/AF9 NRAS cell line, with the exception of bezafibrate where viability went down to approximately 80% with 100µM treatment. The MV4-11, MOLM-13 and THP-1 cell lines showed no sensitivity to any of the three cholesterol synthesis inhibitors, even at the maximum concentrations tested.

3.2.2.6 Summary of dose-response curve testing

In summary, the mouse-derived MLL/AF9 NRAS cells showed some sensitivity (defined as >10% drop in cell viability at the highest concentration tested) to all of the metabolism modifying drugs tested and was the most sensitive of the four cell lines to CX-5461 treatment. Of the human AML cell lines tested, MV4-11 cells were the most sensitive to the metabolism modifying drugs overall and to CX-5461, followed by MOLM-13, then THP-1 which showed no, or limited, sensitivity to any of the metabolism drugs, or to CX-5461, up to the maximum concentrations used for testing.

MV4-11
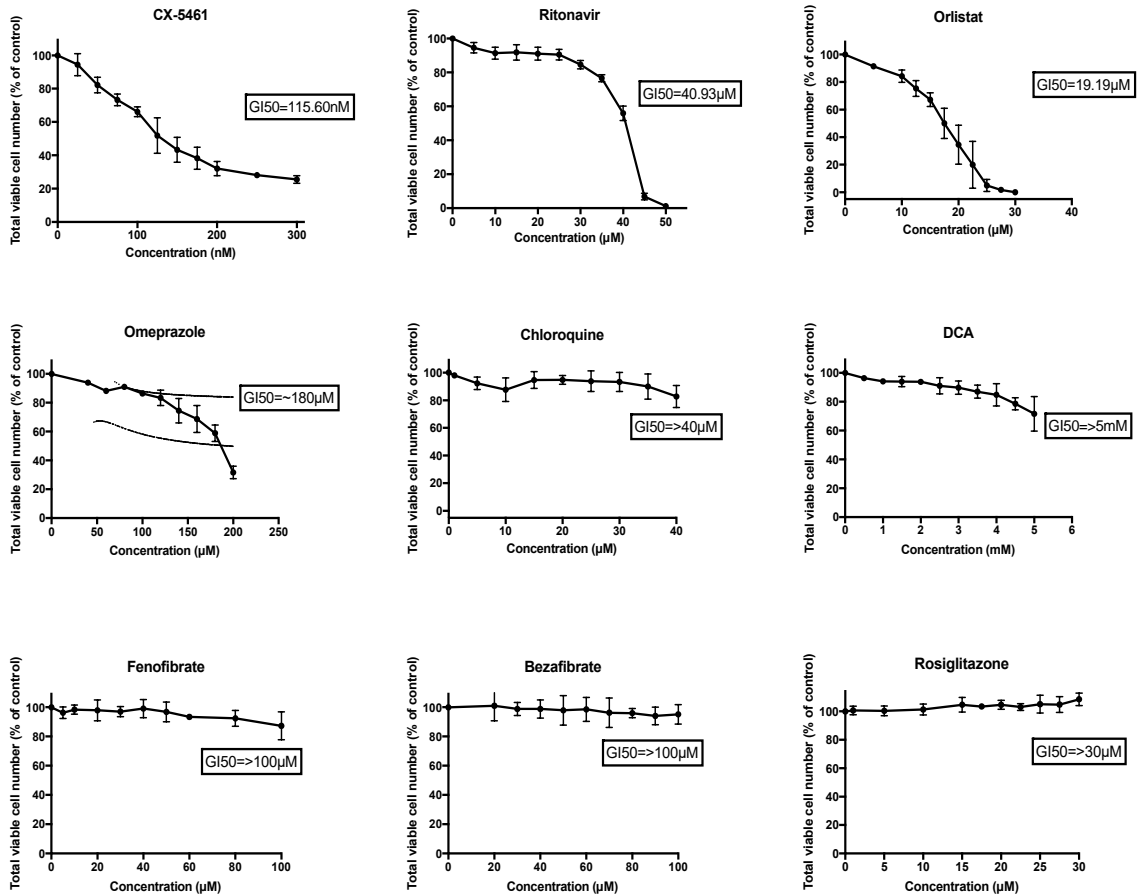
Figure 3-5: Dose response curves and GI$_{50}$s of drugs as single agents in MV4-11 cells.

MV4-11 cells were cultured for 96 h in the presence of the indicated drugs at a range of concentrations, up to a maximum rational concentration for testing (Section 3.1.3). Total viable cell number was determined using MTT (for chloroquine) or neutral red assays (for all other drugs). The dose resulting in a 50% growth inhibition (GI$_{50}$) values were calculated after fitting a non-linear curve to the data points (Methods Section 2.5.5). Graphs show the mean±SD of n=3 experiments.

59
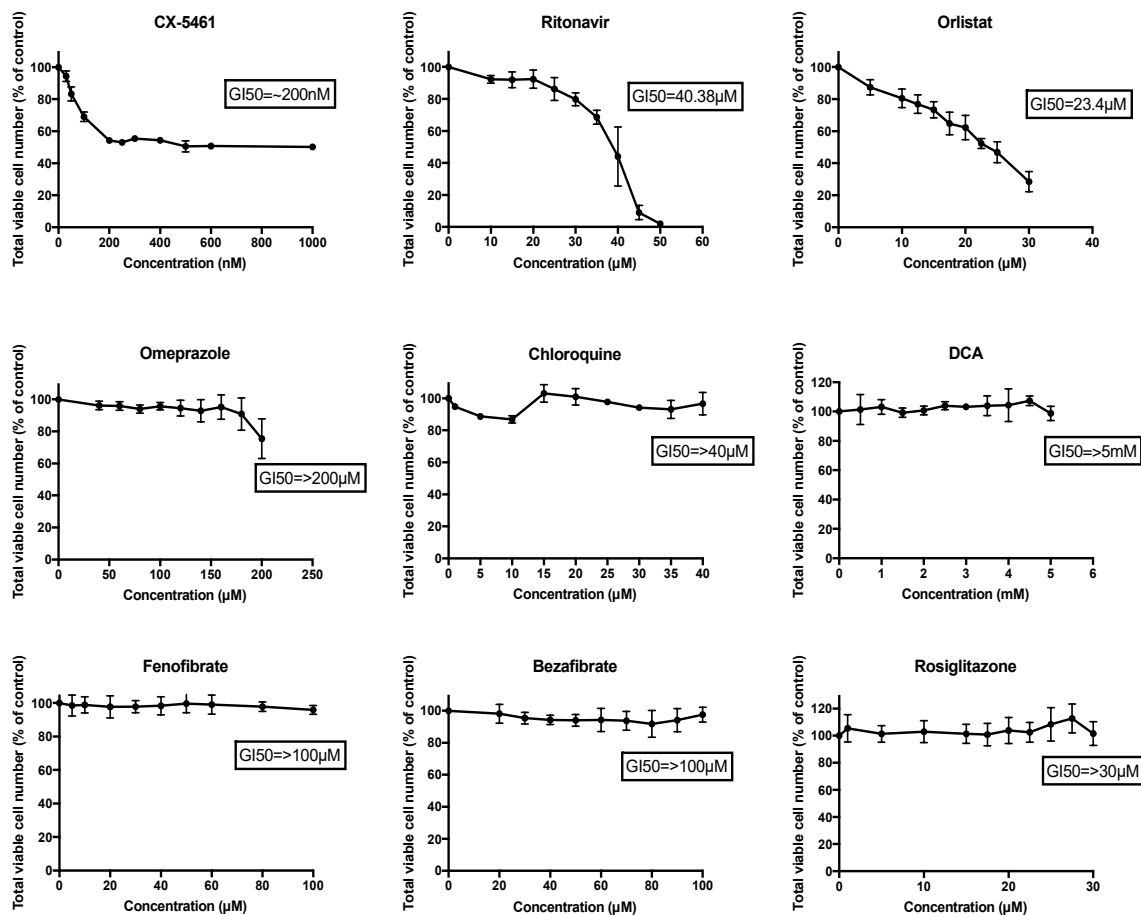
MOLM-13

Figure 3-6: Dose response curves and GI$_{50}$s of drugs as single agents in MOLM-13 cells.

MOLM-13 cells were cultured for 96 h in the presence of the indicated drugs at a range of concentrations, up to a maximum rational concentration for testing (Section 3.1.3). Total viable cell number was determined using MTT (for chloroquine) or neutral red assays (for all other drugs). The dose resulting in a 50% growth inhibition (GI$_{50}$) values were calculated after fitting a non-linear curve to the data points (Methods Section 2.5.5). Graphs show the mean±SD of n=3 experiments.

THP-1
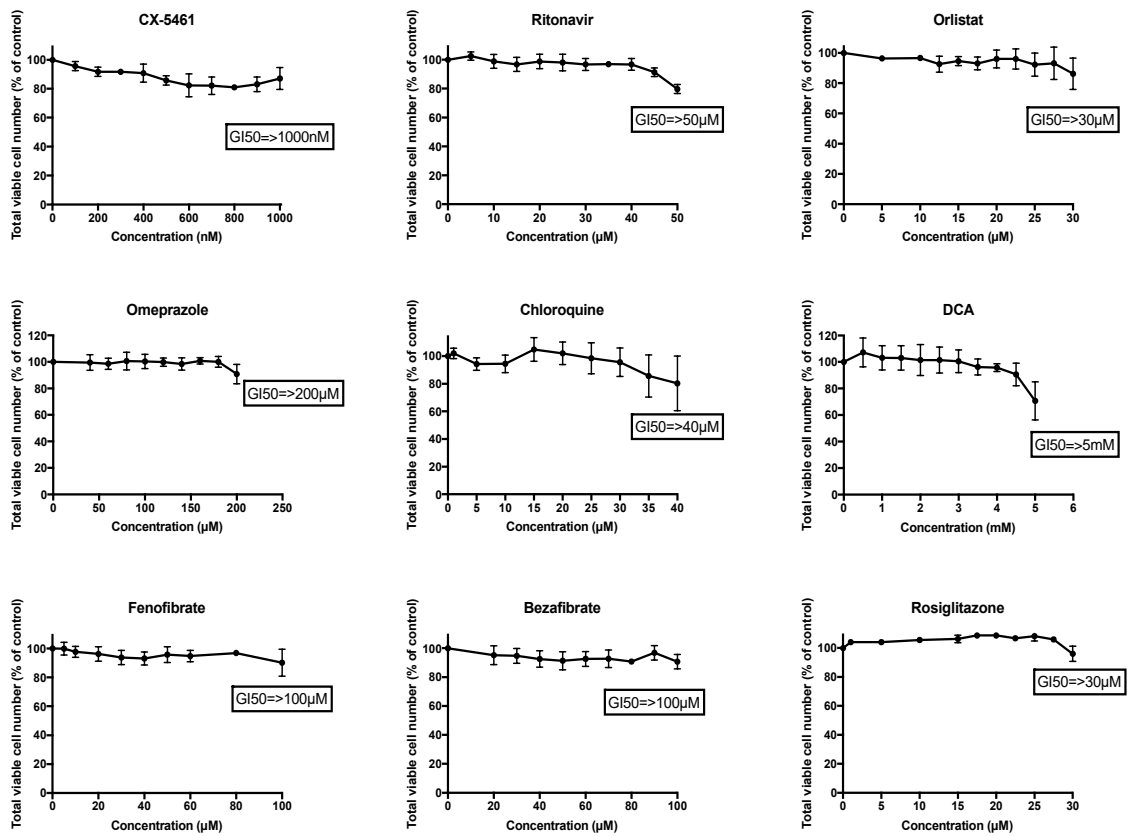
Figure 3-7: Dose response curves and GI$_{50}$s of drugs as single agents in THP-1 cells.

THP-1 cells were cultured for 96 h in the presence of the indicated drugs at a range of concentrations, up to a maximum rational concentration for testing (Section 3.1.3). Total viable cell number was determined using MTT (for chloroquine) or neutral red assays (for all other drugs). The dose resulting in a 50% growth inhibition (GI$_{50}$) values were calculated after fitting a non-linear curve to the data points (Methods Section 2.5.5). Graphs show the mean±SD of n=3 experiments.

MLL/AF9 NRAS
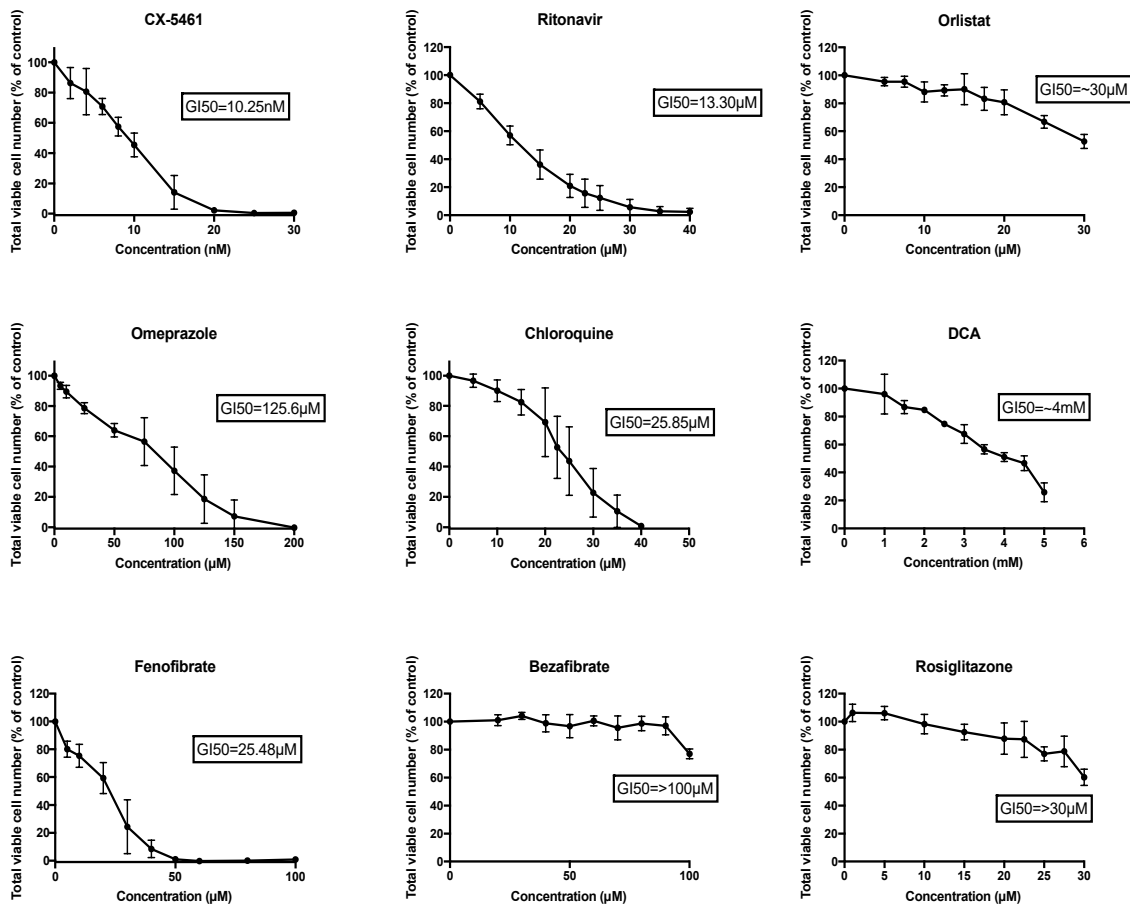
Figure 3-8: Dose response curves and GI$_{50}$s of drugs as single agents in MLL/AF9 NRAS cells.

MLL/AF9 NRAS cells were cultured for 96 h in the presence of the indicated drugs at a range of concentrations, up to a maximum rational concentration for testing (Section 3.1.3). Total viable cell number was determined using MTT (for chloroquine) or neutral red assays (for all other drugs). The dose resulting in a 50% growth inhibition (GI$_{50}$) values were calculated after fitting a non-linear curve to the data points (Methods Section 2.5.5). Graphs show the mean±SD of n=3 experiments.

3.2.3 Combination testing of metabolism drugs with CX-5461 (4 main cell lines)

Based on the results from the viability assays with the drugs as single agents (Table 3-4), non-constant ratio combination testing was performed with five concentrations of CX-5461 and three concentrations of the metabolism drugs, up to the $GI_{50}s$ previously determined or the maximum concentration tested, whichever was lower. Total viable cell number was determined after 96 h of treatment and the combination index calculated using CompuSyn (Methods section 2.5.5). Synergy was defined as a combination index below 0.75 (based on recommended guidelines for categorising synergism [123])and drug combinations were considered promising if synergy was observed in 2 or more cell lines. Figure 3-9 to Figure 3-16 show the viability results and CI values, which are summarised in Table 3-6.

3.2.3.1 CX-5461 + ritonavir

The best combination effect of CX-5461 and ritonavir was observed in the MLL/AF9 NRAS cell line (Figure 3-9d), where 14/15 of the drug combinations tested were synergistic, particularly at the highest concentration of ritonavir used (12μM). In the MOLM-13 cell line (Figure 3-9b) 9/15 of the drug combinations were synergistic, particularly with the lowest dose of ritonavir used (25μM). In the MV4-11 cell line (Figure 3-9a) none of the combinations had a synergistic effect on cell viability. The THP-1 cell line (Figure 3-9c), combination testing resulted in no obvious change in viability from the single agents, however, the CIs indicated the combinations were synergistic (with 50 μM ritonavir) or highly antagonistic (>1000; with 15 or 30μM ritonavir). These CI appear to result from calculation artefacts, the cause of such calculation artefacts is discussed in Section 3.1.3.

Figure 3-9: Combination testing of CX-5461 with ritonavir in AML cell lines.

AML cell lines a) MV4-11, b) MOLM-13, c) THP-1 and d) MLL/AF9 NRAS were cultured for 96 h in the presence of CX-5461 or ritonavir (rit), as single agents or in combination. Total viable cell number was determined using the neutral red assay. Graphs show the mean±SD of n=3 experiments. To determine if a combination was synergistic, the combination index (CI) of each data point was calculated using CompuSyn and displayed in the inlayed table (CI <0.75 considered synergistic, shaded green). Where CI values were greater than 1000, '>1000' only was displayed.

CX-5461 + Ritonavir

a) MV4-11
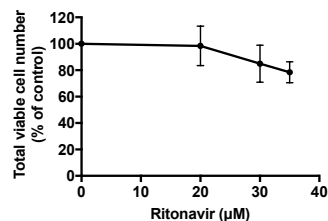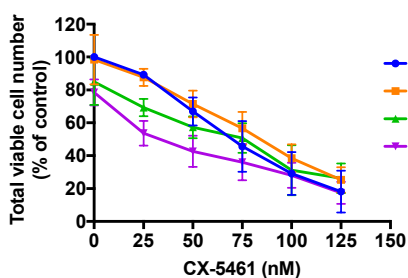
Combination index (CI)		CX-5461 (nM)				
		25	50	75	100	125
Ritonavir (µM)	20	1.568	1.677	1.752	1.632	1.523
	30	1.345	1.584	1.833	1.641	1.743
	35	1.226	1.415	1.588	1.655	1.524

b) MOLM-13
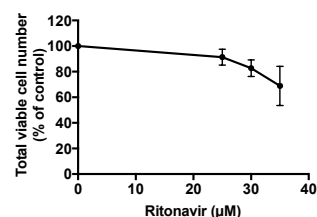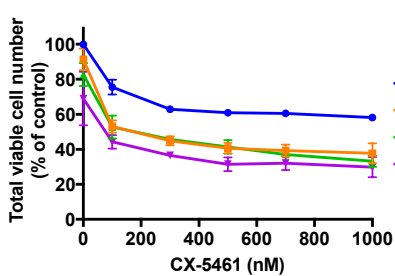
Combination index (CI)		CX-5461 (nM)				
		100	300	500	700	1000
Ritonavir (µM)	25	0.683	0.651	0.631	0.637	0.647
	30	0.802	0.778	0.752	0.712	0.680
	35	0.823	0.773	0.735	0.751	0.737

c) THP-1
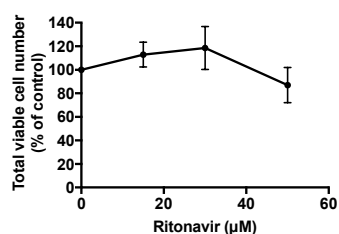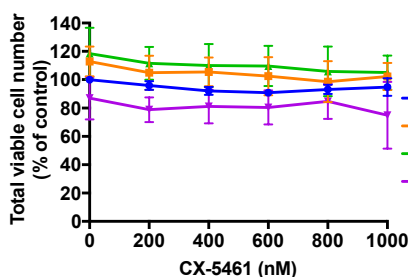
Combination index (CI)		CX-5461 (nM)				
		100	300	500	700	1000
Ritonavir (µM)	15	>1000	>1000	>1000	>1000	>1000
	30	>1000	>1000	>1000	>1000	>1000
	50	0.651	0.678	0.669	0.735	0.616

d) MLL/AF9 NRAS
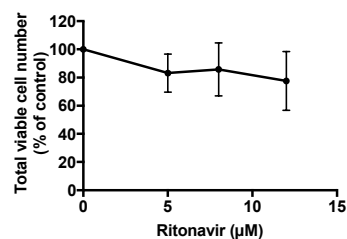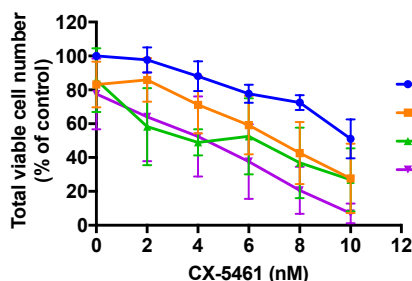
Combination index (CI)		CX-5461 (nM)				
		2	4	6	8	10
Ritonavir (µM)	5	1.666	0.679	0.685	0.645	0.589
	8	0.261	0.375	0.602	0.577	0.579
	12	0.368	0.422	0.444	0.395	0.279

3.2.3.2 CX-5461 + orlistat

In the MV4-11 cell line (Figure 3-10a) 10/15 of the combinations of CX-5461 and orlistat were synergistic, particularly with concentrations of >50nM CX-5461 and 8μM or 11μM orlistat. In the MOLM-13 cell line (Figure 3-10b) 11/15 of the combinations were synergistic. In contrast, none of the combinations of CX-5461 and orlistat in the MLL/AF9 NRAS cell line (Figure 3-10d) were synergistic. The THP-1 cell line (Figure 3-10c) did not provide useful CI readouts due to calculation artefacts, as for the CX-5461 and ritonavir combination (see Section 3.2.3.9).

Figure 3-10: Combination testing of CX-5461 with orlistat in AML cell lines.

AML cell lines a) MV4-11, b) MOLM-13, c) THP-1 and d) MLL/AF9 NRAS were cultured for 96 h in the presence of CX-5461 or orlistat (orl), as single agents or in combination. Total viable cell number was determined using the neutral red assay. Graphs show the mean±SD of n=3 experiments. To determine if a combination was synergistic, the combination index (CI) of each data point was calculated using CompuSyn and displayed in the inlayed table (CI <0.75 considered synergistic, shaded green). Where CI values were greater than 1000, '>1000' only was displayed.

CX-5461 + Orlistat

a) MV4-11

Combination index (CI)		CX-5461 (nM)				
		25	50	75	100	125
Orlistat (µM)	5	1.030	0.989	0.906	0.651	0.516
	8	0.865	0.747	0.666	0.581	0.589
	11	0.866	0.724	0.613	0.373	0.510

b) MOLM-13

Combination index (CI)		CX-5461 (nM)				
		100	300	500	700	1000
Orlistat (µM)	10	0.861	0.582	0.747	0.831	0.966
	20	0.812	0.640	0.616	0.588	0.611
	30	0.570	0.270	0.329	0.310	0.311

c) THP-1

Combination index (CI)		CX-5461 (nM)				
		200	400	600	800	1000
Orlistat (µM)	10	0.948	0.866	0.671	0.607	0.699
	20	1.145	1.359	1.089	0.905	0.885
	30	1.339	1.031	0.986	1.175	0.914

d) MLL/AF9 NRAS

Combination index (CI)		CX-5461 (nM)				
		2	4	6	8	10
Orlistat (µM)	10	1.012	1.160	1.023	1.057	0.960
	20	0.937	1.095	1.223	1.298	1.262
	25	1.273	1.390	1.346	1.239	0.847

3.2.3.3 CX-5461 + omeprazole

The best combination effect of CX-5461 and omeprazole was observed in the MOLM-13 cell line (Figure 3-11b), where all 15 combinations were synergistic. In the MLL/AF9 NRAS (Figure 3-11d) one combination was synergistic, the lowest of each of the drugs used (2nM CX-5461 with 30µM omeprazole). In contrast, none of the combinations of CX-5461 and omeprazole were synergistic in the MV4-11 cell lines (Figure 3-11a). The THP-1 cell line (Figure 3-11c) did not provide useful CI readouts due to calculation artefacts (see Section 3.2.3.9).

Figure 3-11: Combination testing of CX-5461 with omeprazole in AML cell lines.

AML cell lines a) MV4-11, b) MOLM-13, c) THP-1 and d) MLL/AF9 NRAS were cultured for 96 h in the presence of CX-5461 or omeprazole (ome), as single agents or in combination. Total viable cell number was determined using the neutral red assay. Graphs show the mean±SD of n=3 experiments. To determine if a combination was synergistic, the combination index (CI) of each data point was calculated using CompuSyn and displayed in the inlayed table (CI <0.75 considered synergistic, shaded green). Where CI values were greater than 1000, '>1000' only was displayed.

CX-5461 + Omeprazole

a) MV4-11

Combination index (CI)		CX-5461 (nM)				
		25	50	75	100	125
Omeprazole (µM)	125	1.335	1.340	1.388	1.231	1.046
	150	1.218	1.216	1.353	1.194	1.097
	175	1.204	1.163	1.168	1.021	0.931

b) MOLM-13

Combination index (CI)		CX-5461 (nM)				
		100	300	500	700	1000
Omeprazole (µM)	100	0.692	0.329	0.332	0.311	0.268
	150	0.410	0.232	0.231	0.202	0.179
	200	0.288	0.206	0.169	0.141	0.093

c) THP-1

Combination index (CI)		CX-5461 (nM)				
		200	400	600	800	1000
Omeprazole (µM)	100	0.670	0.667	0.614	0.621	0.604
	150	0.844	0.799	0.861	0.886	0.830
	200	1.045	1.044	0.982	0.965	0.836

d) MLL/AF9 NRAS

Combination index (CI)		CX-5461 (nM)				
		2	4	6	8	10
Omeprazole (µM)	30	0.686	0.949	1.056	1.068	1.014
	60	0.801	0.925	1.117	1.187	1.214
	90	1.095	1.182	1.250	1.091	0.838

3.2.3.4 CX-5461 + chloroquine

There was a strong combination effect of CX-5461 + chloroquine in the MOLM-13 cell line (Figure 3-12b), with doses of chloroquine as low as 5μM resulting in a synergistic effect on cell viability when combined with CX-5461, and a total of 12/15 synergistic combinations. In the MV4-11 cell line (Figure 3-12a) 9/15 of the combinations were synergistic, particularly with CX-5461 and 40μM chloroquine. In the MLL/AF9 cell line (Figure 3-12d) 5/15 of the combinations are synergistic, particularly with combinations of 10nM or 12nM CX-5461 with 20μM or 25μM chloroquine. Interestingly, in the THP-1 cell line (Figure 3-12c) there is a decrease in viability with increasing concentrations of CX-5461 and 40μM chloroquine, dropping to approximately 50% viability with the 1000nM CX-5461 combination and 3/15 of the combinations are synergistic. In contrast to the combinations with other metabolism-modifying drugs were the CIs result from calculation artefacts, this appears to be the only true combination effect in the THP-1 cell line.

Figure 3-12: Combination testing of CX-5461 with chloroquine in AML cell lines.

AML cell lines a) MV4-11, b) MOLM-13, c) THP-1 and d) MLL/AF9 NRAS were cultured for 96 h in the presence of CX-5461 or chloroquine (CQ), as single agents or in combination. Total viable cell number was determined using the MTT assay. Graphs show the mean±SD of n=3 experiments. To determine if a combination was synergistic, the combination index (CI) of each data point was calculated using CompuSyn and displayed in the inlayed table (CI <0.75 considered synergistic, shaded green). Where CI values were greater than 1000, '>1000' only was displayed.

CX-5461 + Chloroquine

a) MV4-11
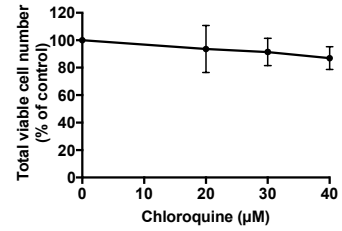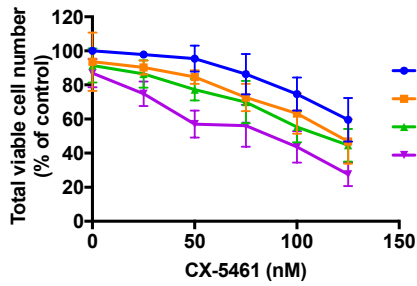
Combination index (CI)		CX-5461 (nM)				
		25	50	75	100	125
Chloroquine (µM)	20	0.969	0.935	0.810	0.827	0.732
	30	0.849	0.745	0.796	0.718	0.710
	40	0.492	0.426	0.581	0.574	0.496

b) MOLM-13
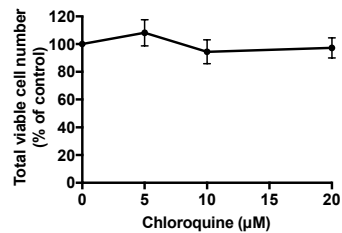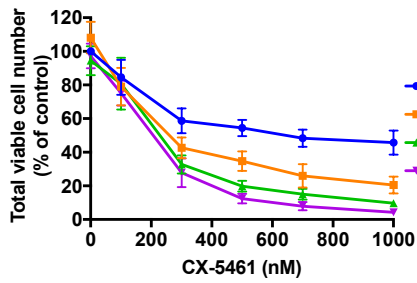
Combination index (CI)		CX-5461 (nM)				
		100	300	500	700	1000
Chloroquine (µM)	5	0.911	0.392	0.418	0.351	0.341
	10	1.176	0.311	0.231	0.208	0.165
	20	1.097	0.360	0.215	0.172	0.124

c) THP-1
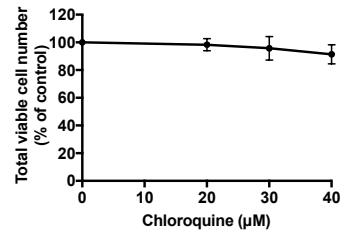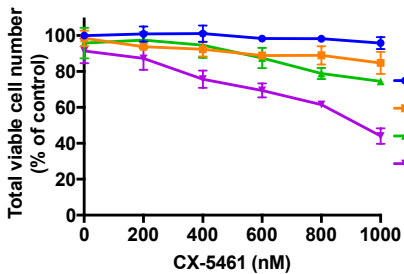
Combination index (CI)		CX-5461 (nM)				
		200	400	600	800	1000
Chloroquine (µM)	20	0.721	0.804	0.806	0.927	0.906
	30	1.474	1.246	0.974	0.849	0.851
	40	0.943	0.775	0.756	0.722	0.593

d) MLL/AF9 NRAS
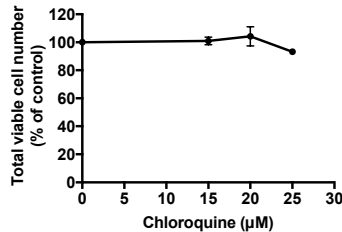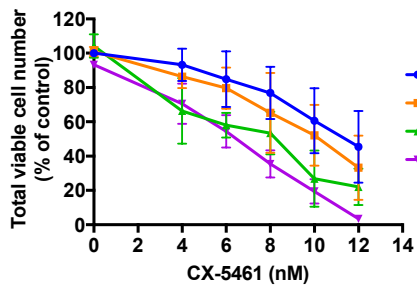
Combination index (CI)		CX-5461 (nM)				
		4	6	8	10	12
Chloroquine (µM)	15	1.127	1.211	1.104	1.054	0.889
	20	0.764	0.847	0.961	0.708	0.737
	25	0.918	0.859	0.747	0.622	0.330

71

CX-5461 + DCA

Of the four cell lines, the MLL/AF9 cell line (Figure 3-13d) had the most robust combination effect with CX-5461 + DCA treatment, with all combinations testing being synergistic. In the MOLM-13 cell line (Figure 3-13b) 6/15 of the combinations were synergistic, particularly in combination with 5mM DCA. In the MV4-11 cell line (Figure 3-13a) 3/15 of the combinations were synergistic. Again, the THP-1 cell line (Figure 3-13c) did not provide useful CI readouts due to calculation artefacts, see Section 3.2.3.9.

Figure 3-13: Combination testing of CX-5461 with DCA in AML cell lines.

AML cell lines a) MV4-11, b) MOLM-13, c) THP-1 and d) MLL/AF9 NRAS were cultured for 96 h in the presence of CX-5461 or DCA, as single agents or in combination. Total viable cell number was determined using the neutral red assay. Graphs show the mean±SD of n=3 experiments. To determine if a combination was synergistic, the combination index (CI) of each data point was calculated using CompuSyn and displayed in the inlayed table (CI <0.75 considered synergistic, shaded green). Where CI values were greater than 1000, '>1000' only was displayed.

CX-5461 + DCA

a) MV4-11
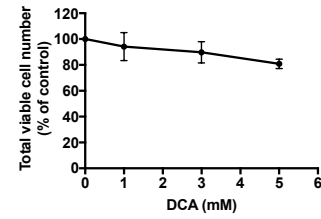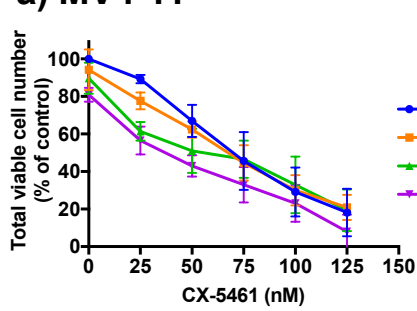
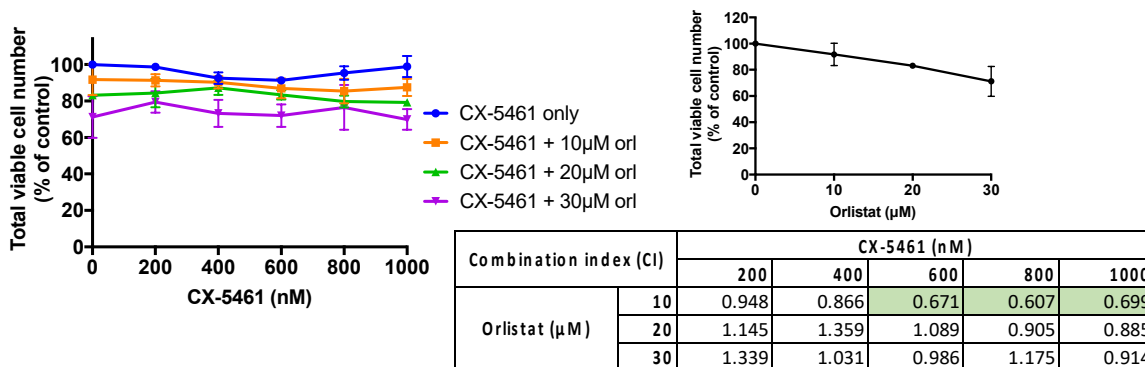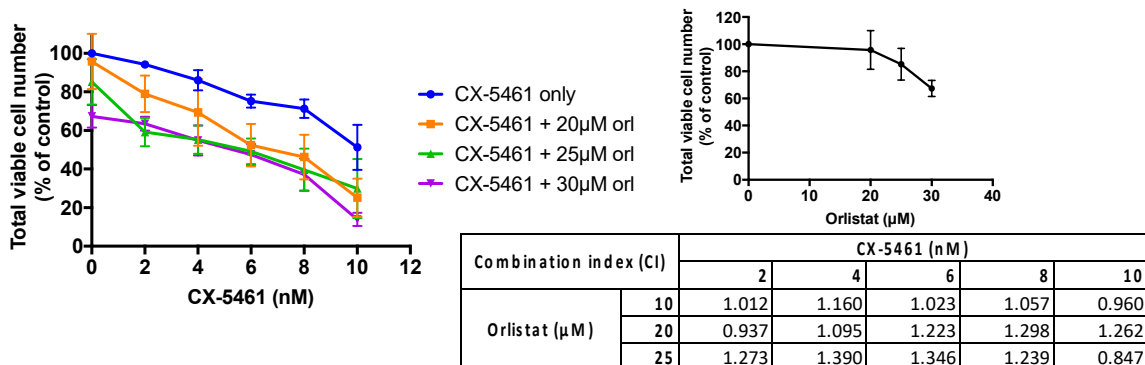| Combination index (CI)		CX-5461 (nM)				
		25	50	75	100	125
DCA (mM)	1	0.786	0.993	1.042	1.037	1.039
	3	0.610	0.853	0.129	1.124	1.002
	5	0.615	0.756	0.876	0.906	0.635

b) MOLM-13
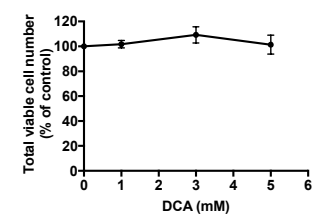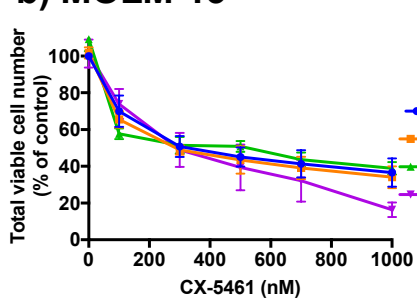
Combination index (CI)		CX-5461 (nM)				
		100	300	500	700	1000
DCA (mM)	1	0.780	0.746	0.859	0.893	0.891
	3	0.449	0.887	1.411	1.218	1.259
	5	1.520	0.746	0.652	0.536	0.176

c) THP-1
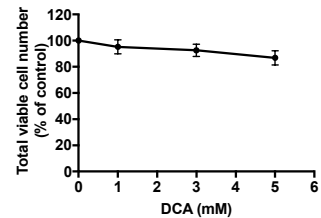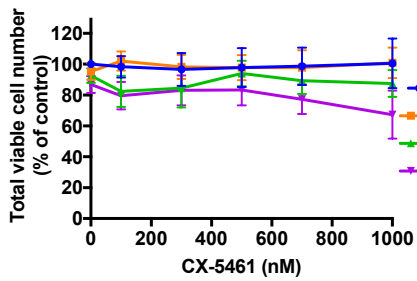
Combination index (CI)		CX-5461 (nM)				
		100	300	500	700	1000
DCA (mM)	1	396.850	5.190	6.280	7.512	396.850
	3	>1000	>1000	224.11	>1000	>1000
	5	>1000	>1000	>1000	>1000	>1000

d) MLL/AF9 NRAS
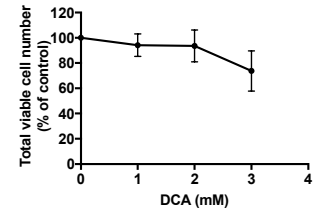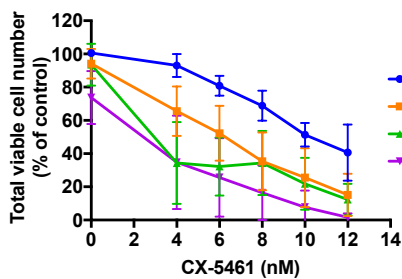
Combination index (CI)		CX-5461 (nM)				
		4	6	8	10	12
DCA (mM)	1	0.524	0.623	0.588	0.584	0.498
	2	0.319	0.458	0.650	0.572	0.470
	3	0.400	0.437	0.409	0.311	0.151

In the MLL/AF9 NRAS cell lines (Figure 3-14d) 1/15 of the combinations of CX-5461 and fenofibrate are synergistic (12nM CX-5461 with 5μM fenofibrate). While in the MV4-11 cell line (Figure 3-14a) none of the combinations of CX-5461 and fenofibrate were synergistic. The combination data in the MOLM-13 (Figure 3-14b) and THP-1 (Figure 3-14c) cell lines did not provide useful CI readouts due to calculation artefacts, see Section 3.2.3.9.

Figure 3-14: Combination testing of CX-5461 with fenofibrate in AML cell lines.

AML cell lines a) MV4-11, b) MOLM-13, c) THP-1 and d) MLL/AF9 NRAS were cultured for 96 h in the presence of CX-5461 or fenofibrate (fen), as single agents or in combination. Total viable cell number was determined using the neutral red assay. Graphs show the mean±SD of n=3 experiments. To determine if a combination was synergistic, the combination index (CI) of each data point was calculated using CompuSyn and displayed in the inlayed table (CI <0.75 considered synergistic, shaded green). Where CI values were greater than 1000, '>1000' only was displayed.

CX-5461 + Fenofibrate
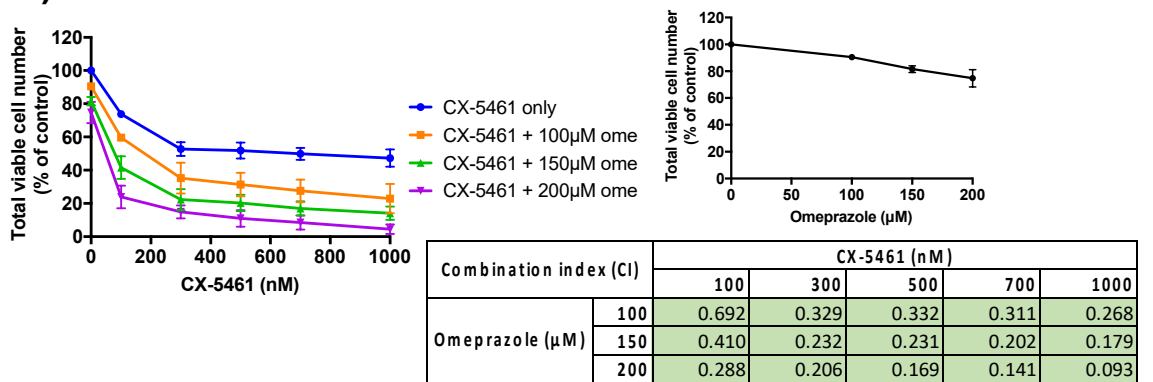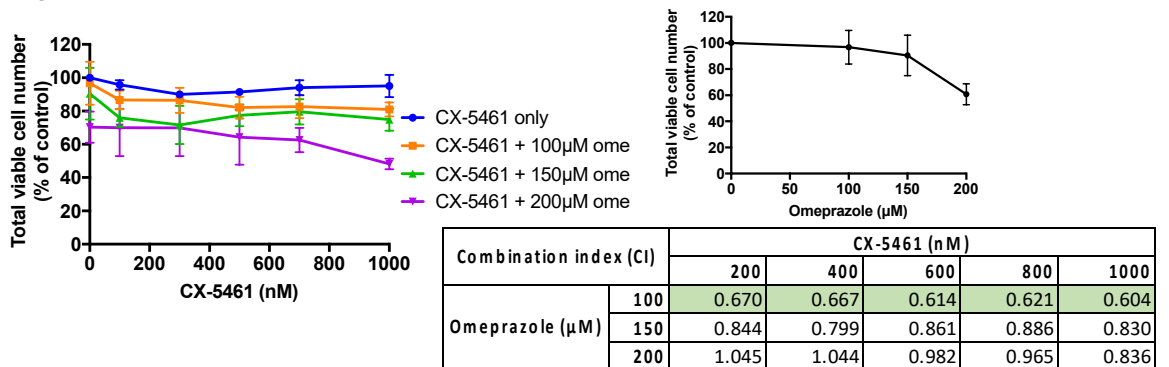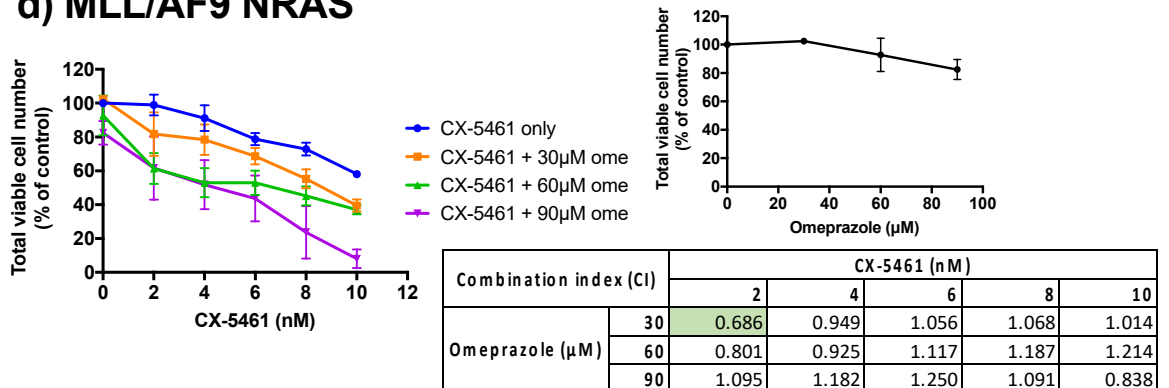
a) MV4-11
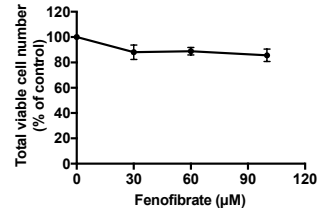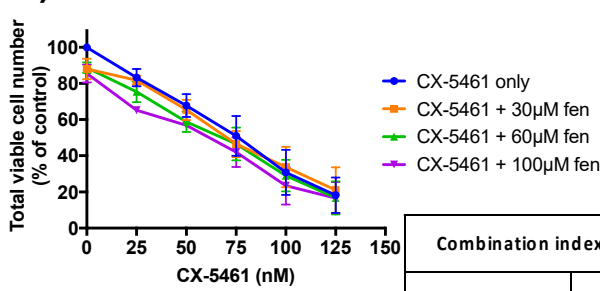
Combination index (CI)		CX-5461 (nM)				
		25	50	75	100	125
	30	1.053	1.173	1.119	1.105	0.968
Fenofibrate (μM)	60	1.001	1.091	1.177	1.031	0.854
	100	0.886	1.152	1.132	0.900	0.869

b) MOLM-13
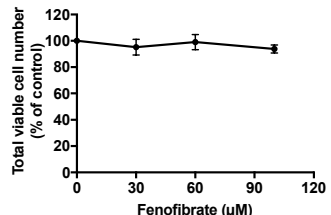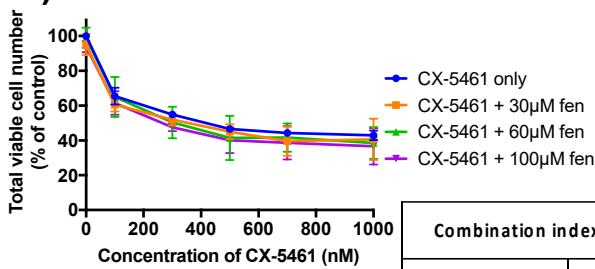
Combination index (CI)		CX-5461 (nM)				
		100	300	500	700	1000
	30	0.620	0.833	0.712	0.592	0.933
Fenofibrate (μM)	60	0.974	0.703	0.504	0.727	0.759
	100	0.684	0.540	0.444	0.537	0.634

c) THP-1
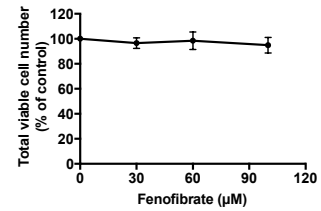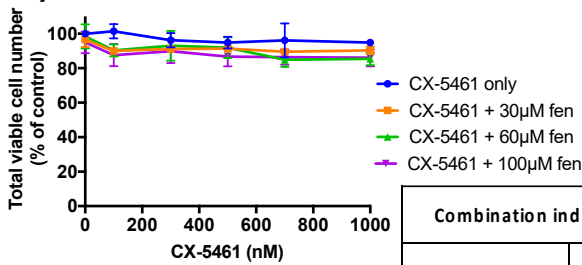
Combination index (CI)		CX-5461 (nM)				
		100	300	500	700	1000
	30	0.100	0.319	0.530	0.655	0.956
Fenofibrate (μM)	60	0.109	0.399	0.569	0.509	0.744
	100	0.089	0.299	0.399	0.549	0.771

d) MLL/AF9 NRAS
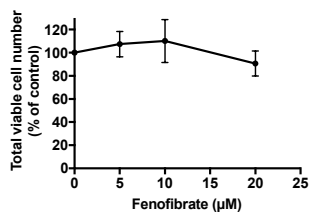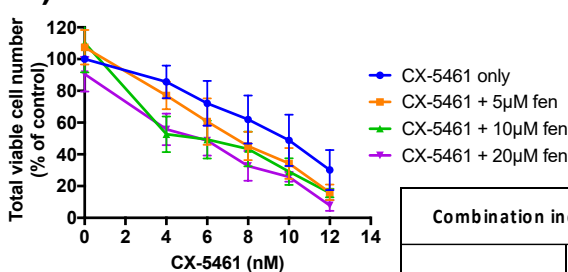
Combination index (CI)		CX-5461 (nM)				
		4	6	8	10	12
	5	0.970	0.982	0.967	0.966	0.748
Fenofibrate (μM)	10	0.809	0.987	1.097	1.016	0.854
	20	1.206	1.317	1.218	1.225	0.830

3.2.3.7 CX-5461 + bezafibrate

In the MV4-11 (Figure 3-15a), MOLM-13 (Figure 3-15b) and MLL/AF9 NRAS (Figure 3-15d) cell lines none of the combinations of CX-5461 and bezafibrate were synergistic. The THP-1 cell line (Figure 3-15c) did not provide useful CI readouts due to calculation artefacts, see Section 3.2.3.9.

Figure 3-15: Combination testing of CX-5461 with bezafibrate in AML cell lines.

AML cell lines a) MV4-11, b) MOLM-13, c) THP-1 and d) MLL/AF9 NRAS were cultured for 96 h in the presence of CX-5461 or bezafibrate (bez), as single agents or in combination. Total viable cell number was determined using the neutral red assay. Graphs show the mean±SD of n=3 experiments. To determine if a combination was synergistic, the combination index (CI) of each data point was calculated using CompuSyn and displayed in the inlayed table (CI <0.75 considered synergistic, shaded green). Where CI values were greater than 1000, '>1000' only was displayed.

CX-5461 + Bezafibrate

a) MV4-11

Combination index (CI)		CX-5461 (nM)				
		25	50	75	100	125
Bezafibrate (µM)	30	0.916	1.236	1.277	1.280	1.208
	60	0.887	1.239	1.402	1.281	1.208
	100	0.825	1.164	1.357	1.289	0.986

b) MOLM-13

Combination index (CI)		CX-5461 (nM)				
		100	300	500	700	1000
Bezafibrate (µM)	30	967.206	>1000	>1000	>1000	>1000
	60	>1000	>1000	>1000	>1000	>1000
	100	>1000	>1000	>1000	>1000	>1000

c) THP-1

Combination index (CI)		CX-5461 (nM)				
		100	300	500	700	1000
Bezafibrate (µM)	30	0.113	0.260	0.348	0.548	0.881
	60	0.102	0.244	0.419	0.494	0.657
	100	0.082	0.223	0.382	0.519	0.679

d) MLL/AF9 NRAS

Combination index (CI)		CX-5461 (nM)				
		4	6	8	10	12
Bezafibrate (µM)	30	1.500	1.512	1.207	1.060	0.871
	60	0.938	1.108	1.134	1.287	1.097
	100	12.727	1.744	1.370	1.202	0.977

In the MV4-11 (Figure 3-16a), MOLM-13 (Figure 3-16b) and MLL/AF9 NRAS (Figure 3-16d) cell lines none of the combinations of CX-5461 and rosiglitazone were synergistic. The THP-1 cell line (Figure 3-16c) did not provide useful CI readouts due to calculation artefacts, see Section 3.2.3.9.

Figure 3-16: Combination testing of CX-5461 with rosiglitazone in AML cell lines.

AML cell lines a) MV4-11, b) MOLM-13, c) THP-1 and d) MLL/AF9 NRAS were cultured for 96 h in the presence of CX-5461 or rosiglitazone (rosi), as single agents or in combination. Total viable cell number was determined using the neutral red assay. Graphs show the mean±SD of n=3 experiments. To determine if a combination was synergistic, the combination index (CI) of each data point was calculated using CompuSyn and displayed in the inlayed table (CI <0.75 considered synergistic, shaded green). Where CI values were greater than 1000, '>1000' only was displayed.

CX-5461 + Rosiglitazone

a) MV4-11

Combination index (CI)		CX-5461 (nM)				
		25	50	75	100	125
Rosiglitazone (μM)	10	1.145	1.206	1.321	1.265	1.140
	20	1.249	1.321	1.440	1.382	1.347
	30	0.949	1.331	1.507	1.244	1.332

b) MOLM-13

Combination index (CI)		CX-5461 (nM)				
		100	300	500	700	1000
Rosiglitazone (μM)	10	2.560	2.631	2.854	2.686	3.088
	20	4.272	4.876	5.383	5.537	5.757
	30	6.198	6.712	7.117	7.338	7.743

c) THP-1

Combination index (CI)		CX-5461 (nM)				
		100	300	500	700	1000
Rosiglitazone (μM)	10	0.453	0.745	0.900	1.249	1.357
	20	3.161	0.693	1.578	1.286	1.276
	30	0.979	1.360	1.767	1.428	1.415

d) MLL/AF9 NRAS

Combination index (CI)		CX-5461 (nM)				
		4	6	8	10	12
Rosiglitazone (μM)	10	1.608	1.293	1.270	1.181	0.934
	20	0.968	1.167	1.349	1.189	1.060
	25	1.238	1.290	1.292	1.156	1.280

3.2.3.9 Apparent CI calculation artefacts

In many cases in the THP-1 cell line, and in some cases in the MOLM-13 cell line, combination testing resulted in no change in viability from the single agents, however this resulted in a CI being calculated that indicated the combination was either highly synergistic or highly antagonistic. For example, in the THP-1 cell line with ritonavir treatment (Figure 3-9c). These CI appear to result from calculation artefacts, the cause of such calculation artefacts is discussed in Section 3.3.2.

3.2.3.10 Summary of combination testing

The combination testing results are summarised in Table 3-6. In summary, evaluation of CX-5461 with various metabolism-modifying drugs identified that CX-5461 and chloroquine was the most promising combination, with synergy observed in all four cell lines tested. Other promising combinations with CX-5461 were orlistat, ritonavir, omeprazole and DCA. Calculation artefacts were pronounced in the THP-1 cell line, and in some cases the MOLM-13 cell line, highlighting some of the limitations of the synergy testing which are further discussed in Section 3.3.2. A schematic summary of the results of the *in vitro* combination testing are shown in Figure 3-19.

3.2.4 Dose-response curves, GI50s and combination testing of chloroquine with CX-5461 (additional cell lines)

The most promising of the drug combinations, CX-5461 and chloroquine, was tested in additional human AML cell lines KG-1 and SKM-1, which were selected based on increasing the range of genetic characteristics being tested to include non-MLL mutants and p53 mutants (Table 3-1). These additional cell lines were tested as above, firstly with the drugs as a single agent over a range of concentrations, the total viable cell number determined using the MTT assay and the GI_{50} calculated (Figure 3-17). The cell viability of SKM-1 cells was not affected by CX-5461 or chloroquine up to the maximum concentration used (as justified in Section 3.1.3). KG-1 cells exhibited approximately a 40% decrease in total viable cell number at the maximum chloroquine concentration (40μM) tested and a GI_{50} of approximately 600nM with CX-5461. In response to CX-5461 treatment, they exhibit a similar dose-response curve to the MOLM-13 cells (Figure 3-6), where the viability plateaus out.

Non-constant ratio combination testing was then performed, as above, and shown in Figure 3-18. In the KG-1 cell line (Figure 3-18a), 3/15 of the combinations of CX-5641 and chloroquine were synergistic, with the greatest combination effect observed with combinations of 500nM and 700nM CX-5461. In the SKM-1 cell line (Figure 3-18b), all 15 combinations of CX-5461 and chloroquine were synergistic, particularly in combination with 40µM chloroquine. These results show that the combination of CX-5461 and chloroquine is effective in non-MLL mutant and p53 mutant AML cell lines.
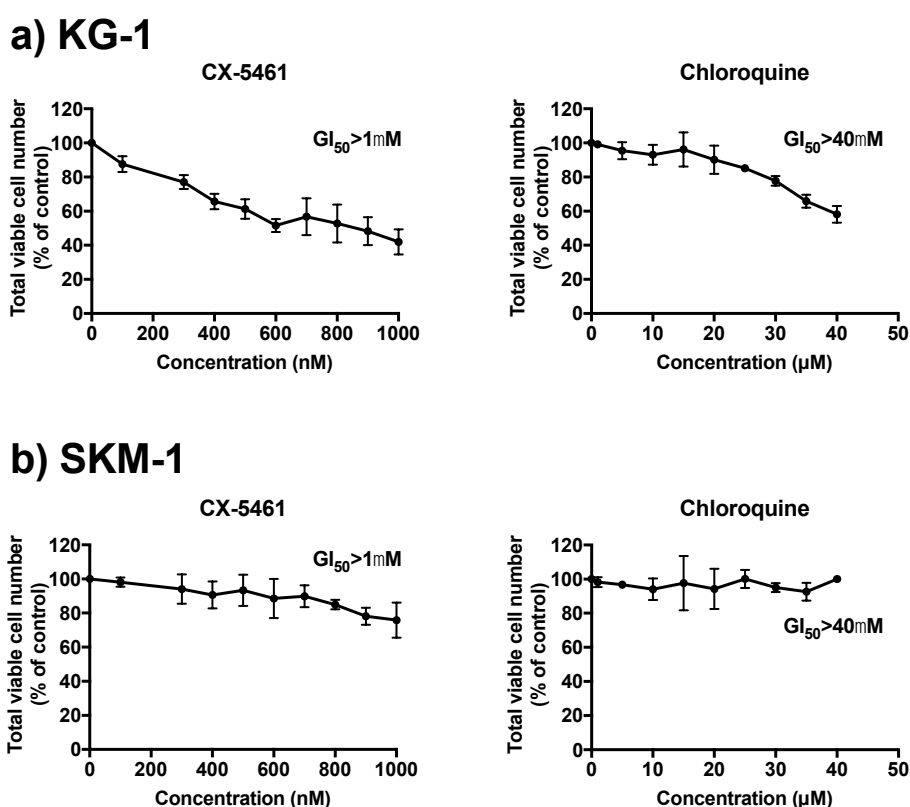
a) KG-1

b) SKM-1

Figure 3-17: Dose response curves and GI$_{50}$s of CX-5461 and chloroquine in additional AML cell lines

AML cell lines a) KG-1 and b) SKM-1 were cultured for 96 h in the presence of the indicated drugs at a range of concentrations, up to a maximum concentration for testing. Total viable cell number was determined using the MTT assay (Methods Section 2.5.2). The dose resulting in a 50% growth inhibition (GI$_{50}$) values were calculated after fitting a non-linear curve to the data points (Methods Section 2.5.5). Graphs show the mean ±SD of n=3 experiments.

Drugs	Maximum concentration tested*	GI$_{50}$±SD	
		Human	
		SKM-1 (No fusion, p53 mutant)	KG-1 (AML1-ETO, p53 null)
CX-5461 (nM)	1000	>1000	~600
Chloroquine (µM)	40	>40	>40

Table 3-5: GI$_{50}$s of CX-5461 and chloroquine in additional AML cell lines

Data from Figure *3-18*. Colour code: No colour = Sensitive (>25% drop in cell viability at maximum concentration Light grey = Some sensitivity (10-25% drop in cell viability at maximum concentration) Dark grey = Not sensitive (<10% drop in cell viability at maximum concentration).* Justified in Section 3.1.3.

CX-5461 + Chloroquine

a) KG-1

Combination index (CI)		CX-5461 (nM)				
		100	200	300	500	700
Chloroquine (µM)	10	1.175	0.805	1.032	0.705	0.621
	20	0.951	1.320	0.882	0.745	0.764
	30	1.035	1.109	0.956	0.797	0.784

b) SKM-1

Combination index (CI)		CX-5461 (nM)				
		100	200	300	500	700
Chloroquine (µM)	10	0.403	0.346	0.354	0.300	0.323
	20	0.563	0.607	0.331	0.344	0.289
	40	0.480	0.430	0.331	0.227	0.159
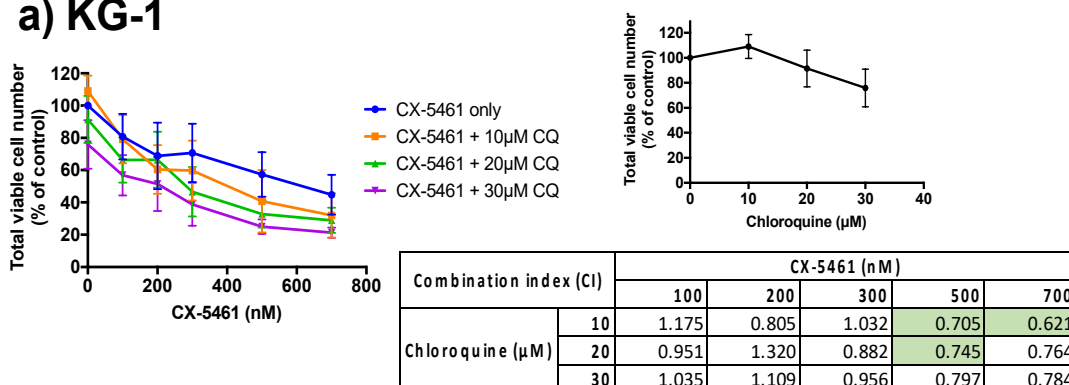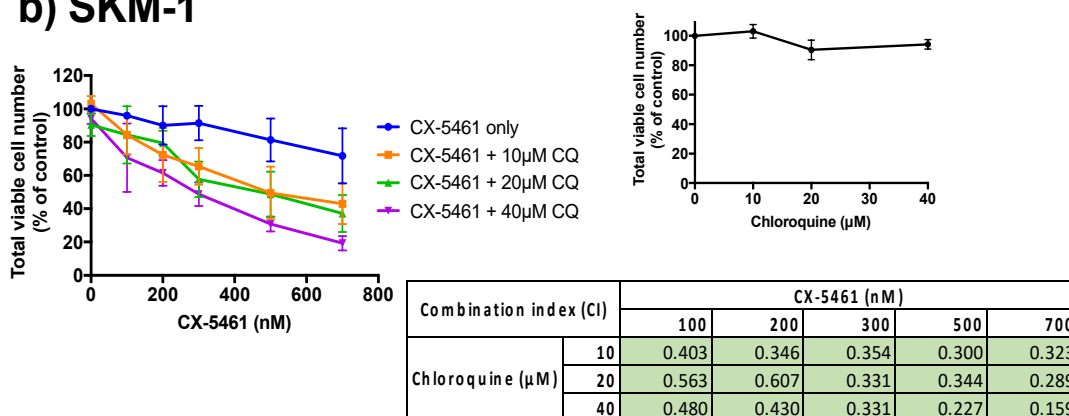
Figure 3-18: Combination testing of CX-5461 and chloroquine in additional AML cell lines.

AML cell lines a) KG-1 and b) SKM-1 cell lines were cultured for 96 h in the presence of CX-5461 or chloroquine (CQ), alone or in combination. Total viable cell number was determined using the MTT assay. Graphs show the mean±SD of n=3 experiments. In order to determine if a combination was synergistic the combination index of each data point was calculated using CompuSyn and displayed in the inlayed table (synergism was designated as a combination index (CI) value <0.75, shown in green).

CX-5461 in combination with:	Synergistic combinations (out of 15)					
	Cell line					
	Human	Human	Human	Mouse	Human	Human
	MV4-11 (MLL/AF4, p53 WT)	MOLM-13 (MLL/AF9, p53 WT)	THP-1 (MLL/AF9, p53 null)	MLL/AF9 NRAS (p53 WT)	KG-1 (AML1-ETO, p53 null)	SKM-1 (No fusion, p53 mutant)
Ritonavir	0	9	5*	14	NT	NT
Orlistat	10	11	3*	0	NT	NT
Omeprazole	0	15	5	1	NT	NT
Chloroquine	9	12	3	5	3	15
DCA	3	6	0	15	NT	NT
Fenofibrate	0	11*	13*	1	NT	NT
Bezafibrate	0	0	14*	0	NT	NT
Rosiglitazone	0	0	3*	0	NT	NT

Table 3-6: Summary of combination testing results

Data summarised from Figure *3-9* to Figure *3-16* and Figure *3-18*. Synergism was defined as a CI below 0.75. NT = not tested. * indicates results which are likely calculation artefacts from CI analysis.

Summary of combination testing with CX-5461

Compatible with neutral red or MTT assays?

NO → **Not evaluated in combination**
- Simvastatin
- Metformin

YES

Assessed combination in 4-6 cell lines

Synergy in ≥2 cell lines

Synergy in ≤1 cell lines

Selected for *in vivo* testing (Chapter 4)
- Orlistat
- Ritonavir
- Omeprazole
- Chloroquine
- DCA

Not tested *in vivo*
- Fenofibrate
- Bezafibrate
- Rosiglitazone
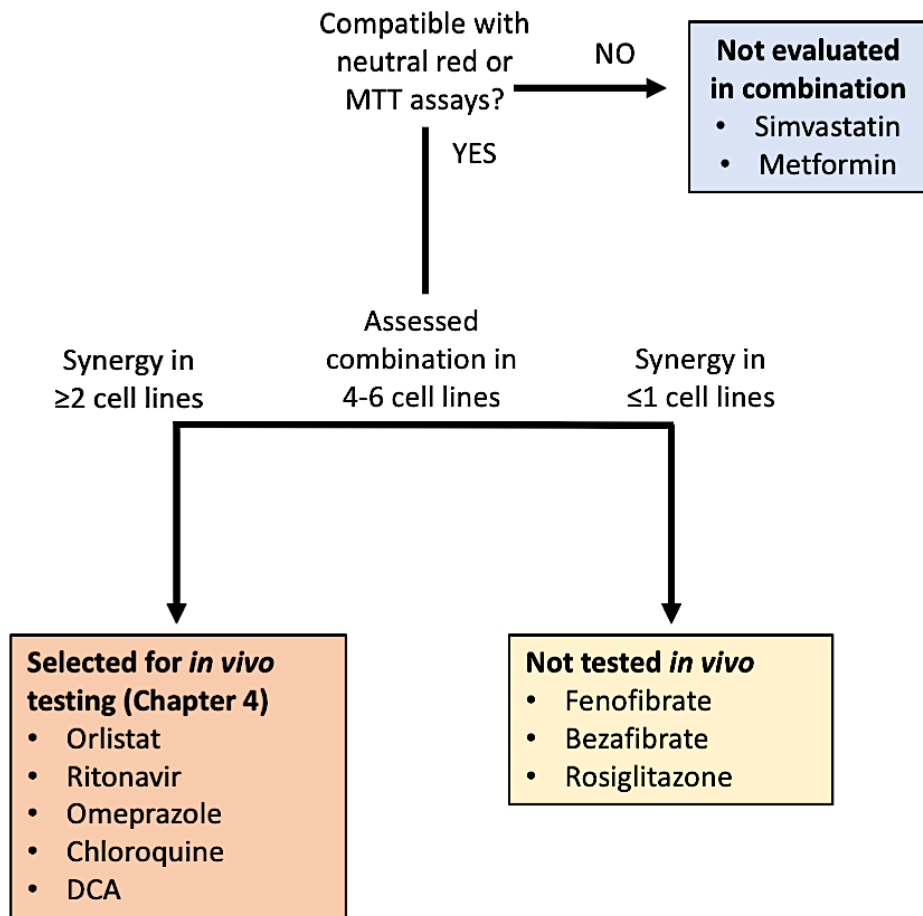
Figure 3-19: Schematic summary of evaluating combinations of metabolism-modifying drugs with CX-5461.

For combination testing, 4 cell lines were used for evaluation, with the exception of CX-5461 + chloroquine where 6 cell lines were used.

3.3 Discussion

This chapter aimed to test CX-5461 for synergy in combination with metabolism-modifying drugs in a panel of AML cell lines.

3.3.1 Dose-response curve analysis

Dose-response analysis of the drugs as single agents (Table 3-4 and Table 3-5) revealed the cell lines varied widely in their sensitivity, however, some patterns emerged.

The mouse-derived MLL/AF9 NRAS showed at least some sensitivity to all the drugs tested, and was more sensitive than the human cell lines, suggesting a greater reliance on ribosome biogenesis and a range of metabolic pathways compared to the human AML cell lines.

In terms of specific biological pathways, targeting ribosome biogenesis with CX-5461 was the most effective single-agent approach, with 5/6 cell lines showing at least some sensitivity up to the maximum concentration of 1µM (as justified in Section 3.1.3), which is consistent with the well-established role of ribosome biogenesis in malignant transformation and progression [78]. Ritonavir was highly effective in reducing cell viability, with 4/4 cell lines tested showing at least some sensitivity to the drug as a single agent. Confirming ritonavir's on-target activity as a glucose uptake inhibitor, at the concentrations used in these experiments, would be important to support this process as a promising therapeutic target. In the MLL/AF9 NRAS and THP-1 cells, this may correlate with a dependence on glycolysis as these cells show at least some sensitivity to DCA as a single agent. As single agents, orlistat, omeprazole and chloroquine were effective in reducing cell viability, as 3/4, 3/4 and 4/6 of the cell lines tested, respectively, showed at least some sensitivity to the drugs. Confirming orlistat and omeprazole's on target activity as fatty acid synthesis inhibitors and chloroquine's as an autophagy inhibitor, at concentrations used in these experiments, would be important to support these processes as promising therapeutic approaches. MLL/AF9 NRAS was the only cell line of the four tested to show a reduction in cell viability in response to fenofibrate, bezafibrate and rosiglitazone treatment as single agents. Confirmation on-target activity of these drugs as cholesterol synthesis inhibitors, at the

concentrations used in these experiments, would be important to determine if this process is a promising therapeutic approach, as it is possible that full inhibition of this pathway was not achieved with the concentrations used.

The mutation status of the cell lines also appears to play a role in the sensitivity of the cell lines to the drugs as single agents. In particular, cell lines with wild type p53 status were more sensitive to CX-5461 than those with mutant or null p53 status. In order of most to least sensitive; MLL/AF9 NRAS (p53 WT), MV4-11 (p53 WT), MOLM-13 (p53 WT), KG-1 (p53 null), SKM-1 (p53 mutant) and THP-1 (p53 null). This is consistent with the reported p53-dependent effects of CX-5461 in AML in Hein et al. [1], (further discussed in Section 5.1.1), however, this same study found no correlation between p53 status and cell viability (in terms of cell death). The discrepancy between the literature and the results in this thesis could be due to the smaller panel of cell lines used in this thesis, or to the different methods used to measure viability (i.e. neutral red or MTT vs. cell death by propidium iodide exclusion). No other pattern between mutation status and drug sensitivity was apparent, given the small panel of cell lines utilised.

3.3.2 Combination testing and synergy analysis

The combination testing was successful in identifying several metabolism-modifying therapies that work synergistically with CX-5461 to reduce cell viability of AML cells *in vitro* (Table 3-6), with CX-5461 and chloroquine being the most promising combination as synergy was observed for all 6 cell lines tested. This suggests a potential role for autophagy in sensitising AML cells to CX-5461 treatment, across a broad range of mutations, including p53, MLL fusion and NRAS status (Table 3-1). Targeting fatty acid synthesis was also promising as a means to sensitise AML cells to CX-5461, as synergy was seen with CX-5461 + orlistat and CX-5461 + omeprazole in multiple cell lines. This is consistent with the sensitivity of the cell lines to the fatty acid synthesis inhibitors as single agents (Table 3-4). Combination testing results also suggest that reversing the glycolytic phenotype with DCA and inhibiting glucose uptake with ritonavir are promising strategies when combined with CX-5461 treatment, in addition to being promising single-agent approaches (Table 3-4). None of the cholesterol-modifying drugs synergised with CX-5461 treatment in any of the cell lines, suggesting that

cholesterol metabolism might not play a pro-survival role in the response of AML cells to ribosome biogenesis inhibition with CX-5461.

However, several caveats must be considered when interpreting the results of the synergy testing. First, the results of the combination testing must be interpreted with caution in the context of the targets of the drugs as many established metabolism-modifying therapies have multiple known targets in healthy tissues as well as cancer. For example, omeprazole is known to inhibit fatty acid synthase [152], modulate the lysosomal transport pathway [154] and act as an AHR ligand [155]. As outlined in Section 3.1.2.7, some of the metabolism-modifying agents have the potential to modulate ribosome biogenesis under certain conditions. This can make biological interpretation of the synergy results difficult, unless further mechanistic analysis, including genetic approaches and alternative inhibitors, is conducted. For this reason, promising combinations from the *in vitro* testing, that also act synergistically to improve survival *in vivo* (Chapter 4), were subjected to mechanistic analysis to determine how they act synergistically together (Chapter 5). A limitation of the studies is that mechanistic analysis was not performed to confirm the action of all the drugs utilised in these studies as metabolism-modifying agents, nor for their effects on ribosome biogenesis.

In addition, a limited range of drug concentrations can be tested: if the concentration of either drug is too high it is difficult to determine if the combination is synergistic as the 'effect' of the single agents is already close to 1. For this reason, the maximum concentrations of the single agents was capped at approximately the GI_{50}. This gives the assay a limited dynamic range and some drug combinations of interest might be missed if synergism is only observed at higher concentrations. Further *in vivo* testing of any promising drug combinations does not suffer from this same limitation, but has different limitations, such as that the maximum drug dosage is dependent on tolerability.

Another limitation of the synergy testing is that the algorithms underlying the CompuSyn program were unable to calculate a reliable CI where there was not a complete dose-response curve of the single drug. There were many instances where a dose-response curve was not achieved with the drugs as single agents, particularly in

the THP-1 cell line (Figure 3-7), and to a lesser extent in the MOLM-13 cell line (Figure 3-6). In order to calculate the CI values, the CompuSyn program requires a dose-response curve of the effects of the drugs as single agents. In the case where a curve cannot be fitted across the data points, the curve is predicted, thus likely to be inaccurate and will affect the results of the synergy testing. This issue is particularly pronounced for the THP-1 cell line, which has no or limited sensitivity to all the drugs tested, where many combinations, according to the CI, appear highly antagonistic (e.g. CX-5461 + DCA, Figure 3-13c) or synergistic (e.g. CX-5461 + fenofibrate, Figure 3-14c), despite the viability curves indicating the combinations have a similar effect on cell viability to the single drugs alone. Thus, CI values must be interpreted with caution in the case where one or both of the drugs do not produce a dose-dependent curve as a single agent. The only drug combination which does appear to have CI values that were not affected by calculation artefacts in the THP-1 cell line is CX-5461 + chloroquine (Figure 3-12c).

3.3.3 Summary of synergy testing

In summary, metabolism-modifying drugs ritonavir, orlistat, omeprazole, chloroquine and DCA were found to act synergistically with ribosome biogenesis inhibitor CX-5461 *in vitro* in multiple AML cell lines. These promising combinations were then taken forward for *in vivo* testing to determine if they synergise to improve the survival of tumour bearing mice (Chapter 4).

Chapter 4   Testing promising combination therapies *in vivo* in transplant models of AML

4.1 Introduction

Testing potential cancer therapeutics in applicable mouse models is important for determining the efficacy of compounds in a more complex whole organism setting and prioritising the transition of only the most effective compounds to human clinical trials. This chapter addresses Aim 2: 'Test promising combination therapies in *in vivo* syngeneic and xenograft models of AML'.

Metabolism-modifying drugs that were found to act synergistically with CX-5461 to reduce AML viability *in vitro* (Chapter 3) were tested for their efficacy in improving survival *in vivo* in transplant models of AML. Compared to *in vitro* assays, several factors can play important roles in these *in vivo* pre-clinical mouse models including the microenvironment, the type of transplant model and the method of tracking disease. Testing potential drug combinations in the context of the tumour microenvironment is important, as it modulates cancer cell growth and drug resistance.

4.1.1 The leukaemia microenvironment

The primary tumour microenvironment of leukaemia cells is the bone marrow, and to a lesser extent secondary lymphoid organs such as the spleen and lymph nodes. The bone marrow niche consists of osteoblasts, osteoclasts, the sympathetic nerve system, blood vessels, immune cells such as macrophages, endothelial cells, mesenchymal stem cells (MSCs) and haematopoietic stem cells (HSCs) [193]. As the location of the HSCs, the bone marrow niche regulates the survival, proliferation and differentiation of these cells, and is the site of production of all blood cells including erythrocytes, monocytes and lymphocytes [194]. The bone marrow niche is also thought to be the primary reservoir of leukemic stem cells, which possess self-renewing properties like HSCs and differentiate into leukemic blasts, such that the bone marrow niche dictates

disease progression, drug resistance and relapse through interactions with the leukaemia cells [195].

Leukemic blasts hijack this supportive environment to support their own survival and proliferation (Figure 4-1). These AML cells reprogram the surrounding cells to their advantage, such as reprogramming bone marrow adipocytes to increase lipolysis, resulting in the increased transfer of fatty acids from adipocytes to leukemic cells to support their metabolic processes [196]. One mechanism via which AML cells can signal to surrounding cells is through excreted vesicles called exosomes. The plasma of AML patients has been reported to be rich in exosomes containing immunosuppressive components which interfere with the anti-tumour immune response [197]. AML-derived
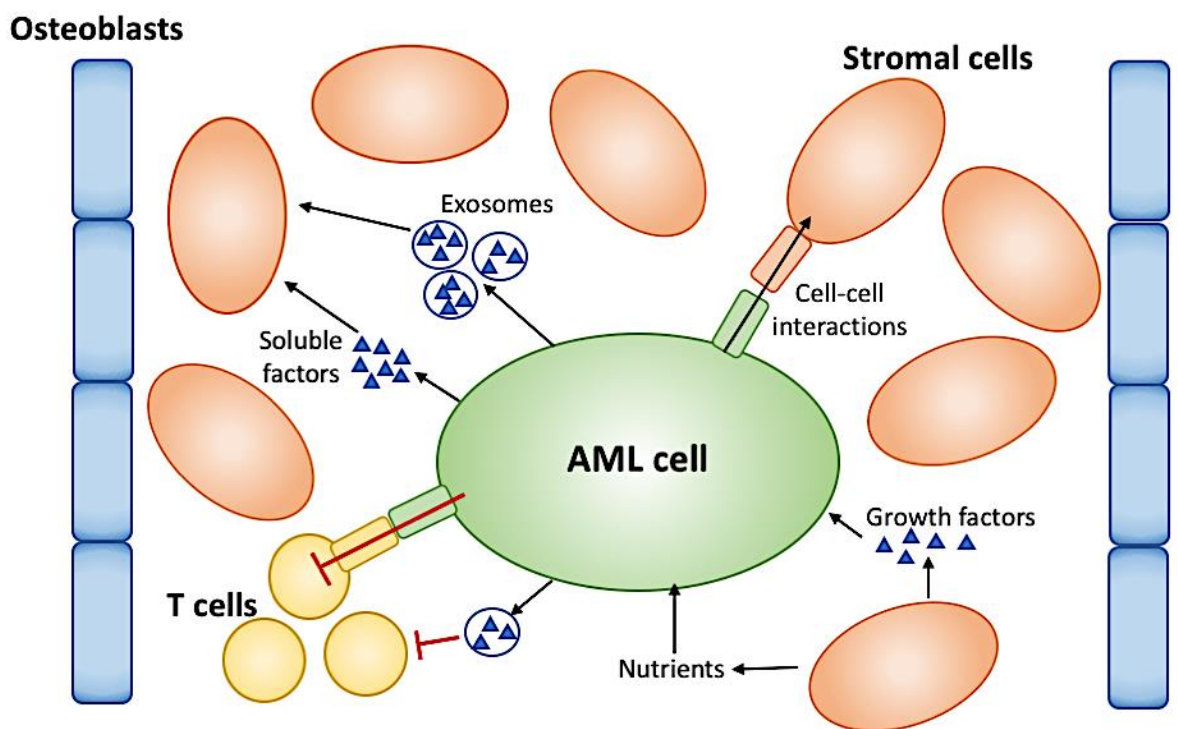
Figure 4-1: The leukaemia microenvironment

The bone marrow environment is the main niche of AML cells and includes osteoblasts (blue), stromal cells (orange) and immune cells such as T cells (yellow). The AML cell signals to the surrounding cells through soluble factors (triangles), vesicles known as exosomes (which contain factors such as signalling molecules) and through direct cell-to-cell interactions. In response, the stromal cells provide the AML cells with nutrients and growth factors, supporting their survival and proliferation. Normal osteoblast function, immune cell function and haematopoiesis is also inhibited. In this manner the bone marrow niche becomes more favourable to the tumour cells and can also increase their chemotherapy resistance.

exosomes are able to remodel the bone architecture and stromal cell compartment, reducing the activity of osteoblasts and also the ability of the stromal cells to support normal haematopoiesis, thus providing a competitive advantage to AML cells [198]. Soluble factors are also utilised by AML cells to signal to surrounding cells. Cytokine-mediated crosstalk between MSCs and AML cells was shown to reduce apoptosis and increase the proliferation of primary AML patient cells in an *in vitro* co-culture model [199], which is in agreement with evidence that AML cells increase the numbers of fibroblasts, which produce pro-survival cytokines and result in reduced chemotherapy sensitivity [200]. AML cells have also been found to communicate to surrounding cells through direct cell-to-cell contact including through gap-junction mediated mechanisms [201] and also via vascular cell adhesion molecule 1 (VCAM-1) and very late antigen-4 (VLA-4) signalling, activating nuclear factor kappa-light-chain-enhancer of activated B cells (NF-κB) pro-survival signalling and leading to chemoresistance [202].

While this is a simplistic view of the bone marrow niche that does not take into account the vast complexities of such a system [203], it is clear that the bone marrow niche plays a significant role in the survival of AML cells and their response to chemotherapy, highlighting the importance of evaluating promising combination therapies in this context, as it will influence the effects of the drugs on the tumour cells.

4.1.2 Types of in vivo transplant models utilised

Various types of *in vivo* mouse transplant models have been developed which differ in the type of cells which are injected (donor cells) and the location within the recipient where the cancer develops. For the studies in this thesis, an established MLL/AF9 NRAS mouse AML cell line [32] was injected intravenously (IV) into C57Bl/6 mice, an immunocompetent strain. This is a syngeneic (strain and species matched), orthotopic (tumours develop in the organ of origin) model. Cell line xenograft models (human cell lines injected into immunocompromised mice) were also utilised. For these studies, established human AML cell lines were injected into NOD/SCID/gamma^{null} (NSG) mice, which lack functional B lymphocytes, T lymphocytes and natural killer cells, thus would mount a limited immune response against the human AML cells [204]. This method of

transplant is well characterised for the human AML cell lines selected for these experiments (MV4-11, THP-1 and MOLM-13) [33 205 206 207 208 209].

A comparison of the observed features of these two types of models is outlined in Table 4-2 and the subsequent benefits or limitations of these models discussed in the Sections 4.3.3 and 4.3.6.

Heterotopic tumour models involve the transplant of tumour cells in an organ that is not the organ of origin, typically tumour cells are injected subcutaneously into the flank of the mouse where the resulting solid tumour can be easily detected and measured with calipers. Indeed, such models have been used for *in vivo* evaluation of AML cell lines including MV4-11 [210-212], MOLM-13 [206,213,214] and THP-1 [215,216]. However, the flank of the mouse is far removed from the natural microenvironment for leukaemia, thus only orthotopic AML models were chosen to test the efficacy of the promising combinations identified in Chapter 3. To facilitate the monitoring of the engraftment and development of leukaemia, live animal imaging with luciferase-tagged cells was employed.

4.1.3 Live animal imaging with luciferase tagged tumours

As orthotopic models of AML do not provide simple visualisation of the tumours, an alternative method of measuring disease progression was required. Orthotopic AML models do not normally feature high numbers of circulating leukaemia cells until close to the ethical endpoint, in the case of the THP-1 xenograft model there is very little circulating disease even at ethical endpoint [207], thus the number of leukaemia cells in the blood is not a robust early measure of tumour burden in these particular models. Live animal imaging of luciferase tagged leukaemia cell lines was used as the measure of tumour burden to overcome this issue (Methods section 2.6). Specifically, the leukaemia cell lines must be tagged with the luciferase enzyme. A few days following IV injection of the leukaemia cells, the mice are injected with the luciferin substrate, anaesthetised and imaged with IVIS Spectrum, a specialised imaging machine for measuring bioluminescence and fluorescence in live rodents. The luciferase enzyme in the AML cells converts luciferin to oxyluciferin and energy is released in the form of bioluminescence [217] which is detected by the camera in the IVIS Spectrum. This technique provides a non-invasive method of confirming engraftment and tracking

disease progression in the same mice over time, and also allows the tumour burden in different areas of the mouse to be visualised [217]. The MLL/AF9 NRAS cell line is a well-established mouse AML cell line which expresses the luciferase enzyme [32], whereas the human AML cell lines used in the *in vitro* screening in the previous chapter were transduced to express the luciferase enzyme, as part of this thesis project (Methods Section 2.9).

4.2 Results

4.2.1 Tolerability testing of metabolism drugs +/- CX-5461 in non-tumour bearing mice

In order to determine a tolerable dose of the metabolism drugs for *in vivo* experiments testing was performed in healthy, non-cancer bearing mice of the relevant background strain (C57BL/6). The tolerability of CX-5461 had already been established by our lab, being a standard dosing schedule of 30-35mg/kg dosed 3 times per week by oral gavage, with a vehicle of 50mM NaH_2PO_4 [1]. In these studies, weight is measured regularly as weight loss is used as a sign of drug toxicity, and general health is also monitored (Methods Section 2.6.1). The maximum tolerated dose (MTD) is defined as the dose which causes a maximum weight loss of 10% from which the mice recover within a week. Once the MTD or tolerable range of the metabolism drug was established, combination tolerability testing with CX-5461 was commenced.

4.2.1.1 Tolerability of orlistat

The published method of orlistat administration *in vivo* is through extraction from commercially-available Xenical capsules, then dosing at 240mg/kg/day injected IP, as 15µL/10g body weight [160]. Orlistat solubility required a high percentage of ethanol (33%), thus the vehicle was also tested. Mice were treated with orlistat at the published dosing schedule for 3 weeks, weighed daily, and a vehicle only group included. Figure 4-2 shows that all mice in the vehicle only group maintained their weight over a 3 week period of dosing, and at the final weigh-in 1 week after dosing was completed, indicating the vehicle was tolerated. In the orlistat treated group two of the mice tracked with the vehicle only mice, however one mouse lost approximately 5% body weight during dosing which then stabilised at this level for the remainder of the dosing period. It was determined that 240mg/kg was a tolerable dose, which is consistent with the literature [119]. Combination tolerability testing with CX-5461 was not performed with orlistat due to the favourable toxicity results of orlistat as a single agent.
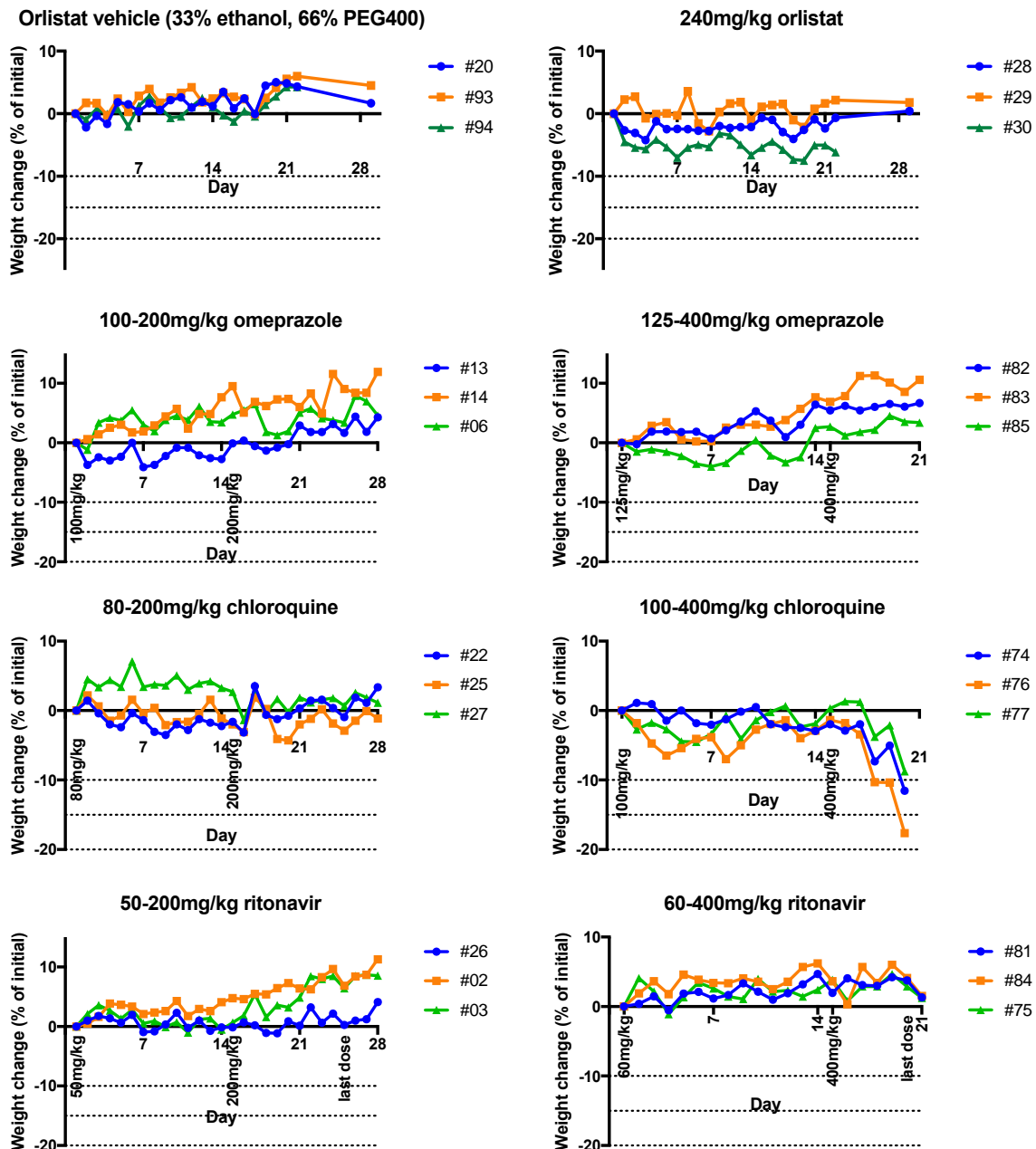
Figure 4-2: Tolerability of metabolism-modifying drugs as single agents in non-tumour bearing mice

Non-tumour bearing C57Bl/6 mice were weighed and dosed with the indicated drug regimes daily for 21 days, followed by monitoring only for 1 week. If no weight change was observed after 2 weeks of dosing, the dose was increased and continued for a further 1-2 weeks. Weight change is shown, as a percentage of the initial weight. -10%, -15% and -20% weight changes are indicated by dotted lines, as >10% weight loss is a sign of drug toxicity and >20% weight loss requires euthanasia, according to ethical requirements. N=3 mice/dosing regime.

35 mg/kg CX-5461 + 200mg/kg DCA

35mg/kg CX-5461 + 100mg/kg chloroquine

35mg/kg CX-5461 + 80mg/kg chloroquine

30mg/kg CX-5461 + 80mg/kg chloroquine

30mg/kg CX-5461 + 50mg/kg chloroquine

Grey = dosing days
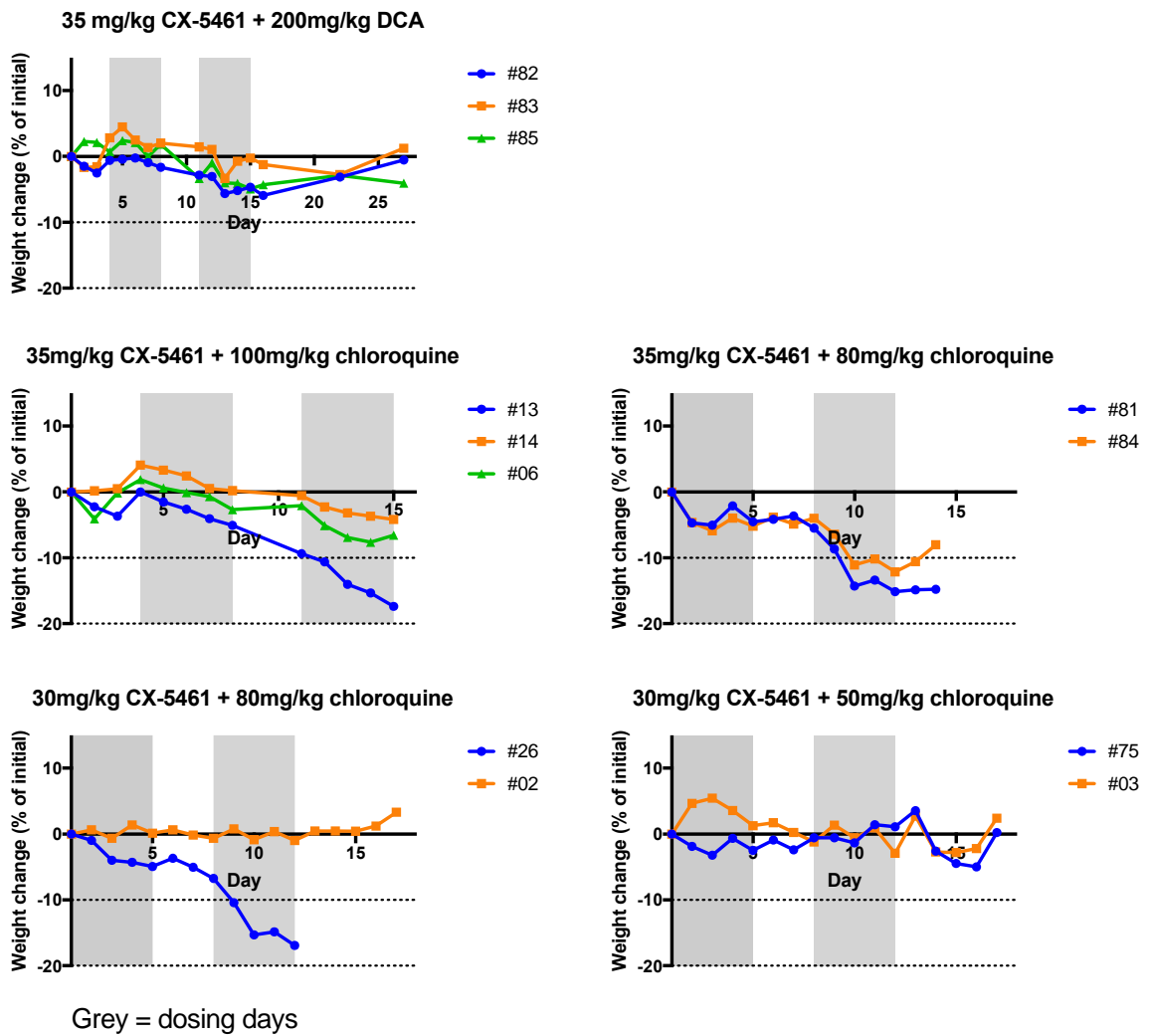
Figure 4-3: Tolerability of CX-5461 + DCA or chloroquine in non-tumour bearing mice

Non-tumour bearing C57Bl/6 mice were weighed and dosed with the indicated drug regimes daily for 14-21 days, followed by monitoring only for 1 week. Grey areas indicate dosing days. Weights are graphed for each individual mouse as weight change, a percentage of the initial weight. -10%, -15% and -20% weight changes are indicated by dotted lines, as >10% weight loss is a sign of drug toxicity and >20% weight loss requires euthanasia, according to ethical requirements. N=2-3 mice/dosing regime.

4.2.1.2   Tolerability of chloroquine +/- CX-5461

Tolerability testing of chloroquine was commenced at 50mg/kg dosed daily by oral gavage. As the vehicle was phosphate-buffered saline (PBS), a vehicle only group was not included. Figure 4-2 shows that the mice maintained their weight after 1 week of treatment with 50mg/kg chloroquine, thus a separate group with 100mg/kg was started. After 2 weeks of dosing the 50mg/kg treated group were still maintaining

weight so their dosing was increased to 200mg/kg for a further 2 weeks during which no toxicity was observed. The 100mg/kg treated group were still maintaining weight after 2 weeks of dosing and as such, dosing was increased to 400mg/kg daily. After 3 doses the mice rapidly lost weight and the experiment was terminated. Autopsies revealed the mice had bloated stomachs and intestines, and pale organs suggesting anaemia. From these single-agent studies, it was determined that 50, 100 and 200mg/kg of chloroquine were tolerable daily dosing schedules in healthy C57Bl/6 mice, while 400mg/kg was not. These results are consistent with the published literature, where daily doses of 50-100mg/kg/day chloroquine have been used as a single agent in various cancer models without significant toxicity [218-220], and the oral 50% lethal dose (LD_{50}) of chloroquine in mice is reported to be 500mg/kg [221].

Based on these studies combination tolerability testing of CX-5461 with chloroquine was performed. Typically when testing combination therapies, a lower dose than the MTD is trialled. Thus, dosing of 80 or 100mg/kg chloroquine was performed daily Monday to Friday (reduced from 7 days a week) with 35mg/kg CX-5461 (Monday, Wednesday and Friday). As chloroquine is soluble in water-based vehicles, for these experiments it was dissolved in 50mM NaH_2PO_4, as is CX-5461. Figure 4-3 shows that 35mg/kg CX-5461 in combination with 80 or 100mg/kg chloroquine was not tolerated, as the mice rapidly lost weight from day 8 of dosing onwards. A lower dose of CX-5461 (30mg/kg) with 80mg/kg chloroquine was potentially intolerable as one mouse maintained weight, while the other lost almost 20% of its weight and required euthanasia after 2 weeks of dosing, whereas 30mg/kg CX-5461 and 50mg/kg chloroquine was found to be tolerable, with weight loss of less than 5% throughout the experiment.

4.2.1.3   Tolerability of DCA + CX-5461

Previous work in our laboratory established the *in vivo* toxicity of DCA as a single agent based on dosing through drinking water, estimated to be equivalent to 200mg/kg/day. As DCA is soluble in water-based vehicles, for these experiments it was dissolved in 50mM NaH_2PO_4, as is CX-5461. Dosing was commenced at 200mg/kg/day DCA with 35mg/kg CX-5461 (Monday, Wednesday and Friday) by oral gavage. Figure 4-3 shows that the mice maintained weight over the two-week schedule (with a maximum weight

loss of 5% after 13 days) and over the following 2 weeks after dosing, thus this dosing schedule was determined to be tolerable. The MTD was not reached, thus higher doses of both drugs could potentially be used.

4.2.1.4   Tolerability of omeprazole

Omeprazole dosing was tested at 100 or 125 mg/kg/day by oral gavage, dissolved in 7.5% ethanol in PBS [155,222] (Figure 4-2). After 2 weeks toxicity was not observed thus the dose was increased to 200 or 400 mg/kg/day respectively for a further 2 weeks, with no observable toxicity. Thus omeprazole at 400mg/kg/day is a tolerable dosing schedule in healthy C57BL/6 mice. This is consistent with the published literature, where doses of 75-100mg/kg/day of omeprazole have been used in various cancer models as a single agent without significant toxicity [155,222] and the oral LD_{50} in mice has been reported to be in excess of 4g/kg [223]. Combination tolerability testing of CX-5461 and omeprazole was not completed due to time constraints, and thus not followed up for testing in tumour models.

4.2.1.5   Tolerability of ritonavir

Ritonavir dosing was tested at 50 or 60 mg/kg/day by oral gavage, dissolved in 7.5% ethanol in PBS [159,224,225] (Figure 4-2). After 2 weeks toxicity was not observed thus the dose was increased to 200 or 400 mg/kg/day respectively for a further 2 weeks, with no observable toxicity. Thus ritonavir at 400mg/kg/day is a tolerable dosing schedule in healthy C57BL/6 mice. This is consistent with the published literature, where doses of 30-50mg/kg/day of ritonavir have been used in various cancer models as a single or combination agent without significant toxicity [159,224,225], and the oral LD_{50} in mice is reported to be in excess of 2.5g/kg [226]. Combination tolerability testing of CX-5461 and ritonavir was not completed due to time constraints, and thus not followed up for testing in tumour models.

4.2.1.6   Summary

In summary, tolerable doses of orlistat, chloroquine, omeprazole and ritonavir as single agents in healthy C57BL/6 mice were determined, in addition to tolerable combination dosing with CX-5461 and DCA, and CX-5461 and chloroquine. Results of the MTD testing are summarised in Table 4-1.

Drug/s	Vehicle	Method of administration	Tolerable doses	Intolerable doses	Maximum tolerated dose (if achieved)
Orlistat	33% ethanol, 66% PEG 400	15µL/10g injected IP, daily	240mg/kg	-	-
Omeprazole	7.5% ethanol in PBS	100µL/10g by oral gavage, daily	100, 125, 200, 400mg/kg	-	-
Ritonavir	7.5% ethanol in PBS	100µL/10g by oral gavage, daily	50, 60, 200, 400mg/kg	-	-
Chloroquine	PBS	100µL/10g by oral gavage, daily	80, 100, 200mg/kg	400mg/kg	>200mg/kg, <400mg/kg
CX-5461 + DCA	50mM NaH_2PO_4	100µL/10g by oral gavage, daily (DCA), M,W,F (CX-5461)	35mg/kg CX-5461 + 200mg/kg DCA	-	-
CX-5461 + chloroquine	50mM NaH_2PO_4	100µL/10g by oral gavage, daily M-F (chloroquine), M,W,F (CX-5461)	30mg/kg CX-5461 + 50mg/kg chloroquine	35mg/kg CX-5461 + 100mg/kg chloroquine, 35mg/kg CX-5461 + 80mg/kg chloroquine	~30mg/kg CX-5461 + 80mg/kg chloroquine

Table 4-1: Summary of drug tolerability studies in non-tumour bearing mice

Data from Figure *4-2* and Figure *4-3*.

4.2.2 Treatment of MLL/AF9 NRAS in vivo

The MLL/AF9 NRAS syngeneic mouse model is a well-established model in our laboratory [1]. Specifically, 5 x 10^5 MLL/AF9 NRAS cells were injected into recipient C57Bl/6 mice and engraftment confirmed 7 days post-transplant by bioluminescent imaging, as previously established. The mice were then randomised into groups and treatment commenced, at a regime informed by the previous tolerability testing (Figure 4-2 and Figure 4-3). 'Survival' was defined as the time taken post-transplant until the mice reached an ethical endpoint and required euthanasia due to symptoms

such as weight loss, reluctance to move and hunching. Median survival times and subsequent statistical analysis of survival times are shown in Appendix Tables 4-1 and 4-2.

4.2.2.1 CX-5461 + orlistat

Orlistat treatment did not alter survival compared to the vehicle-treated mice (median survival of 17 days post-transplant for both groups) (Figure 4-4a), whereas CX-5461 treatment alone significantly improved survival compared to the vehicle and orlistat groups, (median survival of 29 days). The combination of CX-5461 and orlistat had a significantly worse outcome on survival than CX-5461 alone (median survival of 25 days).

This antagonistic effect was also reflected in the spleen weights (Figure 4-4b. Disease-induced splenomegaly was not altered with orlistat treatment, whereas CX-5461 treatment prevented spleen enlargement and the drug combination resulted in an intermediate spleen weight.

Figure 4-4c illustrates a difference in patterning of the bioluminescence between the groups. For example, at 14 days post-transplant the bioluminescent signal in the vehicle and orlistat treated groups had spread throughout the body, with a higher concentration in the midsection. In comparison, the CX-5461 and combination-treated mice had no visible bioluminescent signal in the midsection and reduced levels in the head and pelvic regions. At day 21 post-transplant, the CX-5461 and combination-treated groups still had minimal bioluminescent signal in the mid-section, whereas the disease had progressed in the head and pelvic areas, more in the combination-treated group. At day 28 post-transplant the bioluminescent signal in the head and pelvic areas had increased the remaining three mice of the CX-5461 only group, which were the only mice remaining of all four treatment regimes. Quantification of the bioluminescent imaging revealed that the orlistat-treated mice had significantly elevated total body bioluminescence (BLI) at 14 days post-transplant compared to the vehicle-treated groups, while the CX-5461 and combination-treated groups had a significantly lower BLI (Figure 4-4d).

The weights of the mice remained stable in all the treatment groups for the duration of the experiment, indicating the dosing regime was tolerable in tumour-bearing mice (Appendix Figure 4-1).

Figure 4-4: Combination therapy of CX-5461 and orlistat does not improve survival *in vivo* in a syngeneic transplant model of MLL/AF9 NRAS AML

Mice were transplanted with MLL/AF9 NRAS cells via the tail vein, imaged by bioluminescence to confirm engraftment at day 7 and therapy initiated. Mice were dosed with vehicle (50mM NaH_2PO_4), 240mg/kg orlistat daily, 35mg/kg CX-5461 Monday, Wednesday, Friday, or the combination, until they reached an ethical endpoint. N= 5 mice/treatment group. A) Kaplan-Meier survival curves. Log-rank test with Bonferroni corrected threshold was applied for comparison of multiple survival curves, such that a P value of <0.0083 was considered significant. Key comparisons: * = significant compared to vehicle, # = significant compared to CX-5461. The grey area indicates the dosing period. B) Spleen weight at ethical endpoint. Mean weight ± SD shown. One-way ANOVA was performed with a Tukey's multiple comparison test, the adjusted p-value is shown. NS P > 0.05, *P ≤ 0.05, **P ≤ 0.01, ***P ≤ 0.001, **** P ≤ 0.0001. Compared to vehicle, unless indicated by a bar. C) Bioluminescent images. Imaging was performed weekly from 7 days post-transplant. The day 7 images are shown on a lower image colour scale to the subsequent weeks images, in order to show that engraftment has occurred. D) The total bioluminescence (BLI) of each mouse was quantified from the images. Mean BLI ± SD shown One-way ANOVA was performed with a Tukey's multiple comparison test, the adjusted p-value is shown. Compared to vehicle, unless indicated by a bar.

MLL/AF9 NRAS: CX-5461 + orlistat

A)

B)
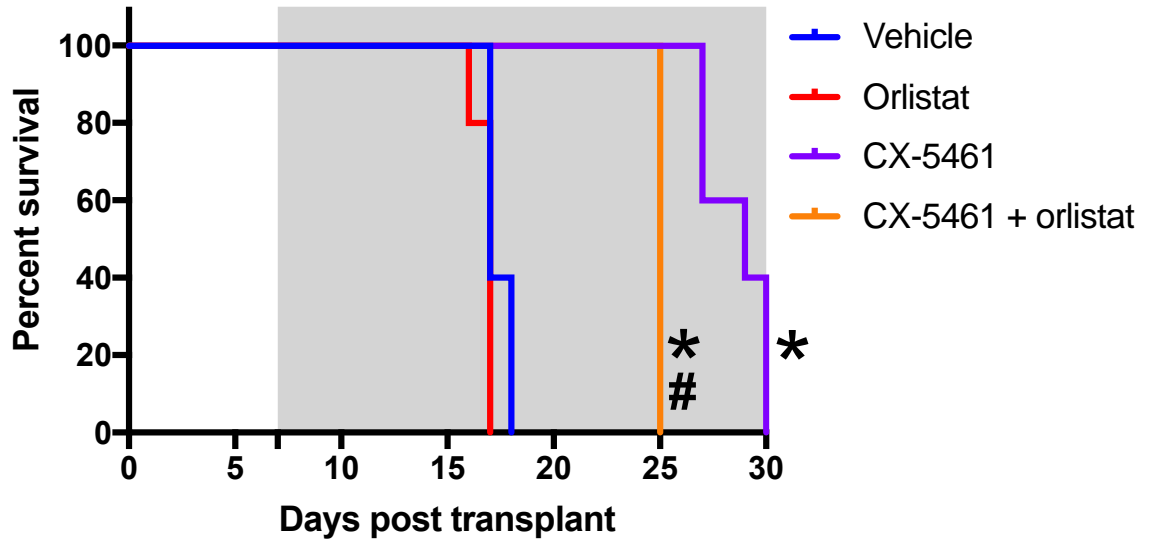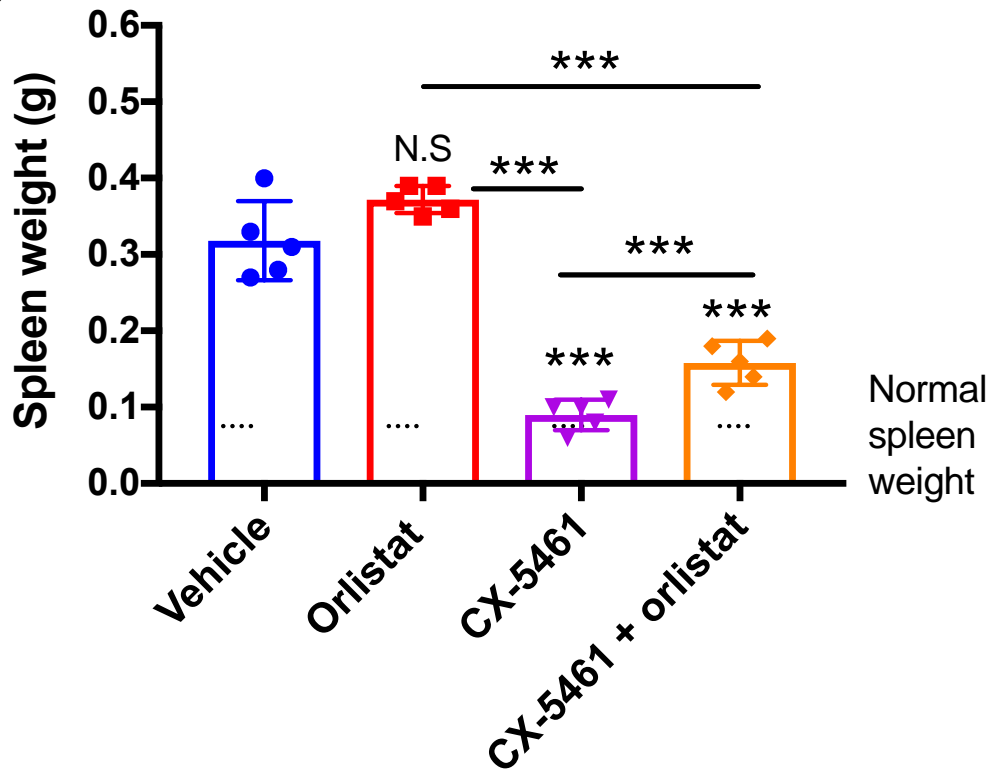
MLL/AF9 NRAS: CX-5461 + orlistat

C)
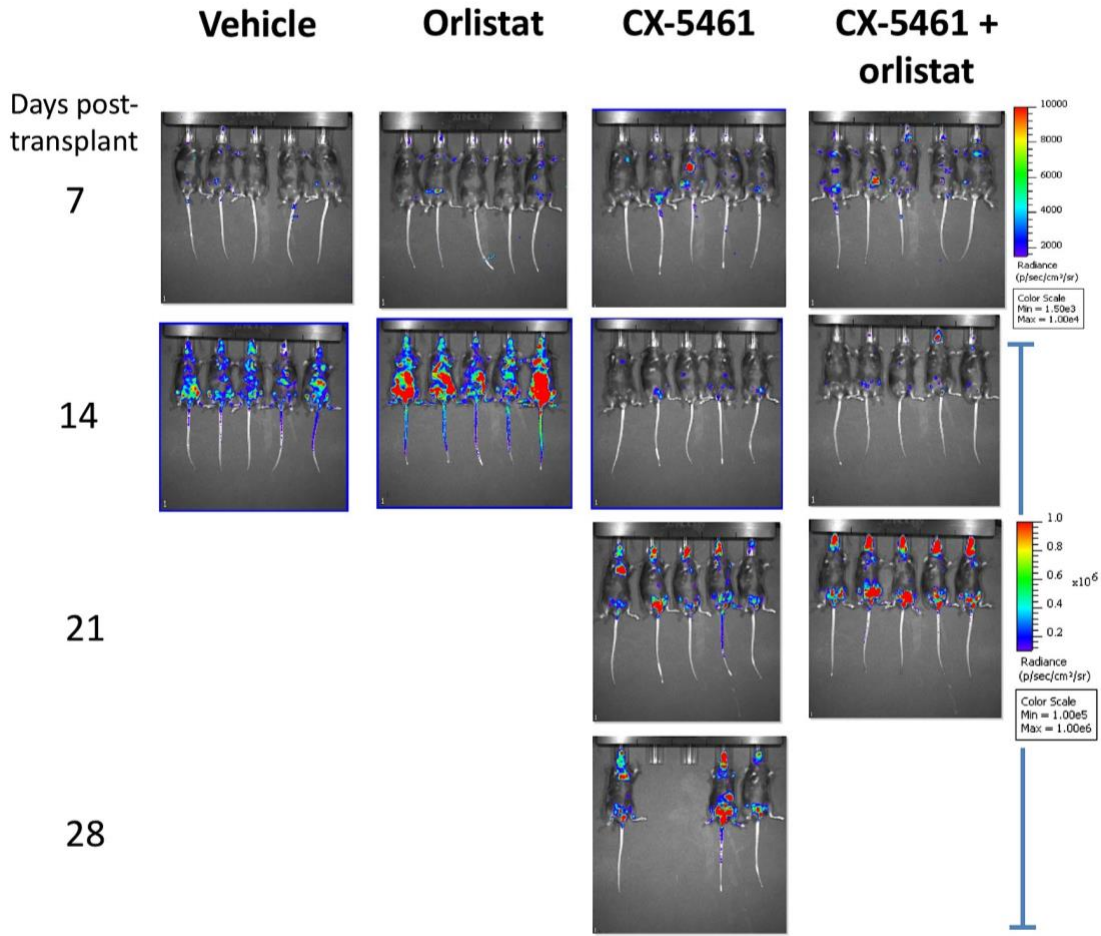
D)
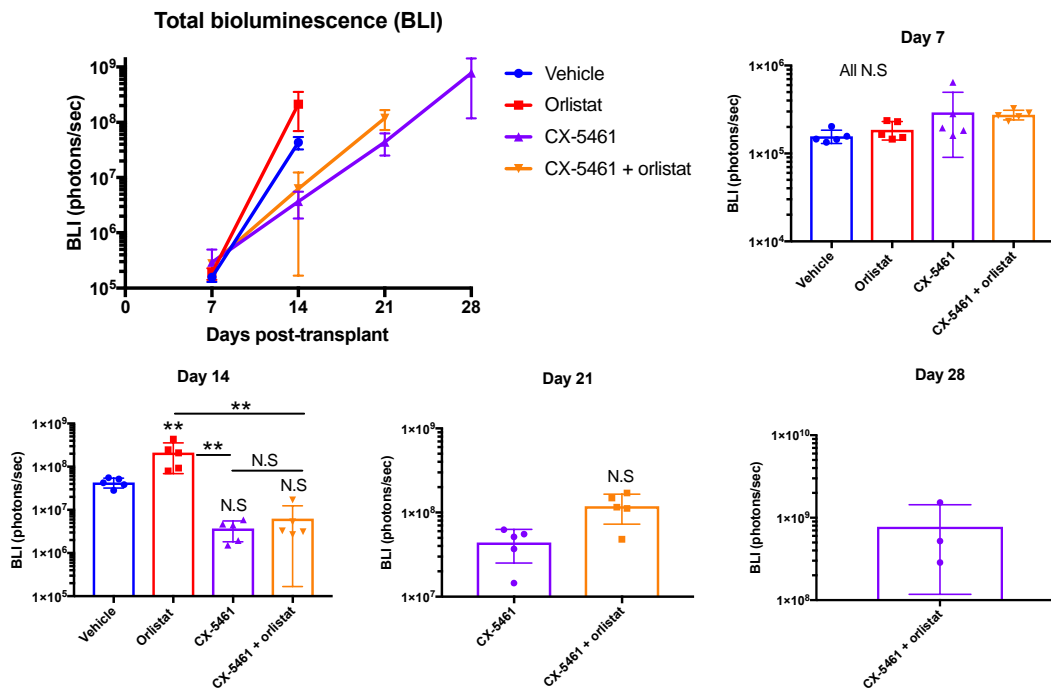
4.2.2.2 CX-5461 + DCA

Similarly to orlistat, DCA treatment alone did not alter survival compared to vehicle treatment (Figure 4-5a). Furthermore, DCA did not confer a survival advantage over 30mg/kg CX-5461 treatment alone (20 days) or combination treatment (19.5 days). Note that as CX-5461 was administered at a lower dose in this experiment (30mg/kg, down from 35mg/kg) compared to the CX-5461 + orlistat experiment, (Figure 4-4) the survival advantage with CX-5461 treatment reduced from 12 to 5 extra days compared to the vehicle. This lower dose of CX-5461 was used to allow any effective combinations to be more apparent and reduce potential dosing side effects considering the extra burden that the tumour cells place on the mice, compared to the healthy mice used in the tolerability studies.

The DCA treated mice had significantly smaller spleens at endpoint than the vehicle-treated mice, (approximately 20% reduction, Figure 4-5b), and while there was no survival advantage, this indicates that DCA as a single agent was able to impact tumour burden *in vivo*, consistent with *in vitro* results (Figure 3-8). Both CX-5461 and the combination-treated mice had spleens that were the same weight as those of a non-tumour bearing mouse.

As with the previous experiment, the bioluminescent imaging shows that by day 14 post-transplant the disease in the vehicle and the DCA treated mice had spread throughout the body, concentrating particularly in the mid-section (Appendix Figure 4-2). However, in line with the spleen weights being significantly lower in the DCA treated mice, the disease levels in the mid-section were marginally lower compared to the vehicle. Figure 4-5c shows that at day 14 post-transplant the BLI of the vehicle and DCA treated mice did not differ, whereas the CX-5461 and combination-treated mice had significantly lower BLI than the vehicle and DCA treated mice. There was no significant difference between the BLI of the CX-5461 and combination-treated groups. There were not enough mice remaining at day 21 to perform robust statistical analysis comparing the BLI of the CX-5461 and combination-treated groups at this timepoint.

The majority of the mice maintained their weight for the duration of the experiment, with the exception of one mouse in the combination-treated group, indicating the dosing regimes were tolerable in tumour-bearing mice (Appendix Figure 4-3).

Figure 4-5: Combination therapy with CX-5461 and DCA does not improve survival *in vivo* in a syngeneic transplant model of MLL/AF9 NRAS AML

Mice were transplanted with MLL/AF9 NRAS cells via the tail vein, imaged by bioluminescence to confirm engraftment at day 7 and therapy initiated. Mice were dosed with vehicle (50mM NaH_2PO_4), 200mg/kg DCA daily Monday-Friday, 30mg/kg CX-5461 Monday, Wednesday, Friday, or the combination, until reaching an ethical endpoint. N=8 mice/ treatment group. A) Kaplan-Meier survival curves. Log-rank test with Bonferroni corrected threshold was applied for comparison of multiple survival curves, such that a P value of <0.0083 was considered significant. Key comparisons: * = significant compared to vehicle. The grey area indicates the dosing period. B) Spleen weight at ethical endpoint. Mean weight ± SD shown. One-way ANOVA was performed with a Tukey's multiple comparison test, the adjusted p-value is shown. NS P > 0.05, *P ≤ 0.05, **P ≤ 0.01, ***P ≤ 0.001, **** P ≤ 0.0001. Compared to vehicle, unless indicated by a bar. C) The total bioluminescence (BLI) of each mouse was quantified from the bioluminescent images (Appendix Figure 4-2). Mean BLI ± SD shown One-way ANOVA was performed with a Tukey's multiple comparison test, the adjusted p-value is shown. Compared to vehicle, unless indicated by a bar.

MLL/AF9 NRAS: CX-5461 + DCA

A)

B)
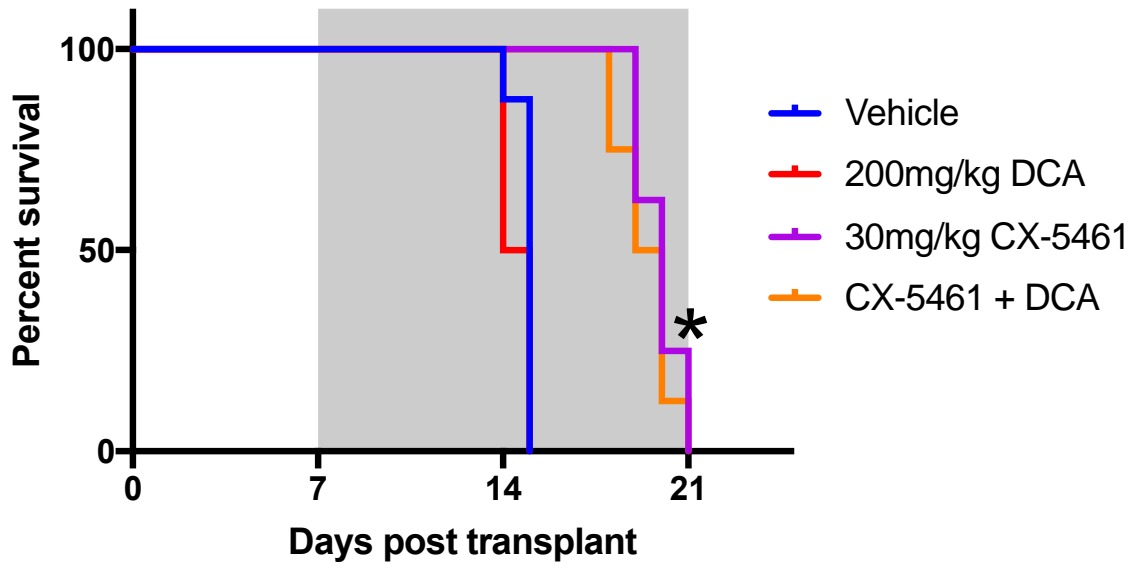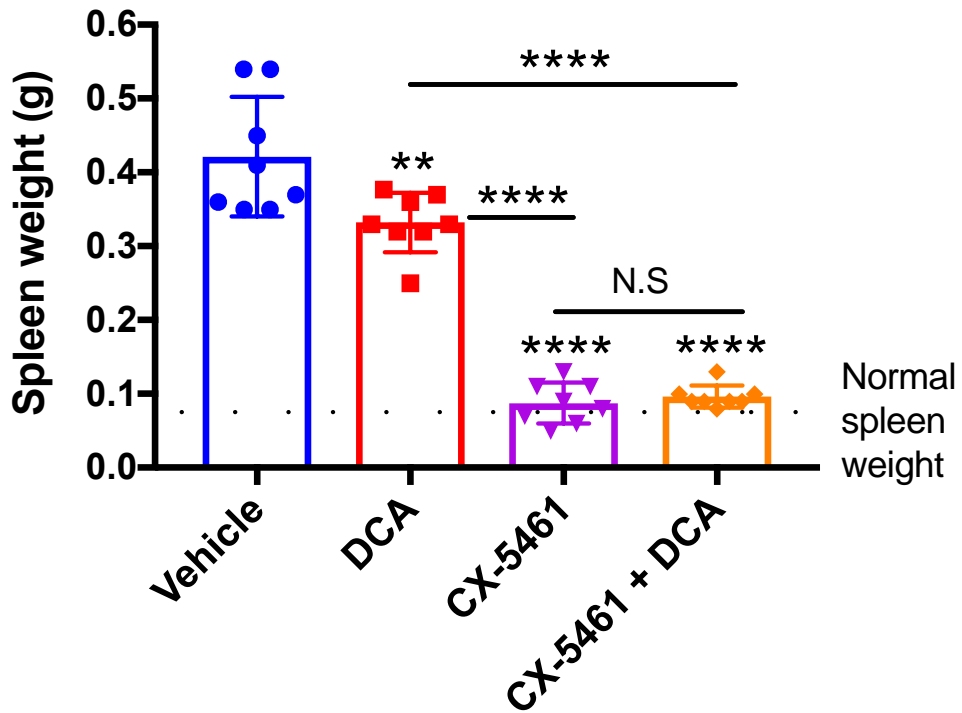
MLL/AF9 NRAS: CX-5461 + DCA

C)
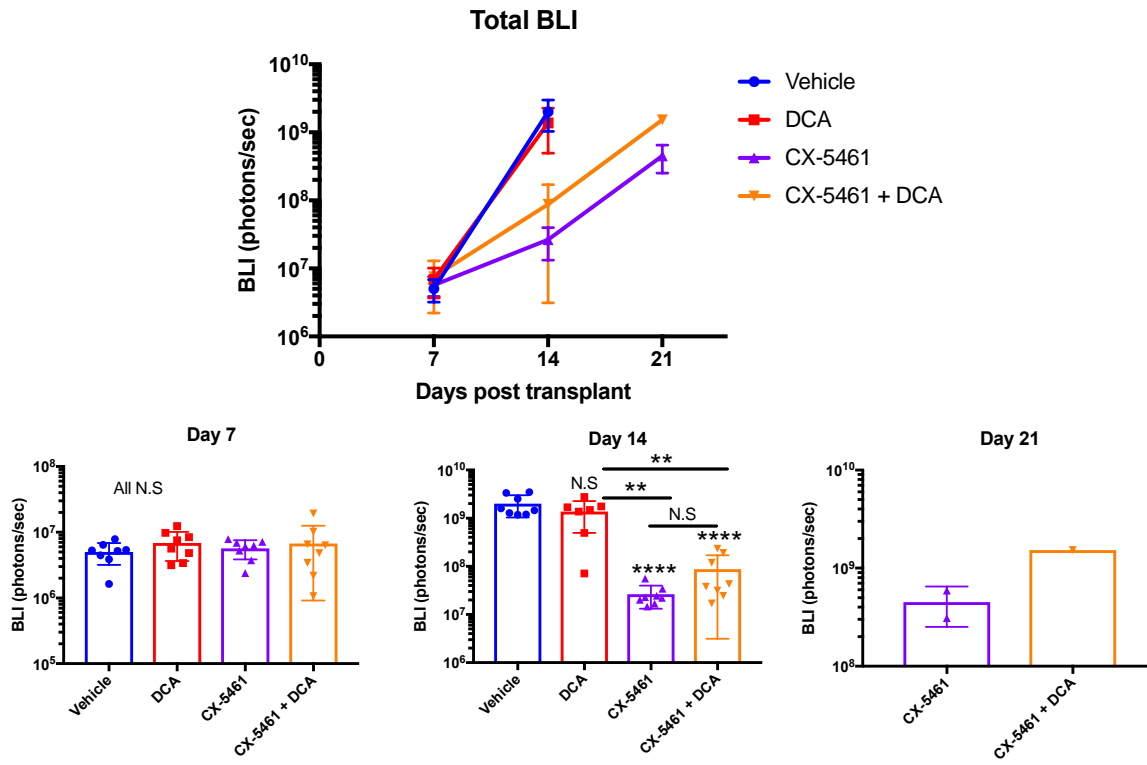
4.2.2.3 CX-5461 + chloroquine

A dosing regime of 30mg/kg CX-5461 and 80mg/kg chloroquine was chosen in order to use the maximal concentrations of the drugs in the mice, however this was lowered to 50mg/kg chloroquine when slight weight loss was observed by day 19. Figure 4-6a shows that chloroquine treatment alone did not alter survival compared to the vehicle-treated mice (15 days compared to 14 days respectively). CX-5461 only treatment resulted in a 5 day survival advantage compared to the vehicle-treated mice (20 days) and the combination-treated mice extended this to 23 days post-transplant, a statistically significant 3 day survival advantage compared to the CX-5461 only group.

The spleen weights of the vehicle and chloroquine treated groups were not significantly different at endpoint, neither were the CX-5461 and combination-treated groups (Figure 4-6b). Both the CX-5461 and combination-treated groups had spleens that were the same weight as a non-tumour bearing mouse and significantly smaller than both the vehicle and chloroquine groups.

The bioluminescent imaging was comparable to the previous experiments, specifically by day 14 post-transplant the vehicle-treated mice had disease spread throughout the body but concentrated in the particularly in the mid-section, while the CX-5461 treated mice show no disease in the mid-section and minimal disease in the head (Appendix Figure 4-4). The bioluminescent patterning of the chloroquine treated group was similar to the vehicle group, whereas the combination-treated group was comparable to the CX-5461 group. This is consistent with the total BLI quantification (Figure 4-6c) with high BLI in the vehicle and chloroquine groups, and significantly lower BLI in the CX-5461 and combination-treated groups.

The weight changes (Figure 4-6d) demonstrate that the vehicle, chloroquine and CX-5461 as single-agent dosing regimes were tolerable, with the exception of one mouse in the CX-5461-treated group which lost more than 10% body weight at day 20. However, more than half of the combination-treated mice had lost 10% of their body weight by day 20 post-transplant. In response to this, the dose of chloroquine was dropped from 80 to 50mg/kg in an attempt to avoid further weight loss, however five of the mice continued to decline in weight and reached 20% weight loss, thus required

euthanasia. This pronounced weight loss indicates that the initial combination dosing regime used in this experiment was not well tolerated in tumour-bearing mice, thus a dosing regime of 50mg/kg chloroquine in combination with 30mg/kg CX-5461 from the beginning of dosing would be preferable.

Interestingly, one of the toxic effects of combining CX-5461 and chloroquine was anaemia. Figure 4-6e illustrates the red cell parameters from a full blood count analysis of cardiac blood collected at the experiment ethical endpoint, with normal reference ranges for comparison. While the total number of red blood cells was in the normal range for the vehicle and CX-5461-treated mice, these were slightly elevated for the chloroquine treated mice and approximately half the lower limit of the normal range in the combination-treated mice, indicating anaemia. The same trend was observed for haemoglobin levels and the hematocrit. The mean corpuscular volume (MCV), or the average size of the red blood cells, followed the same trend as the number of red blood cells. Together these parameters suggest that the dosing regime of CX-5461 with chloroquine used in this experiment resulted in pronounced anaemia, which may explain the weight loss (Figure 4-6d). Although, it should be noted that the blood samples were not collected at the same timepoint post-transplant, and as such, there is a possibility that the additional time that the combination-treated mice were bearing the tumour cells contributed to the anaemia, in addition to the drugs administered.

In conclusion, of the 3 combination therapies tested, the combination of CX-5461 and chloroquine was the only one that improved survival in the MLL/AF9 NRAS model compared to CX-5461 treatment alone. The synergy is clear, as chloroquine alone had no impact on survival compared to the vehicle-treated mice. However, profound weight loss and anaemia in the combination-treated group indicated that the treatment regime was not tolerated and requires optimising for future experiments.

Figure 4-6: Combination therapy with CX-5461 and chloroquine significantly improves survival *in vivo* in a syngeneic transplant model of MLL/AF9 NRAS AML

Mice were transplanted with MLL/AF9 NRAS cells via the tail vein, imaged by bioluminescence to confirm engraftment at day 7 and therapy initiated. Mice were dosed with vehicle (50mM NaH_2PO_4), 80mg/kg chloroquine (CQ) daily Monday-Friday (dropped to 50mg/kg as of day 19), 30mg/kg CX-5461 Monday, Wednesday, Friday, or the combination, until reaching an ethical endpoint. N=8 mice/ treatment group. A) Kaplan-Meier survival curves. Log-rank test with Bonferroni corrected threshold was applied for comparison of multiple survival curves, such that a P value of <0.0083 was considered significant. Key comparisons: * = significant compared to vehicle, # = significant compared to CX-5461.The grey area indicates the dosing period. B) Spleen weight at ethical endpoint. Mean weight ± SD shown. One-way ANOVA was performed with a Tukey's multiple comparison test, the adjusted p-value is shown. NS P > 0.05, *P ≤ 0.05, **P ≤ 0.01, ***P ≤ 0.001, **** P ≤ 0.0001. Compared to vehicle, unless indicated by a bar. C) The total bioluminescence (BLI) of each mouse was quantified from the bioluminescent images (Appendix Figure 4-4). Mean BLI ± SD shown One-way ANOVA was performed with a Tukey's multiple comparison test, the adjusted p-value is shown. Compared to vehicle, unless indicated by a bar. D) The weights of the mice were monitored daily during the dosing period and the weight changes as % of initial weight shown. Grey = dosing days. E) Full blood count analysis at ethical endpoint. Red blood cell count, haemoglobin levels, haematocrit and mean corpuscular volume (MCV) are shown. Grey areas indicate the average and reference ranges based off Charles River guidelines for C57Bl/6 females North American Colonies (January 2008 – December 2012). N=2-5/group.

MLL/AF9 NRAS: CX-5461 + chloroquine

A)

Chloroquine dosing lowered to 50mg/kg as of day 19.

B)

MLL/AF9 NRAS: CX-5461 + chloroquine

C)

Total BLI

Legend:
- Vehicle
- Chloroquine
- CX-5461
- CX-5461 + CQ

Day 7 — All N.S

Day 14 — N.S, ****, ****, N.S

Day 21

D)

Vehicle: #07, #12, #13, #14, #76, #77, #99, #30

80mg/kg chloroquine: #04, #58, #59, #00, #32, #84, #37, #90

30mg/kg CX-5461: #33, #34, #35, #38, #30, #31, #32, #60

CX-5461 + chloroquine: #75, #84A, #85A, #06, #84B, #85B, #86, #87

*Chloroquine lowered to 50mg/kg as of day 19

113

MLL/AF9 NRAS: CX-5461 + chloroquine

E)

Red blood cells

Haemoglobin

Hematocrit
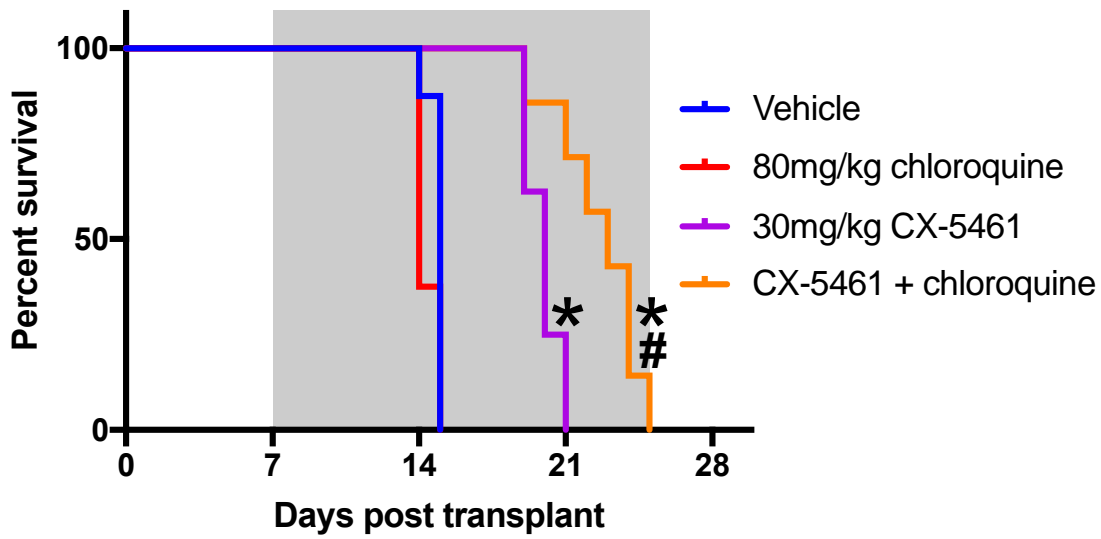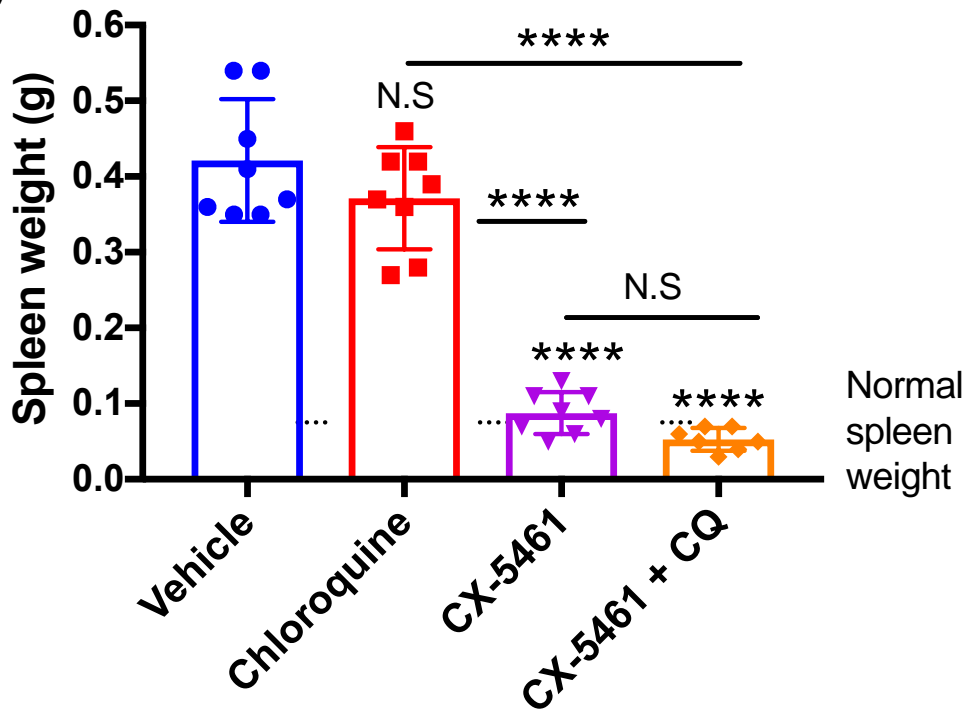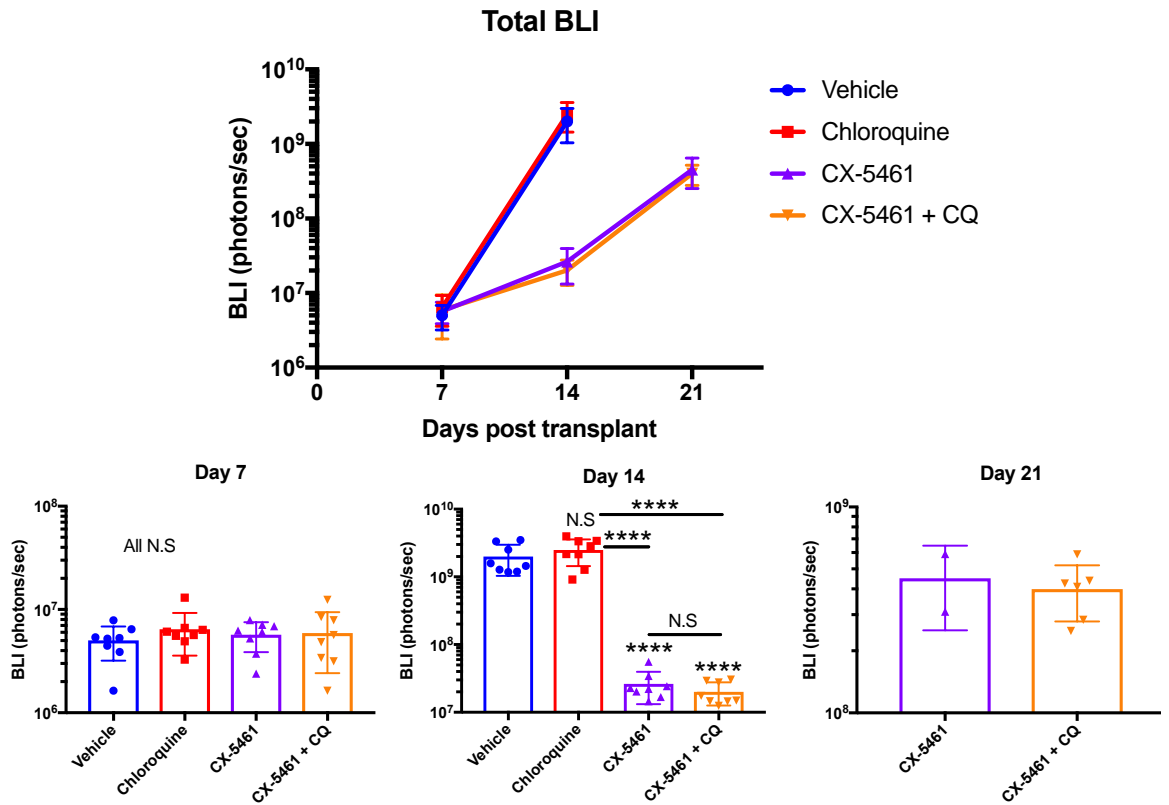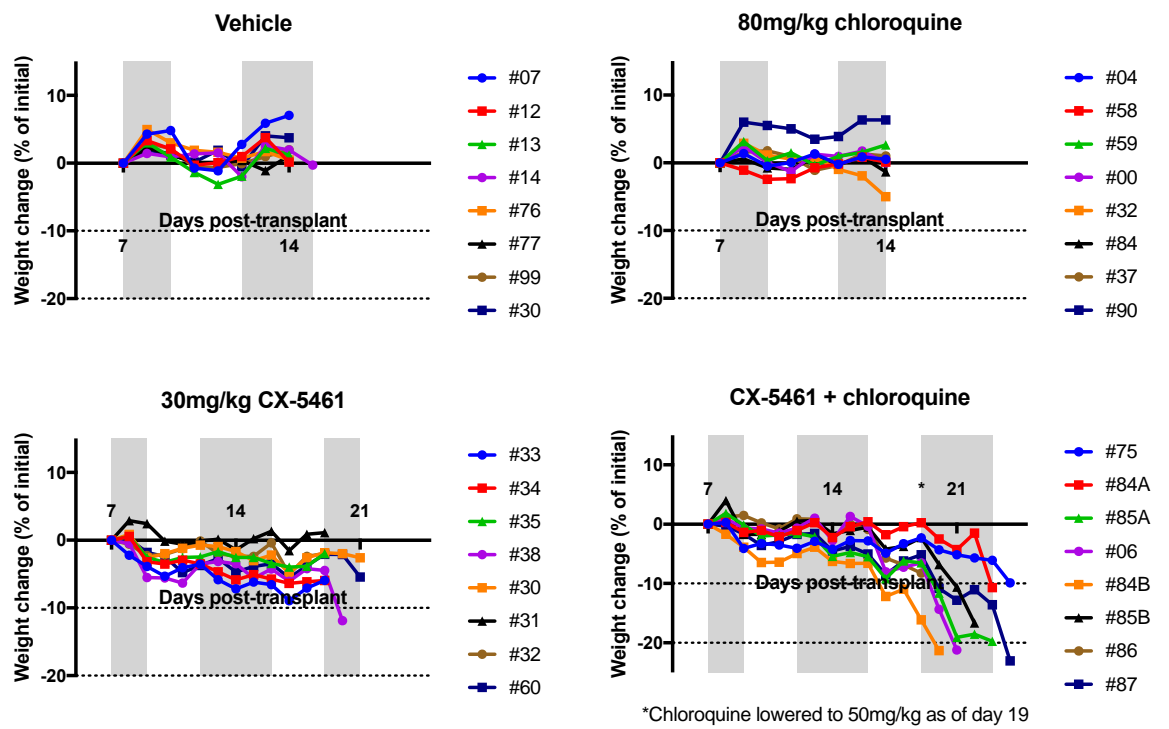
Mean corpuscular volume
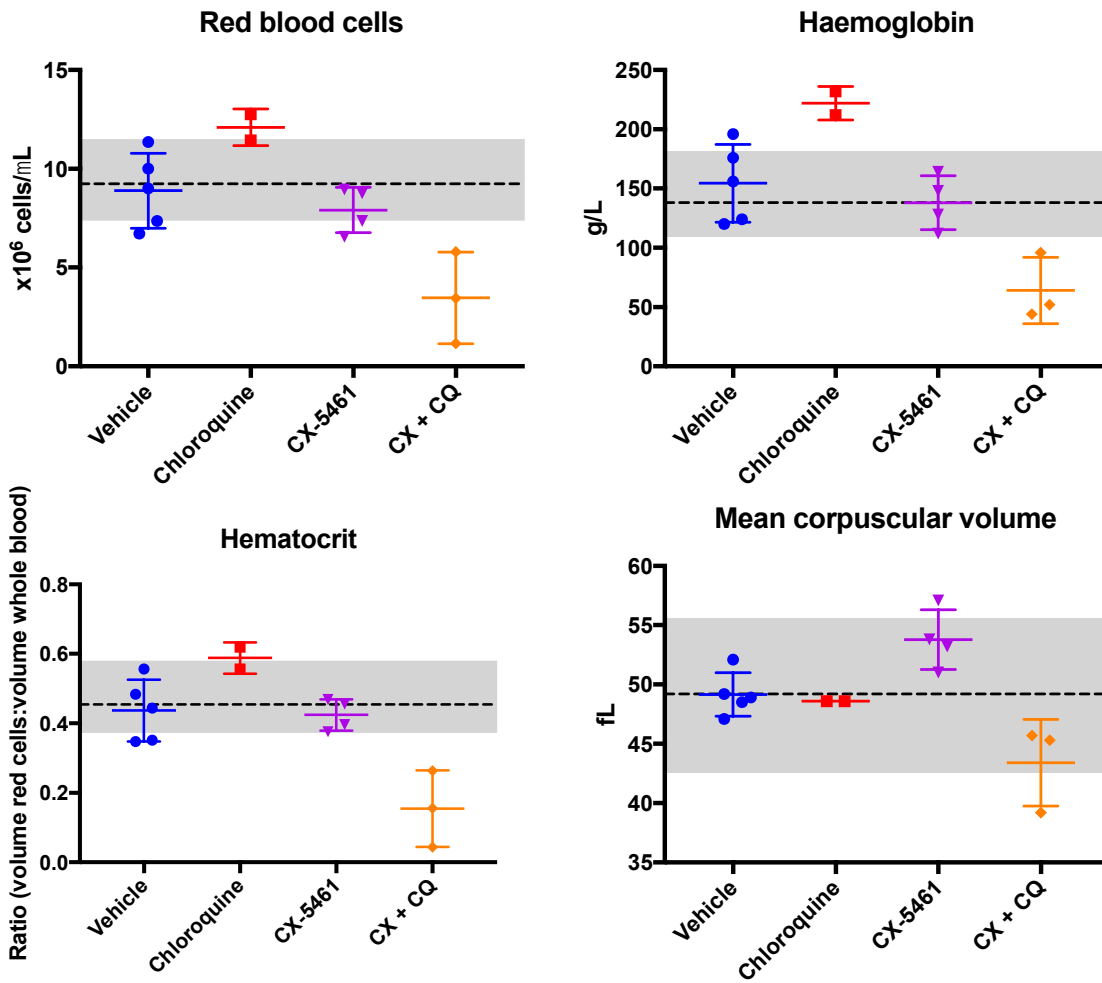
4.2.3 Creation of GFP-luc tagged human AML cell lines and characterising the disease model in vivo in NSG mice

The synergism of CX-5461 and chloroquine was also tested in human cell line xenografts. In order to track the human leukaemia cell lines both *in vivo* by live-animal bioluminescent imaging and potentially *ex vivo* through flow cytometry, the cell lines were tagged with GFP and luciferase (described in Methods Section 2.9). In brief, retroviral particles containing the MSCV-GFP-luc2 construct were used to transduce the MV4-11, THP-1 and MOLM-13 human leukaemia cell lines through retroviral spin infection. The transduced cells were then identified by GFP positivity and cell sorted (results not shown), and the resulting cells named '(cell line) GFP luc'.

In order to characterise the disease produced by these cells *in vivo*, a small cohort of immunocompromised NSG mice (which lack functional B, T and natural killer (NK) cells) were injected with 2 x 10^6 cells IV via the tail vein. For the THP-1 cells, the day before injection the mice were irradiated with 1Gy single dose (sub-lethal dose) in order to facilitate the engraftment of the leukaemia cells by disrupting the complex host bone marrow environment[227] (irradiation has been shown to result in various changes to the bone marrow environment including cytokine release,[228] [229] and lymphodepletion in immunocompetent models [230]). The other cell lines were injected without irradiation of the host mice. Health monitoring was performed daily and bioluminescent imaging was performed every 2 days (MOLM-13 GFP luc) or weekly (THP-1 and MV4-11 GFP luc) to track the progression of the disease. This continued until an ethical endpoint was reached. The features of each of the xenograft models are summarised in Table 4-2 and compared to those of the MLL/AF9 NRAS syngeneic model.

Figure 4-7a shows the overall survival of the three models. The MOLM-13 GFP luc cells produced the most aggressive disease, with a median survival of 14 days post-transplant, followed by the MV4-11 GFP luc cells at 22 days post-transplant. Interestingly, the MV4-11 GFP luc cells generated a more aggressive disease than that published in the literature, 36 days survival post-transplant for the same number of cell injected [33], which may be explained by genetic drift in either the MV4-11 GFP luc cell line or in the NSG mouse colony, or by selection of more aggressive clones during the transduction process. With the exception of one mouse which became unwell at

44 days post-transplant, the mice in the THP-1 GFP luc group remained well at 52 days post-transplant and the experiment was concluded, thus a true survival time was not established.

Bioluminescent imaging (Figure 4-7c) in the MOLM-13 GFP luc model indicated engraftment was faintly visible at day 3 post-transplant, and was well established at day 5 post-transplant, indicating that day 4 post-transplant would be an ideal timepoint to confirm engraftment and begin drug treatment. Over the next week of imaging, the bioluminescent signal in the upper body and hind limbs increased rapidly, appearing to disseminate more broadly by day 14. Since the literature reported that hind limb paralysis is a predominant feature of this model the prone (back) position was also imaged. Bioluminescent signals across and either side of the spine, indicating peripheral organ involvement, were visible from day 7 onwards, as well as in the skull, which is consistent with the literature [206]. The average total BLI of the mice increased rapidly over the 14 day period, to a level higher than that observed in the THP-1 or MV4-11 GFP luc groups at day 7 and day 14 post-transplant (Figure 4-7d). In the MV4-11 GFP luc model, engraftment was visible in the hind limbs at 7 days post-transplant, increasing in intensity at 14 and 21 days post-transplant and spread to the midsection and front limbs. In the THP-1 GFP luc model bioluminescence was first detected in the pelvic region at 7 days post-transplant, spreading to more distal regions at day 14, and continuing to increase predominately in the pelvic and midsection regions over the next 3 weeks. The BLI was similar to the MV4-11 GFP luc group at day 7 and 14 post-transplant (but significantly less than the MOLM-13 GFP luc), however, it surpassed the maximum average BLI of the MOLM-13 GFP luc group (at day 14) when the mice reached day 28 post-transplant.

The spleens of the MOLM-13 GFP luc and MV4-11 GFP luc-bearing mice were significantly enlarged to approximately four times the normal weight (Figure 4-7b), consistent with the literature [33]. Splenomegaly was not observed in the THP-1 GFP luc model. The literature reports that the spleens of THP-1 bearing mice were 2-3 times normal size [208], however, these published experiments were conducted at 10 weeks post-transplant, it is possible that the spleens of the mice in this study may have been

larger if the experiment was continued for a further 3 weeks. What is clear from these results is that spleen enlargement is not an early occurrence in this model.

Figure 4-7: Characterisation of human AML cell line xenograft models

Mice were transplanted with 2×10^6 human AML cell line cells in the tail vein (following 1 Gy single dose irradiation for the THP-1 GFP luc cells), Methods Section 2.6.2.2. General health was monitored daily and the mice were euthanised once an ethical endpoint was reached. N=5 for MV4-11 GFP luc, N= 6 for THP-1 GFP luc, N=3-4 mice/imaging day for MOLM-13 GFP luc. A) Kaplan Meier survival curves. B) Spleen weight at ethical endpoint, mean ± SD. The fold change from a normal NSG spleen shown. C) Bioluminescent imaging. Due to ethical requirements regarding the frequency of imaging, a cohort of mice was injected with the MOLM-13 GFP luc cells then divided into 3 groups which were imaged on different days. Due to hind limb paralysis observed in a pilot study, these mice were imaged both supine (face up) and prone (face down), in order to visualise the spine. Different image colour scales are used between and within the different cell lines. D) Quantification of total bioluminescence (BLI), prone measurements not included for MOLM-13 GFP luc. Not significant (NS) $P > 0.05$, *$P \leq 0.05$, **$P \leq 0.01$, ***$P \leq 0.001$, **** $P \leq 0.0001$. E) Weight changes as % initial weight. F) Images of enlarged organs at autopsy i) Liver of a THP-1 GFP luc injected mouse at 52 days post-transplant ii) Left (L) and right (R) ovaries of a MV4-11 GFP luc injected mouse at 22 days post-transplant, compared to the ovary of a non-tumour bearing NSG mouse of a similar age and weight iii) Ovaries and fallopian tubes of a MV4-11 GFP luc injected mouse at 22 days post-transplant.

Characterisation of human cell line xenograft models

A)
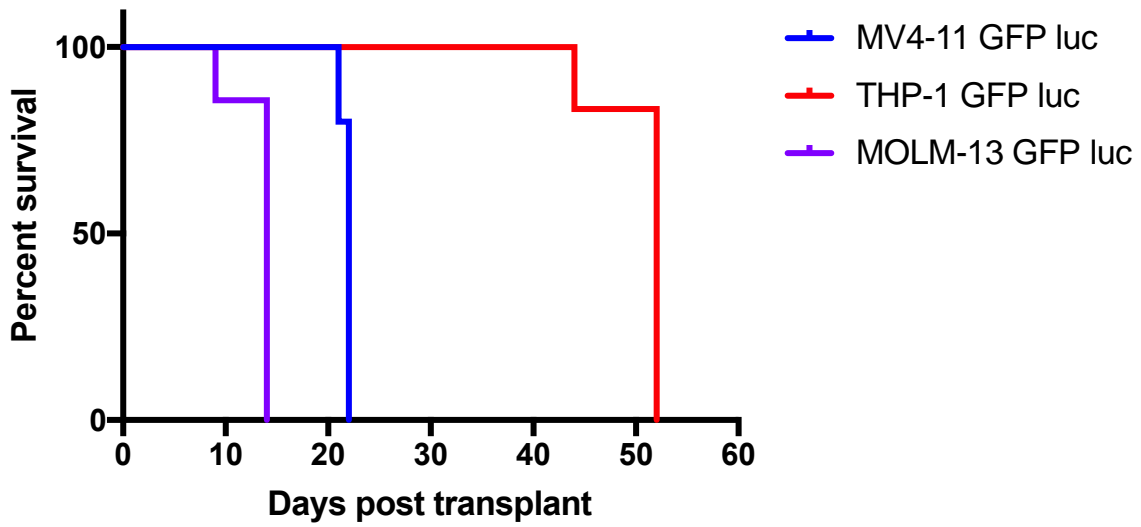
Median survival (days):
MV4-11 GFP luc = 22
THP-1 GFP luc = Unknown (experiment concluded at 52 days)
MOLM-13 GFP luc = 14

B)
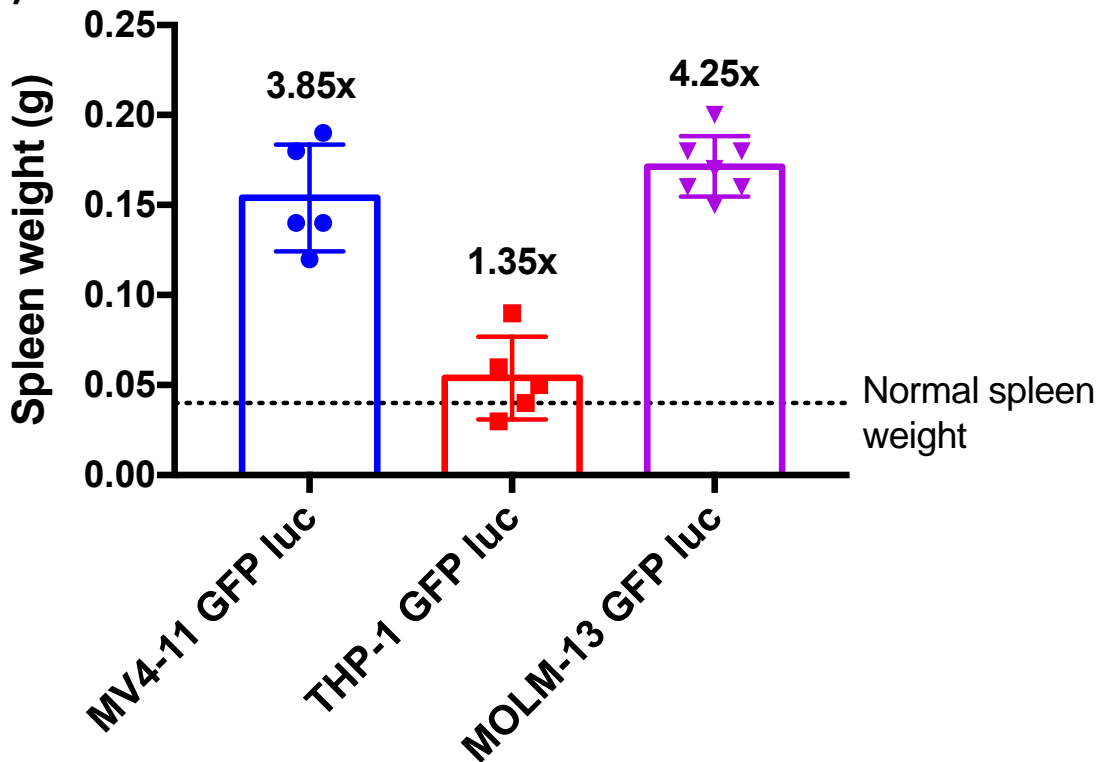
Characterisation of human cell line xenograft models
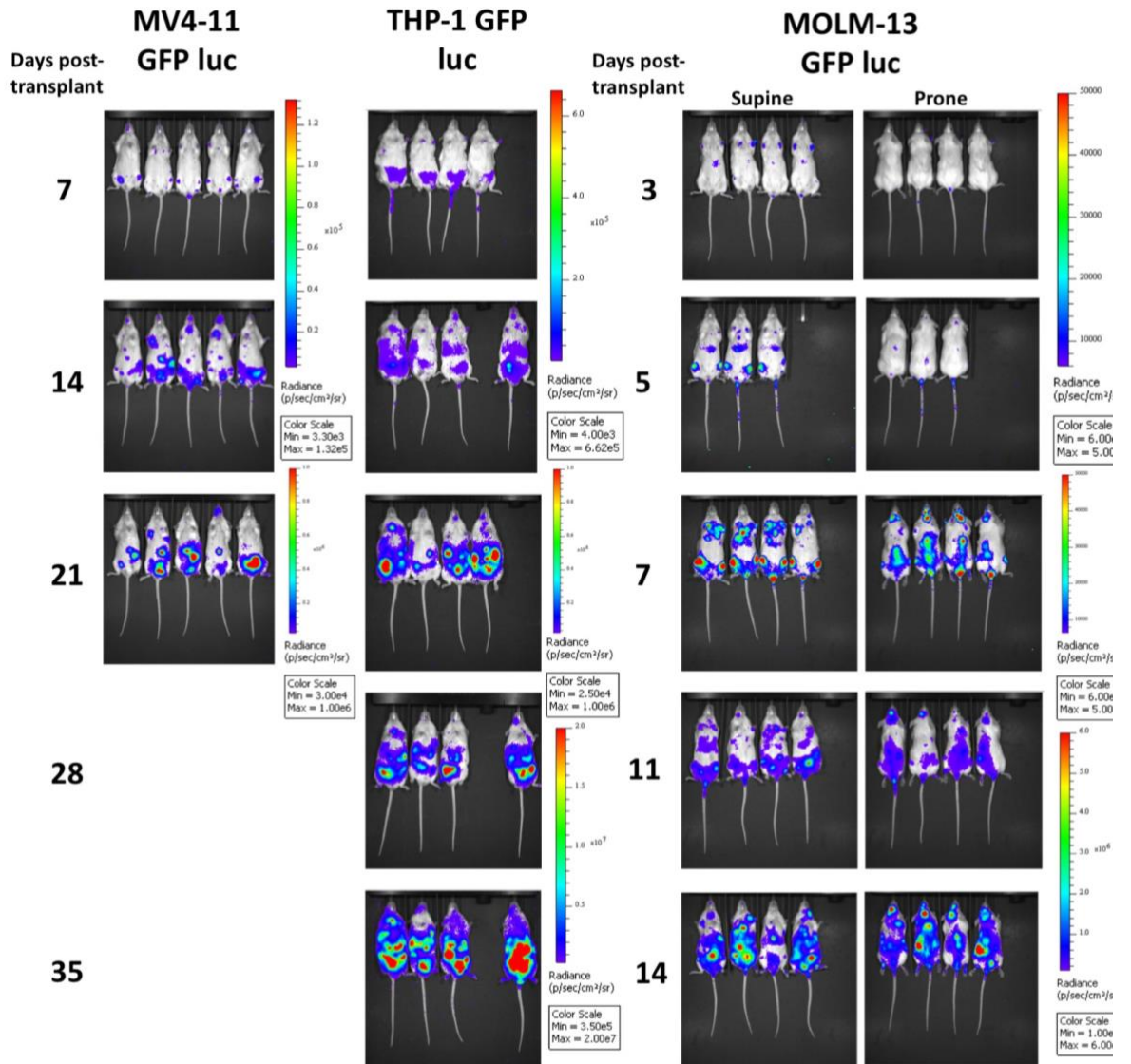
C)

Characterisation of human cell line xenograft models

D)

Total bioluminescence (BLI)

MV4-11 GFP luc
THP-1 GFP luc
MOLM-13 GFP luc

Day 7

NS ** **

Day 14

NS *** ***

E)

MV4-11 GFP luc

#52
#53
#54
#55
#56

THP-1 GFP luc

#67
#81
#82
#64
#65
#66

MOLM-13 GFP luc

#42
#43
#44
#45
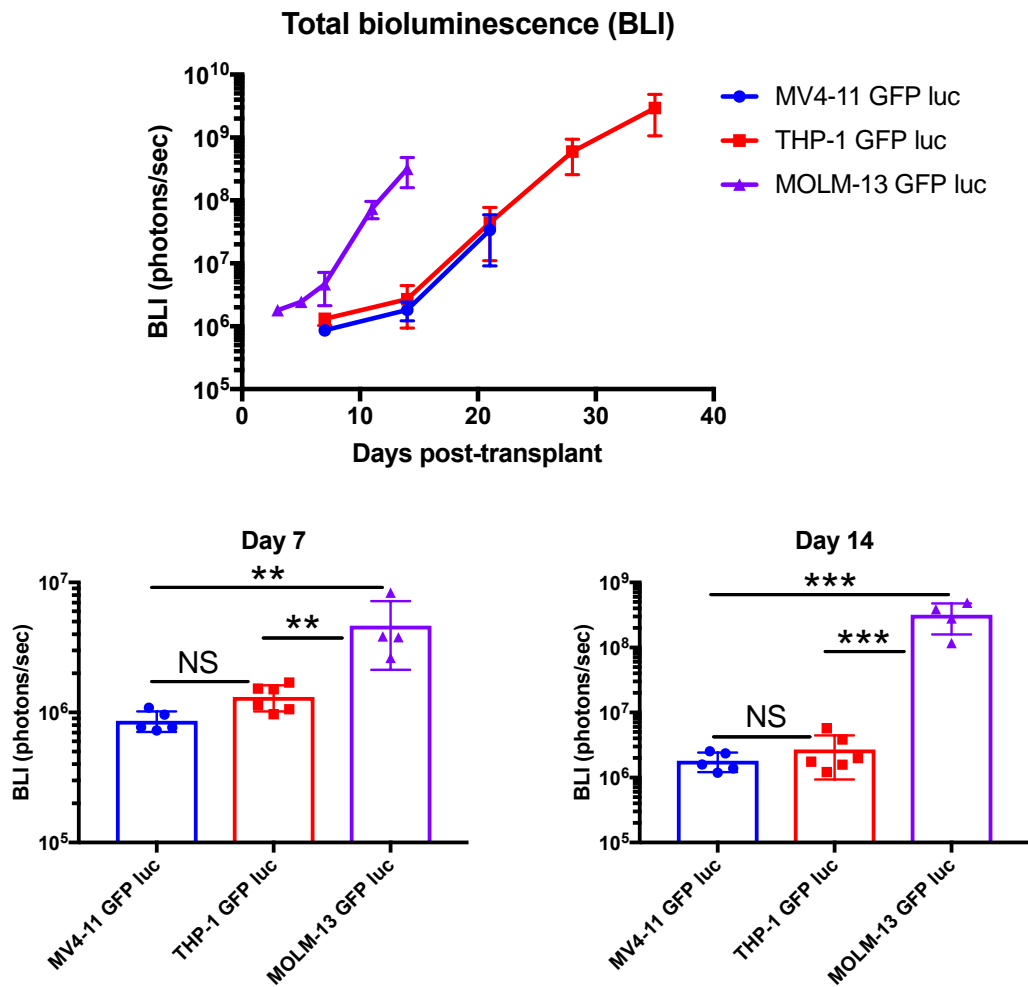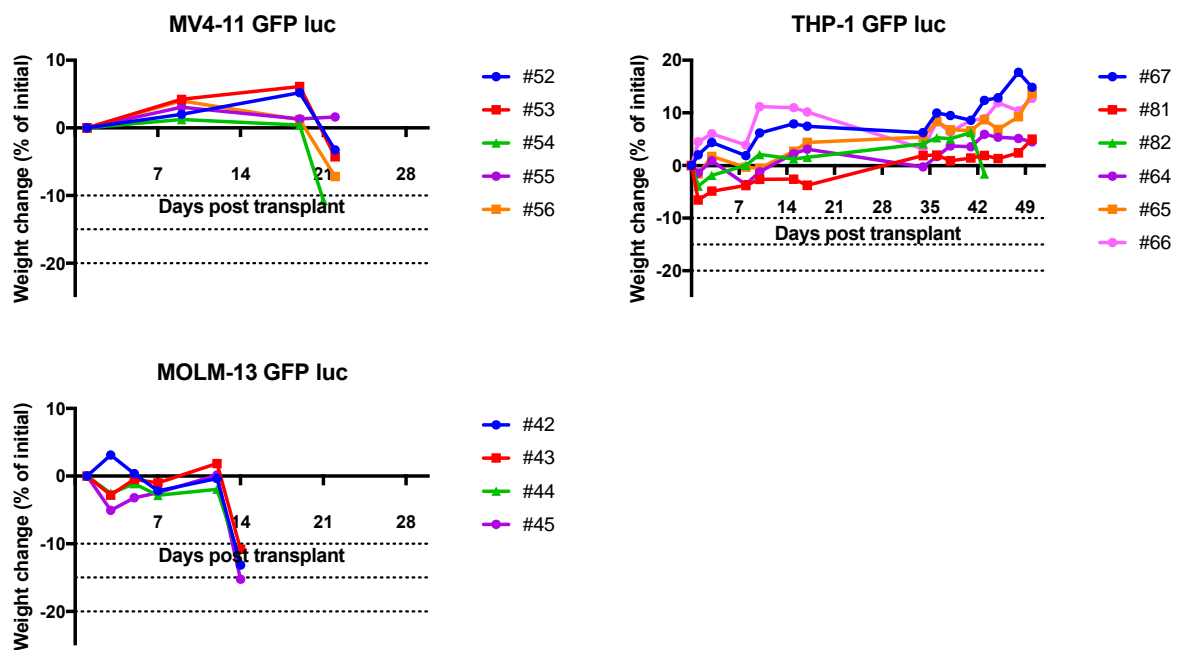
Characterisation of human cell line xenograft models

F)

i) Liver of a THP-1 GFP luc injected mouse

ii) Left (L) and right (R) ovaries of a MV4-11 injected mouse, compared to a normal (N) ovary

iii) Ovaries and fallopian tubes of a MV4-11 GFP luc injected mouse

The predominant features at endpoint varied between the three models. The dominant feature of the MOLM-13 GFP luc model was hind limb paralysis, which likely contributed to the rapid weight loss of 10-20% body weight over 1-2 days (Figure 4-7e) for which the mice required euthanasia. The development of hind limb paralysis is consistent with the reported literature [206], likely due to infiltration of cancer cells in the central nervous system and cord compression, as observed by a high bioluminescent signal around the spine (Figure 4-7b). All of the mice also had enlarged ovaries on one or both sides (consistent with the strong bioluminescent signal observed just below the midsection in the imaging, and sporadic lymph node enlargement, which are both reported features of this model [206,231]. In the MV4-11 GFP luc model hind limb paralysis at the ethical endpoint was occasionally observed, which is a reported feature of the model [205] and explains the rapid weight loss at day 22 (Figure 4-7e), as was ovary enlargement on one or both sides, which has not previously been reported. Interestingly, in the THP-1 GFP luc models the livers were massively enlarged due to the presence of numerous solid tumours (Figure 4-7f), explaining the strong bioluminescent signal from this area during imaging (Figure 4-7c), and the weights of the mice increasing during the course of the experiment, with two mice reaching more than 10% weight gain by day 52 (Figure 4-7e). The enlargement of the liver is a previously reported feature of this model[207]. Other features of this model included lymph node enlargement and tumours behind the eyes and under the skin, which have not previously been reported. Due to the irregularities of this model compared to other established AML transplant models, the THP-1 GFP luc model was not selected for further survival experiments.

The predominant features of the four different orthotopic AML used in this thesis are summarised in Table 4-2. A comparison of the features of these AML transplant models to those of human AML patients is discussed in Section 4.3.3.

Disease characteristics	Orthotopic AML Transplant Models			
	MLL/AF9 NRAS	MV4-11	THP-1	MOLM-13
Syngeneic/xenograft	Syngeneic	Xenograft	Xenograft	Xenograft
Mouse strain	C57Bl/6 (immune competent)	NSG (immune deficient)	NSG (immune deficient)	NSG (immune deficient)
Ethical endpoint reached (days post-transplant)	14	21	N/A (experiment terminated at 52 days)	14
Spleen enlargement	Yes	Yes	Subtle	Yes
Ovary enlargement	No	Yes, occasionally.	No	Yes, common.
Lymph node enlargement	No	Yes, occasionally.	Yes	Yes
Weight loss at endpoint	No	Yes. <10% of initial weight.	No	Yes. >10% of initial weight.
Hind limb paralysis at endpoint	No	Yes, ~25% of mice.	No	Yes, all.
Other features	Enlarged liver.		Numerous solid tumours on liver. Tumours behind eyes and under the skin, occasionally.	

Table 4-2: Comparison of disease characteristics of orthotopic AML models

Characteristics of each of the orthotopic AML transplant models were summarised from trial experiments to determine engraftment and survival time, and from vehicle-only treated mice from drug treatment experiments. NSG = NOD-Scid-gamma.

4.2.4 Treatment of human cell line xenografts

As the most promising drug combination in the MLL/AF9 NRAS model, CX-5461 + chloroquine was tested in human cell line xenograft survival experiments using the MOLM-13 GFP luc and MV4-11 GFP luc models (Methods Section 2.6.2.2). Using the conditions previously established in the model characterisation experiments (Figure 4-7) NSG mice were injected with 2 x 10^6 cells IV in the tail vein, then imaged at day 4

(MOLM-13 GFP luc cells) or day 7 (MV4-11 GFP luc cells) post-transplant to confirm tumour cell engraftment, randomised into treatment groups and dosing commenced. A modified dosing regime of 30mg/kg CX-5461 + 50mg/kg chloroquine was used in order to avoid the side effects observed in the MLL/AF9 NRAS experiment (Figure 4-6). As previously, "survival" was defined as the time post-transplant until the mice reached an ethical endpoint and required euthanasia due to symptoms such as weight loss, reluctance to move and hunching. Median survival times and subsequent statistical analysis of survival times are shown in Appendix Tables 4-1 and 4-2.

4.2.4.1   CX-5461 + chloroquine in MOLM-13 xenograft

Chloroquine treatment at 50mg/kg did not improve survival compared to vehicle treatment, with a median survival time of 14 days post-transplant in both groups (Figure 4-8a). CX-5461 treatment at 30mg/kg improved survival significantly to 15 days post-transplant, as did combination treatment. There was no significant difference between the survival of the CX-5461 and combination-treated groups.

The spleens of the vehicle-treated mice were enlarged (Figure 4-8b), which is consistent with Figure 4-7b. Chloroquine treatment did not significantly impact on spleen enlargement, whereas the spleens of CX-5461 and combination-treated mice were significantly smaller than the vehicle-treated mice, although still enlarged. The addition of chloroquine to CX-5461 treatment did not further reduce disease burden in the spleen.

The bioluminescent imaging (Appendix Figure 4-5) shows disease patterns consistent with the characterisation experiment (Figure 4-6c). Quantification of the bioluminescent imaging showed that the total BLI (supine) of the treatment groups was similar, whereas the prone BLI of the chloroquine treated mice was significantly higher than the vehicle and the combination-treated groups (Figure 4-8d). The same trends in rapid weight loss from day 10 onwards were observed for all the treatment groups, likely due to the hind limb paralysis which is a previously confirmed feature of this model (Figure 4-8e), rather than toxicity of the drugs.

Figure 4-8: Combination therapy with CX-5461 and chloroquine does not improve survival *in vivo* in the MOLM-13 AML cell line xenograft model

Mice were transplanted with MOLM-13 cells via the tail vein, imaged by bioluminescence to confirm engraftment at day 4 and therapy initiated. Mice were dosed with vehicle (50mM NaH_2PO_4), 50mg/kg chloroquine (CQ) daily Monday-Friday, 30mg/kg CX-5461 Monday, Wednesday, Friday, or the combination, until reaching an ethical endpoint. N=8 mice/treatment group. A) Kaplan-Meier survival curves. Log-rank test with Bonferroni corrected threshold was applied for comparison of multiple survival curves, such that a P value of <0.0083 was considered significant. Key comparisons: * = significant compared to vehicle. The grey area indicates the dosing period. B) Spleen weight at ethical endpoint. Mean weight ± SD shown. One-way ANOVA was performed with a Tukey's multiple comparison test, the adjusted p-value is shown. NS $P > 0.05$, *$P \leq 0.05$, **$P \leq 0.01$, ***$P \leq 0.001$, **** $P \leq 0.0001$. Compared to vehicle, unless indicated by a bar. C) The total bioluminescence (BLI) of each mouse was quantified from the bioluminescent images (Appendix Figure 4-5). Mean BLI ± SD shown. Issues with the background levels on day 4 of imaging meant many of the mice had a negative BLI value, so quantification was not shown for this timepoint. One-way ANOVA was performed with a Tukey's multiple comparison test, the adjusted p-value is shown. Compared to vehicle, unless indicated by a bar. D) The weights of the mice were monitored daily during the dosing period and the weight changes as % of initial weight shown.

MOLM-13 xenograft: CX-5461 + Chloroquine

A)
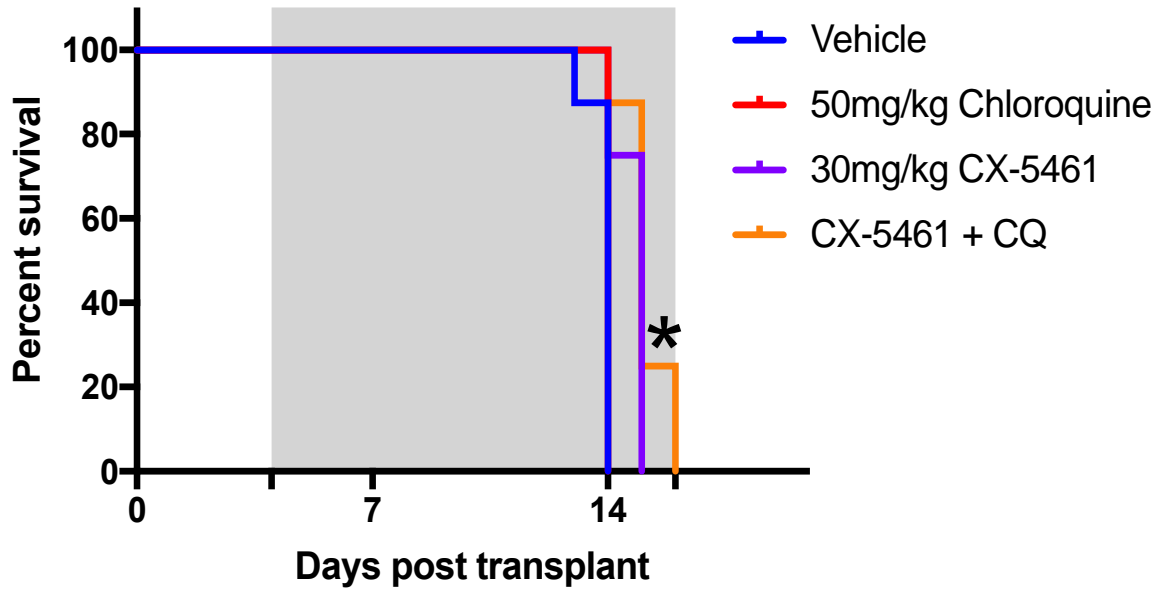
B)
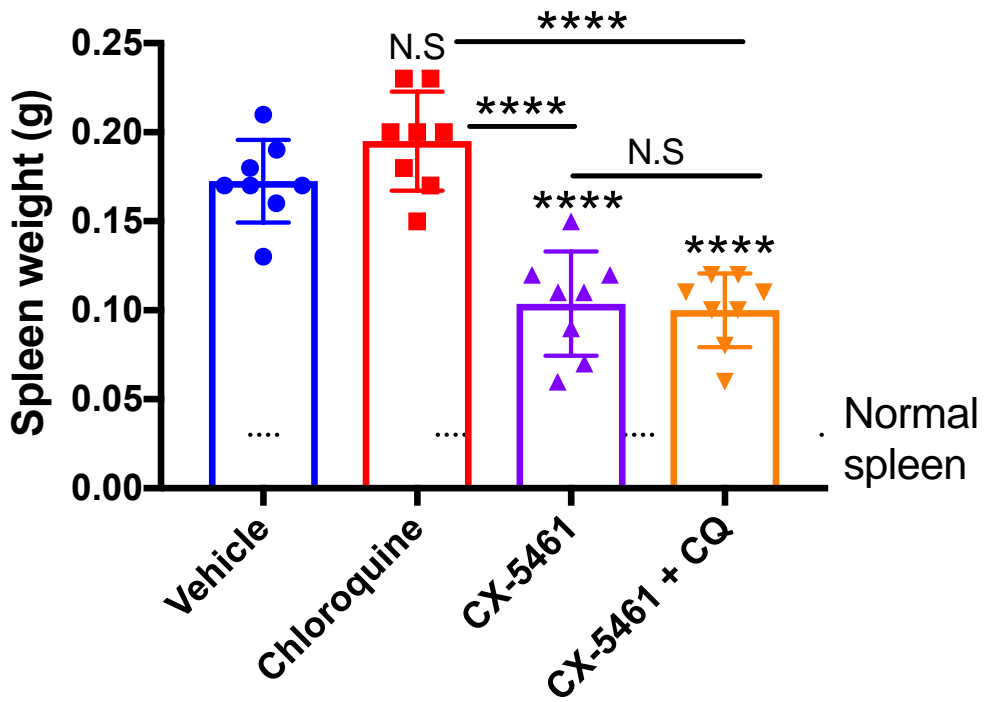
MOLM-13 xenograft: CX-5461 + Chloroquine

C)
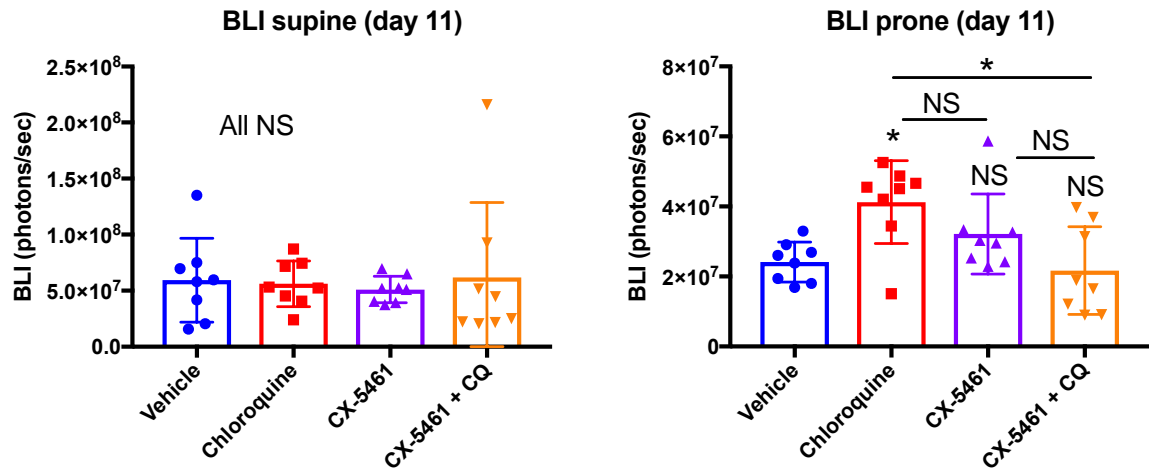
D)
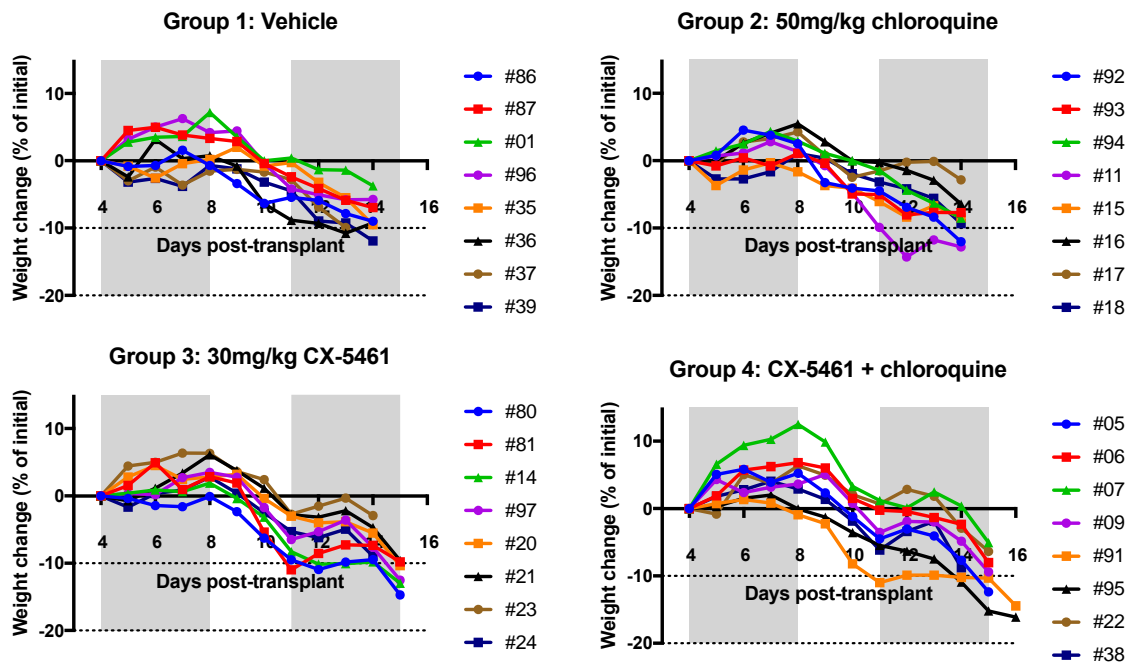
4.2.4.2   CX-5461 + chloroquine in MV4-11 xenograft

In the MV4-11 GFP luc xenograft model the vehicle-treated mice had a median survival of 22 days post-transplant, consistent with the characterisation experiment (Figure 4-7a), CX-5461 treatment or chloroquine treatment did not significantly change median survival (Figure 4-9a). Combination treatment resulted in a small, statistically significant survival advantage of 2-3 days over the other 3 groups, but this may not be biologically significant.

The spleen weights of the vehicle-treated group (Figure 4-9b), as observed in Figure 4-7b, and the chloroquine group were similarly enlarged. The CX-5461 treated mice had significantly smaller spleens than the vehicle mice, but this was not further decreased with the addition of chloroquine.

The bioluminescent imaging (Appendix Figure 4-6) of the treatment groups over the course of the experiment was consistent with the characterisation experiment (Figure 4-7). There was no significant difference in the BLI quantification (Figure 4-9c) between the groups at day 7, 14 and 21 post-transplant, although there is a large amount of variation in the vehicle and combination-treated groups at day 21 post-transplant.

The weights of the mice remained quite stable, in fact increased in a number of cases, over the course of the experiment (Appendix Figure 4-7). The exceptions were spread across the different treatment groups, where rapid weight loss in a 1 day period was likely due to the development of hind limb paralysis. These weight results indicate that the treatment regimes were tolerated in this model.

Figure 4-9: Combination therapy with CX-5461 and chloroquine improves survival *in vivo* in the MV4-11 AML cell line xenograft model

Mice were transplanted with MV4-11 cells via the tail vein, imaged by bioluminescence to confirm engraftment at day 4 and therapy initiated. Mice were dosed with vehicle (50mM NaH_2PO_4), 50mg/kg chloroquine daily Monday-Friday, 30mg/kg CX-5461 Monday, Wednesday, Friday, or the combination, until reaching an ethical endpoint. N=8 mice/treatment group. A) Kaplan-Meier survival curves. Log-rank test with Bonferroni corrected threshold was applied for comparison of multiple survival curves, such that a P value of <0.0083 was considered significant. Key comparisons: * = significant compared to vehicle, # = significant compared to CX-5461. The grey area indicates the dosing period. B) Spleen weight at ethical endpoint. Mean weight ± SD shown. One-way ANOVA was performed with a Tukey's multiple comparison test, the adjusted p-value is shown. NS $P > 0.05$, *$P \leq 0.05$, **$P \leq 0.01$, ***$P \leq 0.001$, **** $P \leq 0.0001$. Compared to vehicle, unless indicated by a bar. C) The total bioluminescence (BLI) of each mouse was quantified from the bioluminescent images (Appendix Figure 4-6). Mean BLI ± SD shown. One-way ANOVA was performed with a Tukey's multiple comparison test, the adjusted p-value is shown. Compared to vehicle, unless indicated by a bar. NS = not significant.

MV4-11 xenograft: CX-5461 + Chloroquine

A)
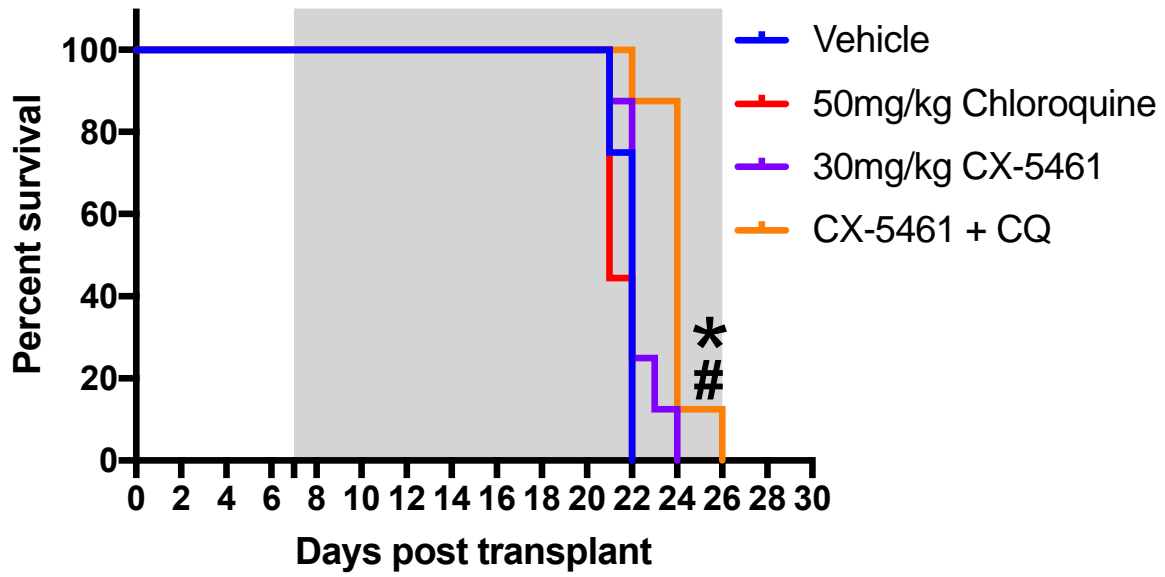
B)
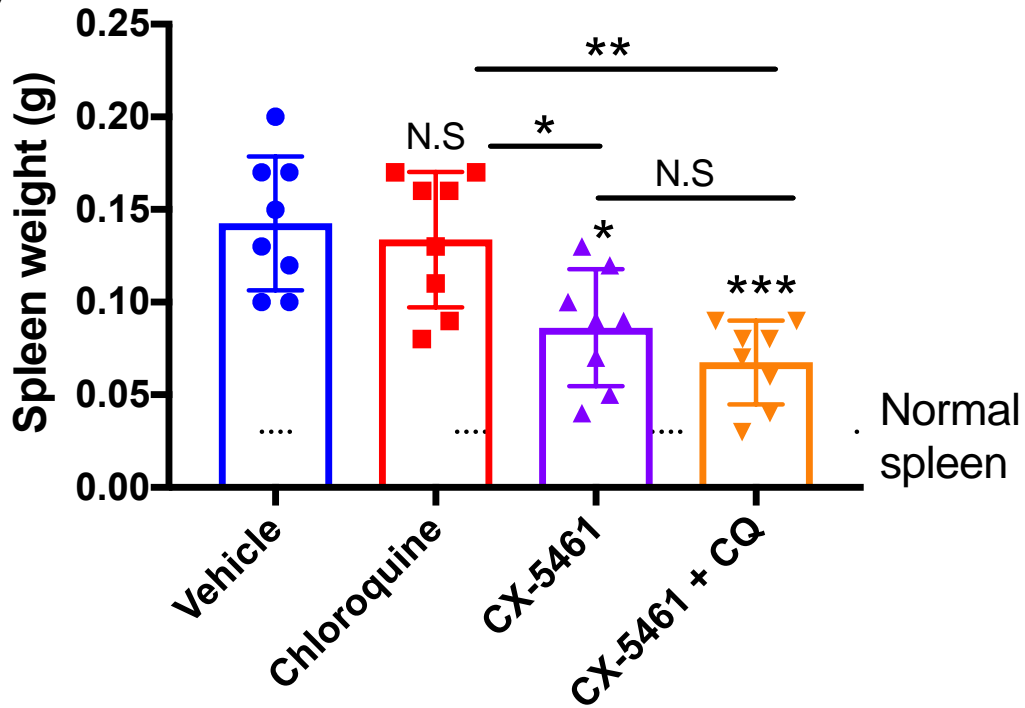
MV4-11 xenograft: CX-5461 + Chloroquine

C)
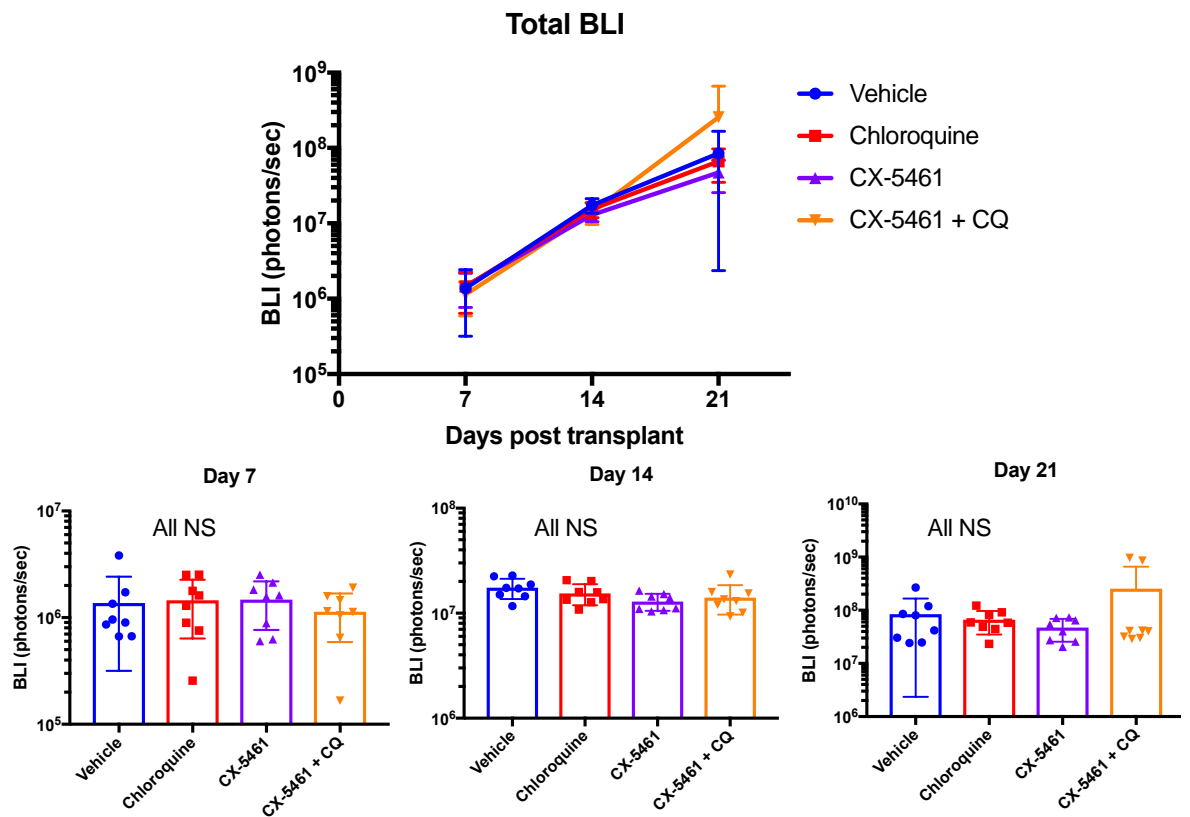
4.2.5 Summary of results

Consistent with the literature, CX-5461 is effective in improving survival and reducing tumour burden in the spleen in the syngeneic MLL/AF9 NRAS model [1]. In the human cell line xenograft models, CX-5461 resulted in limited or no survival advantage, however, it did significantly reduce tumour burden in the spleen. These results show that CX-5461 can target human AML cells *in vivo*, but requires adjustment to the dosing schedule or combination therapy to improve efficacy. Synergism between CX-5461 + chloroquine was shown *in vivo*, with combination therapy significantly improving survival in the MLL/AF9 NRAS and MV4-11 GFP luc models, however it did not reduce tumour burden in the spleen compared to CX-5461 alone.

4.3 Discussion

4.3.1 Combination treatment outcomes

4.3.1.1 Combination treatment outcomes in the syngeneic model

Three drug combinations were tested in the syngeneic MLL/AF9 NRAS model in order to determine if they provided a survival advantage compared to the individual drugs. The combination of CX-5461 plus orlistat (Figure 4-4) or DCA (Figure 4-5) did not alter survival compared to the single agents. However, the combination of CX-5461 with chloroquine significantly increased survival compared to the vehicle, chloroquine and CX-5461 alone (Figure 4-6). As a result, this drug combination was evaluated in human cell line xenograft models (Figure 4-8, Figure 4-9).

This well-established MLL/AF9 NRAS model has benefits, but also limitations, compared to the human cell line xenograft models. Since the cells for the MLL/AF9 NRAS model and the host mice are genetically matched the cells can be transplanted into an immune-competent host. This is important as immune cells are an integral part of the bone marrow microenvironment and play a role in attacking tumour cells (Section 4.1.1) so it is important to evaluate drug efficacy in this context. A limitation using this model specifically related to evaluating CX-5461 is that CX-5461 treatment as a single agent slows the growth of tumour cells in most areas of the mouse body except for the head region (Figure 4-4). This results in the mice eventually developing breathing difficulties for which they required euthanasia, despite minimal disease in the midsection including in vital organs such as the liver. Analysis of the location of the tumour cells revealed they are in the nasal passages, rather than the brain (Hein, unpublished), which may be due to medullary expansion of the turbinates, an area rich in lymphatics [232]. Infiltration of AML cells in the nasal passage is not a reported feature of human disease. A comparison of the features of the MLL/AF9 NRAS model, and the human cell line xenograft models, with those of human AML patients is covered in Section 4.3.3. If the disease levels could be controlled in this region, the survival advantage with CX-5461 treatment would be greatly improved, however, none of the combination therapies tested in the MLL/AF9 NRAS model achieved this outcome.

There are several future experiments which could be conducted in this model. Due to time constraints tolerability testing of the combination of CX-5461 with ritonavir or omeprazole was not completed, and neither were the survival experiments to determine if these combination therapies improved survival of MLL/AF9 NRAS-bearing mice. Of the 3 drug combinations evaluated in the MLL/AF9 NRAS model, CX-5461 + chloroquine was the only one which resulted in a survival advantage (Figure 4-6). In order to evaluate the mechanism behind this survival advantage short term treatment experiments (for example a single dose of individual drugs or the combination for 6 h in mice 10 days post-transplant when tumour levels are high but the mice are not yet compromised) should be performed to determine the initial effects of the drugs on parameters such as cell cycle arrest, apoptosis and cell death, as well as on-target mechanisms of action of the drugs.

4.3.1.2   Combination treatment outcomes in the xenograft experiments

The efficacy of CX-5461 with chloroquine was tested in 2 human AML xenograft models, the MOLM-13 GFP luc and MV4-11 GFP luc. Despite observing a robust synergistic effect of CX-5461 with chloroquine *in vitro*, this did not translate to improved survival in the MOLM-13 GFP luc model (Figure 4-8), however a small survival advantage was observed in the MV4-11 GFP luc model (Figure 4-9). This survival difference, while statistically significant, may not be biologically significant.

To date there are no published accounts of CX-5461 or chloroquine being testing in MOLM-13 xenograft models. However, CX-5461 efficacy has been tested in an MV4-11 xenograft model, where the cells were injected into the flank of the mouse (heterotopic) and tumour volume compared between mice dosed with either vehicle or CX-5461 at 125mg/kg week by intraperitoneal injection for 3 weeks. CX-5461 was found to significantly inhibit tumour growth by 3-fold compared to the vehicle-treated mice. This astounding result contrasts with the lack of efficacy of CX-5461 and CX-5461 with chloroquine observed in this thesis (Figure 4-9). Several factors could account for this discrepancy. Firstly, the location of the tumour cells differs; in the orthotopic model it is possible the bone marrow microenvironment supports the AML cells so they are more drug-resistant (Section 4.1.1). Secondly, the dosing schedule and route of administration differs, specifically in the heterotopic model CX-5461 was

administered intraperitoneally, compared to orally in the orthotopic models, which can alter the accessibility of the drug to the tumour cells as the peritoneum is in close proximity to the flank. CX-5461 was also dosed at a higher dose of 125mg/kg/week, compared to the 30mg/kg 3 times a week used in these studies, which will affect the pharmacodynamics of the drug. Lastly, the strains of mice differed between the experiments. In the heterotopic model used immunocompromised athymic nude mice (CrTac:Ncr-Foxn1nu), compared to the NSG mice used in the orthotopic models. Athymic nude mice only lack functional T cells [233], whereas NSG mice lack functional B, T and NK cells [204]. Thus, if an anti-tumour immune response is important for the efficacy of CX-5461 (further discussed in Section 4.3.6), this would be more impaired in the NSG mice compared to the nude mice. There are no published reports of chloroquine being tested in any MV4-11 xenograft models.

While the combination of CX-5461 + chloroquine was not effective in either of these human cell line xenograft models tested, based on the *in vitro* experiments perhaps *in vivo* testing with the SKM-1 cell line, which demonstrated a robust combination effect (Figure 3-18) would be justified. In order to do so the SKM-1 cell line would require tagging with GFP and luciferase (as completed for the MV4-11, THP-1 and MOLM-13 models, Methods Section 2.9) and disease characterisation, as in Figure 4-7.

4.3.1.3 Correlating drug treatments *in vitro* and *in vivo*

The experiments in this chapter illustrated a discrepancy between the *in vitro* and *in vivo* results. The most obvious example was the strong combination effect of CX-5461 with chloroquine *in vitro* in the MOLM-13 cell line, which was not observed using the MOLM-13 GFP luc model *in vivo*. Several factors could contribute to this inconsistency including the role of the bone marrow microenvironment on the AML cells and the drugs not reaching effective levels or combination ratios *in vivo*.

As mentioned previously, *in vivo* studies, unlike *in vitro* studies, take into account the role of bone marrow microenvironment in the response of AML cells to drugs (Section 4.1.1). It is possible that the bone marrow stroma is providing a permissive environment for the AML cells and affecting their sensitivity to the drugs. Thus perhaps a more accurate method of evaluating drug combinations *in vitro* would be

stromal co-culture experiments. Interestingly there have been studies demonstrating that co-culturing primary AML patient samples with stromal cells reduced their sensitivity to various inhibitors, including topoisomerase II and tyrosine kinase inhibitors, compared to standard culture conditions [234].

Alternatively, the drugs did not reach optimal concentrations *in vivo*, as was achieved *in vitro*. The *in vitro* experiments provide a controlled environment with direct contact between the cells and the drugs. *In vivo,* the drugs undergo a more complicated route to the tumour cells, including the requirement for its absorption, possible protein binding in the bloodstream, drug metabolism and excretion by various methods, which can alter the drug concentration in the blood and various tissues [235]. For example, MLL/AF9 NRAS cells were sensitive to DCA and chloroquine as a single agent *in vitro* (Figure 3-8) but not *in vivo* (Figure 4-5, Figure 4-6), perhaps these drugs are not reaching the tumour cells at a concentration to have an effect. In such a situation increasing the drug dose would be ideal, which is possible for DCA but not for chloroquine due to toxicity (Figure 4-3). Alternatively, the dosing schedule could be altered, such as increasing the frequency to achieve a higher or more sustained drug concentration in the body. In order to determine if the drugs reached the AML cells at an effective dose, a short term drug treatment experiment could be performed. Specifically, tumour-bearing mice would be treated with the drugs of interest for 3, 6, or 24 h and tumour cells harvested to detect drug levels by mass spectrometry, as well as perform on-target assays for the activity of the individual drugs.

A third possibility is that the drugs are not reaching the optimal ratio *in vivo* for synergy. In the *in vitro* studies, the ratio of CX-5461 to the metabolism modifying agents was critical to observe synergy. However, for the *in vivo* studies, the maximum tolerated doses were utilised rather than a set ratio. For example, in the *in vitro* experiments, 1μM of CX-5461 was found to be highly synergistic with 5μM chloroquine (1:5 molar ratio), while for the *in vivo* experiments they were dosed at a molar ratio of approximately 1:1.7 or 1:2.7. In this case, CX-5461 should have potentially been used at a lower dose, in which case it is unlikely to be effective, based on unpublished observations by the laboratory. Alternatively, chloroquine should be used at a higher

dose, however experiments presented here showed this was not possible due to toxicity (Figure 4-3).

Pharmacokinetic (PK) drug-drug interactions, where one drug modulates the absorption, distribution, metabolism, or excretion of another drug [236], could also play a role in the lack of combination efficacy *in vivo,* as well as toxicity. The PK drug-drug interactions of CX-5461 are, as of yet, not well known. PK analysis of the plasma of patients in the first-in-human, Phase I dose-escalation study of CX-5461 in advanced hematologic cancers suggests that CX-5461 undergoes enterohepatic recirculation [82]. Specifically, the liver and the intestine cooperate to 'recycle' a drug for secondary absorption, results in increased drug exposure [237]. Disruption of this process could account for the decrease in survival advantage observed in mice treated with the combination CX-5461 + orlistat, compared to CX-5461 alone in the MLL/AF9 model (Figure 4-4). If orlistat is affecting hepatic metabolism (this has not been established in the literature, as the normal route of orlistat intake is orally, with minimal systemic exposure), then the concentration and efficacy of CX-5461 could be reduced.

The effects of the drugs on expression and activity of drug-metabolising enzymes in the liver must also be considered. The effects of CX-5461 administration on the expression and activity of drug-metabolising liver enzymes is not yet well-characterised. Chloroquine has been shown to inhibit activity of the enzyme cytochrome P450 (CYP) 2D6 in humans, up to 18% after 7 daily doses of 250 mg chloroquine diphosphate [238]. If the metabolism of CX-5461 is dependent on this enzyme, then administration of chloroquine could affect the metabolism of CX-5461. The major enzymes involved in metabolism of chloroquine to its main metabolite desethylchloroquine are CYP3A4/5 and CYP2C8 [239], thus if CX-5461 affects the expression or activity of these enzymes then the metabolism of chloroquine could be affected.

Drug-drug interaction studies between CX-5461 and the metabolism modifying agents will be required to determine if it is the pharmacokinetic interactions that are altering the efficacy of the combinations *in vivo*.

4.3.2 Importance of disease location over total tumour burden

A prominent feature of the different AML models used was that the location of the disease, rather than the total tumour burden, was important for the survival time of the mice. For example, in the syngeneic MLL/AF9 NRAS experiments the CX-5461 treated mice exhibited a higher total BLI at ethical endpoint compared to the vehicle-treated mice (Figure 4-4). As outlined in Section 4.3.1.1, the reason that the CX-5461-treated mice required euthanasia was due to the drug not reducing disease progression in the nasal passages, while still having efficacy in vital organs such as the liver. Another example is that the THP-1 GFP luc injected mice survived weeks longer than the MV4-11 and MOLM-13 GFP luc injected mice, despite having a higher total BLI (Figure 4-7). This indicates that the THP-1 GFP luc cells either do not expand as fast or do not cause as much damage to vital organs as the other cell lines. While the THP-1 GFP luc cells are clearly highly associated with liver involvement, as is evident from the numerous lesions observed (Figure 4-7f), these were superficial and perhaps had minimal effects on liver function, whereas the MLL/AF9 NRAS cells mediated hepatomegaly without discrete lesions (Table 4-2).

4.3.3 Characteristics of AML transplant mouse models and comparison to human AML

A characterisation experiment was performed where the human AML cell lines were injected into NSG mice and the resulting disease monitored (Figure 4-7). The characteristics of each of the syngeneic and xenograft were compiled (Table 4-2) and compared to human AML symptoms in order to determine if the mouse models recapitulate the human disease. In particular, bone marrow involvement and the spread of the disease out of the bone (extramedullary disease) was investigated.

4.3.3.1 Bone marrow involvement

Engraftment in the bone marrow, particularly of the hind limbs and sternum, was visible in all 4 *in vivo* models of AML used in these experiments (Figure 4-4-Figure 4-9), as early as 3-7 days post engraftment indicating the bone marrow is the major site of engraftment and proliferation of the AML cells. This is consistent with the bone marrow being the normal site in which AML cells are found in patients, with the

associated bone marrow microenvironment supporting their growth (Section 4.1.1). As all four transplant models feature bone marrow involvement they are consistent with the predominant feature of the human disease in this aspect.

4.3.3.2 Hind limb paralysis

Hind limb paralysis was observed in all mice engrafted with MOLM-13 GFP luc cells and in some mice engrafted with the MV4-11 GFP luc cells (Table 4-2). A possible cause of this paralysis is infiltration of the cells into the central nervous system (CNS) or enlarged organs pressing on the spinal cord. For example, the enlarged ovaries which were observed in the MOLM-13 and MV4-11 models (Figure 4-7f) may be causing a pressure point on the spine, thus contributing to the limb paralysis. This could be tested by following the progression of disease in male mice injected with MOLM-13 and MV4-11 GFP luc cells.

In adult human patients, the involvement of the CNS is rare, less than 1% at initial diagnosis increasing to 3% at relapse [240]. In paediatric AML cases, the incidence of CNS involvement is more common at 7-29% [241,242]. Furthermore, paralysis as a feature of CNS involvement of AML is rare, with only a limited number of reported cases, of which all presented with solid AML tumours (further discussed in the next paragraph) compressing on the spine [243,244]. While it might be considered that hind limb paralysis in the human AML xenograft mouse models is not highly representative of the human disease, it is likely to be due to extramedullary spread of the AML cells, which itself is a common feature of AML.

4.3.3.3 Solid tumours on the liver

A striking feature of the THP-1 GFP luc model was the numerous solid tumours present on the liver (Figure 4-7f) which is a previously reported feature of this model [207]. In patients, extramedullary AML (also known as chloroma) occurs in up to 24% of AML patients and primarily involves the lymph nodes, and to a lesser extent the spleen, liver, skin, gingiva and (as previously mentioned when discussing hind limb paralysis) the CNS [245]. Around 5% of AML patients have extramedullary AML associated with the liver which is associated with a poorer prognosis [245]. In paediatric AML cases, extramedullary disease is most common in the very young patients, with an incidence

of greater than 30% of cases in children 1-year-old or younger [246]. The THP-1 cell line is derived from a 1-year-old patient with AML (Table 3-1), thus could explain why this particular model features multiple sites of extramedullary disease, including the liver, multiple lymph nodes throughout the body and in the spleen (Table 4-2), whereas the other cell lines, which are derived from older patients, feature this less predominately. Thus, the THP-1 xenograft model could be a useful model for paediatric AML with extramedullary disease.

4.3.3.4   Spleen enlargement

Spleen enlargement was observed in all four orthotopic models; 3-4 times normal spleen weight in the MLL/AF9 NRAS, MOLM-13 GFP luc and MV4-11 GFP luc models and 1.3 times normal spleen weight in the THP-1 GFP luc model. Splenic extramedullary AML is the second most common accumulation of AML cells (after the lymph nodes), and is found in just over 7% of patients [245]. Splenic involvement is a consistent feature in the mouse models used in these studies, and is representative of human disease.

4.3.3.5   Enlarged ovaries

Enlarged ovaries were observed in the MOLM-13 and MV4-11 GFP luc models (Figure 4-7f). As with limb paralysis, ovarian involvement of AML is rare in patients, with only a few reported cases, some even preceding the development of the standard AML phenotype blood and bone marrow disease [247]. Thus, it would be interesting to determine if such tumours would develop in the testes of male mice injected with the same human AML cell lines. It is possible that female sex hormones such as oestrogen may play a role in the infiltration and growth of the AML cells in the reproductive organs, thus the ovary enlargement may be less pronounced in older female mice.

4.3.3.6   Summary of AML xenograft versus patient features

The main characteristic of human AML, bone marrow involvement, occurs in all four models used in these studies. In addition, all four, but particularly the three human cell line xenograft models, show features of extramedullary spread, which is a common occurrence in AML. Alone these observations validate these models as consistent with

the main features of human AML, and can be considered useful as preclinical models to test potential treatments for human AML.

4.3.4 Targeting AML in sanctuary sites

As outlined in the previous section, extramedullary disease is a common feature of AML both in human patients and the mouse models used in these studies. This is clinically significant, as the CNS and gonads are considered sanctuary sites that is have chemical and immunological privilege [248] [249] [250]. In order to target AML cells in these sites, agents capable of penetrating the blood:brain or gonad barrier must be utilised.

CX-5461 does not cross the blood:brain barrier [251], however, second generation Pol I transcription inhibitors are currently in development that have improved blood:brain barrier penetrance, such as PMR-116 [252]. Whether second generation Pol I inhibitors like PMR-116 cross the gonad barrier is yet to be determined. Chloroquine crosses the blood:brain barrier [253], as does metformin [254] and DCA [255] [256], however, it is not clear if these agents also penetrate the gonads. Utilising these metabolism-modifying agents *in vivo* with a second generation Pol I inhibitor that can penetrate the blood:brain barrier, such as PMR-116, could potentially result in greatly improved survival as the AML cells in some sanctuary sites will be accessible.

4.3.5 Limitations of the disease measurements used in the survival experiments

In order to compare the efficacy of the different drug treatments, various parameters were collected as a measure of disease burden in the mice, including overall survival, spleen weight, bioluminescent imaging and weight changes. However, these methods suffer from limitations which can impact on the interpretation of the outcomes of the experiments. Spleen weight is generally a robust measure of disease burden, however this can also be impacted by the presence of an infection [257], for example. The mice are housed in a pathogen-free environment and handled in sterile conditions (and the NSG mice were given antibiotics for the duration of the experiments) so this is unlikely to occur. The bioluminescent imaging could be influenced by injection errors with the luciferin. If the luciferin is injected into the fat pads, or internal organs, rather than the

peritoneum, this will influence its distribution through the body and thus affect the imaging results. The location of the tumour cells can also affect the imaging, specifically tumour cells closer to the skin will give a stronger bioluminescent signal than tumour cells that are deeper internally. This will also be relevant if a drug treatment changes the distribution of the tumour cells to, for example, move them closer to the skin of the mouse which would result in an apparent increase in total tumour burden. An example of this is orlistat treatment (Figure 4-4), which increased the total BLI of the mice compared to the vehicle, however this might have simply been due to the changed distribution of the leukaemia cells to the periphery. Overall survival was defined as the time taken post-transplant until the mice reached an ethical endpoint based on symptoms such as weight loss, reluctance to move and hunching. This ethical endpoint does present a source of human error as the severity of the symptoms being displayed by the mice, and whether these are significant enough to require euthanasia, can be subjective. In order to remove as much of this subjectivity as possible, a clear mouse symptom scoring sheet was utilised in all mouse experiments and observations were made by the same person.

For these reasons, the results of the various measures of disease burden were considered in order to draw conclusions about the efficacy of the drug treatments. Of the disease measurements, weight changes are considered the most robust and accurate, as they reflect the health of the mouse and thus disease burden.

4.3.6 Differences in the outcomes of the syngeneic and xenograft models

Despite the combination of CX-5461 + chloroquine demonstrating synergy *in vitro* in the MLL/AF9 NRAS, MOLM-13 and MV4-11 cell lines, the survival advantage *in vivo* was less robust and significant only in two models. Surprisingly, there was no survival advantage in MOLM-13 GFP luc model (Figure 4-8), despite this cell line having the strongest combination effect *in vitro* (Figure 3-12). Clearly there is a discrepancy between the efficacy of this drug combination between the syngeneic and human cell line xenograft models, where the combination effect appears to be improved from *in vitro* to *in vivo* in the syngeneic model, and the combination effect is much less pronounced in the human cell line xenograft models. A possible reason for the

differences in efficacy of CX-5461 + chloroquine between the different types of models is the absence of an immune response in NSG mice, while the C57Bl/6 mice used in the MLL/AF9 NRAS experiments have an intact immune system. In particular, T cells are important for an anti-tumour response, thus a higher level of T cells, as well as lymphocytes and NK cells, in the bone marrow of AML patients is associated with an improved outcome for patients [258]. It is possible that *in vivo* the efficacy of CX-5461 and/or chloroquine is also dependent on this anti-tumour immune response. An experiment to address this would be to inject the MLL/AF9 NRAS cells into NSG mice, and evaluate the combination of CX-5461 + chloroquine with respect to survival. If the combination was less effective in the same cells in the NSG mice compared to the C57Bl/6 mice, this would support the need for an intact immune system for this response. Thus using a humanised mouse model, such as implanting human mesenchymal stem cells to create a humanised bone marrow niche [259], would be required to test the drug combination in human cell line xenografts experiments or for the engraftment of primary AML patient samples.

As outlined in Section 4.3.1.3, enterohepatic recirculation of CX-5461 has been indicated to occur in patients [82]. Interestingly, intestinal bacteria are known to play a key role in the process of enterohepatic recirculation [237]. It is possible that the antibiotic treatment used in the immunocompromised mice in the human cell line xenograft models (Methods Section 2.6.2.2) compromises the gut microflora, resulting in decreased exposure to CX-5461, and thus reduced efficacy in the xenograft models compared to the syngeneic model. As the antibiotic is provided continuously in the drinking water, supplementation with probiotics would not be feasible in these models.

4.3.7 Outcomes of tolerability testing and limitations of the approach

In order to evaluate the promising combination therapies identified *in vitro* (Chapter 3) in i*n vivo* transplant models of AML, tolerability testing of the metabolism-modifying drugs was performed first in non-tumour bearing mice (Figure 4-2, Figure 4-3). Tolerable doses of the drugs as single agents or in combination with CX-5461 were identified for all of the promising drugs and evaluated in survival experiments. In the

case of CX-5461 with orlistat (Figure 4-4) and CX-5461 with DCA (Figure 4-5) these dosing regimes were also tolerated in MLL/AF9 NRAS tumour bearing mice, as indicated by no significant weight loss during the course of the experiment. However, treatment with CX-5461 + chloroquine (Figure 4-6) was not tolerated over the course of the experiments and thus lower doses were used when tested in the human AML cell line xenograft experiments. This highlights the limitation of tolerability testing in non-tumour bearing mice as it does not always completely predict the tolerability of the drugs in tumour bearing mice as tumour cells place additional burdens on the mice which can lower their tolerability to the drugs [260].

4.3.8 Concluding remarks

CX-5461 + chloroquine was confirmed as a combination therapy of interest based on the survival results in the MLL/AF9 NRAS model, and to a lesser extent the MV4-11 GFP luc xenograft model. However, it is possible that chloroquine levels were not sufficient *in vivo* to have efficacy. In order to understand why CX-5461 + chloroquine act synergistically, and therefore identify alternative, more potent drugs which could be utilised instead of chloroquine to improve the effects of CX-5461, mechanistic analysis was performed (Chapter 5).

Chapter 5 Determining the mechanisms of synergy between CX-5461 and chloroquine

5.1 Introduction

Previous *in vitro* experiments identified the metabolism-modifying agent chloroquine as acting synergistically with CX-5461 to reduce AML cell viability in 6 genetically different cell lines (Chapter 3). This drug combination was also tested using *in vivo* orthotopic transplant models of AML (Chapter 4). The combination of CX-5461 + chloroquine resulted in a statistically significant improvement in survival in the syngeneic MLL/AF9 NRAS model and the MV4-11 GFP luc xenograft model, but not the MOLM-13 GFP luc model despite the drug combination having a robust synergistic effect in this cell line *in vitro*. It is possible that *in vivo* the dose of chloroquine the AML cells was exposed to was not high enough to have efficacy. This is based on the observation that the dose of chloroquine administered in the *in vivo* experiments was limited by toxicity in combination with CX-5461, consequently, this limits the clinical potential of this drug combination in humans. However, by understanding the mechanisms by which CX-5461 + chloroquine were acting synergistically, may uncover other suitable targets and clinically relevant drugs that may not be as toxic.

The following chapter addresses Aim 3: 'Investigate the mechanism/s of synergy for promising drug combinations'. Given the published effects of CX-5461 and chloroquine as individual agents, mechanistic and end-point analysis was performed to determine how the drugs act synergistically together.

5.1.1 Reported effects of CX-5461

5.1.1.1 Background

As outlined in Section 1.2.3, CX-5461 was identified as a potential cancer therapeutic in a screen for inhibitors of rRNA synthesis [81] and has since shown efficacy in a variety of different blood [1,78] and solid cancers [81,83,84] *in vitro* and *in vivo,* leading to the commencement of clinical trials. CX-5461 is a potent and selective inhibitor of rDNA

transcription that can act within 30 minutes of treatment through disruption of the interaction between SL-1 and Pol I[81]. Interestingly, while CX-5461 exhibits similar efficacy on rDNA transcription initiation in both non-malignant and malignant cells, non-malignant cells are approximately 30 times less sensitive to CX-5461 in terms of viability, highlighting the addiction of malignant cells to rDNA transcription [81]. Depending on the cancer type and underlying genetics, the downstream effects of Pol I inhibition by CX-5461 varies.

5.1.1.2 Cell cycle arrest, apoptosis, cell death and senescence

CX-5461 has been reported to induce cell cycle arrest, apoptosis and/or senescence in various cancer types. For example, in the lung cancer cell line A375 and pancreatic cancer cell line MIA PaCa-2, CX-5461 induces autophagic cell death (a mechanism of programmed cell death) and cellular senescence but not apoptosis or necrotic cell death [81]. Alternatively, in the Eμ-Myc mouse lymphoma cell model rapid p53-dependent apoptotic cell death is induced [78]. CX-5461 also mediates apoptosis and G2/M cell cycle accumulation in acute lymphoblastic leukaemia (ALL) cell lines and patient samples *in vitro*, independent of p53 status [261]. Cell cycle progression defects were also reported in AML cells within 24 h of CX-5461 treatment, predominately G2/M phase accumulation [1].

5.1.1.3 Activation of the nucleolar stress response

CX-5461 acts on rDNA transcription which occurs in the nucleolus. Historically known as the site of ribosome biogenesis, the nucleolus has more recently been recognised as a sensor of cellular stress (reviewed in [262]). In response to perturbations of ribosome biogenesis and nucleolar disruption, mediated by inhibition of Pol I transcription by Cx5461 treatment or inactivation of UBF [263] or TIF-1A [264], p53 levels are elevated leading to cell cycle arrest or apoptosis. Under normal growth conditions, p53 is bound and inactivated by MDM2, promoting the rapid degradation of p53 [265]. In response to certain stresses there is excess ribosomal proteins in the cell results in the accumulation of the RPL5/L11/5S ribonucleolar protein (5SRNP) complex, that can bind and sequester MDM2, resulting in increased levels of p53 [266]. This activation of the nucleolar stress response was observed in Eμ-Myc lymphoma cells, with low doses of CX-5461, in as little as 1 hour of treatment[78]. Similarly, in mouse and human AML cells

accumulation of p53 and phosphorylated p53 can be observed as early as 1 hour after CX-5461 treatment[1].

5.1.1.4 Activation of ATM/ATR signalling

As outlined in Section 5.1.1.2, cell cycle progression defects are observed in a variety of cancer types following CX-5461 treatment, and this often correlated often with activation of known components of the DNA damage pathway. For example, in acute lymphoblastic leukaemia cells, 24 hour treatment with CX-5461 induced ATM/ATR signalling, as assessed by phosphorylation of Chk1 and Chk2 [261]. Whereas phosphorylation of Chk1 and Chk2 occurred rapidly (1 hour) in AML cells *in vitro* [1]. Typically DNA damage is required to activate the kinases ataxia-telangiectasia mutated (ATM) and ATM and Rad 3-related (ATR), these mediate a signalling cascade through cell cycle checkpoints, such as p53-dependent activation of Chk1 (ATR mediated) and Chk2 (ATM-mediated) resulting in cell cycle arrest so the DNA can be repaired or apoptosis [267].

Interestingly, in the case of CX-5461 treatment of immortalised human fibroblast cells, there is no global DNA damage, thus the pathway activated has been described as 'DNA damage-like' signalling [268]. The proposed mechanism by which CX-5461 induces this DNA damage-like signalling is due to the reduction of Pol I binding to the rDNA promoter and transcribed regions, resulting in 'exposed' regions of rDNA repeats in open conformation stably bound by UBF, the abnormal configuration of which is hypothesised to induced DNA damage signalling in the absence of DNA damage [268].

5.1.1.5 Effects on the mitochondria

There is no published literature evaluating any direct effects of CX-5461 on the mitochondria. However, from collaborations with the Pearson Lab (Kusnadi et al. Peter MacCallum Cancer Centre), we know that lymphoma cells with acquired resistance to the combination of CX-5461 and everolimus (mTORC1/mRNA translation inhibitor) are significantly more metabolically active compared to drug naïve cells, particularly in terms of their baseline mitochondrial activity [269]. These results suggest that elevated mitochondrial activity is a resistance mechanism to the dual targeting of ribosome biogenesis and function in lymphoma cells, however, it remains to be determined such effects on mitochondria would also be observed in AML or normal cells. Unpublished

work in our laboratory has demonstrated that acute CX-5461 treatment of mouse AML cells *in vivo* alters the mRNA abundance of numerous metabolic genes including the upregulation of transcription of enzymes involved in fatty acid and cholesterol synthesis (Figure 1-5), suggesting that CX-5461 treatment alone may induce functional changes in the mitochondria.

5.1.1.6   Summary

In summary, the reported effects of CX-5461 mediated Pol I transcription inhibition include cell cycle arrest, apoptosis and or/senescence, activation of the nucleolar stress response and DNA damage-like signalling, depending on the cell type. Direct or indirect effects of CX-5461 on mitochondrial activity have not as yet been published, however, our laboratory has unpublished data suggesting this occurs.

5.1.2 Reported effects of chloroquine

5.1.2.1   Background

As briefly outlined in Section 3.1.2.3 chloroquine, a synthetic 4-aminoquinoline molecule, has a long history of use in humans as an anti-malarial drug[270]. Chloroquine, a weakly basic molecule, accumulates in a pH-dependent manner in the acidic food vacuoles of the malarial parasite [271], affecting the pH and function of the food vacuole [272], thus leading to toxic accumulation of heme, a by-product of haemoglobin degradation [273,274]. Other than nausea, vomiting and diarrhoea, the most serious, although uncommon, side effect of chloroquine treatment is permanent retinal toxicity, that is associated with long-term use [275]. Hydroxychloroquine is a derivative of chloroquine that is currently used in the clinic and has a reduced risk of retinal toxicity [275,276]. Both chloroquine and hydroxychloroquine have been approved for clinical use in rheumatoid arthritis [139,277,278] and lupus [279,280] due to immune-modulatory capabilities through affecting auto-antigen processing in antigen-presenting cells [281], inhibiting T cell proliferation [282] and inhibiting NK cell activity [283].

During the decades of clinical use of chloroquine, various mechanisms of action have been identified including autophagy inhibition, DNA intercalation, ATM activation, mitochondrial effects, modulation of lysosomal nutrient signalling, cell cycle arrest, apoptosis and cell death.

5.1.2.2 Inhibition of autophagy

5.1.2.2.1 Overview of autophagy

A well-studied mechanism of action of chloroquine is that of autophagy inhibition. Macroautophagy (hereafter referred to as autophagy) is a conserved intracellular recycling process by which cellular material such as damaged organelles and misfolded proteins are degraded in double-membrane-bound structures, then the nutrient and metabolites are released back to the cell. The process of autophagy is multi-step with many players involved, including autophagy-related proteins (ATGs, Figure 5-1).
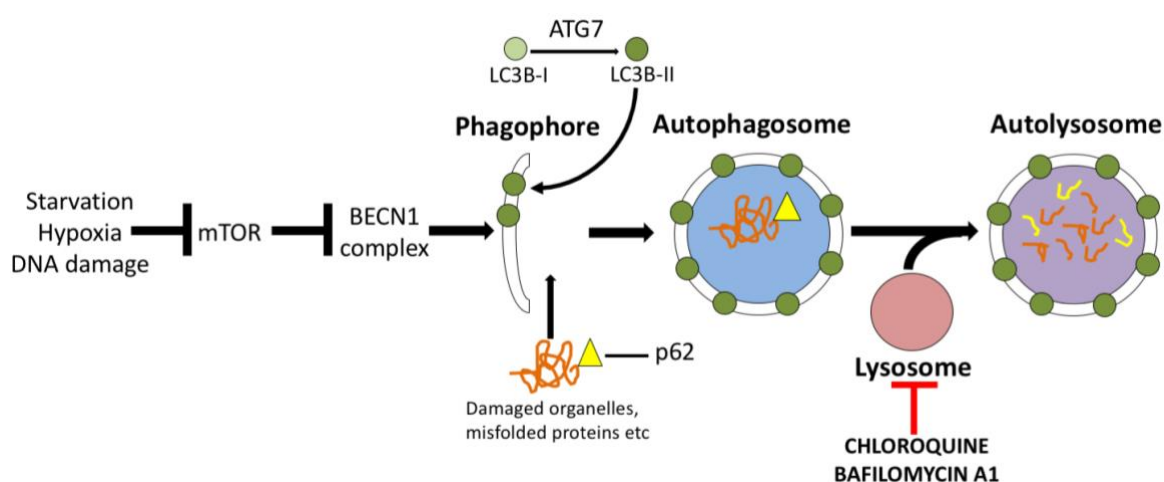
Figure 5-1: Overview of the process of autophagy

Nutrient sensor mammalian target of rapamycin (mTOR) acts as a negative regulator of autophagy in nutrient rich conditions, while in stress conditions the activity of mTOR is inhibited and autophagy is induced. Autophagy begins with the formation of an isolation membrane or phagophore. Initiation (or nucleation) of the phagophore begins when the Beclin-1 (ATG6) complex is activated. Following the nucleation of the phagophore the membrane is elongated, requiring the incorporation of phosphatidylethanolamine-lipidated microtubule-associated protein 1B-light chain 3 (LC3B-II/ATG8), which is formed when the cytosolic LC3-I is conjugated to phosphatidylethanolamine (PE), requiring ATG7. Adaptor proteins such as p62 guide cargo for degradation to the phagophore through interactions with LC3-II. The membrane of the phagophore eventually fuses around the cargo, forming an autophagosome. The phagophore then fuses with lysosomes containing degradative enzymes to form an autolysosome, and the contents are subsequently degraded. P62 and LC3B-II on the inner membrane are also degraded. Chloroquine and bafilomycin A1 interfere with lysosomal function, preventing the fusion of autophagosomes and lysosomes.

Autophagy reduces oxidative stress as dysfunctional mitochondria, a major source of reactive oxygen species (ROS), are removed, thus reducing ROS-induced genomic instability [102]. Under stress conditions, such as nutrient deprivation, autophagy rates increase in order to provide the cell with nutrients and the building blocks required to cope with the stress [101]. If the stress in the cell reaches an unacceptable level then programmed cell death via degradation of essential cell components (autophagic cell death) can occur [284]. Chloroquine inhibits autophagy through interfering with lysosomal function, in a similar mechanism to the food vacuole of the malaria parasite, thus preventing the fusion of lysosomes with autophagosomes [143].

5.1.2.2.2 Dual role of autophagy in cancer

In the context of cancer cells, there is evidence for both tumour suppressive and tumour permissive effects of autophagy, depending on the cancer type and cellular assault.

A reduced rate of autophagy mediates an increase in the number of damaged organelles [111], increasing ROS levels [112], genome instability [102] and inflammation [113], which creates a tumour permissive environment, both for the initiation and progression of cancer. Allelic loss of autophagy gene Beclin 1, which plays a critical role in the initiation stage of autophagy (Figure 5-1), has been reported in 40–75% of sporadic ovarian and breast cancers [285] and its expression is significantly reduced in human brain tumours, which is correlated with a higher disease grade [286]. In mice, heterozygous deletion of Beclin 1 (homozygous deletion is embryonic lethal) renders mice more prone to mammary hyperplasia, lung cancer, liver cancer and lymphoma [287,288].

However, autophagy has also been reported to have a pro-survival role in many cancers, where it acts to help the cell cope with metabolic stresses, for example, increased stress accompanying a high metabolic rate, hypoxia and response to chemotherapy. In hepatocellular carcinoma [289] [290] and pancreatic cell lines [289], treatment with standard chemotherapeutics have been reported to induce autophagy, and genetic or chemical inhibition of autophagy has been shown to synergise with chemotherapy *in vitro* and *in vivo* [290].

In AML the role of autophagy is not straightforward. Heterozygous loss of ATG5 in an MLL/ENL AML model mediated increased proliferation *in vitro* and decreased survival of transplanted mice *in vivo* [114]. Decreased expression of autophagy-related genes, including through hemizygous deletion in some cases, and reduced autophagic flux as assessed by imaging flow cytometry was also reported in AML patient bone marrow samples [114]. Autophagy has also been reported to promote chemoresistance in AML. In human AML cell lines and patient samples treatment with cytarabine, autophagy was induced through inactivation of mTOR, and chemical inhibition of autophagy with bafilomycin or chloroquine, or knockdown of autophagy-related proteins sensitised the cells to the effects of cytarabine by increasing oxidative stress, DNA fragmentation, caspase activation and apoptosis [291]. Cytoprotective autophagy has also been shown to play a role in the maintenance of leukemic stem cells, with inactivation of autophagy by Atg5 or Atg7 knockout resulting in a reduction of leukemic stem cells and prolonged survival in an MLL-ENL mouse model [115]. The role of autophagy in AML cells in the context of CX-5461 treatment remains to be determined.

5.1.2.2.3 Studying autophagy: knockdown approach

As outlined previously in Section 5.1.2.2.1, there are many ATGs which are critical for the process of autophagy. In order to study the combined effects of ribosome biogenesis inhibition (with CX-5461) and autophagy inhibition, the two ATGs Beclin1 and ATG7 (Figure 5-1) were selected to be targeted using an inducible shRNA knockdown approach. Beclin1 (or ATG6) induces autophagy through the formation of the Beclin1-Vps34-Vps15 core complex, leading to the nucleation of the phagophore [292], and control of crosstalk between autophagy and apoptosis through caspase-mediated cleavage [293]. Whereas ATG7, along with ATG3 and ATG12-ATG5-ATG16L multimers, are involved in the conjugation of a phosphatidylethanolamine (PE) moiety to LC3-I, forming LC3-II which subsequently integrates into the forming autophagosome [294]. In the literature both Beclin and ATg7 have been successfully targeted with an shRNA approach.

Significant knockdown of Beclin 1 protein has been reported in sarcoma cells (approximately 50% knockdown, [295]) and the ipsilateral thalamus of rats

(approximately 80% knockdown, [296]). In liver cancer cell line Huh7, 60% knockdown of ATG7 protein was achieved in 48 h using shRNA [297] and up to 90% in human CD34+ hematopoietic stem-progenitor cells [298]. Thus genetic knockdown of Beclin 1 and ATG7 is an achievable approach and in this thesis an inducible shRNA knockdown approach was selected. This was based on the observation that constitutive knockdown or knockout of autophagy genes can mediate compensatory mechanisms in the cell over time, which would make the results difficult to interpret [181].

5.1.2.3 DNA intercalation, changing chromatin structure and ATM activation

It has been recognised for decades that chloroquine can mediate its effects as a DNA intercalator and thus alter chromatin structure. In a cell-free assay, chloroquine reversibly binds calf thymus DNA, with stronger binding to purines [299]. In nuclei or DNA isolated from CV-1 (monkey kidney cell line), chloroquine intercalated almost exclusively to the DNA of the nucleosomal linker regions without affecting nucleosome structure [300] at concentrations of 3mM or higher, but not at 400 or 800μM. Whereas in studies using intact human K562 (erthyroleukaemia) cells, chloroquine intercalated with the DNA of nucleosomal linker regions at concentrations as low as 600μM, again without disruption of the nucleosomes themselves, however this did significantly affect folding of high order chromatin structures [176]. Subsequently, chloroquine has been reported to activate ATM signalling without causing DNA damage (as indicated by the lack of increased gamma H2AX signal), both *in vitro* [301] and *in vivo* [302], improving survival in response to lethal low dose radiation through activation of DNA damage repair pathways.

5.1.2.4 Effects on mitochondria

Chloroquine not only inhibits autophagy, but can inhibit mitophagy, a subset of autophagy specifically involved in the clearance of dysfunctional mitochondria, thus dysfunctional mitochondrial accumulate and ROS increases [303]. In other studies, chloroquine is reported to have direct effects on mitochondria function. In primary rat neurons, chloroquine and an alternative autophagy inhibitor bafilomycin A1, not only reduced mitochondrial quality but modified mitochondrial function [111]. In these cells, 24 hours treatment with chloroquine or bafilomycin did not change mitochondrial number although mitochondrial bioenergetics were reduced including basal

respiration, maximal respiration and spare respiratory capacity, and also reduced the activity of complexes I, II and IV. Metabolomic analysis revealed a significant decrease in Krebs cycle intermediates and an increase in mitochondrial DNA damage. However, in this same study, acute (30 minutes) treatment with chloroquine did not alter mitochondrial respiration, thus it is not conclusive as to if the mitochondrial effects mediated by chloroquine are direct, or an indirect effect of autophagy inhibition.

5.1.2.5 Effects on lysosomal function and nutrient signalling

As previously outlined in Section 5.1.2.2, chloroquine acts an autophagy inhibitor via raising the lysosomal pH and inducing lysosomal dysfunction. However, the cellular effects of this drug is not just limited to inhibiting autophagy. Previously thought to simply be a site for degradation the lysosome has more recently been recognised as a subcellular structure that plays a key role in multiple processes including nutrient signalling. mTOR complex 1 (mTORC1), which regulates cell growth through modulating processes such as autophagy [304], mitochondrial biogenesis [305,306] and nucleotide biosynthesis [307], localises to the lysosomal membrane [308]. Here it is activated by amino acid levels, including through a sensing mechanism involving the proton pump vacuolar H+-ATPase [309] and lysosomal amino acid transporter SLC38A9 [310]. In this manner, the lysosome acts as a hub for nutrient homeostasis and thus inhibition of lysosomal function with chloroquine has the potential to impact on multiple metabolic processes.

5.1.2.6 Cell cycle arrest, apoptosis, and cell death

In the breast cancer cell line Bcap-37, 16µM chloroquine treatment for 48 h resulted in a significant G2/M arrest and elevated expression of apoptotic markers [311]. Whereas 200nM chloroquine induced G2/M phase cell cycle arrest and apoptosis in pancreatic cell lines *in vitro* [312]. In the NB4 cell line (an acute promyelocytic AML cell line) 10µM chloroquine induced apoptosis significantly within 48 hours[147] and an S phase arrest, concomitant with a reduction in the S phase cell cycle regulators cell division cycle 25 A (CDC25A) and cyclin-dependent kinase 2 (CDK2).

5.1.3 Potential mechanisms of synergy

As outlined in Sections 5.1.1 and 5.1.2 there are multiple known mechanisms of action and consequences for CX-5461 and chloroquine treatment as single agents, and interestingly, some of these overlap between the two drugs (Figure 5-2). Potentially, the overlapping mechanisms of action and consequences of exposure may mediate an enhanced effect when the drugs are used in combination (i.e. synergy). Alternatively, the individual effects of the drugs alone may mediate an elevation of cellular stress, thus affecting viability. In this thesis the potential mechanisms of synergy that were assessed included inhibition of autophagy and altering mitochondrial activity or quality, with synergy being assessed via the endpoints of cell cycle arrest and cell death.
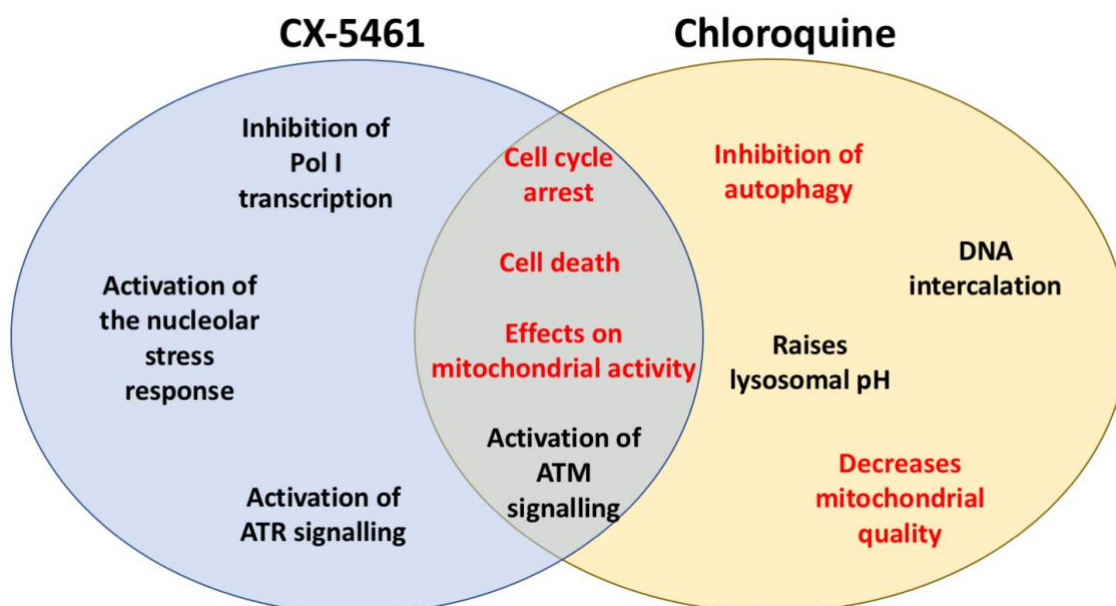
Figure 5-2: Potential mechanisms of synergy between CX-5461 and chloroquine

There are several reported processes altered by CX-5461 and chloroquine that could account for their synergistic action as a drug combination, including mechanisms of action of the drugs and endpoints of exposure to the drugs. Some, like cell cycle arrest, are altered by both drugs alone which could be enhanced when combined. Other effects are unique and in response to the drug combination these effects may combine to cause high levels of cellular stress, thus alter viability. Potential mechanisms of synergy that were investigated in this chapter are shown in red.

5.2 Results

5.2.1 Cell cycle and cell death analysis

Based on the literature demonstrating that CX-5461 exposure results in endpoints of cell cycle arrest and cell death in AML cell lines [1], and that chloroquine causes S phases arrest in the NB4 AML cell line [147], it was hypothesised that CX-5461 and chloroquine act synergistically via an enhancement of their effects on cell cycle arrest and cell death. To test this hypothesis, MV4-11, THP-1, MOLM-13 and MLL/AF9 cells were treated with vehicle, CX-5461, chloroquine or the drugs in combination for 24, 48 and 72 h, then pulsed with BrdU to label newly synthesised DNA, and cell cycle or cell death analysed by determining DNA content and BrdU signal (Section 2.7). The proportion of cells in sub G1, G0/G1, S and G2/M phases are shown (Figure 5-3), with the sub G1 population considered to be indicative of "dead" or non-viable cells (including apoptotic cells) [124].

The percentage of cells in the various cell cycle phases differed significantly between the cell lines treated with vehicle, ranging from 19% to almost 50% of cells in S phase (actively dividing; Figure 5-3). Chloroquine treatment did not alter the cell cycle distribution for any of the four cell lines, whereas CX-5461 treatment induced a G0/G1 cell cycle arrest in 3 cell lines (MV4-11, MOLM-13 and MLL/AF9 NRAS cells) and an S phase delay followed by a G2/M arrest in the THP-1 cell line. This disruption in cell cycle progression in dividing cells following CX-5461 treatment is consistent with the literature findings [1]. In the MOLM-13 cell line, CX-5461 treatment almost completely prevented cells from actively dividing, which was consistent with the plateaued dose-response curve of CX-5461 as a single agent (Figure 3-6). Despite chloroquine not altering the cell cycle as a single agent, chloroquine synergised with CX-5461 to enhance its effects on the cell cycle, specifically by further reducing the S phase population in the MV4-11, MOLM-13 and MLL/AF9 NRAS cells, and also by enhancing the G2/M phase arrest and reduced S phase population in the THP-1 cells.

Sub G1 analysis (Figure 5-3) revealed that as single agents, chloroquine treatment did not alter the percentage of dead cells compared to vehicle treatment, whereas CX-5461 treatment induced cell death in the MV4-11, MOLM-13, and MLL/AF9 NRAS cells,

but not the THP-1 cells, consistent with the insensitivity of THP-1 cells to CX-5461 in the cell viability assays (Table 3-4). Interestingly, despite chloroquine not altering the sub G1 population as a single agent, chloroquine synergised with CX-5461 to induce cell death in the THP-1, MOLM-13 and MLL/AF9 NRAS cells, but not in the MV4-11 cells. The synergistic drug effect observed with cell death was particularly pronounced in the p53 WT MOLM-13 cells, increasing from approximately 30% (CX-5461 alone) to 60% (combination treatment) of the cells classified as SubG1, which is consistent with the strong synergism observed when total viable cell number using the MTT assays was assessed (Figure 3-12). The greatest fold increase (~6-fold) was observed in the p53 null THP-1 cells.

Figure 5-3: Chloroquine enhances the effects of CX-5461 on cell cycle progression and cell death

Quantitation of cell cycle distribution by BrdU incorporation and DNA content (DAPI) was analysed by flow cytometry (Methods Section 2.12) after treatment with CX-5461, chloroquine or the combination of the two after the indicated timepoints. The sub G1 population was considered indicative of cell death. Graphs show the mean $\pm$ SD of n=3 experiments. CX = CX-5461, CQ = chloroquine.

MV4-11
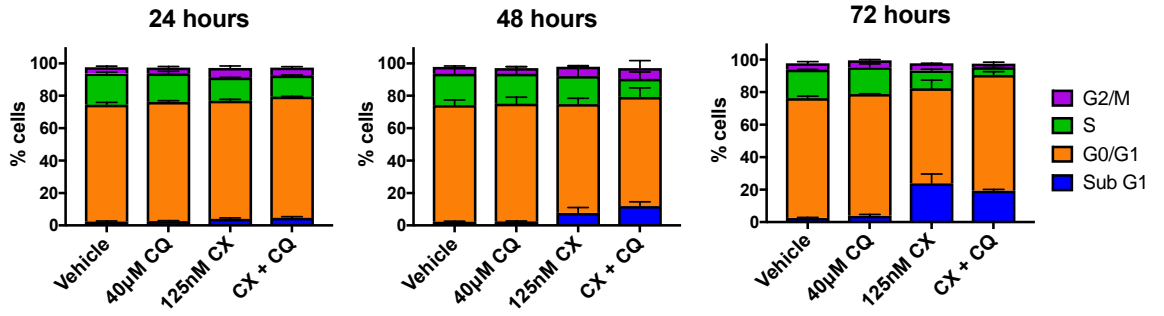
THP-1
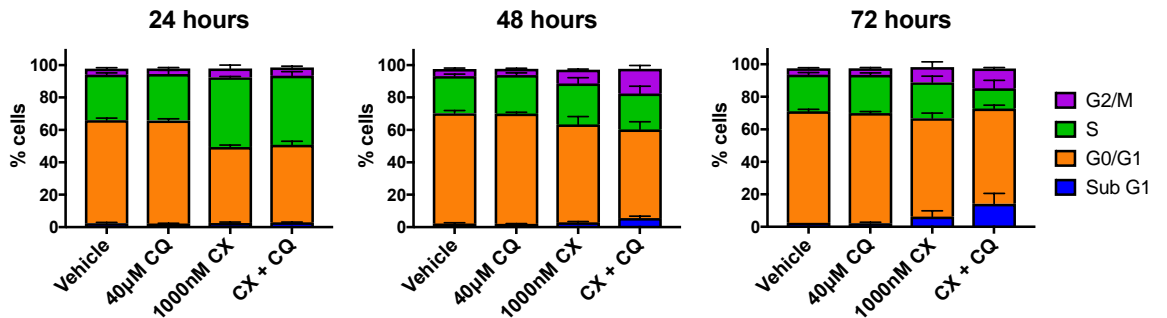
MOLM-13
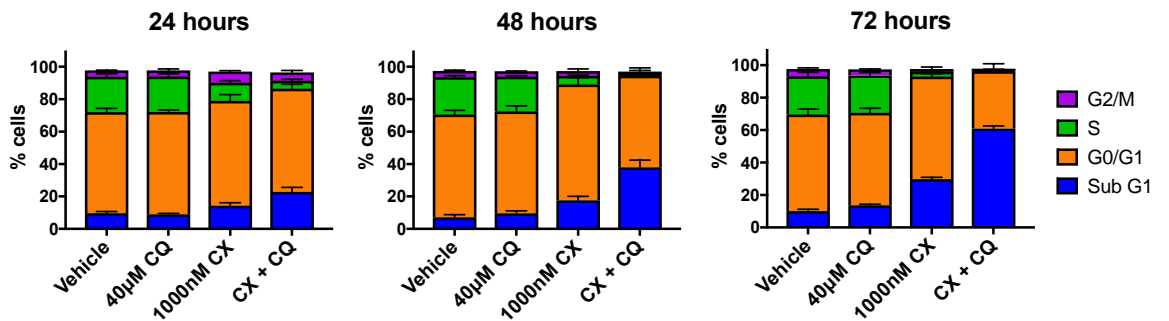
MLL/AF9 NRAS
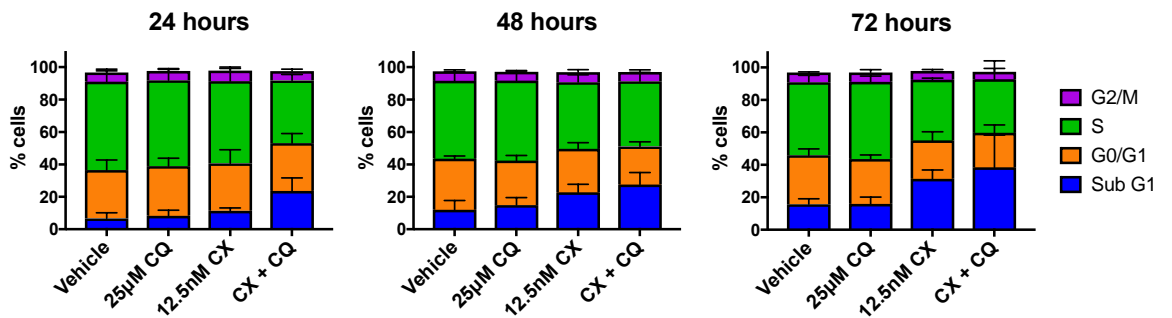
5.2.2 Effect of CX-5461 and chloroquine on autophagy protein expression

Chloroquine is well characterised as an autophagy inhibitor (see Section 5.1.2.2). If CX-5461 and chloroquine were to act synergistically via chloroquine-mediated inhibition of autophagy, this would suggest that cells, in this case, AML cells may upregulate autophagy as a survival mechanism to overcome the effects of CX-5461, as has been published to occur in response to other chemotherapies (Section 5.1.2.2). To test this, three human AML cell lines (MV4-11, THP-1 and MOLM-13) were treated over a time course with a range of concentrations of CX-5461 as a single agent (based on *in vitro* sensitivity determined by viability assay, (Table 3-4)) and the abundance of the autophagy protein LC3B-II was measured by western blot (Figure 5-4). Acute treatment (6 hours) with CX-5461, chloroquine and the combination of drugs was also performed (Figure 5-5). The LC3B-II protein is part of the autophagosome membrane, and thus levels of LC3B are indicative of the number of autophagosomes (Figure 5-1). Thus, if autophagy is upregulated the flux rate (number of autophagosomes) and LC3B-II abundance will increase. If autophagy is blocked at a late stage, such as is observed with chloroquine treatment, autophagosomes will be prevented from merging with lysosomes, leading to their accumulation and LC3B-II expression will increase. If autophagy is also upregulated by CX-5461, there may be a synergistic increase in LC3B-II levels with the combination treatment.

As expected, given the established effect of chloroquine as an autophagy inhibitor, chloroquine treatment mediated an increase in LC3B-II abundance compared to the vehicle in the MV4-11 (Figure 5-5a), THP-1 (Figure 5-5b) and MOLM-13 (Figure 5-5c) cells lines.

The MV4-11 cells (Figure 5-4a) are the most sensitive of the 3 cell lines to CX-5461 in terms of viability (Table 3-4) and interestingly CX-5461 mediated a dose-dependent increase in LC3B-II levels at 3 h, which was maintained at 6 h treatment. By 24 h LC3B-II levels had returned back to basal in the presence of CX-5461, indicating a transient induction of autophagy. In the THP-1 cells (Figure 5-4b), which are insensitive to CX-5461 in terms of viability (Table 3-4), also mediated a dose-dependent increase in LC3B-II abundance detectable at 3 h and 6 h of treatment, with a maximum increase of

3.4 fold compared to the vehicle. However, unlike that observed in the MV4-11 cells, LC3B-II levels remained elevated at 24 h of CX-5461 treatment, indicating that CX-5461 mediated a sustained increase in autophagy in the THP-1 cells. Interestingly, in the MOLM-13 cells (Figure 5-4c), which displayed moderate sensitivity to CX-5461 as a single agent (Table 3-4) and of the 3 cell lines tested displayed the highest degree of synergy with the combination of CX-5461 + chloroquine (Figure 3-12), there were minimal changes in LC3B-II levels detected, in fact at some doses there was a decrease. Together these results suggest that CX-5461 induces autophagy in a cell-dependent manner, and there is no correlation between sensitivity to CX-5461 treatment with respect to viability and induction of autophagy.

The effect of the combination of CX-5461 + chloroquine on LC3B abundance was also evaluated in these cell lines. Human AML cell lines were treated with a single dose of CX-5461, chloroquine or the combination (with the concentration based on *in vitro* sensitivity by viability assay, Table 3-4) for 6 h and the abundance of autophagy marker LC3B-II assessed by western blot. CX-5461 treatment lead to an increase in LC3B-II levels in the MV4-11 cells, but not the THP-1 or MOLM-13 cells, indicating autophagy was not being upregulated at this particular timepoint in these two particular cell lines. This is consistent with the previous results of the single-agent treatment for MV4-11 and MOLM-13 cells, but not the THP-1 cells (Figure 5-4). In all three cell lines, there was no further increase in LC3B-II abundance with combination treatment when compared to chloroquine or CX-5461 treatment alone, indicating that the combination of drugs is not having a synergistic effect on autophagy, or perhaps that the maximum dynamic range of the assay has been reached.

a) MV4-11
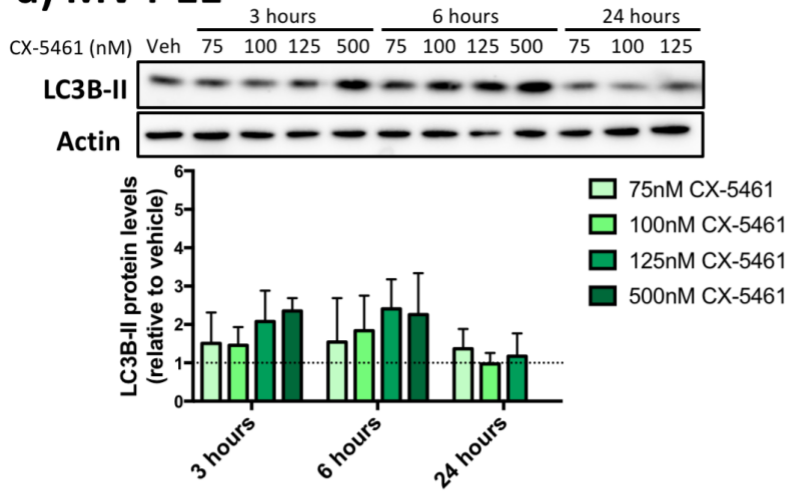
b) THP-1
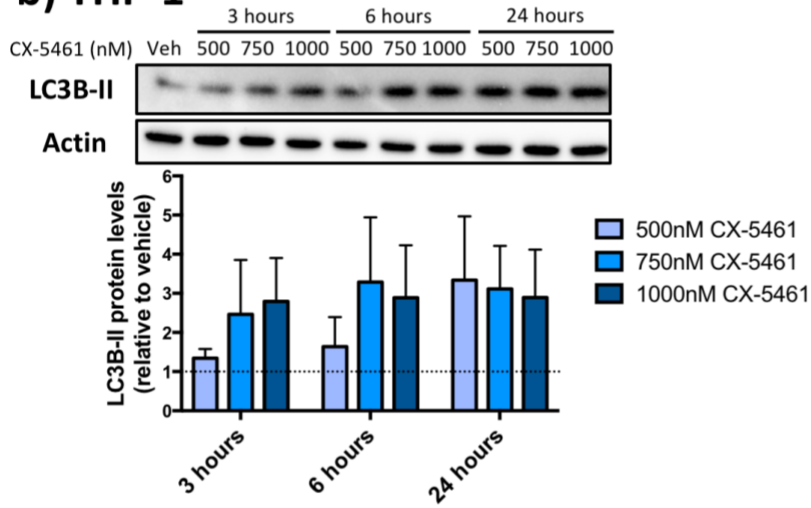
c) MOLM-13
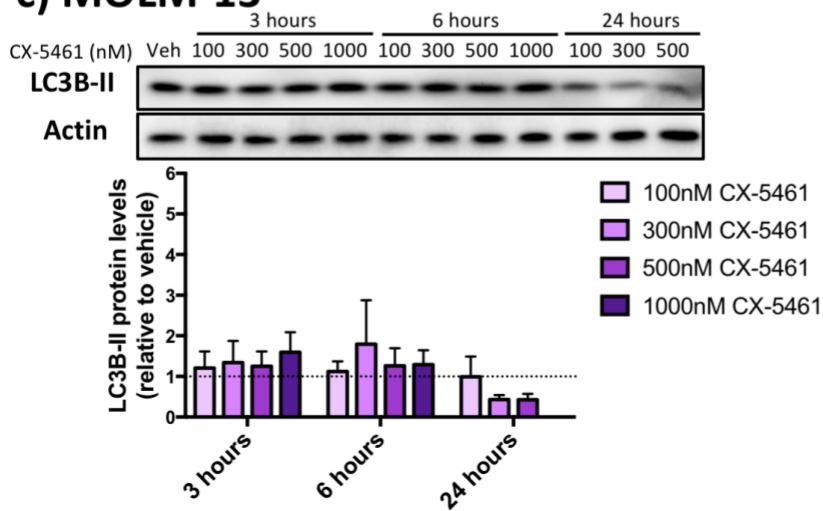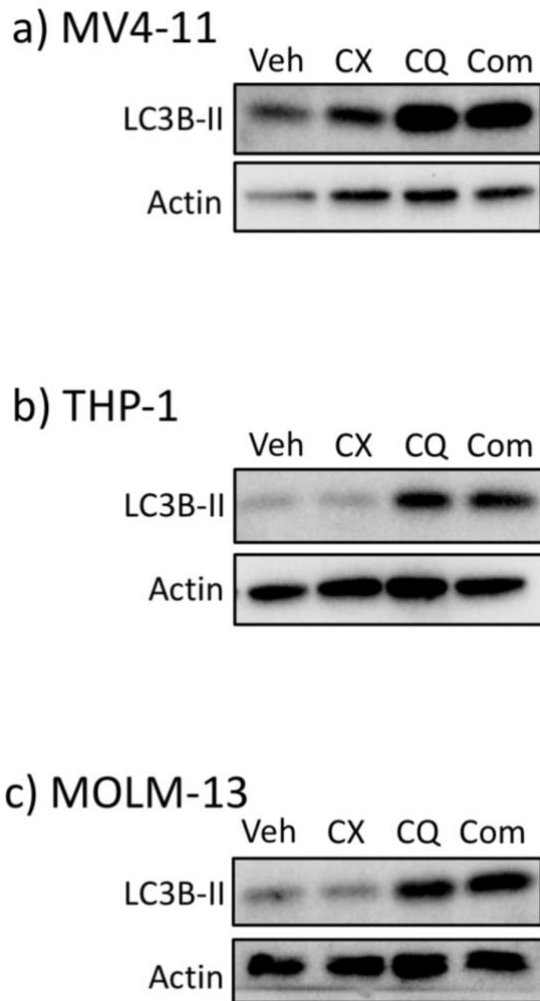
Figure 5-5: Autophagic flux following short term CX-5461 and chloroquine treatment

AML cell lines a) MV4-11, b) THP-1 and c) MOLM-13 were treated with vehicle (Veh), CX-5461 (CX; 125nM for MV4-11, 1000nM for THP-1 and MOLM-13), chloroquine (CQ; 20µM for MOLM-13, 40µM for MV4-11 and THP-1) or the combination of the two drugs (Com) for 6 h. Protein was extracted and 30µg protein separated using SDS-PAGE, followed by immunoblotting for LC3B-II protein levels (Section 2.6). Beta actin was used as a loading control. A representative western blot image of n=2 experiments is shown.

5.2.3 Ultrastructural changes by transmission electron microscopy

Transmission electron microscopy (TEM) was performed to visualise and count the autophagy structures (autophagosomes, autolysosomes and lysosomes, as outlined in Figure 5-1). The human AML cell lines MV4-11, THP-1 and MOLM-13 were treated with vehicle, 1μM CX-5461, 40μM chloroquine or a combination of the two drugs for 24 h, then processed for TEM (Section 2.9). An alternative autophagy inhibitor, bafilomycin, as well as serum starvation, were also included as controls for inhibition and induction of autophagy, respectively. Two representative cells from each treatment are illustrated in Figure 5-6, which also includes a higher magnification view of the cytoplasm for each treatment. In the MV4-11 cells, the number of structures in 10 randomly selected cells were counted (Figure 5-7), however, due to time constraints this experiment was only performed once.

Figure 5-6: Ultrastructural changes following CX-5461 and chloroquine treatment

Human AML cell lines a) MV4-11, b) THP-1 and c) MOLM-13 were exposed to vehicle, serum starvation, 20nM bafilomycin (Baf), 1μM CX-5461, 40μM chloroquine (CQ) or CX-5461+chloroquine (CX+CQ) for 24 h, fixed and processed for transmission electron microscopy (TEM; Section 2.7). Representative cells of each treatment are shown. Scale bar on higher power images = 1μM. N = nucleus, M = mitochondria, A = autophagy structure. n=1.

a) MV4-11
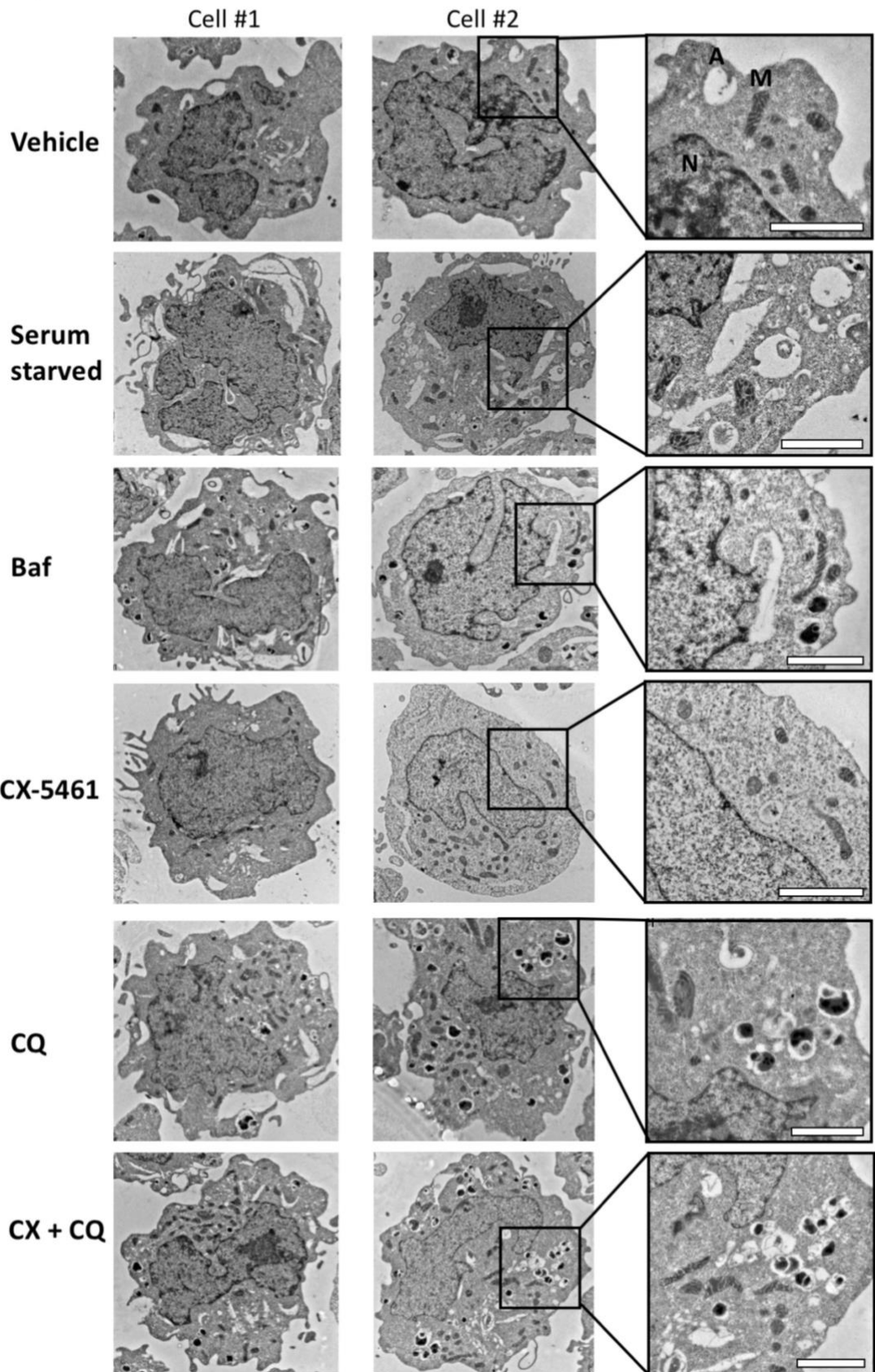
b) THP-1
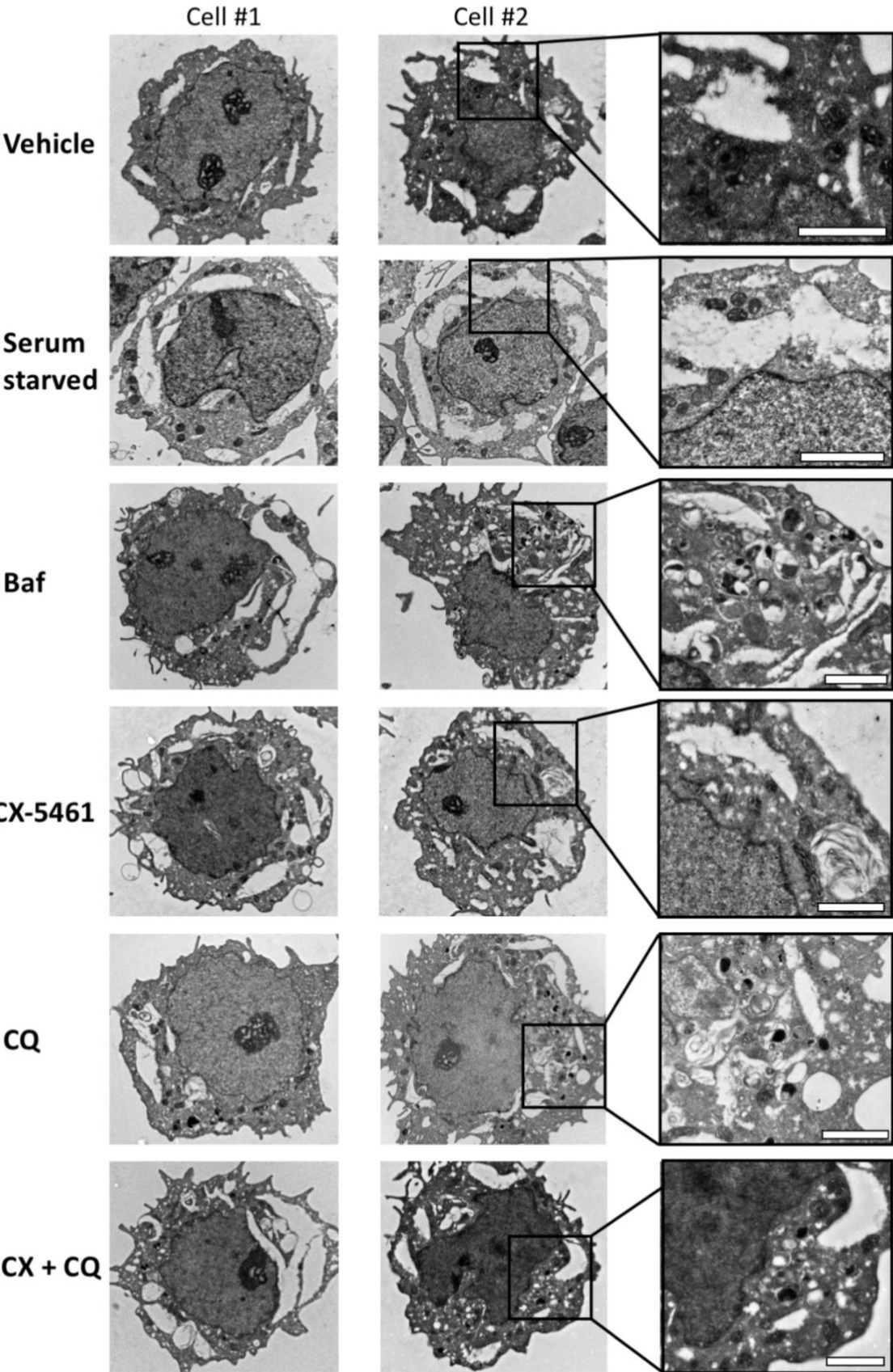
c) MOLM-13
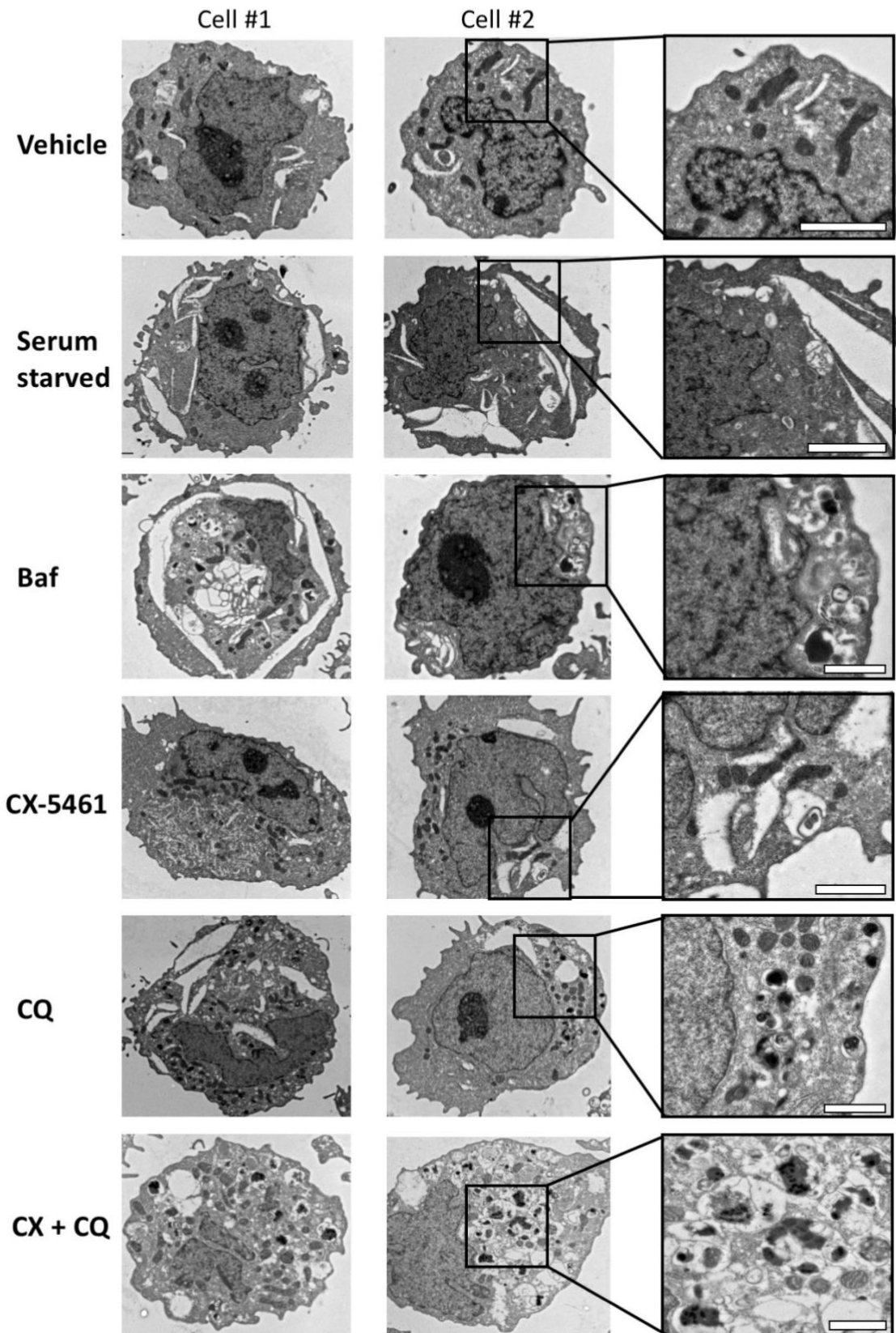
In the vehicle-treated samples, the nuclei and mitochondria are readily visible, as are some small vacuoles and autophagy structures in the cytoplasm. There were relatively few vacuoles in the MV4-11 (Figure 5-6a) and MOLM-13 (Figure 5-6c) vehicle-treated cells compared to the THP-1 cells (Figure 5-6b) which had more and larger vacuoles. Consistent with the LC3B-II levels (Figure 5-5), in chloroquine-treated cells, across all three cell lines, there was an increase in the size and number of vacuoles and autophagy structures, including autophagosomes containing large, electron-dense structures. These were also present in the bafilomycin- and CX-5461 + chloroquine-treated cells. As chloroquine and bafilomycin are late-stage inhibitors of autophagy, specifically blocking the fusion of the autophagosomes with lysosomes, the increased number of autophagosomes containing un-degraded cargo is unsurprising. Serum starvation also mediated an increase in the number and size of cytoplasmic vacuoles and autophagy structures in all 3 cells lines, particularly in the THP-1 cell line. In some of the MV4-11 cells CX-5461 treatment led to a loss of contrast and granular texture in the nucleus and cytoplasm, which may indicate a loss of viability, consistent with the sensitivity of these cells to CX-5461 with respect to viability (Figure 3-5). No obvious changes in the number or size of autophagy structures was observed with CX-5461 treatment, consistent with LC3B-II levels at this timepoint (Figure 5-4). In the THP-1 and MOLM-13 cells CX-5461 treatment mediated an increase in the size and number of vacuoles and autophagy structures, also consistent with the changes in LC3B-II abundance (Figure 5-4).

In addition to visualising autophagy structures, another aim of TEM was to count these structures, however this proved difficult due to limited resolution of the membranes and some uncertainty as to the nature of the structures observed with autophagy inhibitor treatment. A trial counting of autophagy structures, based on guidance from the literature [313] [181] [314], was performed in the MV4-11 samples in order to determine the numbers of autophagosomes, autolysosomes and lysosomes (Figure 5-7). Consistent with the LC3B-II results the number of autophagosomes/cell in the CX-5461 treated samples slightly increased compared to the vehicle, while a 3-fold change was observed in the serum-starved, chloroquine, CX-5461 + chloroquine, and bafilomycin-treated samples compared to vehicle. Autolysosomes were rarely detected across all the samples, and were predominantly identified in the vehicle, serum starved and

CX-5461 -treated samples, with none observed in the chloroquine, CX-5461 + chloroquine and bafilomycin-treated cell. While this was consistent/correlated with the extent of autophagy inhibition, since the overall numbers of structures identified were small definitive conclusions cannot be drawn. Lysosomes were also rarely detected in the samples, with slightly more in the chloroquine, CX-5461 + chloroquine and bafilomycin samples, again consistent with autophagy inhibition.
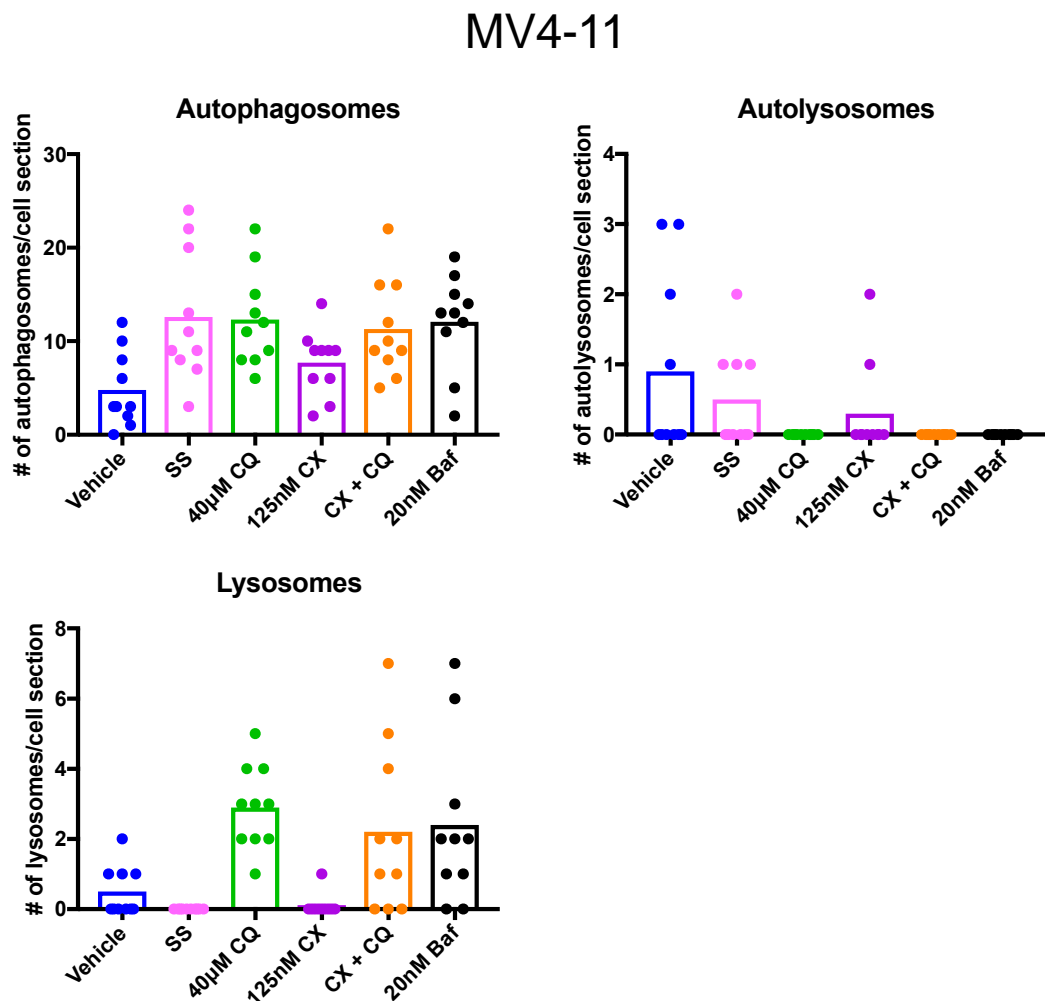
Figure 5-7: Quantification of autophagy structures observed by TEM in MV4-11 cells

The human AML cell line MV4-11 was exposed to vehicle, serum starvation (SS), 20nM bafilomycin (Baf), 1μM CX-5461 (CX), 40μM chloroquine (CQ) or CX-5461+chloroquine (CX+CQ) for 24 h, fixed and processed for transmission electron microscopy (Section 2.7). Samples were de-identified and 10 cells were imaged/treatment. Counting of autophagy structures was performed and then the samples were re-identified. N=1.

5.2.4 Combining alternative autophagy inhibitor bafilomycin with CX-5461

To further evaluate if autophagy inhibition synergises with CX-5461 treatment, combination testing was performed with an alternative autophagy inhibitor, bafilomycin A1 (bafilomycin). Bafilomycin blocks autophagosome-lysosome fusion [315], thus is a late-stage autophagy inhibitor like chloroquine and demonstrated similar effects on the ultrastructure of the AML cells as chloroquine treatment (Figure 5-6). This analysis was performed in the MOLM-13 cell line which demonstrated the most synergy of the four cell lines tested with the combination of CX-5461 + chloroquine (Figure 3-12). Synergy testing was performed as previously (Methods section 2.5.5). Figure 5-8 shows that bafilomycin alone at concentrations up to 15nM had no effect on cell viability. 11/15 of the combinations of CX-5461 with bafilomycin had a synergistic effect on the total viable cell number of MOLM-13 cells, particularly at 300nM CX-5461 or higher. This indicates that bafilomycin, like chloroquine, is synergistic in combination with CX-5461 *in vitro,* supporting the conclusion that autophagy inhibition mediates the synergy between the two drugs. However, like many drugs depending on the concentration evaluated, bafilomycin can mediate other effects in cellular processes, such as directly altering mitochondrial function [316,317], so this evidence should be considered supportive but not definitive. In order to conclusively determine the role of autophagy inhibition in combination with ribosome biogenesis inhibition, a genetic approach is required.

MOLM-13
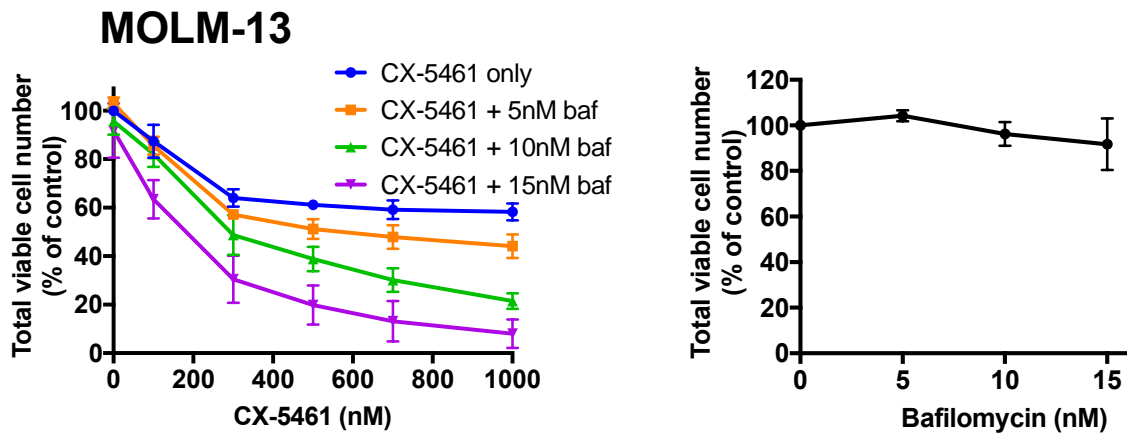
Combination index (CI)		CX-5461 (nM)				
		100	300	500	700	1000
Bafilomycin (nM)	5	1.415	0.612	0.674	0.742	0.820
	10	1.348	0.645	0.595	0.518	0.437
	15	0.888	0.583	0.498	0.432	0.369

Figure 5-8: Alternative autophagy inhibitor bafilomycin A1 synergises with CX-5461 to reduce AML cell number

MOLM-13 cells were cultured for 96 h in the presence of CX-5461 or bafilomycin (baf), as single agents or in combination. Total viable cell number was determined using the MTT assay (Methods section 2.5). Graphs show the mean±SD of n=3 experiments. In order to determine if a combination was synergistic the combination index (CI) of each data point was calculated using CompuSyn (Methods Section 2.5.5) and displayed in the inlayed table (synergism was designated as a CI value <0.75, shown in green).

5.2.5 Combining CX-5461 treatment with genetic knockdown of autophagy proteins

Human AML cell lines MV4-11, THP-1 and MOLM-13 with stable doxycycline-inducible shRNA constructs to Beclin 1 (BECN1) or ATG7 (2 targeting sequences per gene) were generated using lentiviral transduction (Section 2.10). Induction of shRNA expression with doxycycline was performed for 72 h, and the cells then treated with CX-5461 for a further 96 h before cell viability was analysed using the MTT assay (Section 2.5). Knockdown of the autophagy proteins was also assessed by western blot analysis (Section 2.8).

Analysis of the controls (Figure 5-9) shows that the sensitivity of the non-targeting cell lines to CX-5461 is consistent with the viability results of the parental cell lines in Chapter 3 (Table 3-4) and that doxycycline treatment alone did not affect viability in any of the three cell lines compared to the no-doxycycline controls. Western blot analysis revealed that partial knockdown of protein expression was achieved in all the cell lines with the targeting shRNA sequences, but not in the non-targeting control. Neither BECN1 shRNA target nor the two ATG7 shRNA targets lead to a significant change in viability in combination with CX-5461 treatment when compared to the non-targeting control in the 3 cell lines tested (Figure 5-9). Thus, the genetic knockdown of autophagy proteins did not synergise with CX-5461 treatment, which suggests that the synergy observed between CX-5461 + chloroquine (or bafilomycin) is not due to autophagy inhibition.

Figure 5-9: Genetic knockdown of autophagy-related genes BECN-1 and ATG-7 does not synergise with CX-5461 to reduce AML cell number

AML cell lines containing inducible shRNA sequences to BECN1 or ATG7 were treated with doxycycline (dox) for 72 h to induce shRNA expression, then treated with CX-5461 for a further 96 h. Cell viability was assayed with the MTT assay (Section 2.5) and expression of BECN1 and ATG7 protein was assayed by western blot analysis (Section 2.6). A repeated measure two-way ANOVA with Tukey's multiple comparison correction was used to compare the viability between the cell lines with different concentrations of CX-5461. No significant differences were observed. N=3 for the MTT assay, n=1 western blot.

a) MV4-11

b) THP-1

c) MOLM-13

172
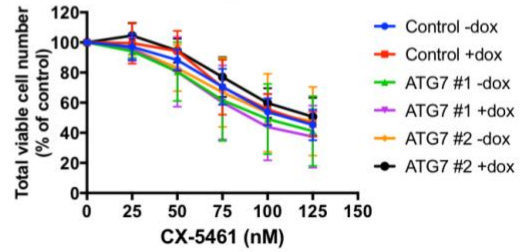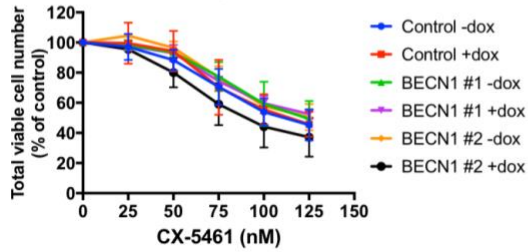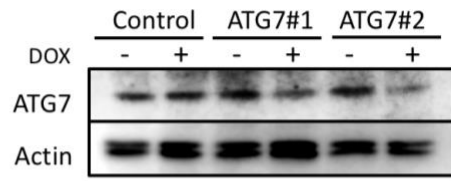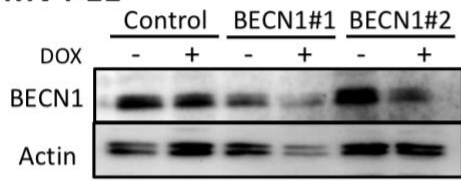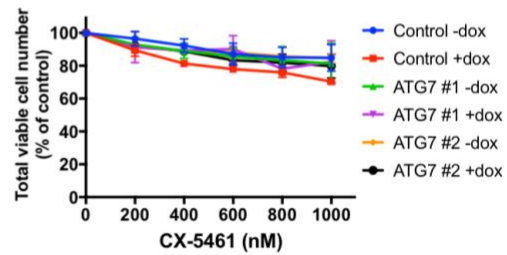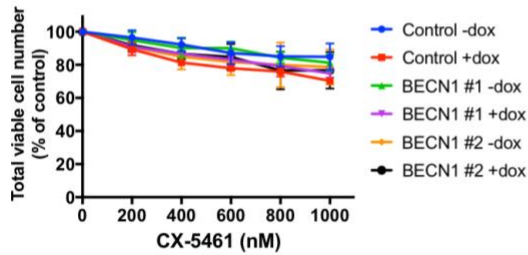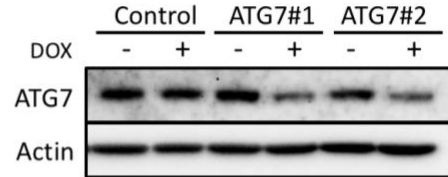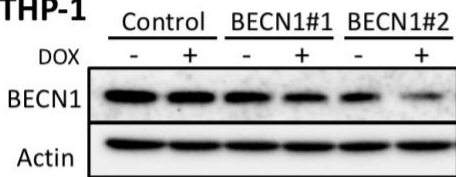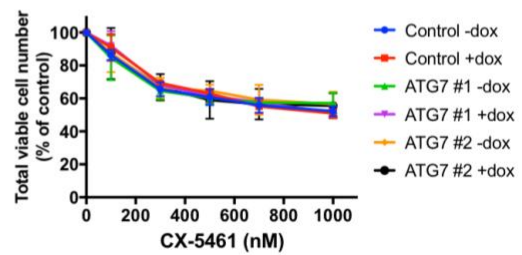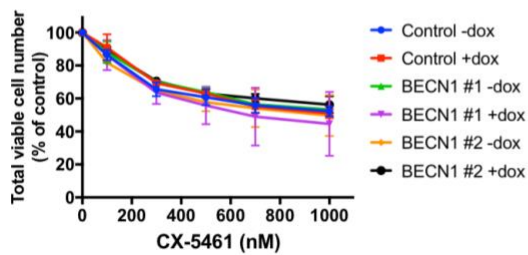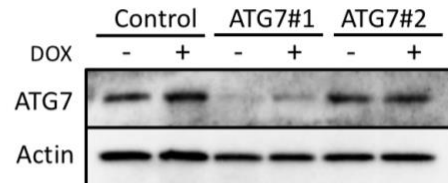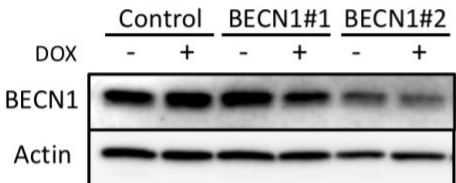
5.2.6 Metabolic flux analysis

Given the reported effects of chloroquine altering mitochondrial function (Section 5.1.2.4), and the appearance of mitophagic-like structures in the TEM in the chloroquine and CX-5461 + chloroquine-treated samples (Figure 5-6), alterations in mitochondrial function were analysed as a potential mechanism of synergy through performing a mitochondrial stress test (Section 2.11). Following 24 h drug pre-treatment, the oxygen consumption rate (OCR) was measured as an indicator of mitochondrial respiration and the extracellular acidification rate (ECAR) as an indicator of glycolysis using the Seahorse Extracellular Flux Analyser. In addition, drug-naïve cells were treated at the time of the assay (acute treatment). Two cell lines were evaluated; the THP-1 cell line (limited sensitivity to CX-5461 + chloroquine by viability assay), and the MOLM-13 cell line (very sensitive to the combination; Figure 3-12).

For the MOLM-13 cells, consistent with them being much more sensitive to combination treatment in terms of viability, the shifts in the energy profile were pronounced (Figure 5-10a). CX-5461 treatment shifted the flux towards mitochondrial respiration and away from glycolysis, whereas the combination treatment shut down both mitochondrial respiration and glycolysis resulting in a quiescent phenotype, represented by a significantly lower rate of basal respiration compared to the vehicle, CX-5461 or chloroquine-treated cells (Figure 5-10b). Consistent with the THP-1 cells being less sensitive to the drugs, both individually and in combination, any shifts in the energy profile (Figure 5-10a) were minimal. Specifically, CX-5461 treatment significantly increased the maximal respiration (Figure 5-10c) and spare respiratory capacity (Figure 5-10d) in the MOLM-13 cells, with an upward trend observed in the THP-1 cells, while chloroquine significantly decreased the maximum respiration rate in the MOLM-13 cells. Interestingly, combination treatment had the opposite effect on the respiratory capacity of the two cells lines. In the THP-1 cells combination treatment significantly increased the maximal respiration and spare respiratory capacity, while in the MOLM-13 cells it was significantly decreased. These results suggest that CX-5461 mediates mitochondrial stress and the cells are adapting to this, however, combination treatment mediates loss of mitochondrial viability due to the effects of chloroquine, explaining why MOLM-13 cells are particularly sensitive to the combination treatment in terms of viability.

Acute drug treatment at the time of the assay indicated that CX-5461 and chloroquine as single agents did not significantly affect respiratory capability compared to vehicle (Appendix Figure 5-1), indicating that these drugs are not likely to be directly affecting the mitochondria.

Figure 5-10: CX-5461 and chloroquine synergise to alter mitochondrial function

AML cell lines THP-1 and MOLM-13 were treated with vehicle, 1µM CX-5461 (CX), 40µM chloroquine (CQ) or CX-5461+chloroquine (CX+CQ) for 24 h, equal cell number plated, then metabolic flux analysed using a mitochondrial stress test on the Seahorse XFe97 analyser (Section 2.11). a) Energy map of basal levels of oxygen consumption rate (OCR) and extracellular acidification rate (ECAR), b) Basal respiration rates c) Maximal respiration rate following mitochondrial uncoupling with FCCP, d) Spare respiratory capacity (difference in the OCR between the maximum respiration rate and basal rate). One-way ANOVA was performed with a Tukey's multiple comparison test, the adjusted p-value is shown. Not significant $P > 0.05$, *$P \leq 0.05$, **$P \leq 0.01$, ***$P \leq 0.001$, **** $P \leq 0.0001$. Significant results only marked. N=3. Compared to vehicle, unless indicated by a bar.
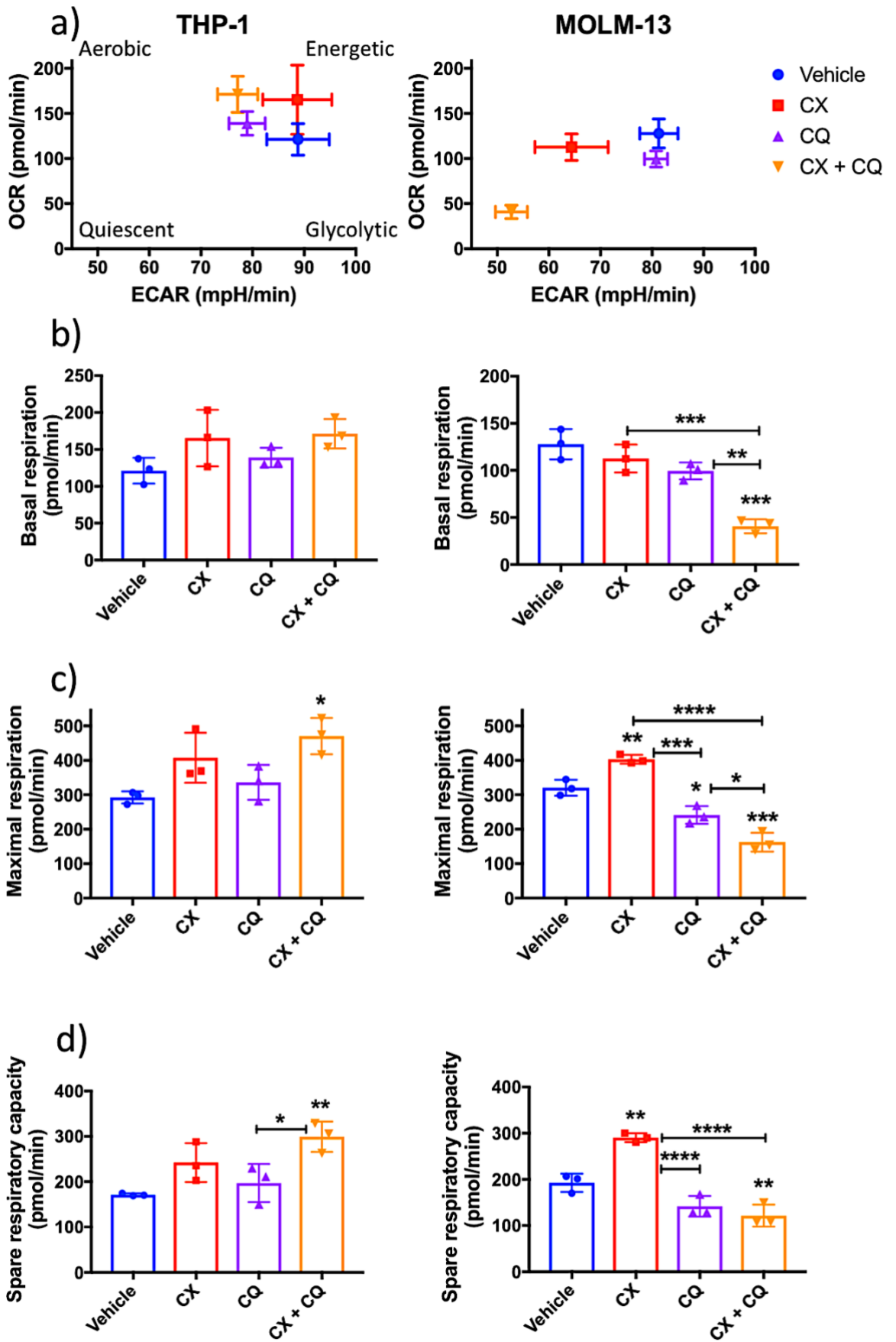
5.3 Discussion

5.3.1 Summary of results and synergy hypothesis

In this chapter, four potential mechanisms and endpoints of synergy between CX-5461 and chloroquine were assessed; cell cycle, cell death, inhibition of autophagy and altered mitochondrial activity. Chloroquine enhanced the cell cycle and cell death endpoints of exposure to CX-5461. While CX-5461 induced autophagy in some cell lines and the alternative autophagy inhibitor bafilomycin also synergised with CX-5461 to reduce AML cell viability, however, the genetic knockdown of autophagy genes did not synergise with CX-5461 treatment, suggesting that autophagy does not play a significant role in the synergy between CX-5461 and chloroquine. Interestingly, metabolic flux analysis revealed that the combination of drugs caused significant changes in mitochondrial respiration which is a potential mechanism of synergy.

Based on the results presented in this chapter, the following hypothesis was devised to account for the synergy observed between CX-5461 and chloroquine in AML cells (Figure 5-11). As an established autophagy inhibitor chloroquine blocks autophagy, including mitophagy (the recycling of mitochondria), thus can result in an accumulation of dysfunctional mitochondria in the cell. In addition, metabolic flux analysis suggests that the combination of CX-5461 and chloroquine may indirectly impact on the mitochondria, placing the cells under a high degree of metabolic stress and leading to the endpoints of cell cycle arrest and cell death.
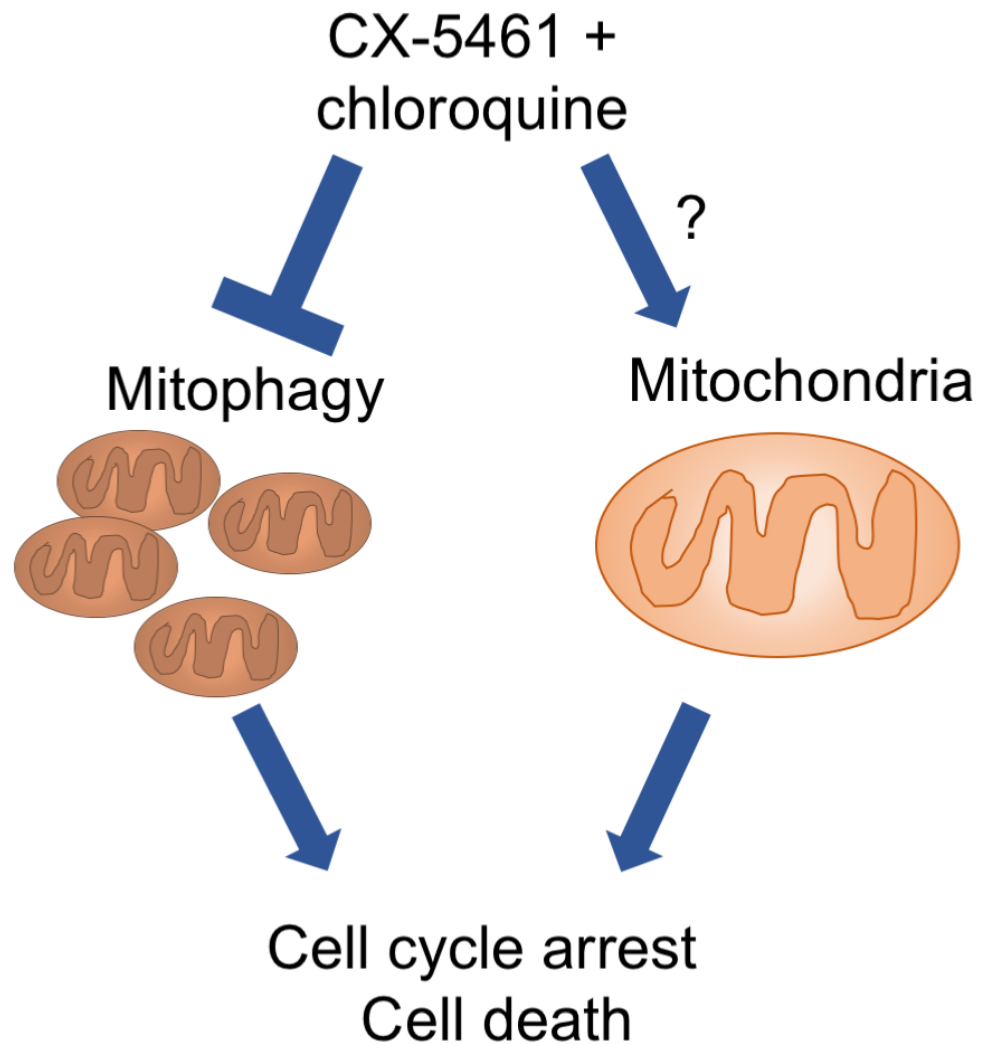
Figure 5-11: Hypothesis of the mechanisms of synergy between CX-5461 and chloroquine

Based on the results presented in this chapter the following hypothesis was devised to account for the synergy observed between CX-5461 and chloroquine in AML cells. As an established autophagy inhibitor chloroquine blocks autophagy, including mitophagy (the recycling of mitochondria) leading to an accumulation of dysfunctional mitochondria which causes some degree of metabolic stress. Flux analysis results also indicate that the combination of the drugs might be having indirect effects on the mitochondria, placing the cells under a high degree of metabolic stress and leading to cell cycle arrest and cell death.

5.3.2 Autophagy as a potential mechanism of synergy

Interestingly, mechanistic analysis indicated that the synergy observed between CX-5461 and chloroquine is not due to autophagy inhibition by chloroquine, its major, well-characterised mechanism of action (Section 5.1.2.2). It is also surprising that CX-5461 does not appear to robustly induce autophagy in all AML cell lines (Figure 5-4) given the link between inhibition of Pol I transcription and autophagy induction. Specifically, inhibition of Pol I transcription with adriamycin and actinomycin-D, or knockdown of Pol I transcription factors in a breast cancer cell line induces nucleolar disruption mediated autophagy [318] and CX-5461 induces autophagic cell death in osteosarcoma cell lines [83]. While LC3B-II levels usually indicate changes in autophagic flux there are some exceptions. In ovarian cancer cell lines elevated LC3B-II following oxidative stress was shown not to be associated with induction of autophagy but rather anoikis (detachment-induced programmed cell death) [319]. Furthermore, accumulation of LC3B-II protein is cell line dependent following autophagy induction by nutrient starvation [320]. An alternative method of measuring autophagic flux following CX-5461 and combination treatment would be to use the long-lived protein degradation assay, where the degradation of radiolabelled long-lived proteins is used as a readout of autophagic activity, as has been utilised to study autophagic flux in AML cells in response to differentiation induction [321], providing a more direct measure of autophagy.

TEM analysis is also considered a reliable method of observing autophagic activity, however counting the number of autophagy structures proved challenging. Overall, while the results are consistent with the changes in LC3B-II abundance, the variation was consistently high across all the samples (Figure 5-7), and counting 3D structures in a 2D context is not ideal. Thus, an alternative assay to count the number of autophagy structures would be to perform immunofluorescence with the LC3B antibody and count the number of LC3B positive puncta, which mark the membrane of the autophagosomes and autolysosomes [322]. A technique known as correlative light and electron microscopy (CLEM), which combines light and electron microscopy on the same sample, would also be a beneficial technique to utilise here as the data of light and electron microscopy could be correlated on the same sample to identify the

membrane of the autophagy structures based on LC3B expression, then characterise the structures as autophagosomes or autolysosomes based on appearance by TEM.

Due to the multiple effects of chloroquine (Section 5.1.2), a genetic approach is also recommended to assist in the identification of mechanisms of action[181]. Interestingly, genetic knockdown of autophagy-related genes Beclin 1 and ATG7 did not synergise with CX-5461 to reduce AML cell number (Figure 5-9), indicating that CX-5461 and chloroquine are not acting synergistically through the action of chloroquine as an autophagy inhibitor. However, the success of the knockdown needs to be considered. Western blot analysis confirmed that partial, but not complete, knockdown of Beclin 1 and ATG7 protein expression was achieved. Other studies confirmed that a 50% knockdown of expression of these proteins has functional effects in other cell types [295,297]; whether this knockdown is sufficient to inhibit autophagy in AML cells is unknown and should be assessed through methods such as LC3B-II expression by western blot (as in Figure 5-4) or long-lived protein degradation assay [321], particularly in the context of autophagy induction through serum starvation, for example. It is also possible that there was some kind of compensatory mechanisms that occurred over the course of the experiments, and this could be further analysed by knocking down two or more autophagy-related genes. Gene editing technology (for example CRISPR deletion) could be employed as an alternative approach to knockdown [181].

5.3.3 Mitochondrial effects as a potential mechanism of synergy

TEM analysis revealed numerous electron-dense structures in the bafilomycin, chloroquine, and CX-5461 + chloroquine-treated cells. Such electron-dense structures have previously been identified as mitophagy structures (autophagosomes containing mitochondria) in a study evaluating the effect of the MDM2 inhibitor Nutlin 3a in AML cell lines [323]. As chloroquine and bafilomycin are late-stage inhibitors of autophagy, blocking the fusion of autophagosomes with lysosomes, the increased appearance of autophagosomes containing un-degraded cargo is unsurprising. However, the frequency of autophagosomes containing mitochondria suggests that mitophagy is upregulated, thus the autophagy inhibitors could be indirectly affecting mitochondrial function, as has been previously suggested [111]. A technique to identify the contents of these electron-dense structures would be immunofluorescence using the autophagy

marker LC3B in combination with mitochondrial or lysosomal markers in order to evaluate co-localisation, a technique which has been used to study mitophagy in the context of heart infarctions [324]. CLEM could also be used to correlate autophagy, mitochondrial and lysosomal markers by immunofluorescence with the electron-dense structures identified by TEM. This technique has been used to study autophagosome biogenesis in HeLa cells [325] and to study the autophagy in the context of *Mycobacterium* infection in a whole organism Zebrafish model [326].

Mitochondrial flux analysis indicated that the combination of CX-5461 and chloroquine lead to significant changes in mitochondrial function, perhaps due to inducing mitochondrial stress (Figure 5-10). Changes in the OCR, such as elevated maximal respiration and spare respiratory capacity in MOLM-13 following CX-5461 treatment (Figure 5-10b,c), could be due to changes in mitochondrial number, expression and/or the activity of mitochondrial complexes or mitochondrial viability. Mitochondria number can be assessed by determining mitochondrial DNA content using qPCR [111,327] or digital droplet PCR [328]. The expression of mitochondrial complexes, including aconitase, citrate synthase and complex IV subunits, can also alter cellular respiration rate which can be assessed by western blot [111]. Activity of the individual mitochondrial complexes can be determined by permeabilising the cells and measuring the OCR with Complex I, II or IV-linked substrates using the Seahorse, as has been performed in primary neurons with chloroquine and bafilomycin treatment [111]. Changes in mitochondrial viability can be assessed using flow cytometry and the membrane-permeant fluorescent dye JC-1, with its localisation in the mitochondria, forming aggregates and leading to a shift in the wavelength of fluorescence emission, being a measure of mitochondrial membrane potential, which has also been utilised to assess mitochondrial changes in AML cell lines treated with chemotherapeutics [106].

A potential mechanism via which CX-5461 and chloroquine are synergising through the mitochondria is by the production of ROS. Autophagy plays a role in controlling ROS levels through removing dysfunctional mitochondria [102], as such is in unsurprising that blocking autophagy (genetically or chemically) mediates increased ROS levels in various cell types [329], including cancer cells such as hepatocellular carcinoma [330]. It has also been shown that inhibition of ribosome biogenesis with CX-5461 leads to ROS

accumulation in aortic medial smooth muscle cells [331], however, the effects of CX-5461 on ROS levels in AML cells is not yet characterised. If CX-5461 does elevate ROS levels in AML cells, this could be a mechanism by which CX-5461 and chloroquine synergise, which presumably is mitochondria-dependent, to affect AML cell viability. Since AML cells are more sensitive to oxidative stress than normal cells [332] this would fit with our hypothesis. To evaluate this possibility, the level of intracellular ROS following CX-5461, chloroquine or combination treatment could be measured using flow cytometry [331].

Narrowing down the mechanism of action in the mitochondria will greatly assist in guiding the rational choice of alternative inhibitors to combine with CX-5461. Further discussion of targeting mitochondria in cancer, including mitochondrial inhibitors with its clinical potential, is explored in Chapter 6.

5.3.4 Other potential mechanisms of synergy

There are multiple other potential mechanisms of synergy that, due to time limitations, were not assessed in this thesis. These include the nucleolar stress response, DNA damage signalling, effects on Pol I transcription and lysosomal effects (Figure 5-2).

5.3.4.1 Nucleolar stress response

The nucleolar stress response is activated by multiple cellular stresses, including Pol I transcription inhibition, resulting in accumulation of p53 (Section 5.1.1.3). It was recently demonstrated that autophagy induction is a downstream consequence of such stress signalling. Chemical inhibition of Pol I transcription and siRNA knockdown of basal Pol I transcription factor Transcription Initiation Factor IA (TIF-IA) resulted in nucleolar disruption and autophagy induction, and this was dependent on nucleolar protein nucleophosmin (NPM) [318]. By inhibiting autophagy with chloroquine this may enhance nucleolar stress signalling resulting in reduced cell viability. This can be assessed by determining p53 and p21 expression by western blot [1] and assessing the translocation of the nucleolar marker protein nucleolin through immunofluorescence as a measure of nucleolar disruption [318].

5.3.4.2 DNA damage signalling

Chloroquine has long been known to have DNA intercalating properties, mediating activation of ATM signalling (Section 5.1.2.3) which may be the focal point for synergy with the DNA damage-like signalling induced by CX-5461 (Section 5.1.1.4). In erythroleukaemia cells, a subset of AML, DNA intercalation was not observed below 600μM chloroquine treatment [176], thus as the highest concentration of chloroquine used in these *in vitro* experiments was 40μM, it is unlikely to have a significant DNA intercalating effect. However, there is the potential that chloroquine might accumulate to higher levels in different AML cell lines so it should still be considered. This could be assessed through western blot analysis of p53, Chk1, Chk2, pChk1 and pChk2 expression [1], in addition to expression of the DNA double-strand break marker γH2AX to check for global DNA damage [268].

5.3.4.3 Pol I transcription inhibition

While CX-5461 is a well-established inhibitor of Pol I transcription, including in AML cells [1], the effects of chloroquine on Pol I transcription have not been reported thus far. Due to its DNA intercalating properties [176], there is the potential that chloroquine could disrupt rDNA transcription. This could be assessed with qRT-PCR for 45S pre-rRNA [81] or [^{32}P] orthophosphate labelling to measure 45S pre-RNA synthesis [1,78]. If chloroquine was to also inhibit ribosome biogenesis, this may be the focus of the synergy observed in combination with CX-5461.

5.3.4.4 Lysosomal effects

As outlined in Section 5.1.2.5, in addition to a role in autophagy, lysosomes also act as hubs for nutrient signalling through mTORC1. Metabolic flux analysis revealed that the combination of CX-5461 and chloroquine altered mitochondrial respiration (Figure 5-10), which may be due to chloroquine inhibiting lysosome function, specifically the nutrient signalling pathways. This could also explain why the alternative inhibitor bafilomycin A1 also synergises with CX-5461 and reduces AML cell number (Figure 5-8), specifically bafilomycin A1 inhibits lysosomal function through its actions on the vacuolar-ATPase [315] (which is known to play an important role in the nutrient signalling of the lysosome through mTORC1 [309]). Activation of mTORC1 following CX-5461, chloroquine or combination treatment can be assessed by western blot for phosphorylation of mTORC1 downstream target S6K1 (pT398) in the presence or

absence of amino acids, also using immunofluorescence to evaluate co-localisation of mTORC1 and the lysosomal marker lysosomal-associated membrane protein 1 (LAMP1) [309].

5.3.5 Conclusion

Thus far, the mechanistic and endpoint analysis of the synergy between CX-5461 and chloroquine indicates that cell cycle arrest, cell death and altered mitochondrial activity are likely to be the processes involved in the synergy. The drug's effects on the mitochondria are novel and a promising finding. While there appears to be limited clinical potential for the use of chloroquine in combination with CX-5461 (as addressed in Chapter 4) this data does present an alternative avenue for combination therapy, thus narrowing down the search for drugs that may have improved efficacy and reduced toxicity when combined with CX-5461, further discussed in Chapter 6.

Chapter 6   Discussion

6.1 Summary of results

Targeting ribosome biogenesis, a cellular process frequently upregulated in cancer, with the novel Pol I transcription inhibitor CX-5461 is highly efficacious in pre-clinical models of solid and haematological cancers [1,81], which lead to Phase I and I/II clinical trials [82,85]. However, as is common with single-agent therapies, the *in vivo* studies demonstrated that eventually, resistance to CX-5461 occurs, highlighting the need for a drug combination approach. Based on the well-established link between ribosome biogenesis and cellular metabolism, both in normal cells and also a cancer setting, it was hypothesised that targeting these two processes in combination would prove more efficacious in AML, a model of aggressive malignancy with poor therapeutic options when compared to the single drugs alone. *In vitro* synergy testing in AML cell lines was performed to identify promising drug combinations of interest (Chapter 3), which were then tested for efficacy in *in vivo* transplant models of AML (Chapter 4). Finally, *in vitro* mechanistic analysis of the most promising drug combination was performed (Chapter 5).

In vitro testing of the novel ribosome biogenesis inhibitor CX-5461 in combination with 10 clinically-approved metabolism-modifying drugs (Chapter 3) confirmed that of these 5 drugs (orlistat, DCA, ritonavir, omeprazole and chloroquine) acted synergistically with CX-5461 to reduce AML cell viability (Figure 3-19), with the autophagy inhibitor chloroquine being the most effective (Figure 3-12). Three synergistic combination therapies were further evaluated in an *in vivo* syngeneic mouse AML model (Chapter 4). Orlistat and DCA treatment did not improve survival when combined with CX-5461 and compared to CX-5461 alone (Figure 4-4, Figure 4-5), whereas chloroquine did (Figure 4-6). CX-561 + chloroquine treatment was also evaluated in human cell line xenograft mouse models, but found to have limited efficacy (Figure 4-8, Figure 4-9), despite robust *in vitro* synergy. As the dosing of CX-5461 and chloroquine could not be increased further due to toxicity, mechanistic analysis was then performed in order to identify an alternative to chloroquine with reduced toxicity, and potentially improved efficacy (Chapter 5). CX-5461 + chloroquine

synergy was observed at the level of cell cycle arrest and cell death in all four cell lines tested (Figure 5-3), and the upstream mechanisms of synergy leading to this was then assessed. The role of autophagy in the synergy between CX-5461 and chloroquine was not definitive. CX-5461 induced autophagy in some cell lines but not others, and this did not correlate with sensitivity to CX-5461 with respect to viability (Figure 5-4, Figure 5-5). In addition the autophagy inhibitor bafilomycin also synergised with CX-5461 (Figure 5-8), however genetic knockdown of autophagy-related genes, Beclin 1 and ATG7, did not synergise with CX-5461 treatment (Figure 5-9), suggesting autophagy may not be the mechanism of synergy between CX-5461 and chloroquine, although the knockdown was partial (and the phenotypic consequences of the knockdown on autophagy are yet to be confirmed) and there might have been compensatory mechanisms involved (as outlined in Section 5.3.2), thus conclusions regarding the role of autophagy cannot be drawn yet. Metabolic flux analysis revealed that the drug combination significantly affected mitochondrial activity (Figure 5-10), decreasing respiration in the MOLM-13 cell line which was very sensitive to the drug combination with respect to viability, whereas increased respiration in the THP-1 cell line which had limited sensitivity to the drug combination. These results indicate that the combination of CX-5461 and chloroquine can place cells under mitochondrial stress and that drug combination sensitivity may be dependent on the cells ability to adapt/respond to such stress. Therefore, direct drug targeting of the mitochondria was identified as a promising combination with ribosome biogenesis inhibition, and potentially more efficacious than CX-5461 plus chloroquine.

6.2 Targeting mitochondria in AML

Mechanistic analysis of CX-5461 and chloroquine in Chapter 5 revealed that combination therapy with these drugs significantly affected mitochondrial respiration (Figure 5-10), which is a published effect of chloroquine via inhibition of mitophagy and perhaps other indirect effects on the mitochondria [111], however, this is a novel response to CX-5461 treatment. Interestingly, in the AML cell lines, a significant decrease in maximum mitochondrial respiration was observed in the MOLM-13 but not the THP-1 cell line, thus the response was not common to all cell lines. Potentially a more selective mitochondrial inhibitor is required to:

- Directly target mitochondrial activity;

- Reduce side effects that might make some cells not responsive;

- Obtain a more uniform response in all cells.

Thus ,directly targeting mitochondrial function was identified as a promising approach in combination with ribosome biogenesis inhibition. There are currently several clinically-used medications that target well defined mitochondrial functions including metformin, phenformin, tigecycline and doxycycline (Figure 6-1).
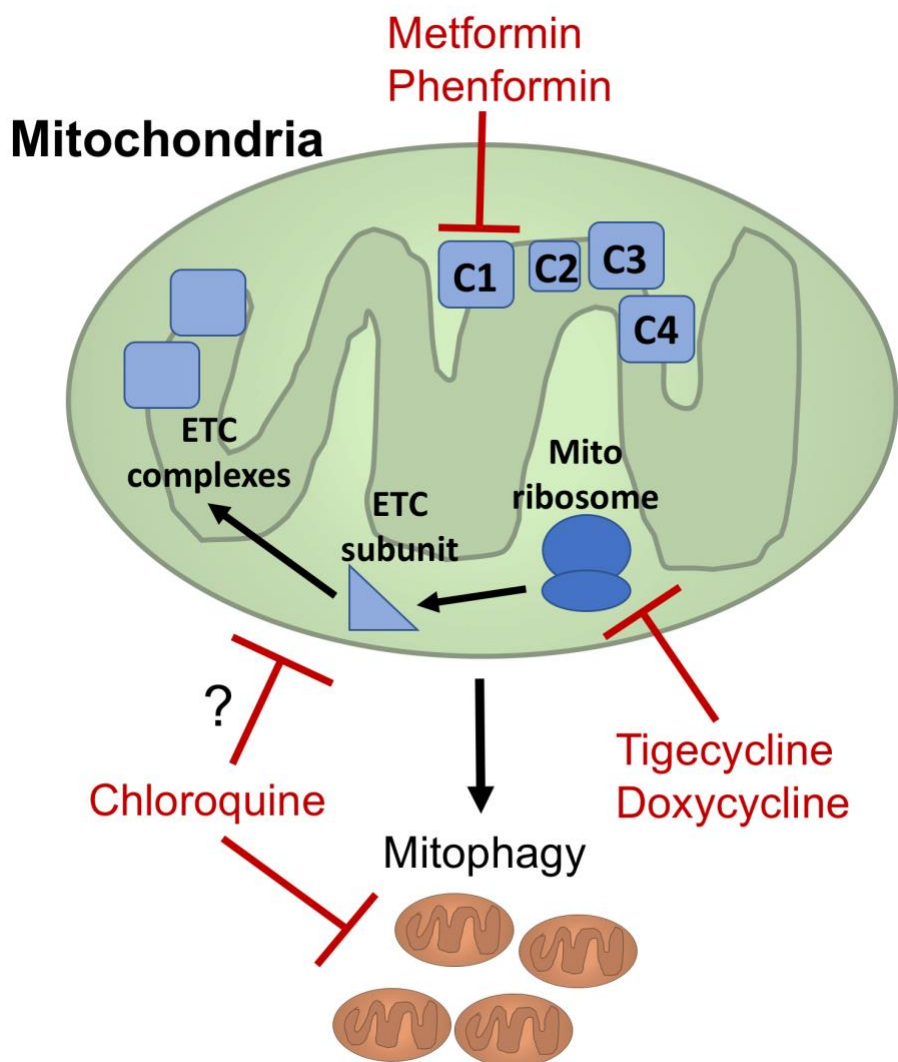
Figure 6-1: Targeting cancer mitochondria

Various clinically approved drugs target the mitochondria and could be repurposed as cancer therapeutics. Chloroquine is known to inhibit mitophagy (the recycling of damaged mitochondria) through inhibition of autophagy, and potentially has direct effects on mitochondrial function through unknown mechanisms. Anti-diabetic medications metformin and phenformin target complex I of the electron transport chain (ETC). Antibiotic tigecycline inhibits the function of the mitochondrial ribosome to translate components of the ETC complexes.

6.2.1 Clinical agents for targeting mitochondria

Metformin is an anti-diabetic medication that interferes with mitochondrial function by inhibiting complex I of the mitochondrial electron transport chain (Section 3.1.2.2)[132]. Metformin was selected as a candidate for evaluation with CX-5461 *in vitro* in Chapter 3, but was not evaluated further as it interfered with the mechanism of

action of both viability assays used (Figure 3-3, Figure 3-4). Entry of metformin into cells is mediated by organic cation transporters (OCTs), particularly OCT1 [333,334], which are highly expressed only on certain cell types including hepatocytes [334] and adipocytes [335], facilitating the effects of metformin as an anti-diabetic. In other cell types expression of OCTs is often low, including in AML patient bone marrow samples [336]. Metformin has shown efficacy in AML cells *in vitro* but only at concentrations of 10mM [134], which is more than 10-fold higher than plasma concentrations achieved in human patients [178], and this is likely due to the low expression of OCTs in these cells. In the same study daily dosing of metformin by IP injection significantly reduced tumour volume in a subcutaneous AML cell line xenograft model, however as discussed in Section 4.3.1.2, dosing via IP might result in higher concentrations of drug reaching the subcutaneous AML cells than achieved in a orthotopic model and also does not represent the normal oral dosing route for human patients. In a retrospective analysis of diabetic patients with AML, metformin treatment did not have an effect on overall survival or disease-free progression[337], potentially due to the drug not reaching the cancer cells at a high enough concentration to have efficacy. Together these factors suggest that metformin could be useful for *in vitro* mechanistic analysis with CX-5461, but potentially have limited clinical use in AML, unless a novel formulation is devised to improve uptake and targeting to the mitochondria (for example metformin coupled to a mitochondrial vector showed efficacy in pancreatic cancer *in vitro* and *in vivo* [338]).

Phenformin is an alternative to metformin, another anti-diabetic medication that inhibits complex I of the electron transport chain[339]. While phenformin is also transported into hepatocytes by OCT1, it displays a higher affinity for the transporter and transport activity compared to metformin [333], and thus could be a better alternative to treat cancer cells that have low OCT expression. However, the clinical use of phenformin has been stopped due to the incidence of lactic acidosis in patients, particularly those with renal or liver insufficiency [340,341] which would also limit its clinical potential as a therapy in cancer (although the risk: benefit profile can vary greatly between diseases such as diabetes and cancer). There is certainly a need for third-generation derivatives of metformin with improved efficacy and reduced toxicity. A novel metformin derivative HL010183 showed increased efficacy against triple-

negative breast cancer [342] and cutaneous squamous cell carcinoma [343] compared to metformin *in vitro* and *in vivo*, however, it is yet to be assessed in clinical trials.

Tigecycline is a broad-spectrum antibiotic that binds to the bacterial 30S ribosomal subunit, inhibiting translation and thus killing the bacteria [344]. Tigecycline is administrated intravenously and has a favourable clinical profile, causing only mild side effects in most patients, including nausea, diarrhoea and vomiting, which are thought to be due to the drug irritating the gastric mucosa [345]. Due to the similarities between the bacterial and mitochondrial ribosomes, tigecycline has also been shown to affect mitochondrial function in eukaryotic cells by inhibiting the mitochondrial ribosome to translate the 13 proteins encoded by the mitochondrial genome, which comprise components of the mitochondrial electron transport chain complexes I-IV [106], making it of interest as a potential cancer therapeutic. Tigecycline has been shown to have strong efficacy in AML as a single agent [106]. In a panel of 9 human and mouse AML cell lines *in vitro* treatment with tigecycline significantly reduced AML cell viability within 72 hours, and induced apoptosis within 6 hours. Importantly, 20 human patient AML samples, but not normal hematopoietic cells, displayed a similar or greater sensitivity in terms of viability to tigecycline compared to the AML cell lines. Pre-treatment with tigecycline significantly reduced the clonogenic potential of primary AML cells but not normal hematopoietic cells *in vitro,* and similarly reduced the repopulating potential of the AML cells *in vivo* in NSG mice, thus targeting leukaemia-initiating cells. The effects of tigecycline on mitochondrial ribosome translation were confirmed, with a reduction of protein levels and increase in mRNA of the respiratory complex IV subunits cytochrome C oxidase-1 and 2 (cox 1 and 2) which are translated by mitochondrial ribosomes, but not grp78 and X-linked inhibitor of apoptosis protein (XIAP) which are translated by cytosolic ribosomes. Incorporation of [^{3}H]-leucine into mitochondria was also significantly reduced with tigecycline treatment. In the same study [106], in a subcutaneous human cell line xenograft model, twice daily IP injections of 50 or 100mg/kg tigecycline for three weeks significantly reduced tumour growth compared to the control, without gross changes (toxicity) to the organs. Based on these findings a Phase I dose-escalation study of tigecycline in 27 AML patients was commenced, with daily IV dosing 5 or 7 days a week for 2 weeks, followed by 1 week off the drug, and this cycle continued until disease progression [346]. Up to four cycles of treatment were

completed and the maximum tolerated dose was determined to be 300mg/day single dose. Despite reaching a peak serum concentration (C_{max}) of approximately 12μM, which has been demonstrated to be efficacious *in vitro* [106], no partial or complete responses were observed (as measured by number of blasts in the bone marrow, neutrophil count and platelet count) and there was no consistent increase in Cox1 mRNA or decrease in protein (due to inhibition of translation) in peripheral blood mononuclear cells, indicating the drug was not hitting its target. The biological half-life ($t_{1/2}$) was found to be approximately 9.5 hours, 2–6-fold lower than that reported in non-cancer patients [347-349], perhaps explaining the lack of a response. Clearly, further adjustments to the dosing schedule are required in order to achieve efficacy in AML (such as twice daily as performed in non-cancer patients [347-349]), however overall the toxicity results were promising.

Doxycycline is another broad-spectrum antibiotic drug that is being investigated as a potential cancer therapeutic. The semi-synthetic tetracycline drug, doxycycline has been used for decades as an anti-microbial in both animals and humans, with either oral or intravenous administration [350]. Like tigecycline, doxycycline targets bacterial ribosome translation through binding the 30S ribosomal subunit [351] and inhibits mitochondrial ribosome translation in a variety of eukaryotic models at a concentration as low as 0.5μg/mL in some [352]. Doxycycline is commonly used in both *in vitro* and *in vivo* models for research to control gene expression, known as the Tet-On/Off systems (as in Methods 2.10). In the genetic knockdown of autophagy experiments presented in this thesis, there was no synergy between CX-5461 and chloroquine in the context of 1μg/mL doxycycline treatment to induce shRNA expression (Figure 5-8), which does not support the hypothesis that ribosome biogenesis synergises with inhibition of mitochondrial function. However, it is possible that this concentration of doxycycline was insufficient to inhibit mitochondrial translation in the AML cell lines, as was observed in the lung cancer cell line A549 where 1μg/mL doxycycline was insufficient to inhibit mitochondrial ribosome translation and 5μg/mL or higher was required [352]. This requires confirmation experimentally in the AML cell lines, and can be done so by evaluating the protein levels of the mitochondrial ribosome-translated protein Cox 1 [352]. In a variety of solid tumours including breast, prostate and lung cancer mitochondrial biogenesis was

identified as a feature of cancer stem cells and thus targeting this with doxycycline inhibited tumour sphere formation, particularly at 10µM or higher [353]. In a small clinical pilot study of 15 breast cancer patients, 14 days of oral doxycycline therapy significantly reduced biomarkers of stemness CD44 and aldehyde dehydrogenase 1 (ALDH1; markers of cancer stem cells) in almost 90% of patients, however, inhibition of mitochondrial translation was not confirmed [354].

While these clinically-used mitochondria-inhibiting agents directly target mitochondrial activity, some issues with concentration/dosing required to achieve this inhibition, as outlined above, suggests that novel drugs with increased potency for inhibiting mitochondrial activity would be an even more promising approach.

6.2.2 Novel mitochondrial inhibitors

Novel mitochondrial-targeting agents are also in development as cancer therapeutics. One example is the novel compound CCI-006 which has shown efficacy in MLL-translocated AML cell lines through inhibiting mitochondrial respiration, although the exact mechanism of action is still to be determined [355]. A relatively small subset of AML cell lines were not responsive to CCI-006 although they did display a similar reduction in mitochondrial respiration as the CCI-006 sensitive cell lines and had a stronger glycolytic phenotype, highlighting the variability of AML cell lines with respect to reliance on mitochondrial function. Such novel therapies could provide a more targeted approach to inhibiting mitochondrial function in cancer, compared to the clinically-used drugs outlined in Section 6.2.1, but will require considerable study to be translated to the clinic.

6.2.3 Combining CX-5461 with mitochondrial inhibitors

Mitochondrial flux analysis (Figure 5-9) suggested that CX-5461 and chloroquine synergised at the level of mitochondrial function, as such combining drugs that specifically target the mitochondria is a promising approach to improve the efficacy of CX-5461. As outlined in Section 6.2, there are currently several clinically approved drugs that target mitochondrial function that warrant evaluation in combination with CX-5461.

Ideally, these mitochondrial-targeting drugs would be evaluated for synergy with CX-5461 following the experimental approach used in this thesis. Specifically they would first be tested *in vitro* in AML cell lines first (as in Chapter 3), however, a different readout to that used in this thesis may be required since metformin interfered with the readouts for both the neutral red and MTT assays (Figure 3-3, Figure 3-4). One such assay could be using high throughput flow cytometry to determine cell number via physical particle counting (cell size and granularity), which is not dependent on biochemical functions, including mitochondrial function. If synergy is observed with these mitochondrial-targeting agents in combination with CX-5461 in multiple AML cell lines (as in Figure 3-19), as done in Chapter 4 the combination therapy will be evaluated for efficacy using *in vivo* mouse models of AML. Issues with the *in vivo* efficacy of the mitochondria-targeting drugs, as well as clinical translatability, as outlined above, must be kept in mind when testing any promising combinations *in vivo*, so it will be important to include markers of on-target effects in these studies.

If the drug combination improves survival in the mouse models of AML, mechanistic analysis such as those performed in Chapter 5 will be required to confirm the mechanisms of action. Specifically, the drugs effect on mitochondrial function will be evaluated. For metformin and phenformin; inhibition of complex 1 activity will be assessed using the Seahorse XFe analyser [111], for tigecycline; inhibition of mitochondrial translation will be confirmed by measuring mRNA and protein levels of Cox 1 and 2 which are translated by mitochondrial ribosomes [106,352] and comparing these to the levels of cytoplasm-translated succinate dehydrogenase [352], grp78 or XIAP [106] to confirm that global translation is not inhibited. For all 4 drugs metabolic flux analysis, including a mitochondrial stress test and individual complex activity, will be conducted using the Seahorse XFe analyser. These assays will also be conducted with CX-5461 as a single agent and in combination with the mitochondrial-inhibitors. The hypothesis developed in Chapter 5 regarding the mechanism of synergy between CX-5461 and chloroquine (Figure 5-11) would suggest that directly targeting cancer mitochondrial activity in combination with CX-5461 will result in increased synergy *in vitro* and improved efficacy and reduced toxicity *in vivo*, compared to CX-5461 and chloroquine, providing a drug combination with the potential of clinical translation.

6.3 Alternative approaches for improving CX-5461 efficacy

6.3.1 CX-5461 and immunotherapy

Evaluation of promising drug combinations in *in vivo* AML transplant models revealed the interesting suggestion that CX-5461 was more effective in the syngeneic MLL/AF9 NRAS model compared to the xenograft models (Figure 4-6, Figure 4-8, Figure 4-9), which is a trend has also been observed by others in the laboratory (unpublished). Other than the mouse-derived MLL/AF9 NRAS cells being 10 times more sensitive to CX-5461 than the human cell lines (Table 3-4), the major difference between these two types of models is the immunodeficiency of the mice used, suggesting that the immune system could play a role in the response of the AML cells to CX-5461. As suggested in Section 4.3.6, this could be examined by transplanting the mouse-derived MLL/AF9 NRAS cell line into the immunocompromised mice normally used for the cell line xenograft experiments, and comparing the efficacy of CX-5461 treatment. This is important for the clinical development of CX-5461, including any potential of combining it with immunotherapy with the aim to improve efficacy in patients. As outlined in Section 4.1.1, leukaemia cells can influence the surrounding microenvironment, including through preventing the normal immune response to the presence of cancer cells. Immunotherapy has shown astounding results in numerous cancers including through chimeric antigen receptor (CAR) T cells targeting CD-19 in large B cell lymphoma [356] and acute lymphoblastic leukaemia [357]. The most striking has been through blockade of programmed cell death protein 1 (PD-1)/programmed cell death ligand 1 (PD-L1), which mediates an immune checkpoint blockade, in advanced melanoma patients [358], which has opened up this field as viable therapies also in the treatment of AML [359]. Gemtuzumab ozogamicin, a CD33-targeted drug conjugate, is the only currently approved antibody-targeted therapy for AML [360], although others are in clinical development, including immune checkpoint inhibitors [361]. The human cell line xenograft models used in this thesis, could be used to evaluate the efficacy of CX-5461 in combination with immune checkpoint inhibitors including, for example, the THP-1 cell line which highly expresses programmed death receptor ligand 1 (PD-L1) [362]. Testing CX-5461 in combination with PD-1 inhibitors such as pembrolizumab [363] or

nivolumab [364], which are also in clinical trials for use in AML, would be rational choices to evaluate based on the results presented in this thesis.

6.3.2 Potential mechanisms of synergy not explored in this thesis

As outlined in Section 5.3.4 there are other potential mechanisms mediating the synergy between CX-5461 and chloroquine which were not assessed in this thesis. These involve the nucleolar stress response, DNA damage signalling, Pol I transcription inhibition and lysosomal effects. One or more of these mechanisms could also be contributing to the synergy observed between the two drugs, and thus may also reveal novel combination therapy strategies, thus warrant investigation.

6.4 Concluding statement

The results of this thesis support the well-established link between ribosome biogenesis and cellular metabolism within the cell, however importantly for the first time, it also demonstrates that targeting these two processes can effectively treat AML. Specifically, targeting mitochondrial function in combination with inhibition of ribosome biogenesis by CX-5461 is a novel therapeutic approach for AML. Critically, this combination was effective in AML, a model of aggressive disease that currently has limited therapeutic options in the clinic and thus has the potential to have a profound impact on patient care.

While the combination effect of CX-5461 and chloroquine observed *in vitro*, did not always translate well *in vivo* and toxicity issues were observed, the results in this thesis provide a solid platform and rationale to develop similar combinations with limited drug toxicity. This may be achieved by repurposing already clinically-approved metabolism-modifying drugs, such as metformin or tigecycline which directly target the mitochondria and have few side effects, in combination with CX-5461 as cancer therapeutics. Such results, if positive, also mean a more rapid translation of promising combination therapies to the clinic compared to unapproved drugs. Speeding up the process of translating research observations to the clinic from the traditional decades to just years, and would be highly beneficial to patients.

While in a number of cases significant inroads have been made into the treatment, and even cure, in many cancers there are still many where this is not the case. Indeed, for some cancers, the treatments have changed little for decades, such as AML. Thus, this work has provided an important insight into combinations to utilise with CX-5461 in cancer, but especially in an aggressive model of AML. After decades, there is promising data that may facilitate a novel approach to tackle this disease.

References

1   Hein, N. *et al.* Inhibition of Pol I transcription treats murine and human AML by targeting the leukemia-initiating cell population. *Blood* **129**, 2882-2895, doi:10.1182/blood-2016-05-718171 (2017).

2   Cancer Genome Atlas Research, N. *et al.* Genomic and epigenomic landscapes of adult de novo acute myeloid leukemia. *N Engl J Med* **368**, 2059-2074, doi:10.1056/NEJMoa1301689 (2013).

3   Frohling, S. *et al.* Prognostic significance of activating FLT3 mutations in younger adults (16 to 60 years) with acute myeloid leukemia and normal cytogenetics: a study of the AML Study Group Ulm. *Blood* **100**, 4372-4380, doi:10.1182/blood-2002-05-1440 (2002).

4   Kottaridis, P. D. *et al.* The presence of a FLT3 internal tandem duplication in patients with acute myeloid leukemia (AML) adds important prognostic information to cytogenetic risk group and response to the first cycle of chemotherapy: analysis of 854 patients from the United Kingdom Medical Research Council AML 10 and 12 trials. *Blood* **98**, 1752-1759 (2001).

5   Wang, M. L. & Bailey, N. G. Acute Myeloid Leukemia Genetics: Risk Stratification and Implications for Therapy. *Arch Pathol Lab Med* **139**, 1215-1223, doi:10.5858/arpa.2015-0203-RA (2015).

6   Papaemmanuil, E. *et al.* Genomic Classification and Prognosis in Acute Myeloid Leukemia. *N Engl J Med* **374**, 2209-2221, doi:10.1056/NEJMoa1516192 (2016).

7   WHO. World Health Organization Model List of Essential Medicines, 21st List. (World Health Organisation, Geneva, 2019).

8   Swerdlow, S. H. *et al. WHO Classification of Tumours of Haematopoietic and Lymphoid Tissues. 4th ed*. (IARC Press, 2008).

9   Smith, A., Howell, D., Patmore, R., Jack, A. & Roman, E. Incidence of haematological malignancy by sub-type: a report from the Haematological Malignancy Research Network. *British journal of cancer* **105**, 1684-1692, doi:10.1038/bjc.2011.450 (2011).

10   AIHW. Vol. Cancer Series no. 119 (ed AIHW) (AIHW, Canberra, 2019).

11   Juliusson, G. *et al.* Age and acute myeloid leukemia: real world data on decision to treat and outcomes from the Swedish Acute Leukemia Registry. *Blood* **113**, 4179-4187, doi:10.1182/blood-2008-07-172007 (2009).

12   Deschler, B. & Lubbert, M. Acute myeloid leukemia: epidemiology and etiology. *Cancer* **107**, 2099-2107, doi:10.1002/cncr.22233 (2006).

13   Metayer, C. *et al.* Tobacco smoke exposure and the risk of childhood acute lymphoblastic and myeloid leukemias by cytogenetic subtype. *Cancer Epidemiol Biomarkers Prev* **22**, 1600-1611, doi:10.1158/1055-9965.EPI-13-0350 (2013).

14   Mitelman, F. *et al.* Chromosome pattern, occupation, and clinical features in patients with acute nonlymphocytic leukemia. *Cancer Genet Cytogenet* **4**, 197-214 (1981).

15   Taylor, J. A. *et al.* ras oncogene activation and occupational exposures in acute myeloid leukemia. *J Natl Cancer Inst* **84**, 1626-1632, doi:10.1093/jnci/84.21.1626 (1992).

16   Kayser, S. *et al.* The impact of therapy-related acute myeloid leukemia (AML) on outcome in 2853 adult patients with newly diagnosed AML. *Blood* **117**, 2137-2145, doi:10.1182/blood-2010-08-301713 (2011).

17   Shi, J. *et al.* Transformation of myelodysplastic syndromes into acute myeloid leukemias. *Chin Med J (Engl)* **117**, 963-967 (2004).

18   Alexandrov, L. B. *et al.* Signatures of mutational processes in human cancer. *Nature* **500**, 415-421, doi:10.1038/nature12477 (2013).

19   Mrozek, K. *et al.* Prognostic significance of the European LeukemiaNet standardized system for reporting cytogenetic and molecular alterations in adults with acute myeloid leukemia. *J Clin Oncol* **30**, 4515-4523, doi:10.1200/JCO.2012.43.4738 (2012).

20   Verhaak, R. G. *et al.* Mutations in nucleophosmin (NPM1) in acute myeloid leukemia (AML): association with other gene abnormalities and previously established gene expression signatures and their favorable prognostic significance. *Blood* **106**, 3747-3754, doi:10.1182/blood-2005-05-2168 (2005).

21   Liu, Y. *et al.* Prognostic significance of NPM1 mutations in acute myeloid leukemia: A meta-analysis. *Mol Clin Oncol* **2**, 275-281, doi:10.3892/mco.2013.222 (2014).

22   Grimwade, D. *et al.* Refinement of cytogenetic classification in acute myeloid leukemia: determination of prognostic significance of rare recurring chromosomal abnormalities among 5876 younger adult patients treated in the United Kingdom Medical Research Council trials. *Blood* **116**, 354-365, doi:10.1182/blood-2009-11-254441 (2010).

23   Munoz, L. *et al.* Acute myeloid leukemia with MLL rearrangements: clinicobiological features, prognostic impact and value of flow cytometry in the detection of residual leukemic cells. *Leukemia* **17**, 76-82, doi:10.1038/sj.leu.2402708 (2003).

24   Meyer, C. *et al.* The MLL recombinome of acute leukemias in 2013. *Leukemia* **27**, 2165-2176, doi:10.1038/leu.2013.135 (2013).

25   Jansen, M. W., van der Velden, V. H. & van Dongen, J. J. Efficient and easy detection of MLL-AF4, MLL-AF9 and MLL-ENL fusion gene transcripts by multiplex real-time quantitative RT-PCR in TaqMan and LightCycler. *Leukemia* **19**, 2016-2018, doi:10.1038/sj.leu.2403939 (2005).

26   Grignani, F. *et al.* The acute promyelocytic leukemia-specific PML-RAR alpha fusion protein inhibits differentiation and promotes survival of myeloid precursor cells. *Cell* **74**, 423-431 (1993).

27   Gilliland, D. G. & Griffin, J. D. The roles of FLT3 in hematopoiesis and leukemia. *Blood* **100**, 1532-1542, doi:10.1182/blood-2002-02-0492 (2002).

28   Bennett, J. M. *et al.* Proposals for the classification of the acute leukaemias. French-American-British (FAB) co-operative group. *Br J Haematol* **33**, 451-458 (1976).

29   Castoldi, G. L., Liso, V., Fenu, S., Vegna, M. L. & Mandelli, F. Reproducibility of the morphological diagnostic criteria for acute myeloid leukemia: the GIMEMA group experience. *Ann Hematol* **66**, 171-174 (1993).

30   Head, D. R. *et al.* Reproducibility of the French-American-British classification of acute leukemia: the Southwest Oncology Group Experience. *Am J Hematol* **18**, 47-57 (1985).

31   Bairoch, A.   (Swiss Institute of Bioinformatics, Lausanne, Switzerland, 2019).

32   Zuber, J. *et al.* Mouse models of human AML accurately predict chemotherapy response. *Genes & development* **23**, 877-889, doi:10.1101/gad.1771409 (2009).

33   Saland, E. *et al.* A robust and rapid xenograft model to assess efficacy of chemotherapeutic agents for human acute myeloid leukemia. *Blood Cancer J* **5**, e297, doi:10.1038/bcj.2015.19 (2015).

34   Her, Z. *et al.* An improved pre-clinical patient-derived liquid xenograft mouse model for acute myeloid leukemia. *J Hematol Oncol* **10**, 162, doi:10.1186/s13045-017-0532-x (2017).

35   Dombret, H. & Gardin, C. An update of current treatments for adult acute myeloid leukemia. *Blood* **127**, 53-61, doi:10.1182/blood-2015-08-604520 (2016).

36   Lichtman, M. A. A historical perspective on the development of the cytarabine (7days) and daunorubicin (3days) treatment regimen for acute myelogenous leukemia: 2013 the 40th anniversary of 7+3. *Blood Cells Mol Dis* **50**, 119-130, doi:10.1016/j.bcmd.2012.10.005 (2013).

37   Kufe, D. W. & Major, P. P. Studies on the mechanism of action of cytosine arabinoside. *Med Pediatr Oncol* **10 Suppl 1**, 49-67 (1982).

38   Lieberman, M. W. *et al.* A probable role for protein synthesis in intestinal epithelial cell damage induced in vivo by cytosine arabinoside, nitrogen mustard, or X-irradiation. *Cancer research* **30**, 942-951 (1970).

39   Ritter, E. J., Scott, W. J. & Wilson, J. G. Teratogenesis and inhibition of DNA synthesis induced in rat embryos by cytosine arabinoside. *Teratology* **4**, 7-13, doi:10.1002/tera.1420040103 (1971).

40   Bodley, A. *et al.* DNA topoisomerase II-mediated interaction of doxorubicin and daunorubicin congeners with DNA. *Cancer research* **49**, 5969-5978 (1989).

41   Ustun, C., Lazarus, H. M. & Weisdorf, D. To transplant or not: a dilemma for treatment of elderly AML patients in the twenty-first century. *Bone Marrow Transplant* **48**, 1497-1505, doi:10.1038/bmt.2013.67 (2013).

42   O'Donnell, M. R. *et al.* Acute Myeloid Leukemia, Version 3.2017, NCCN Clinical Practice Guidelines in Oncology. *J Natl Compr Canc Netw* **15**, 926-957, doi:10.6004/jnccn.2017.0116 (2017).

43   Azevedo, M. C., Velloso, E. D., Buccheri, V., Chamone, D. A. & Dorlhiac-Llacer, P. E. Possible benefit of consolidation therapy with high-dose cytarabine on overall survival of adults with non-promyelocytic acute myeloid leukemia. *Braz J Med Biol Res* **48**, 178-185, doi:10.1590/1414-431X20144059 (2015).

44   Goldstone, A. H. *et al.* Attempts to improve treatment outcomes in acute myeloid leukemia (AML) in older patients: the results of the United Kingdom Medical Research Council AML11 trial. *Blood* **98**, 1302-1311 (2001).

45   Appelbaum, F. R. *et al.* Age and acute myeloid leukemia. *Blood* **107**, 3481-3485, doi:10.1182/blood-2005-09-3724 (2006).

46   Lancet, J. E. *et al.* Phase 2 trial of CPX-351, a fixed 5:1 molar ratio of cytarabine/daunorubicin, vs cytarabine/daunorubicin in older adults with untreated AML. *Blood* **123**, 3239-3246, doi:10.1182/blood-2013-12-540971 (2014).

47   Holowiecki, J. *et al.* Cladribine, but not fludarabine, added to daunorubicin and cytarabine during induction prolongs survival of patients with acute myeloid leukemia: a multicenter, randomized phase III study. *J Clin Oncol* **30**, 2441-2448, doi:10.1200/JCO.2011.37.1286 (2012).

48   Steinherz, L. J., Steinherz, P. G., Tan, C. T., Heller, G. & Murphy, M. L. Cardiac toxicity 4 to 20 years after completing anthracycline therapy. *JAMA* **266**, 1672-1677 (1991).

49   Slovak, M. L. *et al.* Karyotypic analysis predicts outcome of preremission and postremission therapy in adult acute myeloid leukemia: a Southwest Oncology Group/Eastern Cooperative Oncology Group Study. *Blood* **96**, 4075-4083 (2000).

50   Cornelissen, J. J. *et al.* The European LeukemiaNet AML Working Party consensus statement on allogeneic HSCT for patients with AML in remission: an integrated-risk adapted approach. *Nat Rev Clin Oncol* **9**, 579-590, doi:10.1038/nrclinonc.2012.150 (2012).

51   Sorror, M. L. & Estey, E. Allogeneic hematopoietic cell transplantation for acute myeloid leukemia in older adults. *Hematology Am Soc Hematol Educ Program* **2014**, 21-33, doi:10.1182/asheducation-2014.1.21 (2014).

52   Lipof, J. J., Loh, K. P., O'Dwyer, K. & Liesveld, J. L. Allogeneic Hematopoietic Cell Transplantation for Older Adults with Acute Myeloid Leukemia. *Cancers (Basel)* **10**, doi:10.3390/cancers10060179 (2018).

53   Sanz, M. A. *et al.* Risk-adapted treatment of acute promyelocytic leukemia based on all-trans retinoic acid and anthracycline with addition of cytarabine in consolidation therapy for high-risk patients: further improvements in treatment outcome. *Blood* **115**, 5137-5146, doi:10.1182/blood-2010-01-266007 (2010).

54   Ades, L. *et al.* Very long-term outcome of acute promyelocytic leukemia after treatment with all-trans retinoic acid and chemotherapy: the European APL Group experience. *Blood* **115**, 1690-1696, doi:10.1182/blood-2009-07-233387 (2010).

55   Tallman, M. S. *et al.* All-trans retinoic acid in acute promyelocytic leukemia: long-term outcome and prognostic factor analysis from the North American Intergroup protocol. *Blood* **100**, 4298-4302, doi:10.1182/blood-2002-02-0632 (2002).

56   Avvisati, G. *et al.* AIDA 0493 protocol for newly diagnosed acute promyelocytic leukemia: very long-term results and role of maintenance. *Blood* **117**, 4716-4725, doi:10.1182/blood-2010-08-302950 (2011).

57   Iland, H. J. *et al.* All-trans-retinoic acid, idarubicin, and IV arsenic trioxide as initial therapy in acute promyelocytic leukemia (APML4). *Blood* **120**, 1570-1580; quiz 1752, doi:10.1182/blood-2012-02-410746 (2012).

58   Lallemand-Breitenbach, V. *et al.* Retinoic acid and arsenic synergize to eradicate leukemic cells in a mouse model of acute promyelocytic leukemia. *J Exp Med* **189**, 1043-1052, doi:10.1084/jem.189.7.1043 (1999).

59   Hu, J. *et al.* Long-term efficacy and safety of all-trans retinoic acid/arsenic trioxide-based therapy in newly diagnosed acute promyelocytic leukemia. *Proc Natl Acad Sci U S A* **106**, 3342-3347, doi:10.1073/pnas.0813280106 (2009).

60   Daver, N., Schlenk, R. F., Russell, N. H. & Levis, M. J. Targeting FLT3 mutations in AML: review of current knowledge and evidence. *Leukemia* **33**, 299-312, doi:10.1038/s41375-018-0357-9 (2019).

61   McConkey, E. H. & Hopkins, J. W. The Relationship of the Nucleolus to the Synthesis of Ribosomal Rna in Hela Cells. *Proc Natl Acad Sci U S A* **51**, 1197-1204, doi:10.1073/pnas.51.6.1197 (1964).

62   Worton, R. G. *et al.* Human ribosomal RNA genes: orientation of the tandem array and conservation of the 5' end. *Science* **239**, 64-68 (1988).

63   Gonzalez, I. L. *et al.* Sequence and structure correlation of human ribosomal transcribed spacers. *J Mol Biol* **212**, 27-35, doi:10.1016/0022-2836(90)90302-3 (1990).

64   Erickson, J. M., Rushford, C. L., Dorney, D. J., Wilson, G. N. & Schmickel, R. D. Structure and variation of human ribosomal DNA: molecular analysis of cloned fragments. *Gene* **16**, 1-9 (1981).

65   Panov, K. I., Friedrich, J. K. & Zomerdijk, J. C. A step subsequent to preinitiation complex assembly at the ribosomal RNA gene promoter is rate limiting for human RNA polymerase I-dependent transcription. *Mol Cell Biol* **21**, 2641-2649, doi:10.1128/MCB.21.8.2641-2649.2001 (2001).

66   Comai, L., Tanese, N. & Tjian, R. The TATA-binding protein and associated factors are integral components of the RNA polymerase I transcription factor, SL1. *Cell* **68**, 965-976 (1992).

67   Miller, G. *et al.* hRRN3 is essential in the SL1-mediated recruitment of RNA Polymerase I to rRNA gene promoters. *EMBO J* **20**, 1373-1382, doi:10.1093/emboj/20.6.1373 (2001).

68   Ray, S. *et al.* Topoisomerase IIalpha promotes activation of RNA polymerase I transcription by facilitating pre-initiation complex formation. *Nat Commun* **4**, 1598, doi:10.1038/ncomms2599 (2013).

69   Hung, S. S. *et al.* Cell cycle and growth stimuli regulate different steps of RNA polymerase I transcription. *Gene* **612**, 36-48, doi:10.1016/j.gene.2016.12.015 (2017).

70   Henras, A. K., Plisson-Chastang, C., O'Donohue, M. F., Chakraborty, A. & Gleizes, P. E. An overview of pre-ribosomal RNA processing in eukaryotes. *Wiley Interdiscip Rev RNA* **6**, 225-242, doi:10.1002/wrna.1269 (2015).

71   Ciganda, M. & Williams, N. Eukaryotic 5S rRNA biogenesis. *Wiley Interdiscip Rev RNA* **2**, 523-533, doi:10.1002/wrna.74 (2011).

72   Xu, X., Xiong, X. & Sun, Y. The role of ribosomal proteins in the regulation of cell proliferation, tumorigenesis, and genomic integrity. *Sci China Life Sci* **59**, 656-672, doi:10.1007/s11427-016-0018-0 (2016).

73   Thomas, F. & Kutay, U. Biogenesis and nuclear export of ribosomal subunits in higher eukaryotes depend on the CRM1 export pathway. *J Cell Sci* **116**, 2409-2419, doi:10.1242/jcs.00464 (2003).

74   Thomas, G. An encore for ribosome biogenesis in the control of cell proliferation. *Nat Cell Biol* **2**, E71-72, doi:10.1038/35010581 (2000).

75   McDermott, P. J., Rothblum, L. I., Smith, S. D. & Morgan, H. E. Accelerated rates of ribosomal RNA synthesis during growth of contracting heart cells in culture. *J Biol Chem* **264**, 18220-18227 (1989).

76   Ruggero, D. & Pandolfi, P. P. Does the ribosome translate cancer? *Nature reviews. Cancer* **3**, 179-192, doi:10.1038/nrc1015 (2003).

77   Derenzini, M. *et al.* Nucleolar size indicates the rapidity of cell proliferation in cancer tissues. *The Journal of pathology* **191**, 181-186,

doi:10.1002/(SICI)1096-9896(200006)191:2<181::AID-PATH607>3.0.CO;2-V (2000).

78   Bywater, M. J. *et al.* Inhibition of RNA polymerase I as a therapeutic strategy to promote cancer-specific activation of p53. *Cancer cell* **22**, 51-65, doi:10.1016/j.ccr.2012.05.019 (2012).

79   Burger, K. *et al.* Chemotherapeutic drugs inhibit ribosome biogenesis at various levels. *J Biol Chem* **285**, 12416-12425, doi:10.1074/jbc.M109.074211 (2010).

80   Carter, R. & Drouin, G. Structural differentiation of the three eukaryotic RNA polymerases. *Genomics* **94**, 388-396, doi:10.1016/j.ygeno.2009.08.011 (2009).

81   Drygin, D. *et al.* Targeting RNA polymerase I with an oral small molecule CX-5461 inhibits ribosomal RNA synthesis and solid tumor growth. *Cancer research* **71**, 1418-1430, doi:10.1158/0008-5472.CAN-10-1728 (2011).

82   Khot, A. *et al.* First-in-Human RNA Polymerase I Transcription Inhibitor CX-5461 in Patients with Advanced Hematologic Cancers: Results of a Phase I Dose-Escalation Study. *Cancer Discov* **9**, 1036-1049, doi:10.1158/2159-8290.CD-18-1455 (2019).

83   Li, L. *et al.* CX-5461 induces autophagy and inhibits tumor growth via mammalian target of rapamycin-related signaling pathways in osteosarcoma. *Onco Targets Ther* **9**, 5985-5997, doi:10.2147/OTT.S104513 (2016).

84   Cornelison, R. *et al.* Targeting RNA-Polymerase I in Both Chemosensitive and Chemoresistant Populations in Epithelial Ovarian Cancer. *Clin Cancer Res* **23**, 6529-6540, doi:10.1158/1078-0432.CCR-17-0282 (2017).

85   Hilton, J. *et al.* CCTG IND.231: A phase 1 trial evaluating CX-5461 in patients with advanced solid tumors. *Annals of Oncology* **29** (2018).

86   Hanahan, D. & Weinberg, R. A. Hallmarks of cancer: the next generation. *Cell* **144**, 646-674, doi:10.1016/j.cell.2011.02.013 (2011).

87   Cairns, R. A., Harris, I. S. & Mak, T. W. Regulation of cancer cell metabolism. *Nature reviews. Cancer* **11**, 85-95, doi:10.1038/nrc2981 (2011).

88   Warburg, O. On the origin of cancer cells. *Science* **123**, 309-314 (1956).

89   Warburg, O., Wind, F. & Negelein, E. The Metabolism of Tumors in the Body. *J Gen Physiol* **8**, 519-530, doi:10.1085/jgp.8.6.519 (1927).

90   Vander Heiden, M. G., Cantley, L. C. & Thompson, C. B. Understanding the Warburg effect: the metabolic requirements of cell proliferation. *Science* **324**, 1029-1033, doi:10.1126/science.1160809 (2009).

91   Liberti, M. V. & Locasale, J. W. The Warburg Effect: How Does it Benefit Cancer Cells? *Trends Biochem Sci* **41**, 211-218, doi:10.1016/j.tibs.2015.12.001 (2016).

92   Sun, R. C. *et al.* Reversal of the glycolytic phenotype by dichloroacetate inhibits metastatic breast cancer cell growth in vitro and in vivo. *Breast cancer research and treatment* **120**, 253-260, doi:10.1007/s10549-009-0435-9 (2010).

93   Weinberg, S. E. & Chandel, N. S. Targeting mitochondria metabolism for cancer therapy. *Nat Chem Biol* **11**, 9-15, doi:10.1038/nchembio.1712 (2015).

94   Samudio, I. *et al.* Pharmacologic inhibition of fatty acid oxidation sensitizes human leukemia cells to apoptosis induction. *J Clin Invest* **120**, 142-156, doi:10.1172/JCI38942 (2010).

95   Jurczyszyn, A. *et al.* Plasma fatty acid profile in multiple myeloma patients. *Leuk Res* **39**, 400-405, doi:10.1016/j.leukres.2014.12.010 (2015).

96   Goto, M. *et al.* Importance of glutamine metabolism in leukemia cells by energy production through TCA cycle and by redox homeostasis. *Cancer Invest* **32**, 241-247, doi:10.3109/07357907.2014.907419 (2014).

97   Bajpai, R. *et al.* Targeting glutamine metabolism in multiple myeloma enhances BIM binding to BCL-2 eliciting synthetic lethality to venetoclax. *Oncogene*, doi:10.1038/onc.2015.464 (2015).

98   Kohnken, R., Kodigepalli, K. M. & Wu, L. Regulation of deoxynucleotide metabolism in cancer: novel mechanisms and therapeutic implications. *Molecular cancer* **14**, 176, doi:10.1186/s12943-015-0446-6 (2015).

99   Kong, Y. *et al.* Inhibition of cholesterol biosynthesis overcomes enzalutamide resistance in castration-resistant prostate cancer (CRPC). *J Biol Chem* **293**, 14328-14341, doi:10.1074/jbc.RA118.004442 (2018).

100   Li, H. Y., Appelbaum, F. R., Willman, C. L., Zager, R. A. & Banker, D. E. Cholesterol-modulating agents kill acute myeloid leukemia cells and sensitize them to therapeutics by blocking adaptive cholesterol responses. *Blood* **101**, 3628-3634, doi:10.1182/blood-2002-07-2283 (2003).

101   Mizushima, N., Yamamoto, A., Matsui, M., Yoshimori, T. & Ohsumi, Y. In vivo analysis of autophagy in response to nutrient starvation using transgenic mice expressing a fluorescent autophagosome marker. *Mol Biol Cell* **15**, 1101-1111, doi:10.1091/mbc.e03-09-0704 (2004).

102   Mathew, R. *et al.* Autophagy suppresses tumor progression by limiting chromosomal instability. *Genes & development* **21**, 1367-1381, doi:10.1101/gad.1545107 (2007).

103   Chan, S. M. *et al.* Isocitrate dehydrogenase 1 and 2 mutations induce BCL-2 dependence in acute myeloid leukemia. *Nat Med* **21**, 178-184, doi:10.1038/nm.3788 (2015).

104   Emadi, A. *et al.* Inhibition of glutaminase selectively suppresses the growth of primary acute myeloid leukemia cells with IDH mutations. *Exp Hematol* **42**, 247-251, doi:10.1016/j.exphem.2013.12.001 (2014).

105   Ni, F. *et al.* Critical role of ASCT2-mediated amino acid metabolism in promoting leukaemia development and progression. *Nature Metabolism* **1**, 390-403 (2019).

106   Skrtic, M. *et al.* Inhibition of mitochondrial translation as a therapeutic strategy for human acute myeloid leukemia. *Cancer cell* **20**, 674-688, doi:10.1016/j.ccr.2011.10.015 (2011).

107   Emadi, A. *et al.* Perturbation of cellular oxidative state induced by dichloroacetate and arsenic trioxide for treatment of acute myeloid leukemia. *Leuk Res* **39**, 719-729, doi:10.1016/j.leukres.2015.04.002 (2015).

108   Ju, H. Q. *et al.* ITD mutation in FLT3 tyrosine kinase promotes Warburg effect and renders therapeutic sensitivity to glycolytic inhibition. *Leukemia* **31**, 2143-2150, doi:10.1038/leu.2017.45 (2017).

109   Rudling, M., Gafvels, M., Parini, P., Gahrton, G. & Angelin, B. Lipoprotein receptors in acute myelogenous leukemia: failure to detect increased low-density lipoprotein (LDL) receptor numbers in cell membranes despite increased cellular LDL degradation. *Am J Pathol* **153**, 1923-1935, doi:10.1016/S0002-9440(10)65706-9 (1998).

110   Vitols, S., Norgren, S., Juliusson, G., Tatidis, L. & Luthman, H. Multilevel regulation of low-density lipoprotein receptor and 3-hydroxy-3-methylglutaryl coenzyme A reductase gene expression in normal and leukemic cells. *Blood* **84**, 2689-2698 (1994).

111   Redmann, M. *et al.* Inhibition of autophagy with bafilomycin and chloroquine decreases mitochondrial quality and bioenergetic function in primary neurons. *Redox Biol* **11**, 73-81, doi:10.1016/j.redox.2016.11.004 (2017).

112   Scherz-Shouval, R. *et al.* Reactive oxygen species are essential for autophagy and specifically regulate the activity of Atg4. *EMBO J* **26**, 1749-1760, doi:10.1038/sj.emboj.7601623 (2007).

113   Mathew, R. *et al.* Autophagy suppresses tumorigenesis through elimination of p62. *Cell* **137**, 1062-1075, doi:10.1016/j.cell.2009.03.048 (2009).

114   Watson, A. S. *et al.* Autophagy limits proliferation and glycolytic metabolism in acute myeloid leukemia. *Cell Death Discov* **1**, doi:10.1038/cddiscovery.2015.8 (2015).

115   Sumitomo, Y. *et al.* Cytoprotective autophagy maintains leukemia-initiating cells in murine myeloid leukemia. *Blood* **128**, 1614-1624, doi:10.1182/blood-2015-12-684696 (2016).

116   Tabe, Y. *et al.* Bone Marrow Adipocytes Facilitate Fatty Acid Oxidation Activating AMPK and a Transcriptional Network Supporting Survival of

Acute Monocytic Leukemia Cells. *Cancer research* **77**, 1453-1464, doi:10.1158/0008-5472.CAN-16-1645 (2017).

117   Jiang, C. *et al.* Upregulation of CASC2 sensitized glioma to temozolomide cytotoxicity through autophagy inhibition by sponging miR-193a-5p and regulating mTOR expression. *Biomed Pharmacother* **97**, 844-850, doi:10.1016/j.biopha.2017.10.146 (2018).

118   Farge, T. *et al.* Chemotherapy-Resistant Human Acute Myeloid Leukemia Cells Are Not Enriched for Leukemic Stem Cells but Require Oxidative Metabolism. *Cancer Discov* **7**, 716-735, doi:10.1158/2159-8290.CD-16-0441 (2017).

119   Kridel, S. J., Axelrod, F., Rozenkrantz, N. & Smith, J. W. Orlistat is a novel inhibitor of fatty acid synthase with antitumor activity. *Cancer research* **64**, 2070-2075 (2004).

120   Repetto, G., del Peso, A. & Zurita, J. L. Neutral red uptake assay for the estimation of cell viability/cytotoxicity. *Nat Protoc* **3**, 1125-1131, doi:10.1038/nprot.2008.75 (2008).

121   Riss, T. L. *et al.* in *Assay Guidance Manual*   (eds G. S. Sittampalam *et al.*) (2004).

122   Chou, T. C. Drug combination studies and their synergy quantification using the Chou-Talalay method. *Cancer research* **70**, 440-446, doi:10.1158/0008-5472.CAN-09-1947 (2010).

123   Chou, T. C. Theoretical basis, experimental design, and computerized simulation of synergism and antagonism in drug combination studies. *Pharmacol Rev* **58**, 621-681, doi:10.1124/pr.58.3.10 (2006).

124   Kajstura, M., Halicka, H. D., Pryjma, J. & Darzynkiewicz, Z. Discontinuous fragmentation of nuclear DNA during apoptosis revealed by discrete "sub-G1" peaks on DNA content histograms. *Cytometry A* **71**, 125-131, doi:10.1002/cyto.a.20357 (2007).

125   DiMasi, J. A., Grabowski, H. G. & Hansen, R. W. The cost of drug development. *N Engl J Med* **372**, 1972, doi:10.1056/NEJMc1504317 (2015).

126   Stacpoole, P. W., Harman, E. M., Curry, S. H., Baumgartner, T. G. & Misbin, R. I. Treatment of lactic acidosis with dichloroacetate. *N Engl J Med* **309**, 390-396, doi:10.1056/NEJM198308183090702 (1983).

127   Bonnet, S. *et al.* A mitochondria-K+ channel axis is suppressed in cancer and its normalization promotes apoptosis and inhibits cancer growth. *Cancer cell* **11**, 37-51, doi:10.1016/j.ccr.2006.10.020 (2007).

128   Sun, R. C., Board, P. G. & Blackburn, A. C. Targeting metabolism with arsenic trioxide and dichloroacetate in breast cancer cells. *Molecular cancer* **10**, 142, doi:10.1186/1476-4598-10-142 (2011).

129   Gang, B. P., Dilda, P. J., Hogg, P. J. & Blackburn, A. C. Targeting of two aspects of metabolism in breast cancer treatment. *Cancer biology & therapy* **15**, 1533-1541, doi:10.4161/15384047.2014.955992 (2014).

130   Agnoletto, C. *et al.* Sodium dichloroacetate exhibits anti-leukemic activity in B-chronic lymphocytic leukemia (B-CLL) and synergizes with the p53 activator Nutlin-3. *Oncotarget* **5**, 4347-4360, doi:10.18632/oncotarget.2018 (2014).

131   Zhou, G. *et al.* Role of AMP-activated protein kinase in mechanism of metformin action. *J Clin Invest* **108**, 1167-1174, doi:10.1172/JCI13505 (2001).

132   El-Mir, M. Y. *et al.* Dimethylbiguanide inhibits cell respiration via an indirect effect targeted on the respiratory chain complex I. *J Biol Chem* **275**, 223-228 (2000).

133   Evans, J. M., Donnelly, L. A., Emslie-Smith, A. M., Alessi, D. R. & Morris, A. D. Metformin and reduced risk of cancer in diabetic patients. *BMJ* **330**, 1304-1305, doi:10.1136/bmj.38415.708634.F7 (2005).

134   Scotland, S. *et al.* Mitochondrial energetic and AKT status mediate metabolic effects and apoptosis of metformin in human leukemic cells. *Leukemia* **27**, 2129-2138, doi:10.1038/leu.2013.107 (2013).

135   Zi, F. M. *et al.* Metformin displays anti-myeloma activity and synergistic effect with dexamethasone in in vitro and in vivo xenograft models. *Cancer Lett* **356**, 443-453, doi:10.1016/j.canlet.2014.09.050 (2015).

136   Shank, J. J. *et al.* Metformin targets ovarian cancer stem cells in vitro and in vivo. *Gynecol Oncol* **127**, 390-397, doi:10.1016/j.ygyno.2012.07.115 (2012).

137   Kumar, A., Al-Sammarraie, N., DiPette, D. J. & Singh, U. S. Metformin impairs Rho GTPase signaling to induce apoptosis in neuroblastoma cells and inhibits growth of tumors in the xenograft mouse model of neuroblastoma. *Oncotarget* **5**, 11709-11722, doi:10.18632/oncotarget.2606 (2014).

138   Chou, A. C. & Fitch, C. D. Control of heme polymerase by chloroquine and other quinoline derivatives. *Biochem Biophys Res Commun* **195**, 422-427, doi:10.1006/bbrc.1993.2060 (1993).

139   Popert, A. J., Meijers, K. A., Sharp, J. & Bier, F. Chloroquine diphosphate in rheumatoid arthritis. A controlled trial. *Ann Rheum Dis* **20**, 18-35 (1961).

140   van den Borne, B. E., Dijkmans, B. A., de Rooij, H. H., le Cessie, S. & Verweij, C. L. Chloroquine and hydroxychloroquine equally affect tumor necrosis factor-alpha, interleukin 6, and interferon-gamma production by peripheral blood mononuclear cells. *J Rheumatol* **24**, 55-60 (1997).

141   Kyburz, D., Brentano, F. & Gay, S. Mode of action of hydroxychloroquine in RA-evidence of an inhibitory effect on toll-like receptor signaling. *Nat Clin Pract Rheumatol* **2**, 458-459, doi:10.1038/ncprheum0292 (2006).

142   Bedoya, V. Effect of chloroquine on malignant lymphoreticular and pigmented cells in vitro. *Cancer research* **30**, 1262-1275 (1970).

143   Murakami, N. *et al.* Accumulation of tau in autophagic vacuoles in chloroquine myopathy. *J Neuropathol Exp Neurol* **57**, 664-673 (1998).

144   Hu, T. *et al.* Chloroquine inhibits hepatocellular carcinoma cell growth in vitro and in vivo. *Oncol Rep* **35**, 43-49, doi:10.3892/or.2015.4380 (2016).

145   Jiang, P. D. *et al.* Antitumor and antimetastatic activities of chloroquine diphosphate in a murine model of breast cancer. *Biomed Pharmacother* **64**, 609-614, doi:10.1016/j.biopha.2010.06.004 (2010).

146   Liang, D. H. *et al.* The autophagy inhibitor chloroquine targets cancer stem cells in triple negative breast cancer by inducing mitochondrial damage and impairing DNA break repair. *Cancer Lett* **376**, 249-258, doi:10.1016/j.canlet.2016.04.002 (2016).

147   Liu, S. *et al.* Chloroquine exerts antitumor effects on NB4 acute promyelocytic leukemia cells and functions synergistically with arsenic trioxide. *Oncol Lett* **15**, 2024-2030, doi:10.3892/ol.2017.7488 (2018).

148   Heck, A. M., Yanovski, J. A. & Calis, K. A. Orlistat, a new lipase inhibitor for the management of obesity. *Pharmacotherapy* **20**, 270-279 (2000).

149   Pallasch, C. P. *et al.* Targeting lipid metabolism by the lipoprotein lipase inhibitor orlistat results in apoptosis of B-cell chronic lymphocytic leukemia cells. *Leukemia* **22**, 585-592, doi:10.1038/sj.leu.2405058 (2008).

150   Tirado-Velez, J. M., Joumady, I., Saez-Benito, A., Cozar-Castellano, I. & Perdomo, G. Inhibition of fatty acid metabolism reduces human myeloma cells proliferation. *PLoS One* **7**, e46484, doi:10.1371/journal.pone.0046484 (2012).

151   Zhi, J., Mulligan, T. E. & Hauptman, J. B. Long-term systemic exposure of orlistat, a lipase inhibitor, and its metabolites in obese patients. *J Clin Pharmacol* **39**, 41-46 (1999).

152   Fako, V. E., Wu, X., Pflug, B., Liu, J. Y. & Zhang, J. T. Repositioning proton pump inhibitors as anticancer drugs by targeting the thioesterase domain of human fatty acid synthase. *J Med Chem* **58**, 778-784, doi:10.1021/jm501543u (2015).

153   Wallmark, B., Lorentzon, P. & Larsson, H. The mechanism of action of omeprazole--a survey of its inhibitory actions in vitro. *Scand J Gastroenterol Suppl* **108**, 37-51 (1985).

154   Udelnow, A. *et al.* Omeprazole inhibits proliferation and modulates autophagy in pancreatic cancer cells. *PLoS One* **6**, e20143, doi:10.1371/journal.pone.0020143 (2011).

155   Jin, U. H., Lee, S. O., Pfent, C. & Safe, S. The aryl hydrocarbon receptor ligand omeprazole inhibits breast cancer cell invasion and metastasis. *BMC Cancer* **14**, 498, doi:10.1186/1471-2407-14-498 (2014).

156   Kempf, D. J. *et al.* ABT-538 is a potent inhibitor of human immunodeficiency virus protease and has high oral bioavailability in humans. *Proc Natl Acad Sci U S A* **92**, 2484-2488 (1995).

157   Hull, M. W. & Montaner, J. S. Ritonavir-boosted protease inhibitors in HIV therapy. *Ann Med* **43**, 375-388, doi:10.3109/07853890.2011.572905 (2011).

158   Murata, H., Hruz, P. W. & Mueckler, M. The mechanism of insulin resistance caused by HIV protease inhibitor therapy. *J Biol Chem* **275**, 20251-20254, doi:10.1074/jbc.C000228200 (2000).

159   Dalva-Aydemir, S. *et al.* Targeting the metabolic plasticity of multiple myeloma with FDA-approved ritonavir and metformin. *Clin Cancer Res* **21**, 1161-1171, doi:10.1158/1078-0432.CCR-14-1088 (2015).

160   Adekola, K. U. *et al.* Investigating and targeting chronic lymphocytic leukemia metabolism with the human immunodeficiency virus protease inhibitor ritonavir and metformin. *Leuk Lymphoma* **56**, 450-459, doi:10.3109/10428194.2014.922180 (2015).

161   Goldstein, J. L. & Brown, M. S. Regulation of the mevalonate pathway. *Nature* **343**, 425-430, doi:10.1038/343425a0 (1990).

162   Lishner, M., Bar-Sef, A., Elis, A. & Fabian, I. Effect of simvastatin alone and in combination with cytosine arabinoside on the proliferation of myeloid leukemia cell lines. *J Investig Med* **49**, 319-324, doi:10.2310/6650.2001.33896 (2001).

163   Gronich, N. *et al.* Simvastatin induces death of multiple myeloma cell lines. *J Investig Med* **52**, 335-344 (2004).

164   Wang, T. *et al.* Simvastatin-induced breast cancer cell death and deactivation of PI3K/Akt and MAPK/ERK signalling are reversed by metabolic products of the mevalonate pathway. *Oncotarget* **7**, 2532-2544, doi:10.18632/oncotarget.6304 (2016).

165   Staels, B. *et al.* Mechanism of action of fibrates on lipid and lipoprotein metabolism. *Circulation* **98**, 2088-2093 (1998).

166   Li, T. *et al.* Fenofibrate induces apoptosis of triple-negative breast cancer cells via activation of NF-kappaB pathway. *BMC Cancer* **14**, 96, doi:10.1186/1471-2407-14-96 (2014).

167   Zak, Z., Gelebart, P. & Lai, R. Fenofibrate induces effective apoptosis in mantle cell lymphoma by inhibiting the TNFalpha/NF-kappaB signaling axis. *Leukemia* **24**, 1476-1486, doi:10.1038/leu.2010.117 (2010).

168   Liu, X. *et al.* Expression Profiling Identifies Bezafibrate as Potential Therapeutic Drug for Lung Adenocarcinoma. *J Cancer* **6**, 1214-1221, doi:10.7150/jca.12191 (2015).

169   Prost, S. *et al.* Erosion of the chronic myeloid leukaemia stem cell pool by PPARgamma agonists. *Nature* **525**, 380-383, doi:10.1038/nature15248 (2015).

170   Girnun, G. D. *et al.* Regression of drug-resistant lung cancer by the combination of rosiglitazone and carboplatin. *Clin Cancer Res* **14**, 6478-6486, doi:10.1158/1078-0432.CCR-08-1128 (2008).

171   Hoppe, S. *et al.* AMP-activated protein kinase adapts rRNA synthesis to cellular energy supply. *Proc Natl Acad Sci U S A* **106**, 17781-17786, doi:10.1073/pnas.0909873106 (2009).

172   Tanaka, Y., Konishi, A., Obinata, H. & Tsuneoka, M. Metformin activates KDM2A to reduce rRNA transcription and cell proliferation by dual regulation of AMPK activity and intracellular succinate level. *Sci Rep* **9**, 18694, doi:10.1038/s41598-019-55075-0 (2019).

173   Yilmaz, S. *et al.* Investigation of low-dose ritonavir on human peripheral blood mononuclear cells using gene expression whole genome microarrays. *Genomics* **96**, 57-65, doi:10.1016/j.ygeno.2010.03.011 (2010).

174   Dai, M. S. & Lu, H. Crosstalk between c-Myc and ribosome in ribosomal biogenesis and cancer. *J Cell Biochem* **105**, 670-677, doi:10.1002/jcb.21895 (2008).

175   Costa-Rodrigues, J., Reis, S., Teixeira, S., Lopes, S. & Fernandes, M. H. Dose-dependent inhibitory effects of proton pump inhibitors on human osteoclastic and osteoblastic cell activity. *FEBS J* **280**, 5052-5064, doi:10.1111/febs.12478 (2013).

176   Krajewski, W. A. Alterations in the internucleosomal DNA helical twist in chromatin of human erythroleukemia cells in vivo influences the chromatin higher-order folding. *FEBS Lett* **361**, 149-152 (1995).

177   Stacpoole, P. W., Henderson, G. N., Yan, Z. & James, M. O. Clinical pharmacology and toxicology of dichloroacetate. *Environ Health Perspect* **106 Suppl 4**, 989-994, doi:10.1289/ehp.98106s4989 (1998).

178   Kajbaf, F., De Broe, M. E. & Lalau, J. D. Therapeutic Concentrations of Metformin: A Systematic Review. *Clin Pharmacokinet* **55**, 439-459, doi:10.1007/s40262-015-0323-x (2016).

179   Lee, S. J. *et al.* Chloroquine pharmacokinetics in pregnant and nonpregnant women with vivax malaria. *Eur J Clin Pharmacol* **64**, 987-992, doi:10.1007/s00228-008-0500-z (2008).

180   Moore, B. R. *et al.* Pharmacokinetics, pharmacodynamics, and allometric scaling of chloroquine in a murine malaria model. *Antimicrob Agents Chemother* **55**, 3899-3907, doi:10.1128/AAC.00067-11 (2011).

181   Klionsky, D. J. *et al.* Guidelines for the use and interpretation of assays for monitoring autophagy (3rd edition). *Autophagy* **12**, 1-222, doi:10.1080/15548627.2015.1100356 (2016).

182   Gatti, G. *et al.* The relationship between ritonavir plasma levels and side-effects: implications for therapeutic drug monitoring. *AIDS* **13**, 2083-2089 (1999).

183   Kim, J. *et al.* A population pharmacokinetic-pharmacodynamic model for simvastatin that predicts low-density lipoprotein-cholesterol reduction in patients with primary hyperlipidaemia. *Basic Clin Pharmacol Toxicol* **109**, 156-163, doi:10.1111/j.1742-7843.2011.00700.x (2011).

184   Balfour, J. A., McTavish, D. & Heel, R. C. Fenofibrate. A review of its pharmacodynamic and pharmacokinetic properties and therapeutic use in dyslipidaemia. *Drugs* **40**, 260-290, doi:10.2165/00003495-199040020-00007 (1990).

185   Braeckman, R. A., Stirtan, W. G. & Soni, P. N. Effects of Icosapent Ethyl (Eicosapentaenoic Acid Ethyl Ester) on Pharmacokinetic Parameters of Rosiglitazone in Healthy Subjects. *Clin Pharmacol Drug Dev* **4**, 143-148, doi:10.1002/cpdd.150 (2015).

186   Roell, K. R., Reif, D. M. & Motsinger-Reif, A. A. An Introduction to Terminology and Methodology of Chemical Synergy-Perspectives from Across Disciplines. *Front Pharmacol* **8**, 158, doi:10.3389/fphar.2017.00158 (2017).

187   Vilimanovich, U. *et al.* Statin-mediated inhibition of cholesterol synthesis induces cytoprotective autophagy in human leukemic cells. *Eur J Pharmacol* **765**, 415-428, doi:10.1016/j.ejphar.2015.09.004 (2015).

188   Nazim, U. M. *et al.* Activation of autophagy flux by metformin downregulates cellular FLICE-like inhibitory protein and enhances TRAIL- induced apoptosis. *Oncotarget* **7**, 23468-23481, doi:10.18632/oncotarget.8048 (2016).

189   Feng, Y. *et al.* Metformin promotes autophagy and apoptosis in esophageal squamous cell carcinoma by downregulating Stat3 signaling. *Cell death & disease* **5**, e1088, doi:10.1038/cddis.2014.59 (2014).

190   Andrzejewski, S., Gravel, S. P., Pollak, M. & St-Pierre, J. Metformin directly acts on mitochondria to alter cellular bioenergetics. *Cancer Metab* **2**, 12, doi:10.1186/2049-3002-2-12 (2014).

191   Bridges, H. R., Jones, A. J., Pollak, M. N. & Hirst, J. Effects of metformin and other biguanides on oxidative phosphorylation in mitochondria. *Biochem J* **462**, 475-487, doi:10.1042/BJ20140620 (2014).

192   Schirris, T. J. *et al.* Statin-Induced Myopathy Is Associated with Mitochondrial Complex III Inhibition. *Cell Metab* **22**, 399-407, doi:10.1016/j.cmet.2015.08.002 (2015).

193   Morrison, S. J. & Scadden, D. T. The bone marrow niche for haematopoietic stem cells. *Nature* **505**, 327-334, doi:10.1038/nature12984 (2014).

194   Manesso, E., Teles, J., Bryder, D. & Peterson, C. Dynamical modelling of haematopoiesis: an integrated view over the system in homeostasis and under perturbation. *J R Soc Interface* **10**, 20120817, doi:10.1098/rsif.2012.0817 (2013).

195   Shlush, L. I. *et al.* Tracing the origins of relapse in acute myeloid leukaemia to stem cells. *Nature* **547**, 104-108, doi:10.1038/nature22993 (2017).

196   Shafat, M. S. *et al.* Leukemic blasts program bone marrow adipocytes to generate a protumoral microenvironment. *Blood* **129**, 1320-1332, doi:10.1182/blood-2016-08-734798 (2017).

197   Hong, C. S. *et al.* Circulating exosomes carrying an immunosuppressive cargo interfere with cellular immunotherapy in acute myeloid leukemia. *Sci Rep* **7**, 14684, doi:10.1038/s41598-017-14661-w (2017).

198   Kumar, B. *et al.* Acute myeloid leukemia transforms the bone marrow niche into a leukemia-permissive microenvironment through exosome secretion. *Leukemia* **32**, 575-587, doi:10.1038/leu.2017.259 (2018).

199   Brenner, A. K., Nepstad, I. & Bruserud, O. Mesenchymal Stem Cells Support Survival and Proliferation of Primary Human Acute Myeloid Leukemia Cells through Heterogeneous Molecular Mechanisms. *Front Immunol* **8**, 106, doi:10.3389/fimmu.2017.00106 (2017).

200   Zhai, Y. *et al.* Growth differentiation factor 15 contributes to cancer-associated fibroblasts-mediated chemo-protection of AML cells. *J Exp Clin Cancer Res* **35**, 147, doi:10.1186/s13046-016-0405-0 (2016).

201   Sinyuk, M. *et al.* Cx25 contributes to leukemia cell communication and chemosensitivity. *Oncotarget* **6**, 31508-31521, doi:10.18632/oncotarget.5226 (2015).

202   Jacamo, R. *et al.* Reciprocal leukemia-stroma VCAM-1/VLA-4-dependent activation of NF-kappaB mediates chemoresistance. *Blood* **123**, 2691-2702, doi:10.1182/blood-2013-06-511527 (2014).

203   Calvi, L. M. & Link, D. C. Cellular complexity of the bone marrow hematopoietic stem cell niche. *Calcif Tissue Int* **94**, 112-124, doi:10.1007/s00223-013-9805-8 (2014).

204   Ito, M. *et al.* NOD/SCID/gamma(c)(null) mouse: an excellent recipient mouse model for engraftment of human cells. *Blood* **100**, 3175-3182, doi:10.1182/blood-2001-12-0207 (2002).

205   Zhang, C. C. *et al.* Gemtuzumab Ozogamicin (GO) Inclusion to Induction Chemotherapy Eliminates Leukemic Initiating Cells and Significantly Improves Survival in Mouse Models of Acute Myeloid Leukemia. *Neoplasia* **20**, 1-11, doi:10.1016/j.neo.2017.10.008 (2018).

206   Keegan, K. *et al.* Preclinical evaluation of AMG 925, a FLT3/CDK4 dual kinase inhibitor for treating acute myeloid leukemia. *Mol Cancer Ther* **13**, 880-889, doi:10.1158/1535-7163.MCT-13-0858 (2014).

207   Gritsman, K. *et al.* Hematopoiesis and RAS-driven myeloid leukemia differentially require PI3K isoform p110alpha. *J Clin Invest* **124**, 1794-1809, doi:10.1172/JCI69927 (2014).

208   Tarighat, S. S. *et al.* The dual epigenetic role of PRMT5 in acute myeloid leukemia: gene activation and repression via histone arginine methylation. *Leukemia* **30**, 789-799, doi:10.1038/leu.2015.308 (2016).

209   Mitchell, K. *et al.* IL1RAP potentiates multiple oncogenic signaling pathways in AML. *J Exp Med* **215**, 1709-1727, doi:10.1084/jem.20180147 (2018).

210   O'Farrell, A. M. *et al.* SU11248 is a novel FLT3 tyrosine kinase inhibitor with potent activity in vitro and in vivo. *Blood* **101**, 3597-3605, doi:10.1182/blood-2002-07-2307 (2003).

211   Woessner, R. *et al.* ARRY-520, a novel KSP inhibitor with potent activity in hematological and taxane-resistant tumor models. *Anticancer Res* **29**, 4373-4380 (2009).

212   Gozgit, J. M. *et al.* Potent activity of ponatinib (AP24534) in models of FLT3-driven acute myeloid leukemia and other hematologic malignancies. *Mol Cancer Ther* **10**, 1028-1035, doi:10.1158/1535-7163.MCT-10-1044 (2011).

213   Moore, A. S. *et al.* Selective FLT3 inhibition of FLT3-ITD+ acute myeloid leukaemia resulting in secondary D835Y mutation: a model for emerging clinical resistance patterns. *Leukemia* **26**, 1462-1470, doi:10.1038/leu.2012.52 (2012).

214   Rudolph, D. *et al.* Efficacy and mechanism of action of volasertib, a potent and selective inhibitor of Polo-like kinases, in preclinical models of acute myeloid leukemia. *J Pharmacol Exp Ther* **352**, 579-589, doi:10.1124/jpet.114.221150 (2015).

215   Chiu, C. F. *et al.* T315 Decreases Acute Myeloid Leukemia Cell Viability through a Combination of Apoptosis Induction and Autophagic Cell Death. *Int J Mol Sci* **17**, doi:10.3390/ijms17081337 (2016).

216   Hickey, C. J. *et al.* Lenalidomide-mediated enhanced translation of C/EBPalpha-p30 protein up-regulates expression of the antileukemic microRNA-181a in acute myeloid leukemia. *Blood* **121**, 159-169, doi:10.1182/blood-2012-05-428573 (2013).

217   Edinger, M. *et al.* Advancing animal models of neoplasia through in vivo bioluminescence imaging. *Eur J Cancer* **38**, 2128-2136 (2002).

218   Maes, H. *et al.* Tumor vessel normalization by chloroquine independent of autophagy. *Cancer cell* **26**, 190-206, doi:10.1016/j.ccr.2014.06.025 (2014).

219 Liu, F., Shang, Y. & Chen, S. Z. Chloroquine potentiates the anti-cancer effect of lidamycin on non-small cell lung cancer cells in vitro. *Acta Pharmacol Sin* **35**, 645-652, doi:10.1038/aps.2014.3 (2014).

220 Tuomela, J. *et al.* Chloroquine has tumor-inhibitory and tumor-promoting effects in triple-negative breast cancer. *Oncol Lett* **6**, 1665-1672, doi:10.3892/ol.2013.1602 (2013).

221 Walum, E. Acute oral toxicity. *Environ Health Perspect* **106 Suppl 2**, 497-503, doi:10.1289/ehp.98106497 (1998).

222 Luciani, F. *et al.* Effect of proton pump inhibitor pretreatment on resistance of solid tumors to cytotoxic drugs. *J Natl Cancer Inst* **96**, 1702-1713, doi:10.1093/jnci/djh305 (2004).

223 Ekman, L., Hansson, E., Havu, N., Carlsson, E. & Lundberg, C. Toxicological studies on omeprazole. *Scand J Gastroenterol Suppl* **108**, 53-69 (1985).

224 Srirangam, A. *et al.* Effects of HIV protease inhibitor ritonavir on Akt-regulated cell proliferation in breast cancer. *Clin Cancer Res* **12**, 1883-1896, doi:10.1158/1078-0432.CCR-05-1167 (2006).

225 Pati, S. *et al.* Antitumorigenic effects of HIV protease inhibitor ritonavir: inhibition of Kaposi sarcoma. *Blood* **99**, 3771-3779 (2002).

226 Capsules, S.   (2015).

227 Green, D. E. & Rubin, C. T. Consequences of irradiation on bone and marrow phenotypes, and its relation to disruption of hematopoietic precursors. *Bone* **63**, 87-94, doi:10.1016/j.bone.2014.02.018 (2014).

228 Frasca, D. *et al.* Hematopoietic reconstitution after lethal irradiation and bone marrow transplantation: effects of different hematopoietic cytokines on the recovery of thymus, spleen and blood cells. *Bone Marrow Transplant* **25**, 427-433, doi:10.1038/sj.bmt.1702169 (2000).

229 Andersen, J. *et al.* Differential effect of conditioning regimens on cytokine responses during allogeneic stem cell transplantation. *Bone Marrow Transplant* **37**, 635-640, doi:10.1038/sj.bmt.1705295 (2006).

230 Wrzesinski, C. *et al.* Increased intensity lymphodepletion enhances tumor treatment efficacy of adoptively transferred tumor-specific T cells. *J Immunother* **33**, 1-7, doi:10.1097/CJI.0b013e3181b88ffc (2010).

231 Fazzina, R. *et al.* Generation and characterization of bioluminescent xenograft mouse models of MLL-related acute leukemias and in vivo evaluation of luciferase-targeting siRNA nanoparticles. *Int J Oncol* **41**, 621-628, doi:10.3892/ijo.2012.1504 (2012).

232 Lohrberg, M. & Wilting, J. The lymphatic vascular system of the mouse head. *Cell Tissue Res* **366**, 667-677, doi:10.1007/s00441-016-2493-8 (2016).

233   Kelland, L. R. Of mice and men: values and liabilities of the athymic nude mouse model in anticancer drug development. *Eur J Cancer* **40**, 827-836, doi:10.1016/j.ejca.2003.11.028 (2004).

234   Karjalainen, R. *et al.* JAK1/2 and BCL2 inhibitors synergize to counteract bone marrow stromal cell-induced protection of AML. *Blood* **130**, 789-802, doi:10.1182/blood-2016-02-699363 (2017).

235   Liu, X. & Jia, L. The conduct of drug metabolism studies considered good practice (I): analytical systems and in vivo studies. *Curr Drug Metab* **8**, 815-821 (2007).

236   Palleria, C. *et al.* Pharmacokinetic drug-drug interaction and their implication in clinical management. *J Res Med Sci* **18**, 601-610 (2013).

237   Floch, M. H. Bile salts, intestinal microflora and enterohepatic circulation. *Dig Liver Dis* **34 Suppl 2**, S54-57, doi:10.1016/s1590-8658(02)80165-7 (2002).

238   Adedoyin, A., Frye, R. F., Mauro, K. & Branch, R. A. Chloroquine modulation of specific metabolizing enzymes activities: investigation with selective five drug cocktail. *Br J Clin Pharmacol* **46**, 215-219, doi:10.1046/j.1365-2125.1998.00765.x (1998).

239   Kim, K. A., Park, J. Y., Lee, J. S. & Lim, S. Cytochrome P450 2C8 and CYP3A4/5 are involved in chloroquine metabolism in human liver microsomes. *Arch Pharm Res* **26**, 631-637, doi:10.1007/bf02976712 (2003).

240   Alakel, N. *et al.* Symptomatic central nervous system involvement in adult patients with acute myeloid leukemia. *Cancer Manag Res* **9**, 97-102, doi:10.2147/CMAR.S125259 (2017).

241   Abbott, B. L. *et al.* Clinical significance of central nervous system involvement at diagnosis of pediatric acute myeloid leukemia: a single institution's experience. *Leukemia* **17**, 2090-2096, doi:10.1038/sj.leu.2403131 (2003).

242   Webb, D. K. *et al.* Relationships between age at diagnosis, clinical features, and outcome of therapy in children treated in the Medical Research Council AML 10 and 12 trials for acute myeloid leukemia. *Blood* **98**, 1714-1720 (2001).

243   Asano, K., Wakabayashi, H., Kikuchi, N. & Sashika, H. Acute myeloid leukemia presenting with complete paraplegia and bilateral total blindness due to central nervous system involvement. *Spinal Cord Ser Cases* **2**, 15035, doi:10.1038/scsandc.2015.35 (2016).

244   Kyaw, T. Z. *et al.* Myeloid sarcoma: an unusual presentation of acute promyelocytic leukemia causing spinal cord compression. *Turk J Haematol* **29**, 278-282, doi:10.5505/tjh.2012.94809 (2012).

245   Ganzel, C. *et al.* Extramedullary Disease in Adult Acute Myeloid Leukemia Is Common but Lacks Independent Significance: Analysis of Patients in ECOG-

ACRIN Cancer Research Group Trials, 1980-2008. *J Clin Oncol* **34**, 3544-3553, doi:10.1200/JCO.2016.67.5892 (2016).

246   Stove, H. K. *et al.* Extramedullary leukemia in children with acute myeloid leukemia: A population-based cohort study from the Nordic Society of Pediatric Hematology and Oncology (NOPHO). *Pediatr Blood Cancer* **64**, doi:10.1002/pbc.26520 (2017).

247   Garcia, M. G. *et al.* Myeloid sarcoma involving the gynecologic tract: a report of 11 cases and review of the literature. *Am J Clin Pathol* **125**, 783-790, doi:10.1309/H9MM-21FP-T7YB-L3PW (2006).

248   Puhalla, S. *et al.* Unsanctifying the sanctuary: challenges and opportunities with brain metastases. *Neuro Oncol* **17**, 639-651, doi:10.1093/neuonc/nov023 (2015).

249   Dave, D. S., Leppert, J. T. & Rajfer, J. Is the testis a chemo-privileged site? Is there a blood-testis barrier? *Rev Urol* **9**, 28-32 (2007).

250   Li, N., Wang, T. & Han, D. Structural, cellular and molecular aspects of immune privilege in the testis. *Front Immunol* **3**, 152, doi:10.3389/fimmu.2012.00152 (2012).

251   Kilanczyk, E. *et al.* Pharmacological inhibition of spinal cord injury-stimulated ribosomal biogenesis does not affect locomotor outcome. *Neurosci Lett* **642**, 153-157, doi:10.1016/j.neulet.2017.02.011 (2017).

252   Ferreira, R., Hein, N., Hannan, K. M., Drygin, D. & Hannan, R. D. in *31st Lorne Cancer Conference 2019* Vol. #173   (2019).

253   Firat, E., Weyerbrock, A., Gaedicke, S., Grosu, A. L. & Niedermann, G. Chloroquine or chloroquine-PI3K/Akt pathway inhibitor combinations strongly promote gamma-irradiation-induced cell death in primary stem-like glioma cells. *PLoS One* **7**, e47357, doi:10.1371/journal.pone.0047357 (2012).

254   Labuzek, K. *et al.* Quantification of metformin by the HPLC method in brain regions, cerebrospinal fluid and plasma of rats treated with lipopolysaccharide. *Pharmacol Rep* **62**, 956-965, doi:10.1016/s1734-1140(10)70357-1 (2010).

255   Park, J. M. *et al.* Metabolic response of glioma to dichloroacetate measured in vivo by hyperpolarized (13)C magnetic resonance spectroscopic imaging. *Neuro Oncol* **15**, 433-441, doi:10.1093/neuonc/nos319 (2013).

256   Dunbar, E. M. *et al.* Phase 1 trial of dichloroacetate (DCA) in adults with recurrent malignant brain tumors. *Investigational new drugs* **32**, 452-464, doi:10.1007/s10637-013-0047-4 (2014).

257   Cadman, E. T. *et al.* Alterations of splenic architecture in malaria are induced independently of Toll-like receptors 2, 4, and 9 or MyD88 and may affect antibody affinity. *Infect Immun* **76**, 3924-3931, doi:10.1128/IAI.00372-08 (2008).

258   Ismail, M. M. & Abdulateef, N. A. B. Bone marrow T-cell percentage: A novel prognostic indicator in acute myeloid leukemia. *Int J Hematol* **105**, 453-464, doi:10.1007/s12185-016-2153-5 (2017).

259   Antonelli, A. *et al.* Establishing human leukemia xenograft mouse models by implanting human bone marrow-like scaffold-based niches. *Blood* **128**, 2949-2959, doi:10.1182/blood-2016-05-719021 (2016).

260   Schuh, J. C. Trials, tribulations, and trends in tumor modeling in mice. *Toxicol Pathol* **32 Suppl 1**, 53-66, doi:10.1080/01926230490424770 (2004).

261   Negi, S. S. & Brown, P. rRNA synthesis inhibitor, CX-5461, activates ATM/ATR pathway in acute lymphoblastic leukemia, arrests cells in G2 phase and induces apoptosis. *Oncotarget* **6**, 18094-18104, doi:10.18632/oncotarget.4093 (2015).

262   Nunez Villacis, L. *et al.* New Roles for the Nucleolus in Health and Disease. *Bioessays* **40**, e1700233, doi:10.1002/bies.201700233 (2018).

263   Rubbi, C. P. & Milner, J. Disruption of the nucleolus mediates stabilization of p53 in response to DNA damage and other stresses. *EMBO J* **22**, 6068-6077, doi:10.1093/emboj/cdg579 (2003).

264   Yuan, X. *et al.* Genetic inactivation of the transcription factor TIF-IA leads to nucleolar disruption, cell cycle arrest, and p53-mediated apoptosis. *Mol Cell* **19**, 77-87, doi:10.1016/j.molcel.2005.05.023 (2005).

265   Haupt, Y., Maya, R., Kazaz, A. & Oren, M. Mdm2 promotes the rapid degradation of p53. *Nature* **387**, 296-299, doi:10.1038/387296a0 (1997).

266   Onofrillo, C., Galbiati, A., Montanaro, L. & Derenzini, M. The pre-existing population of 5S rRNA effects p53 stabilization during ribosome biogenesis inhibition. *Oncotarget* **8**, 4257-4267, doi:10.18632/oncotarget.13833 (2017).

267   Abraham, R. T. Cell cycle checkpoint signaling through the ATM and ATR kinases. *Genes & development* **15**, 2177-2196, doi:10.1101/gad.914401 (2001).

268   Quin, J. *et al.* Inhibition of RNA polymerase I transcription initiation by CX-5461 activates non-canonical ATM/ATR signaling. *Oncotarget* **7**, 49800-49818, doi:10.18632/oncotarget.10452 (2016).

269   Kusnadi, E. *Defining the translational landscape of MYC-driven cancer cells in response to therapeutic targeting of the ribosome*, (2018).

270   Loeb, R. F. *et al.* ACTIVITY of a new antimalarial agent, chloroquine (SN 7618). *J Am Med Assoc* **130**, 1069 (1946).

271   Yayon, A., Cabantchik, Z. I. & Ginsburg, H. Susceptibility of human malaria parasites to chloroquine is pH dependent. *Proc Natl Acad Sci U S A* **82**, 2784-2788 (1985).

272   Krogstad, D. J., Schlesinger, P. H. & Gluzman, I. Y. Antimalarials increase vesicle pH in Plasmodium falciparum. *J Cell Biol* **101**, 2302-2309 (1985).

273   Goldberg, D. E., Slater, A. F., Cerami, A. & Henderson, G. B. Hemoglobin degradation in the malaria parasite Plasmodium falciparum: an ordered process in a unique organelle. *Proc Natl Acad Sci U S A* **87**, 2931-2935 (1990).

274   Sullivan, D. J., Jr., Matile, H., Ridley, R. G. & Goldberg, D. E. A common mechanism for blockade of heme polymerization by antimalarial quinolines. *J Biol Chem* **273**, 31103-31107 (1998).

275   Marmor, M. F. *et al.* Revised recommendations on screening for chloroquine and hydroxychloroquine retinopathy. *Ophthalmology* **118**, 415-422, doi:10.1016/j.ophtha.2010.11.017 (2011).

276   Finbloom, D. S., Silver, K., Newsome, D. A. & Gunkel, R. Comparison of hydroxychloroquine and chloroquine use and the development of retinal toxicity. *J Rheumatol* **12**, 692-694 (1985).

277   Freedman, A. & Steinberg, V. L. Chloroquine in rheumatoid arthritis; a double blindfold trial of treatment for one year. *Ann Rheum Dis* **19**, 243-250 (1960).

278   Percival, S. P. & Meanock, I. Chloroquine: ophthalmological safety, and clinical assessment in rheumatoid arthritis. *Br Med J* **3**, 579-584 (1968).

279   Ruiz-Irastorza, G., Ramos-Casals, M., Brito-Zeron, P. & Khamashta, M. A. Clinical efficacy and side effects of antimalarials in systemic lupus erythematosus: a systematic review. *Ann Rheum Dis* **69**, 20-28, doi:10.1136/ard.2008.101766 (2010).

280   Dubois, E. L. Management and prognosis of systemic lupus erythematosus. *Bull Rheum Dis* **18**, 477-482 (1967).

281   Lombard-Platlet, S., Bertolino, P., Deng, H., Gerlier, D. & Rabourdin-Combe, C. Inhibition by chloroquine of the class II major histocompatibility complex-restricted presentation of endogenous antigens varies according to the cellular origin of the antigen-presenting cells, the nature of the T-cell epitope, and the responding T cell. *Immunology* **80**, 566-573 (1993).

282   Kamal, M. A. & Jusko, W. J. Interactions of prednisolone and other immunosuppressants used in dual treatment of systemic lupus erythematosus in lymphocyte proliferation assays. *J Clin Pharmacol* **44**, 1034-1045, doi:10.1177/0091270004267808 (2004).

283   Ausiello, C. M., Barbieri, P., Spagnoli, G. C., Ciompi, M. L. & Casciani, C. U. In vivo effects of chloroquine treatment on spontaneous and interferon-induced natural killer activities in rheumatoid arthritis patients. *Clin Exp Rheumatol* **4**, 255-259 (1986).

284 Yu, L. *et al.* Regulation of an ATG7-beclin 1 program of autophagic cell death by caspase-8. *Science* **304**, 1500-1502, doi:10.1126/science.1096645 (2004).

285 Aita, V. M. *et al.* Cloning and genomic organization of beclin 1, a candidate tumor suppressor gene on chromosome 17q21. *Genomics* **59**, 59-65, doi:10.1006/geno.1999.5851 (1999).

286 Miracco, C. *et al.* Protein and mRNA expression of autophagy gene Beclin 1 in human brain tumours. *Int J Oncol* **30**, 429-436 (2007).

287 Qu, X. *et al.* Promotion of tumorigenesis by heterozygous disruption of the beclin 1 autophagy gene. *J Clin Invest* **112**, 1809-1820, doi:10.1172/JCI20039 (2003).

288 Yue, Z., Jin, S., Yang, C., Levine, A. J. & Heintz, N. Beclin 1, an autophagy gene essential for early embryonic development, is a haploinsufficient tumor suppressor. *Proc Natl Acad Sci U S A* **100**, 15077-15082, doi:10.1073/pnas.2436255100 (2003).

289 Tang, D. *et al.* HMGB1 release and redox regulates autophagy and apoptosis in cancer cells. *Oncogene* **29**, 5299-5310, doi:10.1038/onc.2010.261 (2010).

290 Guo, X. L. *et al.* Targeting autophagy potentiates chemotherapy-induced apoptosis and proliferation inhibition in hepatocarcinoma cells. *Cancer Lett* **320**, 171-179, doi:10.1016/j.canlet.2012.03.002 (2012).

291 Bosnjak, M. *et al.* Inhibition of mTOR-dependent autophagy sensitizes leukemic cells to cytarabine-induced apoptotic death. *PLoS One* **9**, e94374, doi:10.1371/journal.pone.0094374 (2014).

292 Kang, R., Zeh, H. J., Lotze, M. T. & Tang, D. The Beclin 1 network regulates autophagy and apoptosis. *Cell Death Differ* **18**, 571-580, doi:10.1038/cdd.2010.191 (2011).

293 Wirawan, E. *et al.* Caspase-mediated cleavage of Beclin-1 inactivates Beclin-1-induced autophagy and enhances apoptosis by promoting the release of proapoptotic factors from mitochondria. *Cell death & disease* **1**, e18, doi:10.1038/cddis.2009.16 (2010).

294 Mizushima, N. Autophagy: process and function. *Genes & development* **21**, 2861-2873, doi:10.1101/gad.1599207 (2007).

295 Ye, C. *et al.* Beclin-1 knockdown decreases proliferation, invasion and migration of Ewing sarcoma SK-ES-1 cells via inhibition of MMP-9. *Oncol Lett* **15**, 3221-3225, doi:10.3892/ol.2017.7667 (2018).

296 Xing, S. *et al.* Beclin 1 knockdown inhibits autophagic activation and prevents the secondary neurodegenerative damage in the ipsilateral thalamus following focal cerebral infarction. *Autophagy* **8**, 63-76, doi:10.4161/auto.8.1.18217 (2012).

297   Tanida, I. *et al.* Knockdown of autophagy-related gene decreases the production of infectious hepatitis C virus particles. *Autophagy* **5**, 937-945 (2009).

298   Gomez-Puerto, M. C. *et al.* Autophagy Proteins ATG5 and ATG7 Are Essential for the Maintenance of Human CD34(+) Hematopoietic Stem-Progenitor Cells. *Stem Cells* **34**, 1651-1663, doi:10.1002/stem.2347 (2016).

299   Cohen, S. N. & Yielding, K. L. Spectrophotometric Studies of the Interaction of Chloroquine with Deoxyribonucleic Acid. *J Biol Chem* **240**, 3123-3131 (1965).

300   Esposito, F. & Sinden, R. R. Supercoiling in prokaryotic and eukaryotic DNA: changes in response to topological perturbation of plasmids in E. coli and SV40 in vitro, in nuclei and in CV-1 cells. *Nucleic Acids Res* **15**, 5105-5124 (1987).

301   Collis, S. J. *et al.* Evasion of early cellular response mechanisms following low level radiation-induced DNA damage. *J Biol Chem* **279**, 49624-49632, doi:10.1074/jbc.M409600200 (2004).

302   Lim, Y. *et al.* Chloroquine improves survival and hematopoietic recovery after lethal low-dose-rate radiation. *Int J Radiat Oncol Biol Phys* **84**, 800-806, doi:10.1016/j.ijrobp.2012.01.026 (2012).

303   Li, P. *et al.* Chloroquine inhibits autophagy and deteriorates the mitochondrial dysfunction and apoptosis in hypoxic rat neurons. *Life Sci* **202**, 70-77, doi:10.1016/j.lfs.2018.01.011 (2018).

304   Ganley, I. G. *et al.* ULK1.ATG13.FIP200 complex mediates mTOR signaling and is essential for autophagy. *J Biol Chem* **284**, 12297-12305, doi:10.1074/jbc.M900573200 (2009).

305   Cunningham, J. T. *et al.* mTOR controls mitochondrial oxidative function through a YY1-PGC-1alpha transcriptional complex. *Nature* **450**, 736-740, doi:10.1038/nature06322 (2007).

306   Koyanagi, M. *et al.* Ablation of TSC2 enhances insulin secretion by increasing the number of mitochondria through activation of mTORC1. *PLoS One* **6**, e23238, doi:10.1371/journal.pone.0023238 (2011).

307   Ben-Sahra, I., Howell, J. J., Asara, J. M. & Manning, B. D. Stimulation of de novo pyrimidine synthesis by growth signaling through mTOR and S6K1. *Science* **339**, 1323-1328, doi:10.1126/science.1228792 (2013).

308   Sancak, Y. *et al.* Ragulator-Rag complex targets mTORC1 to the lysosomal surface and is necessary for its activation by amino acids. *Cell* **141**, 290-303, doi:10.1016/j.cell.2010.02.024 (2010).

309   Zoncu, R. *et al.* mTORC1 senses lysosomal amino acids through an inside-out mechanism that requires the vacuolar H(+)-ATPase. *Science* **334**, 678-683, doi:10.1126/science.1207056 (2011).

310   Wang, S. *et al.* Metabolism. Lysosomal amino acid transporter SLC38A9 signals arginine sufficiency to mTORC1. *Science* **347**, 188-194, doi:10.1126/science.1257132 (2015).

311   Jiang, P. D. *et al.* Cell growth inhibition, G2/M cell cycle arrest, and apoptosis induced by chloroquine in human breast cancer cell line Bcap-37. *Cell Physiol Biochem* **22**, 431-440, doi:10.1159/000185488 (2008).

312   Monma, H. *et al.* Chloroquine augments TRAIL-induced apoptosis and induces G2/M phase arrest in human pancreatic cancer cells. *PLoS One* **13**, e0193990, doi:10.1371/journal.pone.0193990 (2018).

313   Yla-Anttila, P., Vihinen, H., Jokitalo, E. & Eskelinen, E. L. Monitoring autophagy by electron microscopy in Mammalian cells. *Methods Enzymol* **452**, 143-164, doi:10.1016/S0076-6879(08)03610-0 (2009).

314   Mizushima, N., Yoshimori, T. & Levine, B. Methods in mammalian autophagy research. *Cell* **140**, 313-326, doi:10.1016/j.cell.2010.01.028 (2010).

315   Mauvezin, C. & Neufeld, T. P. Bafilomycin A1 disrupts autophagic flux by inhibiting both V-ATPase-dependent acidification and Ca-P60A/SERCA-dependent autophagosome-lysosome fusion. *Autophagy* **11**, 1437-1438, doi:10.1080/15548627.2015.1066957 (2015).

316   Teplova, V. V., Tonshin, A. A., Grigoriev, P. A., Saris, N. E. & Salkinoja-Salonen, M. S. Bafilomycin A1 is a potassium ionophore that impairs mitochondrial functions. *J Bioenerg Biomembr* **39**, 321-329, doi:10.1007/s10863-007-9095-9 (2007).

317   Zhdanov, A. V., Dmitriev, R. I. & Papkovsky, D. B. Bafilomycin A1 activates respiration of neuronal cells via uncoupling associated with flickering depolarization of mitochondria. *Cell Mol Life Sci* **68**, 903-917, doi:10.1007/s00018-010-0502-8 (2011).

318   Katagiri, N. *et al.* The nucleolar protein nucleophosmin is essential for autophagy induced by inhibiting Pol I transcription. *Sci Rep* **5**, 8903, doi:10.1038/srep08903 (2015).

319   Satyavarapu, E. M., Das, R., Mandal, C., Mukhopadhyay, A. & Mandal, C. Autophagy-independent induction of LC3B through oxidative stress reveals its non-canonical role in anoikis of ovarian cancer cells. *Cell death & disease* **9**, 934, doi:10.1038/s41419-018-0989-8 (2018).

320   Tanida, I., Minematsu-Ikeguchi, N., Ueno, T. & Kominami, E. Lysosomal turnover, but not a cellular level, of endogenous LC3 is a marker for autophagy. *Autophagy* **1**, 84-91 (2005).

321   Schlafli, A. M., Isakson, P., Garattini, E., Simonsen, A. & Tschan, M. P. The autophagy scaffold protein ALFY is critical for the granulocytic differentiation of AML cells. *Sci Rep* **7**, 12980, doi:10.1038/s41598-017-12734-4 (2017).

322   Yoshii, S. R. & Mizushima, N. Monitoring and Measuring Autophagy. *Int J Mol Sci* **18**, doi:10.3390/ijms18091865 (2017).

323   Borthakur, G. *et al.* MDM2 Inhibitor, Nutlin 3a, Induces p53 Dependent Autophagy in Acute Leukemia by AMP Kinase Activation. *PLoS One* **10**, e0139254, doi:10.1371/journal.pone.0139254 (2015).

324   Qiao, H. *et al.* Liraglutide repairs the infarcted heart: The role of the SIRT1/Parkin/mitophagy pathway. *Mol Med Rep* **17**, 3722-3734, doi:10.3892/mmr.2018.8371 (2018).

325   Hamasaki, M. *et al.* Autophagosomes form at ER-mitochondria contact sites. *Nature* **495**, 389-393, doi:10.1038/nature11910 (2013).

326   Hosseini, R. *et al.* Correlative light and electron microscopy imaging of autophagy in a zebrafish infection model. *Autophagy* **10**, 1844-1857, doi:10.4161/auto.29992 (2014).

327   Hunter, S. E., Jung, D., Di Giulio, R. T. & Meyer, J. N. The QPCR assay for analysis of mitochondrial DNA damage, repair, and relative copy number. *Methods* **51**, 444-451, doi:10.1016/j.ymeth.2010.01.033 (2010).

328   Memon, A. A. *et al.* Quantification of mitochondrial DNA copy number in suspected cancer patients by a well optimized ddPCR method. *Biomol Detect Quantif* **13**, 32-39, doi:10.1016/j.bdq.2017.08.001 (2017).

329   Tal, M. C. *et al.* Absence of autophagy results in reactive oxygen species-dependent amplification of RLR signaling. *Proc Natl Acad Sci U S A* **106**, 2770-2775, doi:10.1073/pnas.0807694106 (2009).

330   Mei, L. *et al.* Synergistic anti-tumour effects of tetrandrine and chloroquine combination therapy in human cancer: a potential antagonistic role for p21. *Br J Pharmacol* **172**, 2232-2245, doi:10.1111/bph.13045 (2015).

331   Wu, Q. *et al.* Abnormal Ribosome Biogenesis Partly Induced p53-Dependent Aortic Medial Smooth Muscle Cell Apoptosis and Oxidative Stress. *Oxid Med Cell Longev* **2019**, 7064319, doi:10.1155/2019/7064319 (2019).

332   Sriskanthadevan, S. *et al.* AML cells have low spare reserve capacity in their respiratory chain that renders them susceptible to oxidative metabolic stress. *Blood* **125**, 2120-2130, doi:10.1182/blood-2014-08-594408 (2015).

333   Sogame, Y., Kitamura, A., Yabuki, M. & Komuro, S. A comparison of uptake of metformin and phenformin mediated by hOCT1 in human hepatocytes. *Biopharm Drug Dispos* **30**, 476-484, doi:10.1002/bdd.684 (2009).

334   Nies, A. T. *et al.* Expression of organic cation transporters OCT1 (SLC22A1) and OCT3 (SLC22A3) is affected by genetic factors and cholestasis in human liver. *Hepatology* **50**, 1227-1240, doi:10.1002/hep.23103 (2009).

335   Moreno-Navarrete, J. M. *et al.* OCT1 Expression in adipocytes could contribute to increased metformin action in obese subjects. *Diabetes* **60**, 168-176, doi:10.2337/db10-0805 (2011).

336   Stefanko, E. *et al.* Significance of OCT1 Expression in Acute Myeloid Leukemia. *Pathol Oncol Res* **23**, 665-671, doi:10.1007/s12253-016-0161-7 (2017).

337   Ceacareanu, A. C., Nimako, G. K. & Wintrob, Z. A. P. Missing the Benefit of Metformin in Acute Myeloid Leukemia: A Problem of Contrast? *J Res Pharm Pract* **6**, 145-150, doi:10.4103/jrpp.JRPP_17_37 (2017).

338   Boukalova, S. *et al.* Mitochondrial Targeting of Metformin Enhances Its Activity against Pancreatic Cancer. *Mol Cancer Ther* **15**, 2875-2886, doi:10.1158/1535-7163.MCT-15-1021 (2016).

339   Geoghegan, F., Chadderton, N., Farrar, G. J., Zisterer, D. M. & Porter, R. K. Direct effects of phenformin on metabolism/bioenergetics and viability of SH-SY5Y neuroblastoma cells. *Oncol Lett* **14**, 6298-6306, doi:10.3892/ol.2017.6929 (2017).

340   Assan, R., Heuclin, C., Girard, J. R., LeMaire, F. & Attali, J. R. Phenformin-induced lactic acidosis in diabetic patients. *Diabetes* **24**, 791-800 (1975).

341   Kwong, S. C. & Brubacher, J. Phenformin and lactic acidosis: a case report and review. *J Emerg Med* **16**, 881-886 (1998).

342   Koh, M., Lee, J. C., Min, C. & Moon, A. A novel metformin derivative, HL010183, inhibits proliferation and invasion of triple-negative breast cancer cells. *Bioorg Med Chem* **21**, 2305-2313, doi:10.1016/j.bmc.2013.02.015 (2013).

343   Miao, G., Liu, B., Guo, X., Zhang, X. & Liu, G. J. Reduction behavior induced by HL010183, a metformin derivative against the growth of cutaneous squamous cell carcinoma. *Int J Clin Exp Pathol* **8**, 287-297 (2015).

344   Brodersen, D. E. *et al.* The structural basis for the action of the antibiotics tetracycline, pactamycin, and hygromycin B on the 30S ribosomal subunit. *Cell* **103**, 1143-1154 (2000).

345   Greer, N. D. Tigecycline (Tygacil): the first in the glycylcycline class of antibiotics. *Proc (Bayl Univ Med Cent)* **19**, 155-161 (2006).

346   Reed, G. A. *et al.* A Phase 1 study of intravenous infusions of tigecycline in patients with acute myeloid leukemia. *Cancer Med* **5**, 3031-3040, doi:10.1002/cam4.845 (2016).

347   Muralidharan, G., Micalizzi, M., Speth, J., Raible, D. & Troy, S. Pharmacokinetics of tigecycline after single and multiple doses in healthy subjects. *Antimicrob Agents Chemother* **49**, 220-229, doi:10.1128/AAC.49.1.220-229.2005 (2005).

348   Muralidharan, G., Fruncillo, R. J., Micalizzi, M., Raible, D. G. & Troy, S. M. Effects of age and sex on single-dose pharmacokinetics of tigecycline in healthy subjects. *Antimicrob Agents Chemother* **49**, 1656-1659, doi:10.1128/AAC.49.4.1656-1659.2005 (2005).

349 Meagher, A. K., Ambrose, P. G., Grasela, T. H. & Ellis-Grosse, E. J. Pharmacokinetic/pharmacodynamic profile for tigecycline-a new glycylcycline antimicrobial agent. *Diagn Microbiol Infect Dis* **52**, 165-171, doi:10.1016/j.diagmicrobio.2005.05.006 (2005).

350 Adadevoh, B. K., Ogunnaike, I. A. & Bolodeoku, J. O. Serum levels of doxycycline in normal subjects after a single oral dose. *Br Med J* **1**, 880, doi:10.1136/bmj.1.6014.880 (1976).

351 Goldman, R. A., Hasan, T., Hall, C. C., Strycharz, W. A. & Cooperman, B. S. Photoincorporation of tetracycline into Escherichia coli ribosomes. Identification of the major proteins photolabeled by native tetracycline and tetracycline photoproducts and implications for the inhibitory action of tetracycline on protein synthesis. *Biochemistry* **22**, 359-368 (1983).

352 Moullan, N. *et al.* Tetracyclines Disturb Mitochondrial Function across Eukaryotic Models: A Call for Caution in Biomedical Research. *Cell Rep* **10**, 1681-1691, doi:10.1016/j.celrep.2015.02.034 (2015).

353 Lamb, R. *et al.* Antibiotics that target mitochondria effectively eradicate cancer stem cells, across multiple tumor types: treating cancer like an infectious disease. *Oncotarget* **6**, 4569-4584, doi:10.18632/oncotarget.3174 (2015).

354 Scatena, C. *et al.* Doxycycline, an Inhibitor of Mitochondrial Biogenesis, Effectively Reduces Cancer Stem Cells (CSCs) in Early Breast Cancer Patients: A Clinical Pilot Study. *Front Oncol* **8**, 452, doi:10.3389/fonc.2018.00452 (2018).

355 Somers, K. *et al.* A novel small molecule that kills a subset of MLL-rearranged leukemia cells by inducing mitochondrial dysfunction. *Oncogene*, doi:10.1038/s41388-018-0666-5 (2019).

356 Locke, F. L. *et al.* Long-term safety and activity of axicabtagene ciloleucel in refractory large B-cell lymphoma (ZUMA-1): a single-arm, multicentre, phase 1-2 trial. *Lancet Oncol* **20**, 31-42, doi:10.1016/S1470-2045(18)30864-7 (2019).

357 Maude, S. L. *et al.* Tisagenlecleucel in Children and Young Adults with B-Cell Lymphoblastic Leukemia. *N Engl J Med* **378**, 439-448, doi:10.1056/NEJMoa1709866 (2018).

358 Ott, P. A., Hodi, F. S. & Robert, C. CTLA-4 and PD-1/PD-L1 blockade: new immunotherapeutic modalities with durable clinical benefit in melanoma patients. *Clin Cancer Res* **19**, 5300-5309, doi:10.1158/1078-0432.CCR-13-0143 (2013).

359 Liu, Y., Bewersdorf, J. P., Stahl, M. & Zeidan, A. M. Immunotherapy in acute myeloid leukemia and myelodysplastic syndromes: The dawn of a new era? *Blood Rev* **34**, 67-83, doi:10.1016/j.blre.2018.12.001 (2019).

360   Appelbaum, F. R. & Bernstein, I. D. Gemtuzumab ozogamicin for acute myeloid leukemia. *Blood* **130**, 2373-2376, doi:10.1182/blood-2017-09-797712 (2017).

361   Stahl, M. & Goldberg, A. D. Immune Checkpoint Inhibitors in Acute Myeloid Leukemia: Novel Combinations and Therapeutic Targets. *Curr Oncol Rep* **21**, 37, doi:10.1007/s11912-019-0781-7 (2019).

362   Liu, Y. F., He, P. C. & Zhang, M. [Effect of PD-L1 Expression on Activity of NK Killing AML Cell Lines and Its Mechanisms]. *Zhongguo Shi Yan Xue Ye Xue Za Zhi* **26**, 1317-1322, doi:10.7534/j.issn.1009-2137.2018.05.010 (2018).

363   Zeidner, J. F. *et al.* Phase II Study of High Dose Cytarabine Followed By Pembrolizumab in Relapsed/Refractory Acute Myeloid Leukemia (AML). *Blood* **130**, 1349 (2017).

364   Daver, N. *et al.* Efficacy, Safety, and Biomarkers of Response to Azacitidine and Nivolumab in Relapsed/Refractory Acute Myeloid Leukemia: A Nonrandomized, Open-Label, Phase II Study. *Cancer Discov* **9**, 370-383, doi:10.1158/2159-8290.CD-18-0774 (2019).
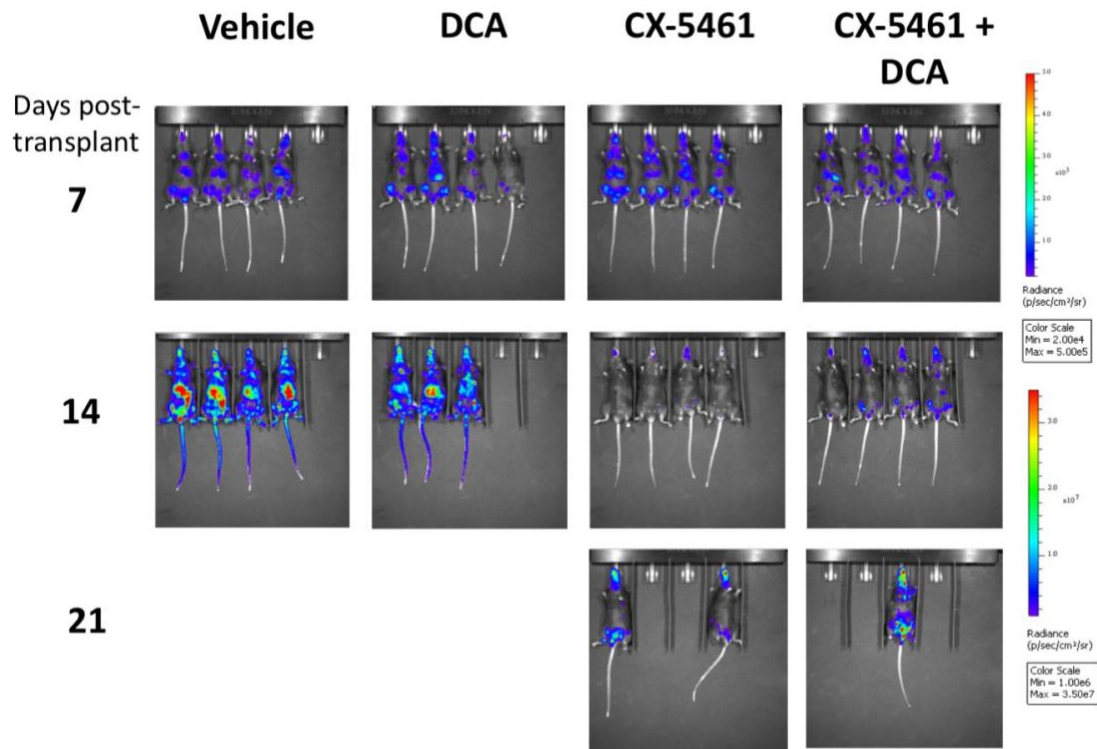
Appendix

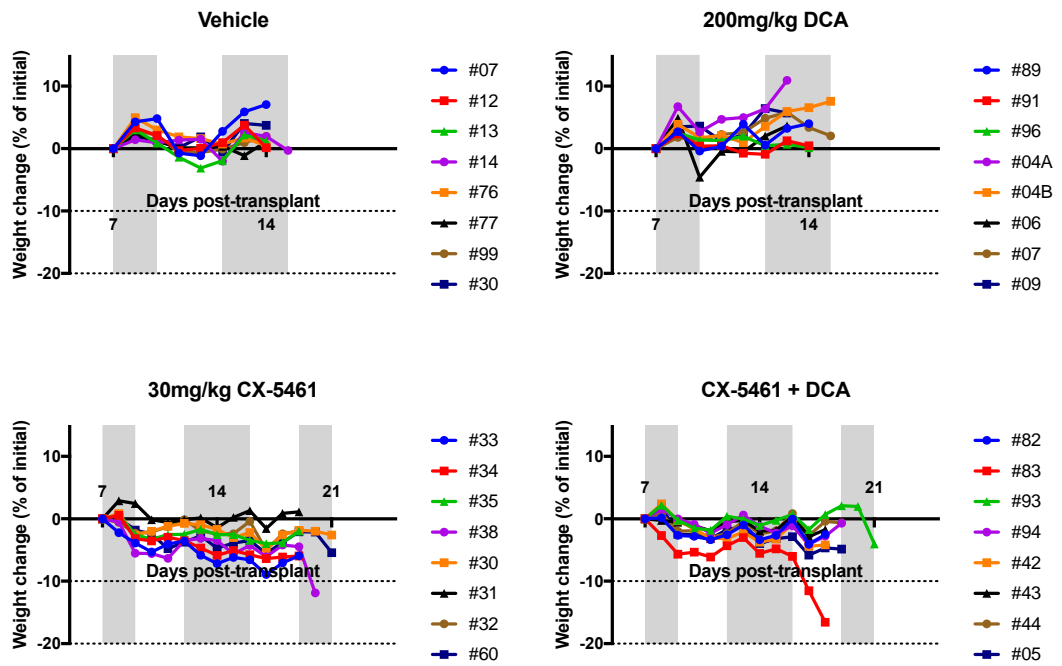## Chapter 4 supplementary data
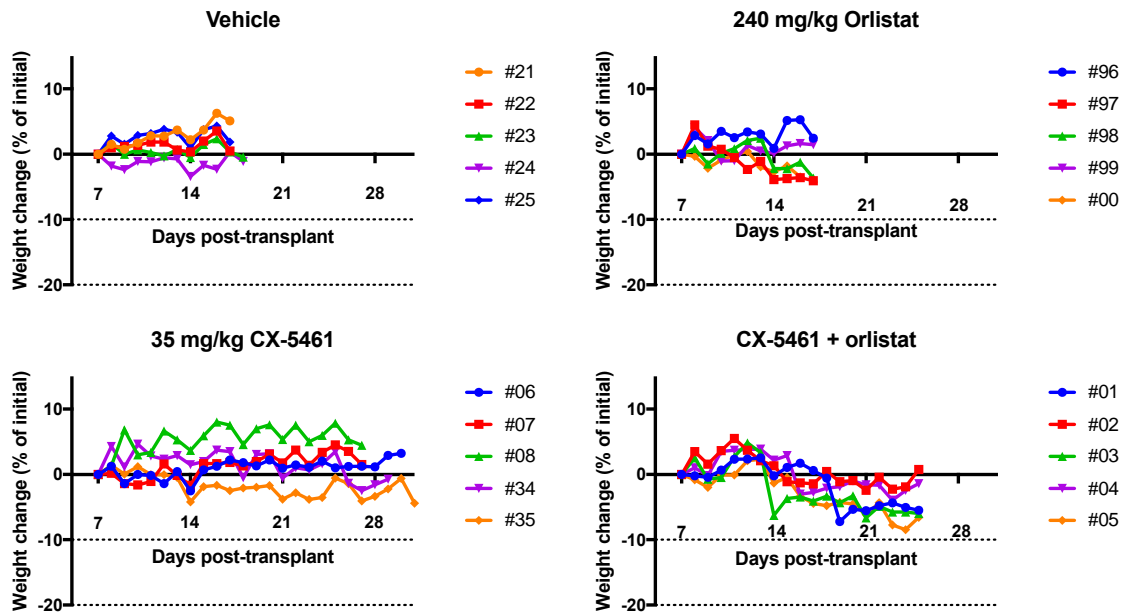
Appendix Figure 4-1: Weight changes from combination therapy of CX-5461 and orlistat in the syngeneic MLL/AF9 NRAS AML model

The weights of the mice were monitored daily during the dosing period and the weight changes as % of initial weight shown. Dosing occurred daily.
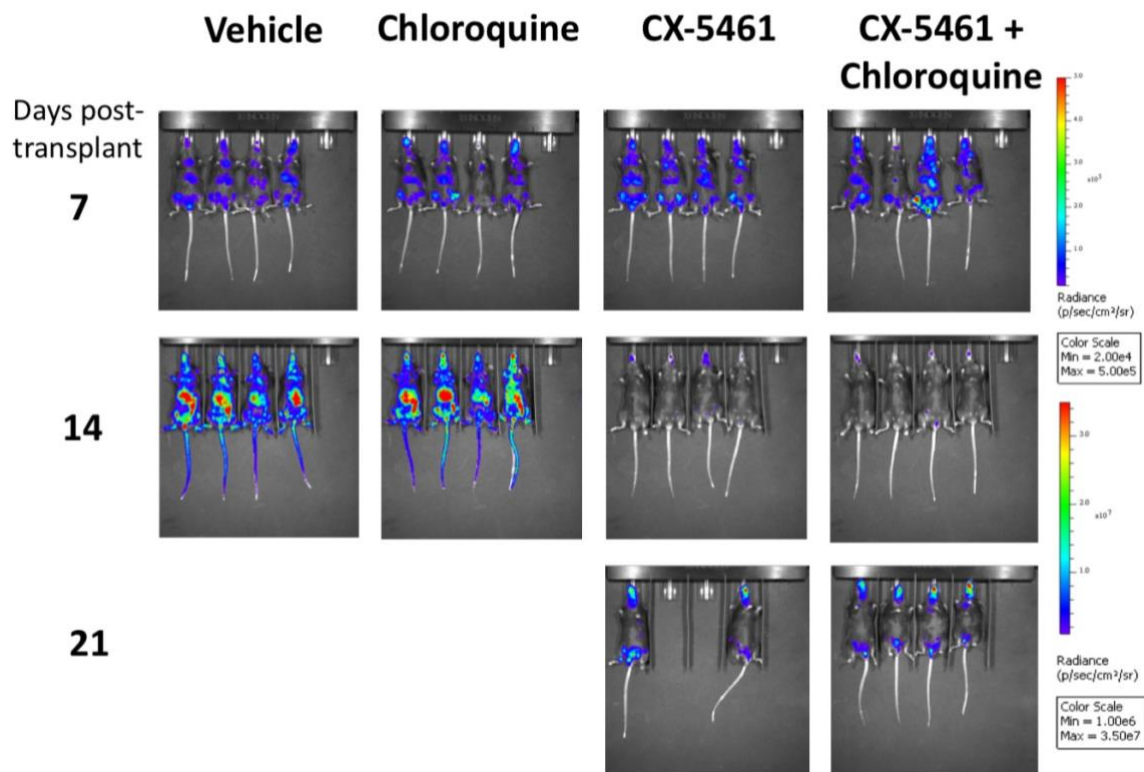
Appendix Figure 4-2: Bioluminescent images from combination therapy of CX-5461 and DCA in the syngeneic MLL/AF9 NRAS AML model

Imaging was performed weekly from 7 days post-transplant. The day 7 images are shown on a lower image colour scale to the subsequent weeks images, in order to show that engraftment has occurred.

Appendix Figure 4-3: Weight changes from combination therapy of CX-5461 and DCA in the syngeneic MLL/AF9 NRAS AML model

The weights of the mice were monitored daily during the dosing period and the weight changes as % of initial weight shown. Dosing days are shown in grey.

Appendix Figure 4-4: Bioluminescent images from combination therapy of CX-5461 and chloroquine in the syngeneic MLL/AF9 NRAS AML model

Imaging was performed weekly from 7 days post-transplant. The day 7 images are shown on a lower image colour scale to the subsequent weeks images, in order to show that engraftment has occurred.
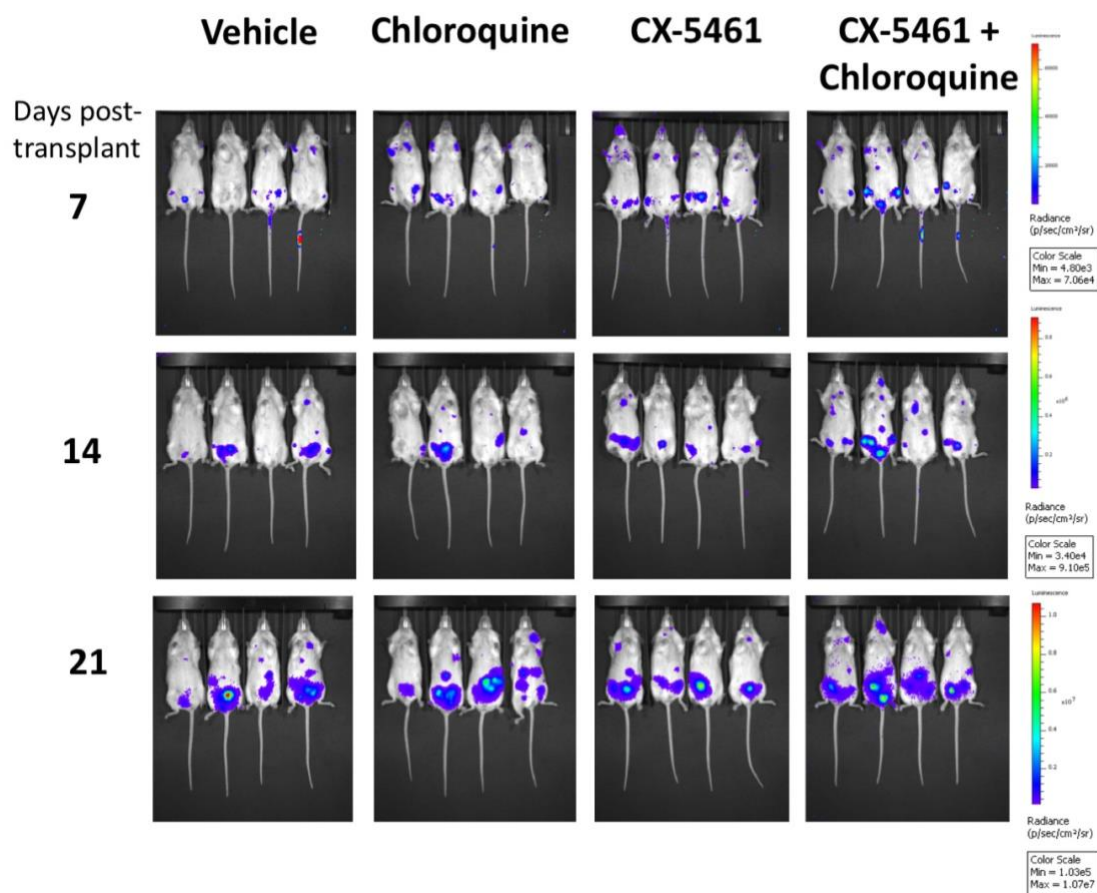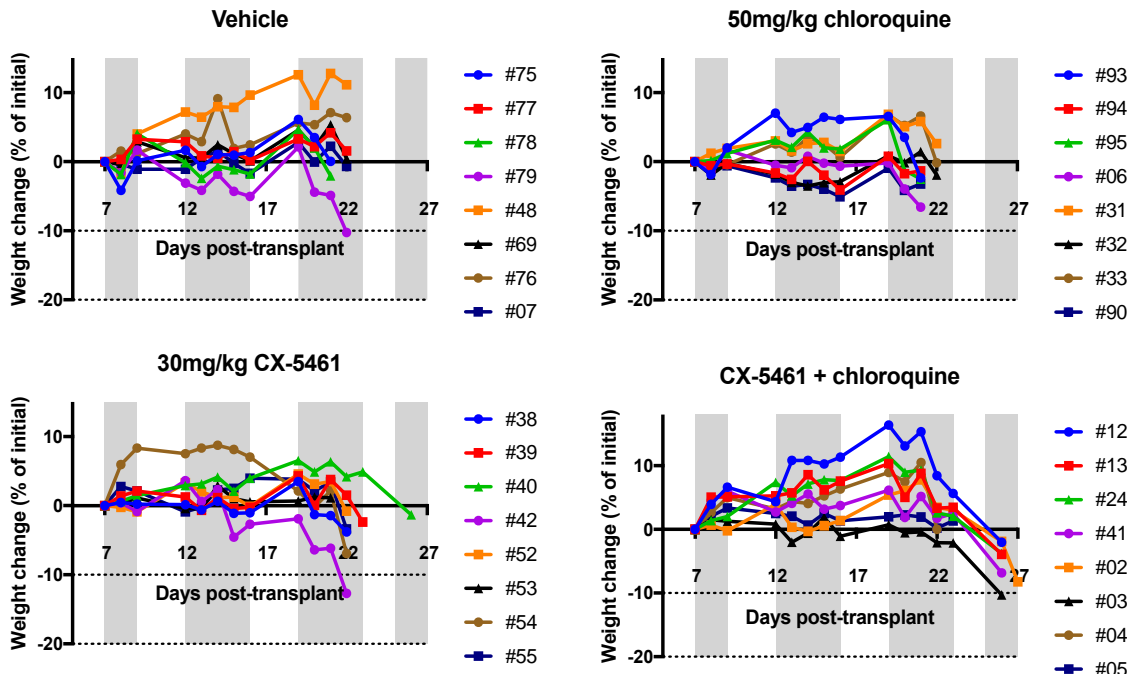
Appendix Figure 4-5: Bioluminescent images from combination therapy of CX-5461 and chloroquine in the xenograft MV4-11 GFP luc model

Imaging was performed weekly from 7 days post-transplant. The day 7 images are shown on a lower image scale to the subsequent weeks images, in order to show that engraftment has occurred.

Appendix Figure 4-6: Weight changes from combination therapy of CX-5461 and chloroquine in the xenograft MOLM-13 GFP luc model

The weights of the mice were monitored daily during the dosing period and the weight changes as % of initial weight shown. Dosing days are shown in grey.

Median survival (days)	Model				
	MLL/AF9 NRAS			MOLM-13 GFP luc	MV4-11 GFP luc
	Treatment regime				
	CX-5461 + orlistat	CX-5461 + DCA	CX-5461 + chloroquine	CX-5461 + chloroquine	CX-5461 + chloroquine
Vehicle	17	15	15	14	22
Metabolism drug	17	14.5	14	14	21
CX-5461	29	20	20	15	22
Combination	25	19.5	23	15	24

Appendix Table 4-1: Survival times from *in vivo* combination treatment experiments

Median survival times of treatment groups were calculated from combination treatment experiments in Sections 4.2.2 and 4.2.4.

P values	Model				
	MLL/AF9 NRAS			MOLM-13 GFP luc	MV4-11 GFP luc
	Treatment regime				
	CX-5461 + orlistat	CX-5461 + DCA	CX-5461 + chloroquine	CX-5461 + chloroquine	CX-5461 + chloroquine
Veh vs. Met	0.0926 N.S.	0.1172 N.S.	0.0455 N.S.	0.2888 N.S.	0.2151 N.S.
Veh vs. CX	0.0023 *	0.0001 ***	0.0001 ***	0.0027 *	0.1750 N.S.
Met vs. CX	0.0035 *	0.0001 ***	<0.0001 ****	0.0017 *	0.0338 N.S.
Veh vs. combo	0.0023 *	0.0001 ***	0.0003 ***	0.0007 **	0.0007 **
Met vs. combo	0.0035 *	0.0001 ***	0.0002 ***	0.0004 **	0.0003 **
CX vs. combo	0.0083 *	0.3840 N.S.	0.0049 *	0.1759 N.S.	0.0032 *

Appendix Table 4-2: Statistical analysis of survival times from *in vivo* combination treatment experiments

Log-rank test with Bonferroni corrected threshold was applied for comparison of multiple survival curves, such that a p-value of <0.0083 was considered significant. Not significant (NS) P > 0.0083, *P ≤ 0.0083, **P ≤ 0.015, ***P ≤ 0.001, **** P ≤ 0.0001. Veh = vehicle, met = metabolism modifying drug, CX = CX-5461.

Appendix Figure 5-1: Acute effects of CX-5461 and chloroquine as individual agents on mitochondrial function

Metabolic flux of AML cell lines THP-1 and MOLM-13 was analysed using a mitochondrial stress test on the Seahorse XFe97 analyser (Section 2.11), with injection of vehicle, 1μM CX-5461 (CX), 40μM chloroquine (CQ) performed during the assay. a) Basal respiration rates, b) Respiration rates following drug injection, c) Maximal respiration rate following mitochondrial uncoupling with FCCP, d) Acute response (difference in the OCR following drug injection and basal respiration, e) Spare respiratory capacity (difference in the OCR between the maximum respiration rate and basal rate). One-way ANOVA was performed with a Tukey's multiple comparison test, the adjusted p-value is shown. Not significant P > 0.05, *P ≤ 0.05, **P ≤ 0.01, ***P ≤ 0.001, **** P ≤ 0.0001. Significant results only marked. N=3.